



Technische Universität München
Fakultät für Elektro- und Informationstechnik
Lehrstuhl für Kognitive Systeme

New Methods for Active Tactile Object Perception and Learning with Artificial Robotic Skin

Mohsen Kaboli

Vollständiger Abdruck der von der Fakultät für Elektro- und Informationstechnik
der Technischen Universität München zur Erlangung des akademischen Grades eines

Doktor-Ingenieur (Dr.-Ing.)

genehmigten Dissertation.

Vorsitzender: Prof. Dongheui Lee, Ph.D.

Prüfer der Dissertation:

1. Prof. Gordon Cheng, Ph.D.
2. Prof. Yasuo Kuniyoshi, Ph.D., University of
Tokyo, Japan
3. Prof. Ravinder S. Dahyia, Ph.D., University
of Glasgow, UK

Die Dissertation wurde am 20.09.2017 bei der Technischen Universität München eingereicht
und durch die Fakultät für Elektrotechnik und Informationstechnik am 21.11.2017 angenom-
men.

Abstract

Sense of touch plays an important role in our daily lives from grasping and manipulating to identifying and interacting with objects. For robotic systems that interact with dynamic environments, it is crucial to recognize objects via their physical properties. However, this is difficult to achieve even with advanced vision techniques due to occlusion and poor lighting conditions. Tactile sensing instead, can simultaneously provide rich and direct feedback to the robotic systems. The performance of the previously proposed tactile object discrimination strategies is dependent on the tactile feature extraction and learning methods designed for particular experimental setup.

Here, I propose novel tactile descriptors which are robust regardless of the number of tactile sensors used in robotic systems, types and techniques of tactile sensors, and structure of objects' surfaces. Previous researchers have used various robotic systems and tactile sensors to passively learn about objects and identify them from each other by utilizing uniformly collected training samples in an offline manner. However, the informativeness of the data varies. Some objects have distinctive tactile properties, which makes them easy to be discriminated. Therefore, collecting many training samples can be redundant.

Contrary to the previous studies, for the first time, I propose a complete probabilistic tactile-based framework consists of an active pre-touch workspace exploration strategy and active tactile object learning method. The robots with the active pre-touch efficiently explore the unknown workspace to estimate the number of objects, their location, and their orientation. With the benefit of the active touch learning algorithm, the robotic systems efficiently learn about objects based on their physical properties with the lowest possible number of samples. Furthermore, I propose a full-fledged touch-based probabilistic framework consisting of an active workspace exploration, active object discrimination, and active target object search. Taking advantage of my previously proposed active tactile object learning and my new active object discrimination algorithm, the robotic system efficiently distinguishes between objects and searches for specified target objects by strategically selecting the optimal exploratory actions.

I also introduce a newly developed tactile-based method to determine the center of mass of rigid objects. Although several strategies have been proposed to robotic systems to learn about objects, robots are still unable to re-use their prior tactile experience while learning new objects. To tackle this problem, I developed the first tactile transfer learning algorithm to enable robotic systems to autonomously exploit their prior tactile knowledge while learning about a new set of objects.

Moreover, I improved this strategy by combining the previously proposed active learning, active object discrimination method and the tactile transfer learning. This new algorithm named as active tactile transfer learning is to further reduce training samples by strategically selecting and exploiting relevant prior tactile knowledge. I also introduce novel tactile-based strategies for detecting slips and regulating grasping forces to enable robots to manipulate deformable objects with the dynamic center of mass safely. My proposed method does not require any prior knowledge of the contact surface and friction coefficient.

Recent advances in tactile sensing have opened up new pathways for humanoids to more accurately communicate with humans. Through tactile interaction, various touch modalities may be carried out; a robot may be patted, slapped, punched, or tickled. For any robotic system that is to work in close cooperation with humans, evaluation and classification of these touch modalities are vital. Taking advantage of my proposed tactile descriptors, I present a novel approach for touch pattern identification during the tactile human-robot interaction.

kurzfassung

Der Tastsinn spielt eine wichtige Rolle in unserem Alltag: vom Greifen und Handhaben von Objekten bis hin zu ihrer Identifikation und dem Interagieren mit ihnen. Für Robotersysteme, die mit einer sich ständig verändernden Umgebung interagieren, ist es entscheidend, Objekte anhand ihrer physikalischen Eigenschaften zu erkennen. Allerdings ist das selbst mit den modernsten visuellen Techniken nicht einfach, besonders bei verdeckten Gegenständen und schlechten Lichtverhältnissen. Die haptische Wahrnehmung kann stattdessen gleichzeitig direkte und aussagekräftige Informationen an das Robotersystem liefern.

Der Erfolg bisher postulierter haptischer Methoden zur Objekterkennung war stets von der haptischen Merkmalsextraktion und der eingesetzten Lernmethode abhängig die jeweils nur für individuelle Versuchsaufbauten eingesetzt werden konnten.

In dieser Arbeit postulieren wir neuartige haptische Deskriptoren, die unabhängig von der Struktur des Objekts, des Typs und der Anzahl der haptischen Sensoren des Robotersystems, zuverlässige Ergebnisse liefern. Bisher haben Forscher verschiedene Robotersysteme und haptische Sensoren verwendet, um Gegenstände passiv zu lernen und sie voneinander zu unterscheiden, indem sie auf zuvor gleichartig gesammelte Trainingsversuche offline zurückgreifen. Jedoch variiert der Informationsgehalt solcher Daten.

Einige Gegenstände sind durch ihre ausgeprägten tastbaren Eigenschaften einfach zu unterscheiden, was das Sammeln zahlreicher Trainingsversuche überflüssig macht. Im Gegensatz zu bisherigen Studien, postulieren wir zum ersten Mal ein vollständig probabilistisches auf Haptik basierendes System, bestehend aus einer aktiven Erkundung des Arbeitsbereichs vor der Berührung des Objekts und einer aktiven haptischen Objekterkennungsmethode. Dabei erkunden die Roboter vor der Berührung sehr effektiv den unbekanntem Arbeitsraum, um die Anzahl der Objekte, deren Lage und deren Orientierung einzuschätzen.

Mit Hilfe des “active touch” Lernalgorithmus lernen die Robotersysteme sehr effizient und mit der geringstmöglichen Anzahl an Trainingsversuchen durch die physikalischen Eigenschaften viel über die Objekte.

Weiterhin präsentieren wir ein umfassendes haptisches auf Berührung basierendes probabilistisches System, welches aus aktiver Erkundung des Arbeitsbereiches, aktiver Unterscheidung von Objekten, sowie aktiver Zielobjektsuche besteht. Indem es sich den bereits bekannten aktiven haptischen Objekterkennungs-Algorithmus und den neuen Algorithmus zur aktiven Objektunterscheidung zu Nutze macht, kann das Robotersystem effizient Objekte unterscheiden, sowie gezielt nach spezifizierten Objekten suchen, indem es strategisch die optimalen exploratorischen Handlungen auswählt.

Ebenso führen wir eine neu entwickelte haptische Methode zur Erkennung des Massenschwerpunktes von starren Objekten ein. Obwohl verschiedene Strategien präsentiert wurden, mit deren Hilfe Robotersysteme Objekte erlernen sollen, sind Roboter immer noch nicht in der Lage, ihre vorherigen haptischen Erfahrungen bei der Erkundung neuer Objekte zu nutzen. Um dieses Problem zu lösen, haben wir erstmalig einen "transfer learning" Algorithmus entwickelt, der es Robotersystemen ermöglicht, ihre vorherigen haptischen Kenntnisse zu nutzen, um neue Objekte kennenzulernen. Weiterhin haben wir diese Strategie verbessert, indem wir das bereits bekannte aktive Lernen, das aktive Unterscheiden von Objekten mit dem haptischen "transfer learning" kombinieren. Dieser neue Algorithmus, welcher "active tactile transfer learning" genannt wird, ermöglicht es, die Zahl an Trainingsversuchen zu reduzieren, indem bereits erlernte haptische Informationen strategisch ausgewählt und genutzt werden.

Des Weiteren stellen wir ein neues haptisches System vor, das ein Abrutschen erkennen kann und die Greifkraft so reguliert, dass Roboter auch verformbare Objekte mit einem veränderlichen Massenschwerpunkt sicher handhaben können. Unser System benötigt bezüglich der Kontaktfläche und des Reibungskoeffizienten keine Vorkenntnisse.

Neueste Fortschritte in der haptischen Wahrnehmung haben den humanoiden Robotern neue Wege eröffnet, genauer mit Menschen zu kommunizieren. Durch haptische Interaktion können verschiedene Arten der Berührung ausgeführt werden; ein Roboter kann getätschelt, geschlagen oder gekitzelt werden. Die Evaluation und Klassifikation dieser Berührungsarten ist von entscheidender Bedeutung für jedes Robotersystem, das eng mit Menschen zusammenarbeiten soll. Indem wir uns die entwickelten haptischen Deskriptoren zu Nutze machen, präsentieren wir eine neue Herangehensweise zur Identifizierung von Berührungsarten bei der haptischen Interaktion zwischen Mensch und Roboter.

*To my beloved parents and sister,
my lovely wife, Dr. Silke Herzer,
and all my teachers.*

Acknowledgements

If I have seen further it is by standing on the shoulders of giants.

(Issac Newton)

I have been incredibly fortunate and honored to be a Ph.D. student of Prof. Gordon Cheng, the best supervisor that I could ever have. Gordon guided me to a fundamental and exciting field of research in robotics which involved all my potentials and scientific passions. I would like to express my gratitude for his consistent support, encouragement, and advice which made my doctoral research studies a fruitful, rewarding, and worthwhile accomplishment. Gordon guided me to achieve a Marie Curie fellowship within the framework of the CONTEST project (COLlaborative Network for Training in Electronic Skin Technology). The CONTEST was a multi-site initial training network (ITN) for expanding the field of flexible and large area tactile sensing with the application in robotics which was perfectly aligned with my scientific desirous and longings.

Moreover, I have been extremely auspicious to be co-advised by Prof. Yasuo Kuniyoshi, the best co-supervisor, and mentor that I could ever have. I would like to express my sincere appreciation for his fundamental insights and ideas in whole body tactile sensing and embodiment in robotics and also for hosting me in his lab, the Intelligent Systems and Informatics (ISI) for four months. I also would like to thank all team member of ISI lab for various discussions and the warm welcome and guidance while I was at the University of Tokyo, Japan. I enjoyed an amazing and influential research environment at ISI lab.

I would like to extend my sincere acknowledgment to Prof. Ravinder Dahiya and Dr. Leandro Lorenzelli for successfully leading the CONTEST project. I would like to thank both of them for creating an excellent opportunity for me to carry out my research and Ph.D. study. I would also like to acknowledge Prof. Etienne Burdet for hosting me in his lab, the Human Robotics lab at the Imperial College London.

I would also like to thank Dr. Sae Franklin and Dr. David Franklin for generously spending their time to proof read my thesis.

I would also like to thank all my friends and colleagues in TUM, especially at the Institute for Cognitive Systems (ICS), Dynamic Human-Robot Interaction (DHRI), and Neuroscientific System Theory (NST). I have been fortunate to have the companionship of my dear friends and colleagues. In particular, I would like to acknowledge Dr. John Nassour, Prof. Vincent Hugel, Dr. Agnieszka Wykowska, Dr. Takaaki Kuratate, Dr. Andreas Holzbach, Dr. Ewald Lutscher, Dr. Hamid Sadeghian, Dr. Pablo Lanillos, Dr. Philipp Mittendorfer, Dr. Sophon Somlor, Dr. Marion Leibold, Dr. Dirk Wollherr, Dr. Sosnowski, Stefan Ehrlich, Erhard Wieser, Brennan Pierce, Quentin Leboutet, Ilya Dianov, Julio Rogelio Guadarrama, Wibke Borgesser, Florian Bergner, Ilona Nar-Witte, Matteo Saveriano, and Dr. Pietro Falco.

I would like to further thank all colleagues at the Shadow Robot Company for hosting in their company, especially Rich Walker, Nike Singer, Gavin Cassidy, Armando De La Rosa T., Matjaz Ogrinc. My particular thanks to all colleagues at the ISI lab, the University of Tokyo, Prof. Ryuma Niiyama, Prof. Satoshi Nishikawa, Dr. Yoshiyuki Ohmura, Dr. Hoshinori Kanazawa, Dr. Kazutoshi Tanaka, Keiko Fujii, Akimasa Nakashima, Mohamed Haggag, Hiromi Kitaura, Chang Shih-Yin, and Mioko Tomaru.

I would like to acknowledge the direct contributions of all my students that have been working with me, Alex Long, Kunpeng Yao, Di Feng, Shoubhik Debnath. I hope to have been a good teacher, but also a good learner. Exceptional thanks to my friends in Heidelberg, Dr. Viola Nordström and Dr. Jackie Nordström for proofreading my manuscripts.

I would like to thank Prof. Jun Nakanishi for teaching me how to write an excellent article. He generously spend his time to improve my writing skill.

I would like to express my deepest gratitude to my parents Fariba and Mostafa Kaboli, my sister, Maryam Kaboli, and my mother and father in law, Adelheid and Rüdiger Herzer. I could not have completed this dissertation without your support. Words are not enough to express all my gratitude to you.

My most heartfelt and genuine appreciation is for my lovely wife, Dr. Silke Herzer for all her love and valuable support along my study. I would not have made it without her; of this, I am honestly sure.

Several of the topics presented in this thesis is presented in published papers. The reproductions of the materials (text, formulas, figures, and tables) in this dissertation were performed with permission from respective journals, wherever applicable, and the corresponding papers, manuscripts or drafts were cited according to the latest status of the peer-review process. Also, I appreciate all the coauthors have worked with me during my doctoral studies, discussions or corrections to the material presented here or in the papers.

Munich, September 2017

Mohsen Kaboli

List of Publications

Parts of the thesis “*New Methods for Active Tactile Object Perception and Learning with Artificial Robotic Skin*” have been published in:

Journals

1. **Mohsen Kaboli**, Di Feng, Kunpeng Yao, Pablo Lanillos, Gordon Cheng
"A Tactile-based Framework for Active Object Learning and Discrimination using Multimodal Robotic Skin" IEEE Robotics and Automation Letters 2(4), pp.2143-2150, 2017
2. **Mohsen Kaboli**, Di Feng, Gordon Cheng
"Active Tactile Transfer Learning for Object Discrimination in an Unstructured Environment using Multimodal Robotic Skin" International Journal of Humanoid Robotics (IJHR), 15(1), 2017
3. **Mohsen Kaboli**, Gordon Cheng
"Robust Tactile Descriptors for Discriminating Objects from Textural Properties via Artificial Robotic Skin" IEEE Transaction on Robotics (TRO), Accepted, 2017
4. **Mohsen Kaboli**, Kunpeng Yao, Di Feng, Gordon Cheng
"Tactile-based Active Object Learning and Discrimination in an Unknown Workspace" Autonomous Robots Journal, under review, 2017
5. Di Feng, **Mohsen Kaboli***, Gordon Cheng
"Active Prior Tactile Knowledge Transfer for Learning Tactual Properties of New Objects" Sensors Journal, under review, 2017 “ * Corresponding author.”
6. **Mohsen Kaboli**, Alex Long, Gordon Cheng
"Humanoids learn touch modalities identification via multi-modal robotic skin and robust tactile descriptors" Advanced Robotics Journal, pub. Taylor & Francis, vol. 29, pp. 1411-1425, 2015

7. Nivasan Yogeswaran, Wenting Dang, William Taube Navaraj, Dhayalan Shakthivel, Saleem Khan, Emre Ozan Polat, Shoubhik Gupta, Hadi Heidari, **Mohsen Kaboli**, Leandro Lorenzelli, Gordon Cheng, Ravinder Dahiya
"New materials and advances in making electronic skin for interactive robots" Advanced Robotics Journal, pub. Taylor & Francis, vol. 29, pp. 1359-1373, 2015

International Conferences

1. Yao Kunpeng, **Mohsen Kaboli***, Gordon Cheng
"Tactile-based Object Center of Mass Exploration and Discrimination"
IEEE International Conference on Humanoids Robot (Humanoids), 2017 “ * Corresponding author.”
2. **Mohsen Kaboli**, Di Feng, Kunpeng Yao, Pablo Lanillos, and Gordon Cheng
"A Tactile-based Framework for Active Object Learning and Discrimination using Multimodal Robotic Skin" IEEE International Conference on Intelligent Robots and Systems (IROS), 2017
3. **Mohsen Kaboli**, Rich Walker, Gordon Cheng
"Re-using prior tactile experience by robotic hands to discriminate in-hand objects via texture properties" IEEE International Conference on Robotics and Automation (ICRA), pp. 2242-2247, 2016
4. **Mohsen Kaboli**, Kunpeng Yao, Gordon Cheng *"Tactile-based manipulation of deformable objects with dynamic center of mass"* IEEE-RAS International Conference on Humanoid Robots (Humanoids), pp. 752-757, 2016
5. **Mohsen Kaboli**, Gordon Cheng
"Dexterous Hands Learn To Re-Use The Past Experience To Discriminate In-Hand Objects From The Surface Textures" 33rd Annual Conference of the Robotics Society of Japan, 2015
6. **Mohsen Kaboli**, T De La Rosa, Rich Walker, Gordon Cheng
"In-hand object recognition via texture properties with robotic hands, artificial skin, and novel tactile descriptors" IEEE-RAS International Conference on Humanoid Robots, pp.1155-1160, 2015

7. **Mohsen Kaboli**, Philipp Mittendorfer, Vincent Hugel, Gordon Cheng

"Humanoids learn object properties from robust tactile feature descriptors via multi-modal artificial skin" IEEE-RAS International Conference on Humanoid Robots, pp.187-192, 2014

International Workshops

1. **Mohsen Kaboli**, Gordon Cheng

"Novel Tactile Descriptors and a Tactile Transfer Learning Technique for Active In-Hand Object Recognition via Texture Properties" IEEE International Conference on Humanoid Robots (Humanoids)-workshop on tactile sensing for manipulation: new progress and challenges, 2016

Contents

Abstract	iii
	ix
List of Publications	xi
Contents	xiv
List of Figures	xx
List of Tables	xxx
List of Algorithms	xxxii
Notations	xxxiii
1. Introduction	1
1.1. Motivation	1
1.2. Challenges	2
1.3. Contributions	3
1.4. Thesis Outline	7
2. Related Work	11
2.1. Tactile Sensing Technology	11
2.2. Tactile Object Properties Perception	12
2.3. Tactile Object Learning	19
2.4. Tactile Transfer Learning	22
2.5. Tactile-based slip detection and object manipulation	24
2.6. Tactile Human-Robot Interaction	27
2.6.1. Touch identification	28

3. Robust Tactile Descriptors	31
3.1. Introduction	31
3.2. Proposed robust tactile descriptors	32
3.2.1. <i>Proposed tactile descriptors for a large skin area</i>	34
3.2.2. <i>Properties of the proposed tactile descriptors</i>	36
3.3. System description	37
3.3.1. <i>Robotic Skin: BioTac®</i>	37
3.3.2. <i>Robotic Skin: Cellular Skin</i>	37
3.3.3. <i>The Shadow Hand</i>	38
3.3.4. <i>NAO Humanoid Robot</i>	38
3.4. Robust feature extraction	39
3.4.1. <i>Tactile descriptors for the Shadow Hand</i>	39
3.4.2. <i>Tactile descriptors for the NAO</i>	42
3.5. Tactile exploration with a robotic hand	43
3.5.1. <i>Material exploration with the Shadow Hand</i>	43
3.5.2. <i>In-hand object exploration with the Shadow Hand</i>	50
3.6. Tactile exploration with a humanoid	52
3.6.1. <i>Material surface exploration with NAO</i>	52
3.6.2. <i>Large object exploration with NAO</i>	56
3.7. Experimental results	58
3.7.1. <i>Experimental evaluation with the Shadow Hand</i>	58
3.7.2. <i>Experimental results with NAO</i>	63
3.7.3. <i>Unsupervised materials and large objects categorization</i>	66
3.8. Summary and discussion	66
4. Active Pre-touch and Touch for Object Learning in an Unknown Workspace	69
4.1. Introduction	69
4.2. Active pre-touch for workspace exploration	70
4.2.1. <i>Problem Definition</i>	70
4.2.2. <i>Robotic system with multimodal robotic skin</i>	71
4.2.3. <i>Methodology</i>	72
4.3. Objects' physical properties perception	74
4.4. Active touch for physical properties learning (AT-PPL)	76
4.4.1. <i>Problem definition</i>	76
4.4.2. <i>Methodology</i>	76

4.5.	Experimental results	78
4.5.1.	<i>Properties of experimental objects</i>	79
4.5.2.	<i>Active learning about objects' physical properties</i>	79
4.6.	Summary	83
5.	Active Touch for IObject Discrimination and Target Object Search	85
5.1.	Introduction	85
5.2.	System description	87
5.2.1.	<i>Robotic gripper</i>	87
5.2.2.	<i>Tactile sensors</i>	87
5.3.	Active touch for unknown workspace exploration	88
5.3.1.	<i>Tactile point cloud construction</i>	89
5.3.2.	<i>Workspace modeling</i>	91
5.3.3.	<i>Next exploratory position selection</i>	91
5.3.4.	<i>One-shot data collection for initializing the GPR</i>	92
5.3.5.	<i>Updating the total uncertainty of TPC</i>	92
5.3.6.	<i>Stop criteria</i>	93
5.3.7.	<i>Object localization and mapping</i>	93
5.4.	Objects' physical properties perception	95
5.4.1.	<i>Stiffness property</i>	95
5.4.2.	<i>Surface texture property</i>	96
5.4.3.	<i>Center of mass property</i>	97
5.4.4.	Object rotation detection for torque condition verification	99
5.4.5.	CoM Exploration	100
5.5.	Active touch for learning physical properties	102
5.5.1.	<i>Problem definition</i>	102
5.5.2.	<i>Methodology</i>	103
5.6.	Active touch for object discrimination	105
5.6.1.	<i>Problem definition</i>	105
5.6.2.	<i>Methodology</i>	106
5.6.3.	<i>Next optimal exploratory action selection</i>	107
5.7.	Active touch for target object search	108
5.7.1.	<i>Baseline: Expected Entropy Reduction (EER)</i>	109
5.8.	Experimental results	111
5.8.1.	<i>Properties of experimental objects</i>	112

5.8.2.	<i>Active Touch for Object Learning in Unknown Workspace</i>	112
5.8.3.	<i>Evaluation of active tactile object learning (AT-LPP)</i>	118
5.8.4.	Evaluation of Active Object Discrimination	122
5.8.5.	Evaluation of active target object search	123
5.9.	Summary and discussion	125
6.	Online Tactile Transfer Learning	129
6.1.	Introduction	129
6.1.1.	<i>Problem definition</i>	131
6.2.	Prior tactile knowledge construction	131
6.3.	Prior tactile knowledge selection	132
6.4.	Online learning methodology	132
6.5.	Tactile transfer learning methodology	133
6.5.1.	<i>Updating and re-weighting the prior textures models</i>	134
6.6.	Tactile perception and data collection	136
6.6.1.	Properties of experimental objects	136
6.6.2.	<i>Data collection with prior objects</i>	136
6.6.3.	<i>Data collection with new objects</i>	136
6.6.4.	<i>Feature extraction methodology</i>	137
6.7.	Experimental evaluation and results	137
6.7.1.	<i>Constructing prior tactile models</i>	137
6.7.2.	<i>Evaluating the performance of Online Transfer Learning</i>	137
6.7.3.	<i>Baseline</i>	138
6.7.4.	<i>Decreasing number of prior objects</i>	138
6.7.5.	<i>Negative knowledge transfer</i>	139
6.8.	Summary	141
7.	Active Tactile Transfer Learning	143
7.1.	Introduction	143
7.2.	Active pr-touch for workspace exploration	144
7.3.	Active tactile transfer learning (ATTL)	145
7.3.1.	<i>Problem definition</i>	145
7.3.2.	<i>Methodology</i>	146
7.4.	Experimental evaluation and results	151
7.4.1.	<i>Experimental Objects</i>	151
7.4.2.	<i>Experimental setting</i>	152

7.4.3.	<i>Workspace exploration</i>	152
7.4.4.	Evaluation of Active Tactile Transfer Learning (ATTL)	153
7.4.5.	<i>Test data collection for new objects</i>	153
7.4.6.	<i>Baselines</i>	153
7.4.7.	<i>Evaluation of ATTL for negative tactile knowledge transfer</i>	157
7.5.	Summary and discussion	160
8.	Manipulation of Deformable Objects	163
8.1.	Introduction	163
8.2.	Methodology	164
8.2.1.	<i>Problem definition</i>	164
8.2.2.	<i>Deformation prevention</i>	165
8.2.3.	<i>Slip correction and force regulation</i>	167
8.2.4.	<i>Manipulation of Deformable Heavy Object</i>	169
8.3.	System description	171
8.3.1.	<i>Robotic systems</i>	171
8.3.2.	<i>Tactile sensors</i>	172
8.3.3.	<i>Experimental Objects</i>	172
8.4.	Experimental results	173
8.4.1.	<i>Gripper's built-in adaptive grasping mechanism</i>	173
8.4.2.	<i>Minimum grasping force</i>	174
8.4.3.	<i>Evaluation of the proposed grasping strategy</i>	174
8.4.4.	Comparison of Three Different Grasping Approaches	176
8.4.5.	<i>Evaluation of the proposed strategy for manipulation of deformable heavy objects</i>	178
8.5.	Summary	179
9.	Touch Modality Identification on Humanoids with Sensitive Body	181
9.1.	Introduction	181
9.2.	Touch perception methodology	182
9.2.1.	<i>Touch perception via multi-modal robotic skin</i>	182
9.2.2.	Data collection	183
9.2.3.	<i>Single touch action</i>	183
9.2.4.	Multiple simultaneous touch actions	185
9.3.	Representative of touch signals	187
9.3.1.	<i>Dynamic Cell Selection</i>	187

9.3.2. <i>Pre-Processing</i>	188
9.4. Adapted existing touch classification approaches	188
9.4.1. <i>Adapted Naya [1]</i>	189
9.4.2. <i>Adapted Silvera-Tawil [2]</i>	189
9.4.3. <i>Adapted Koo [3]</i>	190
9.5. Experimental evaluation and results	191
9.5.1. <i>Touch modality identification results</i>	191
9.5.2. <i>Touch clustering results</i>	193
9.5.3. <i>Comparison with existing approaches</i>	193
9.6. Summary and discussion	195
10. Conclusion and future study	197
10.1. Conclusion	197
10.2. Future study	202
A. Uniform Pre-touch Strategy for Workspace Exploration	203
A.1. Workspace Definition	203
A.2. Methodology	204
B. Gaussian Process	205
C. Normalized Mutual Information method (NMI)	207
Bibliography	209

List of Figures

1.1.	The Illustration of thesis organization.	8
2.1.	(A) The graphene-based flexible capacitive tactile sensors mounted on the intermediate and proximal phalanges of an i-Limb [4]. (B) The Robotiq adaptive gripper with 132 capacitive taxels 3 three-axis accelerometers mounted on the back of each distal phalanx [5]. (C) The Gifu Hand III [6].	12
2.2.	(A) A lightweight, conformable and scalable large area robotic skin [7]. (B) RI-Man is a humanoid robots capable interacting through whole-body contact [8]. (C) The iCub humanoid robot is equipped with large number of capacitive tactile sensors [9].	13
2.3.	(A) Surface texture classification using a biologically inspired artificial finger composed of silicon with two PDVF pressure sensors and two strain gauges embedded within it [10]. (B) Object classification using one finger of the Shadow Hand and the BioTac via Bayesian exploration approach [11]. (C) The BioTac sensor was mounted on a linear stage to classify 117 different textures [12].	14
2.4.	(A) Classification of uniform surface textures with a humanoid with a three-axis accelerometer mounted on an artificial fingernail [13]. (B) Classification of objects with the PR2 robot with two BioTac sensors on its gripper [14]. (C) Online object identification during grasping using only pressure/normal force data [15].	16
2.5.	(A) Active discrimination among different cups using combined Gaussian process latent variable and nonlinear dimensionality reduction method [16]. (B) Determination of the viscosity of different liquids from tactile feedback using an active sequential framework based on Gaussian approximation and Monte Carlo sampling method [17]. (C) Object shape estimation using the Gaussian process classifiers (GPCs) as observation models of both of the object surface and the background [18].	19

2.6.	(A) Grasping deformable objects by measuring the reduction of normal force as well as detecting micro-vibration on the BioTac sensors [19]. (B) Precision grasps, consisting of a slip signal detector and a grasping force set points generator [20]. (C) Utilizing a slip classification result in the feedback loop of an object stabilization controller [21].	25
3.1.	(A) The Shadow Hand with five BioTac on fingertips. (B) The BioTac [®] multimodal tactile sensor. (C) The BioTac [®] sensors with its 19 impedance electrodes and one pressure sensor (The figure is adapted from [22]).	38
3.2.	(A) NAO is equipped with 116 multi-modal artificial skin (Cellular skin) including: 32 skin cells on the chest and 14, 12, and 16 skin cells on each hand, fore arm, and upper arm respectively. (B) and (C) show the front and back of the Cellular skin. (D) shows the skin cells and NAO in rviz. I integrated skin cells with NAO via ROS.	39
3.3.	The selected experimental materials consist of 120 different natural and synthetic textures with uniform (regular) and non-uniform (irregular) structures including: Papers and vinyl wallpapers (Tex.#1-Tex.#37), Textiles (Tex.#38-Tex.#57), Carpets and mats (Tex.#58-Tex.#78), Foams and sponges (Tex.#79-Tex.#82), Fibers (Tex.#83, Tex.#84), PVC and rubber type surfaces (Tex.#85-Tex.#95), Leathers and furs (Tex.#96-Tex.#100), Wooden surfaces (Tex.#101-Tex.#109), metal surfaces (Tex.#110-Tex.#113), Fibreglass and glass surfaces (Tex.#114-Tex.#118), and Carbon sheets (Tex.#119, Tex.#120). All materials acquired from Bauhaus (www.bauhaus.info).	44
3.4.	The Shadow Hand is exploring the textural properties of materials. (A) shows the execution of the lateral and medial exploratory movements. In (B), the Shadow hand performs human-like circular exploratory motion. In (C) an experimental material rotates underneath of the fingertips of the Shadow hand with a constant velocity. (D) and (E) demonstrate the BiTac sensors with its 19 impedance electrodes and one pressure sensor (The figures are adapted from [22]).	45
3.5.	Kinematics Diagram of the Shadow Hand.	46
3.6.	In-hand uniform shaped objects.	49
3.7.	In-hand complex shape objects.	50

3.8.	(A) NAO executes lateral, medial, or circular exploratory movements to sense the textural properties of the object (active exploration). (B) The experimental material/texture rotates underneath of NAO’s hand with a constant velocity (passive exploration). (C) The large object was held by NAO with its upper body slides gradually between its hands, arms, and chest (passive exploration). (D) The kinematics of NAO’s arm which is adapted from <i>www.doc.aldebaran.com</i> .	53
3.9.	Results of On-line Material Classification by the Shadow Hand	61
3.10.	Results of On-line In-Hand Objects Classification by Shadow Hand	62
3.11.	Results of On-line Material Texture Classification by NAO	64
3.12.	Results of On-line Large objects Classification by NAO	65
4.1.	Experimental setup. The UR10 robotic arm mounted with the multi-modal artificial skin on its end-effector.	70
4.2.	Proposed Active Pre-Touch Algorithm for Workspace Exploration.	71
4.3.	An illustration of active pre-touch process.	72
4.4.	Exploratory actions: pressing, sliding, and static contact	74
4.5.	Proposed Active Touch for Learning about Objects via their Physical Properties (AT-PPL).	77
4.6.	Experimental objects. The physical properties are evaluated subjectively by human subjects and are indicated in the panel to the upper right of each object (S: stiffness, T: roughness of surface textures, C: thermal conductivity. ++: very high; +: high; O: middle; -:low; –: very low).	79
4.7.	Statistical evaluation of the active pre-touch method with random and uniform strategies. The horizontal axis shows the number of movements the robot has when exploring the workspace. The vertical axis shows the Shannon entropy in the workspace.	80
4.8.	(A)The unknown workspace which the robot explored. (B)-(D): Trajectories of the robot’s end-effector during the exploration of the workspace and the localization results using three methods. (B): Active pre-touch strategy. (C): Uniform strategy. (D): Random strategy. (E): Statistical evaluation of the active pre-touch method with random and uniform strategies. The horizontal axis shows the number of movements the robot has when exploring the workspace. The vertical axis shows the Shannon entropy in the workspace.	81

4.9.	(A): Evaluation of AT-PPL with three physical properties (stiffness, surface textures, and thermal conductivity). (B)-(D): Evaluation of AT-PPL by learning about the experimental objects via one physical property (B):Surface textures.(C): Stiffness. (D): Thermal conductivity. The horizontal axis represents the learning steps (at each step a new training sample is collected), and the vertical axis represents the value of recognition accuracy on the test dataset averaged over 30 runs.	82
5.1.	The experimental setup. A Robotiq three-finger adaptive robot gripper is equipped with OptoForce sensors and mounted on a UR10 robotic arm	86
5.2.	My proposed probabilistic active touch method for workspace exploration. . .	88
5.3.	The illustration of the active exploration process of an unknown workspace \mathbb{W}_{d_4} (workspace in $d_4 = Y_+$ direction). The uncertainties (variance) at different positions are revealed by the color. Red color represents high uncertainty, while blue color represents low uncertainty.	90
5.4.	(A) Pressing, to measure the stiffness.(B) Sliding, to perceive the textural property. (C) Lifting, to check if the current position is the CoM.	96
5.5.	The analysis of lifting forces (i.e. frictions) at different lifting positions along the length edge of a target object. (A),(C),(E),(G): The robot lifts object at different positions. The real CoM of the object is marked by the red ribbon in each figure. A),(C),(E),(G): The sequence of corresponding lifting force signals from each contact point during lifting process. If the object is lifted almost at its CoM (D), the frictions measured on the contact points on the same side are almost the same (H), owe to the positional symmetry.	98
5.6.	The target object was lifted up at 41 sequential positions along its length edge, and at each lifting position, the measured sequences of frictions from contact points A , B , and C , were recorded during the lifting process. The abscissa scale denotes the lifting positions sequentially distributed along the object, from one tail (1) to the other tail (41). The ordinate scale represents the calculated cross-correlation of signal sequences. (A) The cross-correlation ρ_{BC} is used to determine if the corresponding lifting position can be determined as the real CoM. (B) The relationship of ρ_{AB} and ρ_{AC} is used to guide the selection of the next lifting position.	99
5.7.	my proposed probabilistic active touch algorithm for efficient learning about objects' physical properties (texture, stiffness, center of mass)	102

5.8. My proposed probabilistic active touch for discrimination among objects based on their physical properties.	106
5.9. My proposed probabilistic active touch strategies for searching a target object/s in the workspace that contains unknown objects.	109
5.10. Experimental objects. The physical properties are evaluated subjectively by human subjects and are indicated in the panel to the upper right of each object (S: stiffness, very soft (- -) and very hard (++) T: roughness of surface textures, very smooth (- -) and very rough (++) C: center of mass, far from the centroid (- -), close to the centroid (++)).	112
5.11. The active exploration results of the unknown workspace in the first scenario (see Sec. 5.8.3). (WS-1) The layout of the workspace in the first scenario. From left to right, each one of the three sub-figures aligned in a row illustrates the constructed TPC, clustering result of TPC, and result of object localization. (a) The active exploration results of the unknown workspace by applying my proposed strategy. (b) The active exploration results of the unknown workspace by applying random sampling strategy. (c) The active exploration results of the unknown workspace by applying uniform sampling strategy. . .	114
5.12. The statistical comparison of the performance of the proposed active exploration strategy (GPR), uniform strategy, and random strategy for exploring the unknown workspace. Each small sub-figure on the right side named $S_1 - S_{30}$ corresponds with one experimental scenario and illustrates the change of total variance in one exploratory direction (here I take $X +$ direction as an example) as the number of samples increases, by applying different exploratory strategies. The large sub-figure on the left side shows the averaged total variance over all the 30 scenarios with the shadowed area denoting the standard deviation.	115
5.13. Distributions of the features extracted from the test dataset. (A) The resultant force response for stiffness. (B) CoM. (C) Robust textural descriptors. The observation distributions for object stiffness and CoM are modeled by univariate Gaussian distribution. To visualize the distribution of textures, I first reduce the 12 dimensional texture descriptor to 2D vector via Principle Component Analysis (PCA). Then I model the distributions of features by multivariate Gaussian distribution.	117

5.14. Active learning about objects based on their physical properties. The horizontal axis represents the number of training data collected thus far. The vertical axis shows the mean value of the classification accuracy of evaluation dataset averaged over 30 runs.	119
5.15. An example of learning five objects with three physical properties. Three object and exploratory action selection methods are compared. (a) Proposed active learning method AT-LPP.(b) Uniform sampling method. (c) Random sampling method. The lower bar shows the exploratory actions at each time step ("P" for pressing, "S" for sliding, "L" for lifting). The upper bar shows the object to explore at each step. The vertical axis shows the classification accuracy on the test database.	120
5.16. Active learning each object physical property individually. (A) Learning object's stiffness. (B) Learning object's surface textures. (C) Learning object's CoM. The horizontal axis represents the growing number of training data, and the vertical axis represents the value of classification accuracy on the test data averaged over 30 runs.	121
5.17. The active exploration results of the unknown workspace in the second scenario (see Sec. 5.8.4) by applying my proposed strategy. (WS-2) The layout of the workspace in the second scenario. (a-1) The constructed TPC. (a-2) Clustering result of TPC. (a-3) Object localization result.	122
5.18. Evaluating active object discrimination and target object search. Average decision steps the robot takes to discriminate objects.	123
5.19. The active exploration results of the unknown workspace in the third scenario (see Sec. 5.8.5) by applying my proposed strategy. (WS-3) The layout of the workspace in the third scenario. (a-1) The constructed TPC. (a-2) Clustering result of TPC. (a-3) Object localization result.	124
5.20. Evaluating active object discrimination and target object search. Average decision steps the robot takes to find the target objects.	125
5.21. Evaluating active object discrimination and target object search. Average decision steps leave the non-target objects.	125

6.1.	The Shadow Hand with BioTac robotic skin. Employing the proposed tactile transfer learning method the Shadow Hand could re-use its prior knowledge while discriminating new objects from their texture with a very few trials. The illustrated formula is the regularizer term of the adapted LS-SVM in (6.2). The weight assigned to each prior knowledge λ was found by minimizing Eq.(6.2). K is the number of prior knowledge.	130
6.2.	The figure shows the recognition results on a separate test data for the online tactile transfer learning and PA online learning (No-Transfer) methods. (A)-The robot is re-used the obtained tactile knowledge was constructed with 10 prior objects. (B)-The robot had access to 5 prior knowledge.The recognition results on the new test set were plotted as a function of the number of the training samples.	139
6.3.	This figure shows the confusion matrix for the clustering of 20 objects via texture properties using EM method.	140
6.4.	The figure shows the recognition results corresponding to the hybrid tactile transfer learning and traditional transfer learning (No-Transfer) in which the new surface textures were dissimilar to the prior textures. The recognition results on the new test set were plotted as a function of the number of the training samples	141
7.1.	The scenario of active tactile transfer learning for object discrimination in the unstructured environment. The robotic arm (A) equipped with multimodal artificial skin (B) can actively learn about prior objects (C) in an unstructured environment to build the tactile knowledge of these objects. Then it can leverage this tactile knowledge (D) to actively learn about new objects (E) in another unknown workspace	144
7.2.	The proposed method of the probabilistic tactile-based active tactile transfer learning for object discrimination in unstructured environment.	145
7.3.	Prior objects.The physical properties are evaluated subjectively by human subjects and are indicated in the panel to the upper right of each object (S: stiffness, T: roughness of surface textures, C: thermal conductivity. ++: very high; +: high; -:low; -: very low.)	151
7.4.	New objects.	151
7.5.	(A) The unknown workspace which the robot explored. (B) Trajectories of the robot's end-effector during the exploration of the workspace and the localization results using active pre-touch strategy.	152

7.6.	Evaluation of the active tactile learning performance using ten prior objects. The right small plots show the results from 10 groups of prior objects. Their averaged performance is plotted on the left. The figure illustrates the comparison results between ATTL and ATL (no transfer) as well as uniform (no transfer) methods. The horizontal axis represents the growing number of feature observations, and the vertical axis represents the averaged value of discrimination accuracy on the test data set. The figure illustrates Learning about the new objects based on three physical properties.	154
7.7.	(A) Evaluation of the active tactile learning performance based on only stiffness property. (B) Evaluation of the active tactile learning performance based on only surface texture. (C) Evaluation of the active tactile learning performance based on only thermal conductivity.	154
7.8.	Evaluation of the ATTL performance using different number of prior objects. (A) Learning about the new objects based on three physical properties; (B) based on only stiffness; (C) based on only surface texture; (D) based on only thermal conductivity.	156
7.9.	Learning about new objects with different number of prior objects. The new objects and the prior objects were randomly selected, following the uniform distribution.	157
7.10.	Confusion matrix for stiffness of 28 objects (prior objects (from 1 till 21) + new objects (22 till 28)). The blue index indicates the prior objects, and the red index new objects.	158
7.11.	Confusion matrix for surface texture of 28 objects (prior objects (from 1 till 21) + new objects (22 till 28)). The blue index indicates the prior objects, and the red index new objects.	159
7.12.	Confusion matrix for thermal conductivity of 28 objects (prior objects (from 1 till 21) + new objects (22 till 28)). The blue index indicates the prior objects, and the red index new objects.	159
7.13.	Evaluation of active tactile learning with negative prior knowledge constructed by deliberately selected five prior objects that were unrelated to the new objects. (A) Learning about the new objects based on three physical properties, prior objects: object {2, 3, 6, 10, 13}; (B) based on only stiffness, prior objects: object {1, 2, 3, 10, 18}; (C) based on only surface texture, prior objects: object {6, 7, 9, 10, 21}; (D) based on only thermal conductivity, prior objects: object {4, 6, 8, 10, 13}.	160

8.1. (A)Three-finger adaptive robot gripper from Robotiq is equipped with Opto-Force sensors and mounted on the UR10 robotic arm (B). Experimental objects are shown in (C).	164
8.2. Tangential force and normal force signals exerted by one of the fingers (here finger B) during rotating a deformable bottle filled with 300g water by $\pi/3$. .	165
8.3. Estimation of the friction coefficient	166
8.4. Slip Correction and Force Regulation	167
8.5. Human-like Strategy for Manipulating Deformable Heavy Object	170
8.6. Grasping deformable objects using gripper’s built-in adaptive grasping mechanism.	174
8.7. Manipulation of deformable objects with different characteristics, such as stiffness, surface texture, and center of mass, using minimum grasping force. .	175
8.8. Manipulation of deformable objects with different characteristics, such as stiffness, surface texture, and center of mass, using Algorithm 8.1.	176
8.9. Normal force and tangential force exerted by one of the fingers (here finger A) recorded while manipulating a deformable bottle of 300mL water.	177
8.10. Manipulating a deformable heavy jar by applying Algorithm 8.2. Plots show the recorded normal and tangential forces exerted by (here finger B) during the manipulation process.	177
8.11. Comparison of deformation extents of grasped objects, using gripper’s built-in adaptive grasping mechanism and the proposed slip correction and force regulation framework, respectively.	179
9.1. The upper body of the NAO was covered with 32 skin cells, 16 cells on the front and 16 cells on the back. The skin cells are called Cellular skin.	182
9.2. Illustrations of the nine touch modalities enacting on the NAO’s body.	184
9.3. Illustrations of the multiple touch actions enacting simultaneously on the NAO’s body.	187

10.1. (A) shows the Noby robot (nine-month-old baby robot) which has built at the Intelligent System and Informatics lab (IS), the University of Tokyo directed by Prof. Yasuo Kuniyoshi. I have covered the whole body of Noby with 4000 foldable tactile sensors. (B) shows the NAO with the whole body multimodal skin cells. I have covered the NAO with robotic skin at the Institute for Cognitive System(ICS), Technical university of Munich directed by Prof. Gordon Cheng. (C) Illustrates that the Noby explores the floor with whole body to perceive the textural properties.	201
A.1. An illustration of an unknown workspace exploration.	203

List of Tables

2.1. Summary of the state-of-the-art tactile feature descriptors for discriminating objects/surfaces from their textural properties.	17
2.2. SUMMARY OF EXISTING SLIP DETECTION METHODS	26
2.3. Summary of the existing touch classification approaches	28
3.1. The Cellular skin characteristics.	39
3.2. Surface textures classification by Shadow Hand. The best regularizer value that was found by CV for all experiments is $C = 0.001$	59
3.3. In-Hand objects classification with SVM by Shadow Hand. The best regularizer value that was found by CV for all experiments is $C = 0.003$	62
3.4. Results of Materials and In-hand Objects Categorization by the Shadow Hand.	63
3.5. Surface textures classification by NAO. The best regularizer value that was found by CV for all experiments is $C = 0.005$	64
3.6. Large objects discrimination with SVM by NAO. The best regularizer value that was found by CV for all experiments is $C = 0.003$	65
3.7. Results of Materials Categorization by NAO.	66
5.1. Evaluation of clustering performance based on the normalized mutual information (NMI).	116
9.1. Selected touch modalities.	185
9.2. Multiple touch actions.	186
9.3. Confusion matrix for single touch classification (NAO in stationary position).	194
9.4. Confusion matrix for single touch classification (NAO in motion).	194
9.5. Confusion matrix for single touch classification (Training: NAO in stationary position. Evaluation: NAO in motion).	194
9.6. Confusion matrix for multiple touch action classification (Training: NAO in stationary. Evaluation: NAO in motion).	194

9.7.	Single and multiple touch modality categorization results using EM and the proposed tactile descriptors. Single touch stationary-stationary: EM was trained with unlabelled touch data from the back of the NAO (NAO was in stationary position) and evaluated with the test set obtained from the front of the NAO (NAO was in stationary position). Single touch-moving-moving: EM was trained and tested with touch data collected from back and front of the NAO respectively (in both case NAO was in motion). Single touch-stationary-moving: EM was trained and tested with touch data collected from back (NAO was in stationary position) and front of the NAO respectively (NAO was in motion). Multiple touch-stationary-moving: EM was trained with single touch data collected from the back of the NAO (NAO was in stationary position) and evaluated with multiple touch actions from front of the NAO (NAO was in motion)	195
9.8.	Comparison with the adapted existing touch classification approaches	196

List of Algorithms

5.1. Active unknown workspace exploration	94
5.2. Active touch for object learning	104
5.3. Active touch for object discrimination	107
5.4. Active touch for target object search	110
6.1. Online Tactile Transfer Learning	135
7.1. Active Tactile Transfer Learning	149
8.1. Slip Correction and Grip Force Regulation	168
8.2. Manipulation of Deformable Heavy Object	171
A.1. Uniform strategy for workspace exploration	204

Notations

Abbreviations

3D	3 Dimensional
GP	Gaussian Process
GPR	Gaussian Process Regression
GPC	Gaussian Process Classifier
SVM	Support Vector Machine
LS-SVM	Least Squares Support Vector Machine
PA	Passive Aggressive
EM	Expectation Maximization
NMI	Normalize Mutual Information method
FFT	Fast Fourier Transform
DFT	Discrete Fourier transform
STFFT	Short Time Fast Fourier Transform
DWT	Discrete wavelet transform
TPC	Tactile Point Cloud
BCI	Brain Computer Interface
KNN	K Nearest Neighbors
HMM	Hidden Markov Model
ANN	Artificial neural network
RTD	Robust Tactile Descriptor
CoM	Center of Mass
PVDF	Polyvinylidenfluorid
AT-PLL	Active touch for physical properties learning
OTLL	Online Tactile Transfer Learning
ATTL	Active Tactile Transfer Learning
CMUM	Confusion Matrix-based Uncertainty Minimization
EER	Expected Entropy Reduction
ATOR	active tactile object recognition
LOO	Leave One Out
CV	Cross Validation
ATL	Active Tactile Learning
WCF	World Coordinate Frame
SCF	Sensor Coordinate Frame
OCF	Object Coordinate Frame
MAP	Maximum A Posteriori
WS	Workspace

Symbols

activity	A
mobility	M
complexity	C
linear correlation	L
three dimensional non-linear correlation	N
workspace	W_{XYZ}
Shannon entropy	\mathcal{H}
linear acceleration	<i>a</i>
force	<i>f</i>
variance	σ
four directions of the workspace	\mathbb{W}_{d_4}
pressure	P
impedance electrode	E
distance from i -th skin cell	d_i
upper bound of x axis	\underline{x}
lower bound of x axis	\bar{x}
k number of objects' cluster	\mathbb{O}_k
positive direction of x axis	X_+
negative direction of x axis	X_-
resultant force	<i>f</i> ^{RES}
normal force	<i>f</i> _T
tangential force	<i>f</i> _N
friction coefficient	μ
set of real numbers	\mathbb{R}
set of natural numbers	\mathbb{N}

Operators

time derivative	$\frac{d}{dt}(\cdot)$
euclidean norm	$\ \cdot\ $
absolute value	$ \cdot $
summation sequence	$\sum_{n=1}^N f(n)$
product sequence	$\prod_{n=1}^N f(n)$
squared root	$(\cdot)^{-1/2}$
transposed	$(\cdot)^T$
inverse	$(\cdot)^{-1}$
Hadamard multiplication	$(\cdot) \circ (\cdot)$
logical comparisons	$>, <, ==$
union	\cup

Functions

time continuous function	$f(t)$
time discrete function	$f[n]$
multi-dimensional function	$\mathbf{f}(\cdot)$
exponential	$\exp(\cdot)$ or $e^{(\cdot)}$
maximum	$\max(\cdot)$
minimum	$\min(\cdot)$
sinus	$\sin(\cdot)$
cosinus	$\cos(\cdot)$
conditional probability	$p(a b)$
normal distribution function	$\mathcal{N}(\cdot)$
uniform distribution function	$\mathcal{U}(\cdot)$
probability density function	$p(\cdot)$
probability mass function	$P(\cdot)$
minimization in x	$\operatorname{argmin}_x f(x)$
maximization in x	$\operatorname{argmax}_x f(x)$
variance	$\operatorname{Var}(\cdot)$
covariance	$\operatorname{cov}(\cdot)$
logarithm base 2	\log_2

CHAPTER 1

Introduction

The tactual properties of our surroundings do not chatter at us like their colors; they remain mute until we make them speak . . . Eye movements do not create color the way finger movements create touch.

(Katz D. (1925): The World of Touch, trans. L. E. Krueger, 1989. Hillsdale, NJ: Lawrence Erlbaum)

1.1. Motivation

The sense of touch plays an important role in our daily lives from perceiving the environment, grasping and manipulating to identifying, learning about and interacting with objects. Compensating for the lack of touch with other human senses is hardly feasible. What happens if we have lack of tactile sensing? For instance, consider a scenario of touching objects after keeping hands on an ice block for a while. Westling et al. [23] experimented by anesthetizing the skin of the hand from human subjects. In this way, the mechanoreceptors which are specialized nerve endings for responding mechanical stimulations were no longer available to the brain. In this case, the subjects could not grasp the experimental objects as the hand and finger movement become inaccurate and unstable.

We perceive the physical properties of objects (such as stiffness, textures, temperature, shape, and a center of mass) via the sense of touch by executing different exploratory actions. Experimental psychologists have summarized six types of exploratory actions (also known as "Exploratory Procedure": EP) which we perform to explore objects tactile properties [24]: (1) sliding to sense the textural properties of the objects; (2) pressing to perceive the stiffness; (3) static contact to measure the thermal conductivity; (4) enclosure to roughly estimate the

shape of the objects; (5) contour following to precisely determine the shape of the objects; (6) unsupported holding for estimating object weight and we add one more action (7) lifting objects from different location to explore the center of mass of the rigid objects. After applying various exploratory actions on an object, we can attain its different tactile properties.

Moreover, we use efficiently our sense of touch to actively explore our environment and objects across their tactual properties. In this regard, we strategically select exploratory actions to perceive physical properties of the objects. Active tactile exploration is a complicated procedure which requires efficient tactile perception and learning methods.

Furthermore, we intelligently re-use our previously acquired tactile knowledge while learning about new objects. Our prior tactile knowledge, or past tactile experience, helps us to explore unknown objects efficiently. Therefore, we learn about new objects with fewer training samples or even one (one-shot learning) while re-using our previously obtained prior tactile knowledge.

For robotic systems that interact with dynamic environments, it is crucial to recognize objects via their physical properties (such as surface texture, stiffness, center of mass, and thermal conductivity) [25]. However, this is difficult to achieve even with advanced vision techniques, which are often marred by occlusion, poor lighting situations, and a lack of precision. As an alternative, tactile sensing can simultaneously provide rich and direct feedback to the robotic systems from abundant contact points [26]. The cognitive robots having the sense of touch need to learn continuously and efficiently from tactile experience and update their models of the objects and environment. This tactile learning strategy keeps a robot stable and adaptable to respond to new stimuli receiving from the surrounding. In traditional tactile learning approaches updating the constructed observation models with new objects is conceivable only via a thorough re-training of the learning algorithms. Since there are so many objects with common intrinsic tactual properties in the real world, it is possible for autonomous robots to re-use their acquired tactile experience while learning about new objects. In real-world applications collecting many training data is costly and not always possible. In this condition, tactile learning methods fail to construct robust models from a few training samples.

1.2. Challenges

In recent decades, tactile sensing technology has achieved lots of progress. Currently, advanced tactile sensors have been deployed to cover the body of robots to provide them with the sense of touch, the robot hand to improve the dexterous object manipulation, and on wearable devices to facilitate the safe human-robot interaction, etc.

Contrary to the rapid progress of tactile sensor advancement, considerably less attention has been given to research in tactile information processing and modeling. The performance of tactile systems depends not only on the technological aspects of sensory devices, but also on the design of the efficient tactile exploration and perception strategies, tactile feature representation, and active tactile learning methods. Tactile sensing is crucial for a robotic system to recognize its surrounding objects via its physical properties. With the help of tactile information, the robot can feel what it is holding and understand its grasp posture and manipulate the object properly. To increase the autonomy of a robotic system during the tactile-based object recognition, the robot should be able to autonomously explore unknown workspace, actively detect the number of objects as well as estimate their positions in the workspace.

Moreover, the informativeness of training data obtained with each object is different. Some objects have discriminant tactile properties that make them easier to be identified from the others. Therefore, collecting too many training samples with these objects is redundant, whereas, for objects, which are easily confused with each other due to their similar properties, it is necessary to collect sufficient samples to construct reliable and robust observation models. Furthermore, to efficiently discriminate among objects the autonomous robot should strategically select and execute the exploratory actions that provide the robotic system with the maximum informativeness.

Furthermore, collecting training samples are time and memory consuming, and there may not always be sufficient training data available. In addition, executing many exploratory actions on the objects may destroy tactile sensors or robotics skins. In this case, re-using previously obtained tactile knowledge together with a few number of training samples or even one (one-shot learning) can improve the robotic performance of learning about new objects (tactile transfer learning).

1.3. Contributions

In previous work, the performance of the tactile object discrimination via textural properties is dependent on the tactile feature extraction and learning methods designed for particular experimental setup (such as specific tactile sensor technology, well-controlled tools, predefined exploratory movements). All have to be individually configured to perform efficiently. In this thesis, to tackle the problems as mentioned earlier, I propose a set of robust tactile descriptors, to enable robotic systems equipped with an artificial skin to perceive the textural properties of objects while sliding their sensitive skin across the objects' surfaces. Unlike existing tactile feature extraction method, using my proposed tactile descriptors the robots can

extract robust tactile features regardless of the number of tactile sensors (large-scale robotic skin) and their sensing technology. The proposed tactile descriptors are invariant respect to specific exploratory movements and their corresponding parameters (exploration time, velocity and applied force) of exploratory actions and textural properties of the materials and objects (periodic and non-periodic surface texture). Previous researchers have used various robotic systems and tactile sensors to explore objects via their physical properties passively and to discriminate among objects by utilizing uniformly collected training samples in an offline manner. However, the informativeness of the training data gathered from each object is different. Some objects have distinctive tactile properties, which makes them easy to be discriminated. Therefore, collecting too many training samples by applying exploratory actions is redundant; whereas for objects, whose physical properties are similar and thus can be easily confused with other objects' properties, it is necessary to collect sufficient samples to construct reliable and robust observation models. Moreover, the location and orientation of the experimental objects in the workspace were known and fixed. In this thesis, I propose an active pre-touch approach and a touch-based strategies to enable robotic systems to autonomously and efficiently explore the unknown workspace to calculate the number of objects, find their location, and estimate their orientation.

Moreover, using my active tactile learning method the robotic systems can efficiently learn about objects based on their physical properties (surface textures, stiffness, and thermal conductivity) with the least possible number of tactile exploratory actions (sliding, pressing, and static contact) to construct reliable prior observation models of objects.

Besides, I propose a touch-based probabilistic framework consisting of an active workspace exploration, active object discrimination, and active target object search.

Following my touch-based active workspace exploration method, the robotic system autonomously and efficiently explores an unknown workspace to collect tactile data to construct tactile point cloud dataset. The captured tactile point cloud (TPC) are then clustered to determine the number of objects in the workspace and estimate the location and orientation of each object. In this regard, the robot systems strategically select the next position in the workspace to explore, so that the total variance of the workspace can be reduced as soon as possible. Afterwards, the robots efficiently learn about the objects' physical properties, such that with a smaller number of training data, reliable observation models can be constructed using the Gaussian process for stiffness, surface texture, and center of mass.

Taking advantage of the prior constructed observation models and my active object discrimination algorithm, the robotic system efficiently distinguish between objects via their physical properties and search for specified target objects by strategically selecting the optimal ex-

ploratory actions to apply on objects to perceive the corresponding physical property (sliding to sense textural properties, pressing to measure stiffness, lifting to determine center of mass). Furthermore, for the first time, the center of mass of rigid objects is considered as an intrinsic property for object learning and discrimination.

Although my active tactile learning method enables robotic systems to efficiently learn about tasks by strategically collecting training samples, in case of learning new task it needs to be re-trained from scratch. In other words, robots are still unable to exploit their prior tactile knowledge when they learn a new set of unknown objects.

Instead, *transfer learning strategy* aims at leveraging the prior knowledge from the related tasks which the robotic systems have learned previously, in order improve the performance of the current task.

To tackle this issue, for the first time in the tactile domain, I present an online tactile transfer learning (OTTL) algorithm to enable robotic systems to re-use their constructed prior learning models while learning about new objects via their textural properties with a few number of training samples or even one (one-shot learning). However, employing my OTTL, the robot constructs prior knowledge by collecting data uniformly. I improved my OTTL method by proposing a novel probabilistic tactile-based active transfer learning method (ATTL) that enables robotic systems to autonomously selects and exploits their relevant prior tactile knowledge while learning about new objects via their physical properties (surface textures, stiffness, and thermal conductivity) with a few number of tactile exploratory actions (sliding, pressing, and static contact) or training samples.

Tactile sensing enables robotic systems to interact safely with humans and surrounded objects. Tactile sensing feedback provides feasible solutions to slip detection problem, which is crucial to regulate grasping force in dexterous robotic manipulation. In this thesis, I present a novel tactile-based approach for correcting slips and regulating grasping forces in dynamic manipulation tasks consists of a tangential force based slip detection method to correct slip and a deformation prevention method to regulate grasping force.

I also present a novel approach for touch modality identification (such as poking, tickling, pushing, patting, rubbing, stroking, scratching, punching, and slapping) during tactile human-robot interaction. By taking advantage of my proposed approach humanoid robots with the sensitive body can distinguish between different touch modalities that are enacted on their body skin. The contribution of this thesis has seven folds:

1. I propose a set of robust tactile descriptors to enable robotic systems equipped with an artificial skin to perceive the textural properties of objects while sliding their sensitive skin across the objects' surfaces. Using the proposed tactile descriptors, the robots can extract robust tactile features regardless of the number of tactile sensors (large-scale robotic skin) and their sensing technology. The proposed tactile descriptors are invariant respect to specific exploratory movements and their corresponding parameters (exploration time, velocity and applied force) of exploratory actions and textural properties of the materials and objects (periodic and non-periodic surface texture).
2. I propose a probabilistic pre-touch and touch-based framework to enable robotic systems to autonomously explore unknown workspace, actively learn about objects' properties utilizing of their physical properties. The proposed framework consists of two components; (I) an active pre-touch approach to enable the robotic systems to autonomously and efficiently explore the unknown workspace in order to calculate the number of objects, find their location, and estimate their orientation; (II) an active touch method to learn the physical properties of objects (surface textures, stiffness, and thermal conductivity) with the least possible number of training samples in order to construct reliable objects' observation models.
3. I propose a probabilistic touch-based active workspace exploration and active touch object recognition framework. The proposed touch-based framework has four parts; (I) an active touch-based strategy to enable robotic systems to autonomously explore unknown workspaces in order to collect tactile data of the object, which are then clustered to determine the number of objects in the workspace and estimate their poses; (II) an active object discrimination strategy to efficiently distinguish between objects by strategically selecting the optimal exploratory actions to apply on objects to perceive the corresponding physical property (sliding to sense textural properties, pressing to measure stiffness, lifting to determine center of mass); (III) an active touch-based method to search for target objects in a workspace that contains both known and unknown objects, by strategically selecting a sequence of exploratory movements to apply on the objects.
4. I propose an online tactile transfer learning algorithm. Taking advantage of my proposed tactile transfer learning strategy, the robotic system exploits the former constructed model of objects' physical property while discriminating among new objects with a few training samples or even one.

5. I propose a novel active tactile transfer learning method to enable the robotic systems to re-use their prior tactile experience while discriminating among new objects in the unknown environment with a few number of training samples or even one. Taking advantage of the attained prior tactile knowledge, the autonomous robot that used my proposed method could efficiently discriminate among new objects with higher discrimination accuracy compared to my previously proposed active touch learning methods in which the robot was not able to exploits its prior tactile knowledge. Furthermore, the experimental results show that my proposed algorithm is robust against transferring negative tactile knowledge.
6. I propose a novel tactile-based framework for correcting slips and regulating grasping forces in dynamic manipulation tasks. My framework has three components; (I) a tangential-force based slip detection method to correct slip; (II) a deformation prevention approach to regulate grasping force, which adjusts the relative positions of fingers in real time, and is realized by estimating the weight of the grasped object; (III) a new strategy for manipulating deformable heavy objects by changing their poses.
7. I propose a novel approach for touch modality identification via tactile sensing on humanoid robots. Using my proposed approach humanoids with the sensitive body can identify touch actions are enacted simultaneously with another action on a different body part. Moreover, the humanoids accurately can discrimination among different touch modalities regardless of the location or orientation of the interaction.

1.4. Thesis Outline

The remaining parts of this thesis are divided into seven chapters:

Chapter 2 gives a concise overview of the related works on artificial robotic skin technology, tactile object physical properties, tactile object learning, tactile transfer learning, tactile-based slip detection and grip force regulation, human-humanoid interaction and touch identification, and whole body tactile exploration.

Chapter 3 introduces my proposed novel and robust tactile descriptors for the robotic systems with the sense of touch to discriminate among objects/ materials via their textural properties.

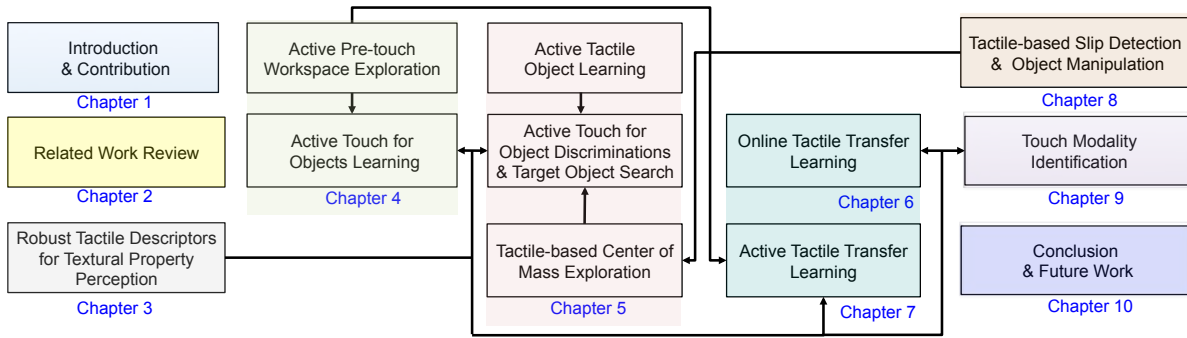


FIGURE 1.1. The Illustration of thesis organization.

Chapter 4 introduces a probabilistic pre-touch and touch-based framework to enable robotic systems to autonomously explore unknown workspace and effectively learn about objects' physical properties. Using my proposed active pre-touch approach robotic systems can autonomously and efficiently explore the unknown workspace. By taking advantage of my proposed active touch method and robust tactile descriptors autonomous robot efficiently learn about the physical properties of objects with the least possible number of training samples.

Chapter 5 explains my proposed touch-based strategies for active workspace exploration and active object discrimination as well as target object search. Following my proposed touch-based workspace exploration, the robotic system autonomously and efficiently explores an unknown workspace to construct tactile point cloud dataset, which are then clustered to determine the number of objects and estimate the location in the workspace. By taking advantage of the proposed active object discrimination strategy, autonomous robots can efficiently distinguish between objects via their physical properties and strategically search for specified target objects in the workspace. Furthermore, this chapter describes my proposed tactile-based algorithm to estimate the center of mass of rigid objects.

Chapter 6 introduces my proposed online tactile transfer learning algorithm. Taking advantage of my proposed method the robotic system exploits their prior constructed object's learning models to discriminating among a new set of objects with a few training samples or even one.

Chapter 7 presents my proposed probabilistic active transfer learning method that enables robotic system to re-use their past tactile experience or prior tactile knowledge while learning about new objects via their physical properties. Using the proposed tactile transfer learning method autonomous robot can automatically select and exploit its prior tactile knowledge while learning new objects with a few number of training samples or even one (one-shot-learning).

Chapter 8 describes my novel method for tactile-based deformable objects with dynamic center of mass. This method includes a novel tactile-based slip detection and grip force regulation as well as a novel strategy for manipulating deformable heavy objects.

Chapter 9 introduces a novel approach for touch modality identification (such as Poking, Tickling, pushing, patting, rubbing, stroking, scratching, punching, and slapping) during tactile human-robot interaction. Using the proposed approach humanoid robots with the sense of touch can distinguish between different touch modalities that are enacted on their body skin.

Chapter 10 briefly summarizes the thesis and discusses about the potential future works.

Appendix A describes the workspace exploration with uniform strategy. **Appendix B** briefly introduces the Gaussian Process (GP) method. **Appendix C** presents the Normalized Mutual Information (NMI) method .

CHAPTER 2

Related Work

Many hands make light work.

(John Heywood)

In this chapter, I would like to give a concise overview of the recent works in developing tactile sensors and their application in the robotic tasks. First, I briefly review the existing tactile sensing technologies. Then, I discuss in detail about the application of the tactile sensing in robotics, from tactile object properties perception and tactile signal and information processing to tactile object learning via objects' physical properties as well as tactile transfer learning. Furthermore, I review the existing strategies and methods in tactile object manipulation and slip detection and grip force regulation. Finally, I present the state-of-the-art methods in tactile human-robot interaction and multiple touch identification.

2.1. Tactile Sensing Technology

Tactile sensing in robotics has a crucial role in the development of cognitive and intelligent robotic systems, since it enables intelligent systems to be capable autonomously explore their surroundings and interact with them [26]. Developing tactile sensing in robotic systems has been investigated for several years. Over the last decade, tactile sensing devices have evolved from being located on a fingertip [4] (Fig. 2.1-A) to full hand [5, 6] (Fig. 2.1-B,C) and even whole body of a humanoid robot [8] (Fig. 2.2). However, developing a robust tactile sensing and efficient tactile perception and learning strategies are still challenging tasks in field of robotics. In this regard, many tactile sensors with various sensing principles and technologies have been developed, e.g., resistive [27, 28], capacitive [29–31], optical [7, 32], piezoelectric [33, 34], acoustic [35, 36] and recently organic bendable [37, 38] and stretchable [39–41], etc.

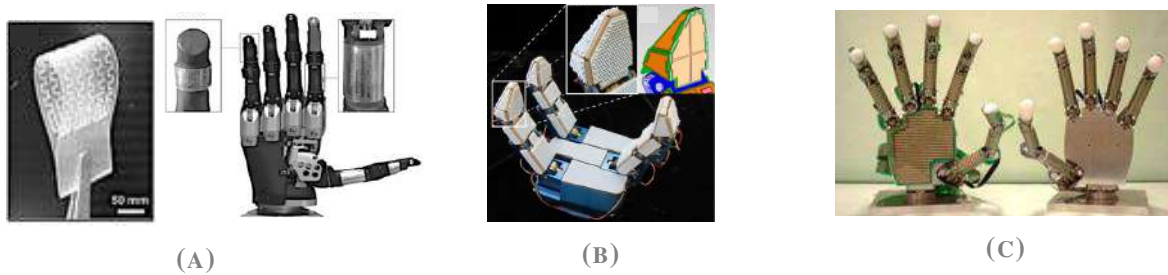


FIGURE 2.1. (A) The graphene-based flexible capacitive tactile sensors mounted on the intermediate and proximal phalanges of an i-Limb [4]. (B) The Robotiq adaptive gripper with 132 capacitive taxels 3 three-axis accelerometers mounted on the back of each distal phalanx [5]. (C) The Gifu Hand III [6].

2.2. Tactile Object Properties Perception

The haptically-accessible object characteristics can be divided into three general classes: (I) geometric information; (II) material properties; and (III) center of mass and weight. The geometric properties can be recognized by object shape via either proprioceptive receptors [42–45] or cutaneous receptors by exhaustively touching a single object in a grid via active exploration approach [18, 46–48]. For example, Jamali et al. [18] trained the Gaussian process classifiers (GPCs) as observation models of both of the object surface and the background in order to estimate the shape of the object (see Fig. 2.5-C). A similar work has been done in [49]. Dragiev et al. [50] obtained the estimation of the implicit shape of the target object as the posterior mean of the Gaussian process model that they constructed based on contact information collected during exploration. The stiffness of objects can be measured by pressing on the object with fingertips [51]. The thermal conductivity of materials can be perceived by lightly contacting the finger on the objects (static contact). For instance, Bhattacharjee et al. measured the thermal conductivity of the objects by making static contact with the finger with the objects' surfaces [52]. In order to find the center of mass (CoM), which is an intrinsic physical property of the rigid object, several interactions with the object are required. For example, humans usually search for the center of mass of a rigid object by lifting it at different positions to feel the difference in the applied lifting force.

Center of mass is an important inherent physical property of the objects. It reveals the distribution of the object's mass. In particular, the CoM position is constant with respect to rigid objects. However, CoM has never been used in robotic to discriminate among objects due to the complexity and difficulty in its determination. Vision-based approaches may fail to solve this problem, since it is difficult to infer the CoM position from the outside. In contrast, tactile signals can be utilized to sense the CoM of the object. Consider several rigid objects with the same shape, stiffness, thermal conductivity, and textural properties but different centers of

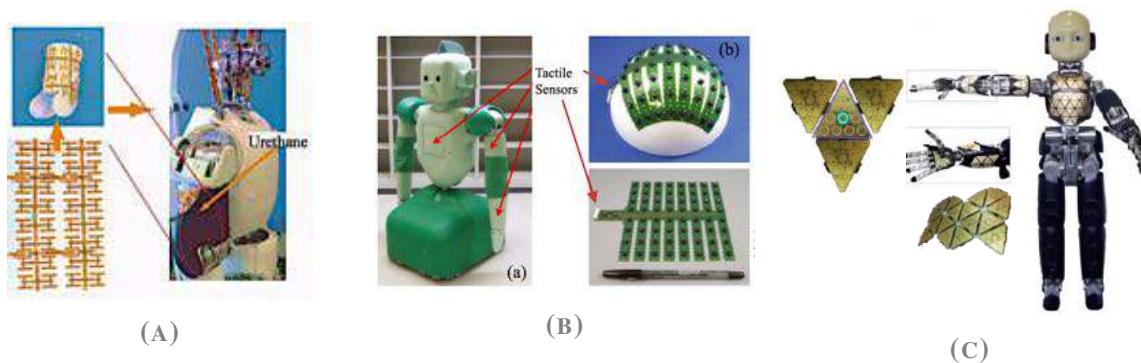


FIGURE 2.2. (A) A lightweight, conformable and scalable large area robotic skin [7]. (B) RI-Man is a humanoid robots capable interacting through whole-body contact [8]. (C) The iCub humanoid robot is equipped with large number of capacitive tactile sensors [9].

mass. I can distinguish between objects via their centers of mass. Although there are several approaches for estimating CoM, to the best of my knowledge there is no work related to object classification via an object's center of mass.

Atkeson *et al.* [53] used a force/torque sensor to estimate the CoM of a rigid load by solving dynamic equations of the robotic system during a manipulation task. This approach has high computational complexity and requires an accurate model of the robotic system. Yu *et al.* [54–56] estimated the center of mass of a target object by determining at least three planes or lines that pass through the center of mass of the object. The robot tips the object repeatedly, and the function of the plane or line can be estimated using the fingertip position and force signals.

However, these approaches require accurate estimations of the force vectors. In addition, the target object is assumed to maintain its stability as it is being toppled, which is often not the case. In this thesis, I propose a purely tactile-based approach to explore the center of mass of the target object, and formulate the center of mass information as an intrinsic feature of the object. The object material can be also characterized and identified via its textural properties through cutaneous tactile receptors by moving fingertips (even other sensitive body parts) over the surface of objects or when objects move on a sensitive skin area [51]. Tactile object classification from textural properties is a complicated task in robotics especially when a large number of tactile sensors are involved to sense the textural properties objects. This is also difficult if the velocity and time of the sliding exploratory movements as well as the force applied on the surface of the objects vary during tactile perception. To overcome this complexity, many researchers have mounted only one or a few number of tactile sensors to the robotic systems and exploited well-defined exploratory trajectories with constant time and/or velocity parameters during surface texture exploration in which the applied force needs to be

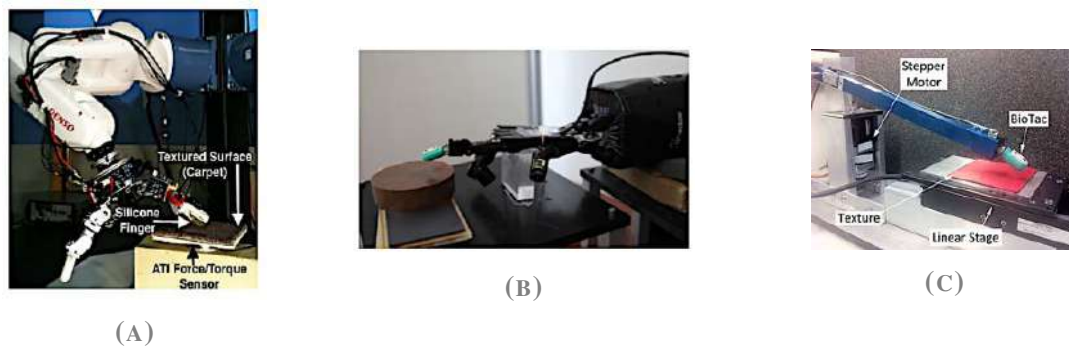


FIGURE 2.3. (A) Surface texture classification using a biologically inspired artificial finger composed of silicon with two PDVF pressure sensors and two strain gauges embedded within it [10]. (B) Object classification using one finger of the Shadow Hand and the BioTac via Bayesian exploration approach [11]. (C) The BioTac sensor was mounted on a linear stage to classify 117 different textures [12].

known as well.

Previously, customized simple tools or robotic end-effectors with various tactile sensors have been used to discriminate between objects via their textural properties. For instance, Dallaire *et al.* [57] managed to classify 28 different surfaces such as aluminum, Plexiglas, kitchen towel, and etc. with 90% accuracy with SVM and Pitman-Yor process algorithms. To do this, a three-axis accelerometer was placed on a stylus, which was then mounted above a well controlled rotating table on which, the surface was placed. Here, in order to generate tactile features, a set of parameters including variance, skewness, kurtosis, fifth moment, sum of the variation over time, and sum of higher half of amplitude spectrum were computed from the recorded data. The same parameters have been used [58] to differentiate ten different indoor and outdoor surfaces from each other. In this study, an accelerometer mounted on a probe was employed to slide over experimental surfaces such as wooden flooring, short hair carpet, and tile linoleum flooring. The authors reported the classification rate of 89.9% and 94.6% with 1s and 4s time windows of data respectively. In other work, in order to classify 7 wooden surfaces Chaturanga *et al.* [59] used a biomimetic fingertip with three commercial accelerometers and seven force sensors, which was then fixed to a horizontal linear stage. In this experiment in order to collect data the artificial fingertip moved forward and backward on the wooden surfaces with a half second pause between each single movement. The applied vertical force and the velocity of movement were kept constant during entire training and testing data collection procedure. In this work, three feature parameters, including wavelet energy, variance of approximate signal, and mean of approximate signal were calculated from the recorded tactile signals. Using an artificial neural network (ANN) the authors classified 7 wooden surfaces with a 65% success rate.

In another work Jamali *et al.* [10] (see Fig. 2.3-A) fabricated a bio-mimetic sensor made of

silicon, which has two PVDF pressure sensors and two strain gauges. The finger was mounted on a robotic gripper and scraped over eight materials to classify the test surfaces. Fourier transform as a feature descriptor and various learning algorithms have been used to find the optimal technique for the texture recognition problem. In this research, the feature descriptor heavily depends on the applied force and sliding duration. Moreover, it can only identify materials with periodic textural structure. In [12] (see Fig. 2.3-C) the BioTac sensor, a biomimetic tactile sensor that measures temperature, pressure, and fingertip deformations, was mounted on a linear stage to classify 117 different textures. Features like roughness, fineness, and traction were identified from the literature on human perception, and then modeled analytically. Although the authors reported a 95.4% classification rate, the proposed features are highly sensitive to the small variation in sliding time and velocity. In addition, the applied force needed to be kept constant during training and testing data collection. Other roboticists, Sinapov *et al.*, employed a humanoid with a three-axis accelerometer mounted on an artificial fingernail to classify 20 different uniform textures (see Fig. 2.4-A). In this instance, the robot scratched on the experimental surfaces with a controlled applied force, fixed velocities, and well-defined scratching movements. Faster scratches usually turned out to have a higher recognition accuracy. Additionally, combining the result of multiple scratches was more accurate than only performing a single scratch [13]. Here, discretized spectrogram as a feature descriptors were used for surface classification task [13]. Recently, Xu *et al.* in [11] used the Shadow Hand with the BioTac sensor on its index finger (see Fig. 2.3-C) to execute exploratory movements over the objects' surface; *pressure* to obtain flexibility information, *sliding* to obtain vibro-tactile information, and *contact* to measure heat flow. In my study, in order to differentiate objects from each other via textural properties, the authors considered only the data that was recorded during the middle of the sliding movements, and the contribution of the generated vibro-tactile signal at the start of the sliding as well as at the end of the movements were eliminated. In order to implement an expert system able to learn object identification information online from a multivariate data stream [15], the authors obtained data while grasping an object with an iCub's hand (see Fig. 2.4-C). The mean, standard deviation, skewness, max value and min value are calculated across the 12 sensors on each finger of the iCub for each time step. These features are accumulated into signature blocks. The encoder values for each DOF are also recorded. For a signature block, one row represents a tactile feature vector, with one column per finger. Thus one vertical slice represents the features for an entire hand, with the x-axis showing change over time. A new learning method abbreviated as STORK-GP is used, which combines sparse online Gaussian processes learning (GP) with a recursive kernel (STORK). However, using the current sensor, objects were classified via their stiffness prop-

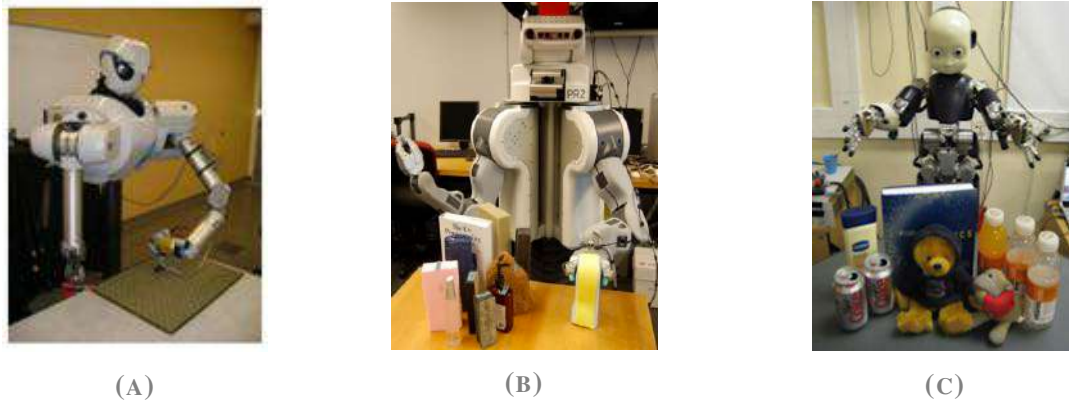


FIGURE 2.4. (A) Classification of uniform surface textures with a humanoid with a three-axis accelerometer mounted on an artificial fingernail [13]. (B) Classification of objects with the PR2 robot with two BioTac sensors on its gripper [14]. (C) Online object identification during grasping using only pressure/normal force data [15].

erty, and the properties such as surface texture were ignored.

Other work was done by Chu *et al.* in which they used the PR2 robot with two BioTac sensors on its gripper to classify 60 objects via their physical properties such as stiffness, temperature, volume, and textures [14, 60] (see Fig. 2.4-B). In this case, the robot applied a series of five predefined well-controlled exploratory motions on each of 60 experimental objects: tap, squeeze, static hold, slow slide, and fast slide. They computed two set of features called static features and dynamic features. To generate static features the authors computed mean and maximum value of low frequency signal measured by the BioTac. Moreover, they converted the recorded high frequency signals into a non-normalized energy spectral density (ESD). To represent the ESD via single valued feature, they calculated the total energy of ESD curve, plus the spectral centroid, variance, skewness, and kurtosis. To obtain the dynamic features they used Hidden Markov Models to capture the variations in the recorded tactile data followed with three pre-processing steps. The static and dynamic features had 188 and 16 elements respectively. Although the proposed methods showed promising results in object recognition through multiple object adjectives, identifying objects among textures properties still was unsolved.

In order to tackle surface texture classification problems in [61] a force sensor, an accelerometer, and a position-orientation sensor were used to develop a haptic tool which was then utilized by a robotic hand to identify surface textures. The exploratory action was a sliding of the tool over the surface with constant velocity and normal force. Another related work conducted by Watanabe *et al.* in which the authors tried to differentiate various kinds of papers from each other by pushing and sliding of a tactile sensor on the papers [62]. To do this, the authors fabricated a tactile sensor consisting of micro-cantilevers with a strain gauge film on Si. The sensor

TABLE 2.1. Summary of the state-of-the-art tactile feature descriptors for discriminating objects/surfaces from their textural properties.

Study	Tactile Sensor	Feature descriptors	Learning methodology	Exploratory action
Dallaire et al. [57]	Three-axis accelerometer (MEMS)	(1) Variance (2) Skewness (3) Kurtosis (4) fifth moment (5) Sum of the variation over time (6) Sum of higher half of amplitude spectrum	SVM, Pitman Yor	A turntable rotating underneath of a prob with steel stylus an attached accelerometer
Chathuranga et al. [59]	Three-axis accelerometer (MEMS) Force sensor	(1) Wavelet Energy (2) Variance of approximate signal (3) Mean of approximate signal	ANN	Sliding with a bio-mimetic soft fingertip
Jamali et al. [10]	PVDF gauge	Strain (1) FFT (5 Relevant Spectral Peaks)	SVM, Naive Bayes, Decision Tree, Naive Bayes Tree	Sliding with a bio-inspired artificial finger
Sinapov et al. [13]	Three-axis accelerometer	(1) Spectrotemporal Histogram (STFT)	SVM, KNN	Lateral and medial scratching with an artificial nail
Xu et al. [11]	BioTac	(1) log(variance) (2) Temperature (3) Joint angle	Bayesian Exploration	Lateral sliding with the index finger of the Shadow Hand (2 DOF)
Chu et al. [60]	BioTac	(1) Area under the ESD curve (2) Weighted averaged over ESD (3) Spectral centroid (4) Spectral variance (5) Statistical variance of ESD (6) Spectral skewness (7) Spectral kurtosis (8) PCA and fifth order polynomial coefficient	Gradient Boosting	Lateral sliding with PR2 gripper

was then fixed on a X-Y stage and a six-axis force sensor on a jig was mounted under the Z-stage. A set of actions like pushing and sliding with constant velocity and force were applied to explore the properties of various papers. In another work, five textiles were explored and classified during an active sliding with constant velocity and through an array of MEMS in the distal phalanx of a robotic finger [63]. In order to classify four objects, Tanaka *et al.* in [64] used the Shadow Hand with three BioTac sensors and an active learning approach in which a latent variable estimation is carried out to learn individual object models. The exploratory motions were selected by the robot while modifying the parameters to dynamic motion primitive. The authors utilized stiffness, temperature, and textural properties to identify 6 objects. However, their proposed method require high computational complexity. In [65] a robotic arm equipped with accelerometers was used to classify 18 metal surfaces. In this scenario, tactile

information was recorded during the sliding motion of the robotic arm with a constant velocity. The obtained tactile data was entered into a neurorobotic texture classifier with a recurrent spiking neural network. To match the spiking activity of mechanoreceptor cells, the sensor data was encoded and then modelled. The resulting high-dimensional features were then continuously classified with a neurally implemented SVM. This proposed approach suffers high computational complexity as well.

Fast Fourier transform (FFT) was used in many studies to classify textures. The obtained tactile signals were transformed into the frequency domain to find the principal frequency of each material. Afterwards, the computed fundamental frequencies were used to classify different textures. For instance, Hu *et al.* classified five different fabrics by sliding a finger-shaped sensor over their surfaces [66]. To classify cotton, linen, silk and denim fabrics, Song *et al.* designed a mechanism to generate the relative motion at a certain speed between the PVDF film and surface of the perceived fabric [67]. Another study employed a piezoelectric microphone. The obtained sound waves were segmented by FFT. A supervised learning vector quantization technique was then used to discriminate 18 materials [68]. An artificial finger equipped with a piezoelectric sensor has been used to detect surface textures of different dimensions [69]. Tactile signals generated during the exploratory movement of the finger were converted to the frequency domain via FFT.

Although many roboticists have used FFT to generate tactile features to identify different textures, the main limitations of this method is its ability to classify only materials with periodic or regular textures, and the need for the sliding time and velocity to be constant and known.

The performance of the tactile object discrimination reviewed above is dependent on the tactile feature extraction and learning methods designed for particular experimental setup (such as specific tactile sensor technology, well-controlled tools, predefined exploratory movements with constant applied force, time or/and velocity parameters, pose of objects and materials in a known workspace). All have to be individually configured to perform efficiently.

In contrast to previous work, I propose a set of novel tactile descriptors which are robust regardless of the number of tactile sensors used in robotic systems (large-scale robotic skin), tactile sensor technology, exploratory sliding movements and textural properties of the objects and materials (periodic and non-periodic surface texture).

I evaluated the robustness of my proposed tactile descriptors with two different robotic platforms with different sensing technology to discriminate among large numbers of objects or materials via their textural properties.

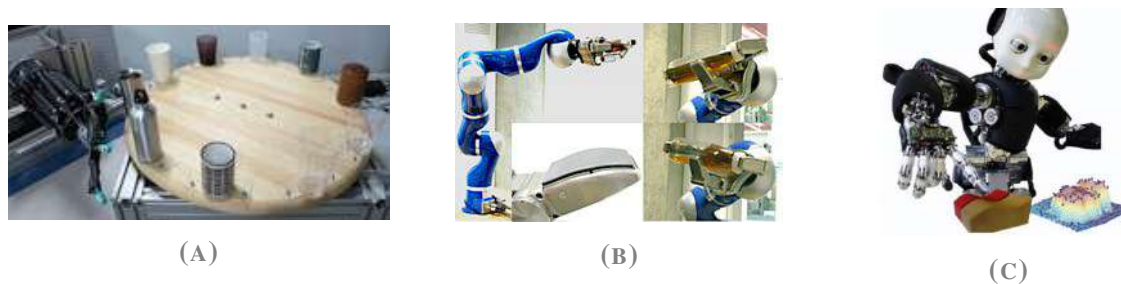


FIGURE 2.5. (A) Active discrimination among different cups using combined Gaussian process latent variable and nonlinear dimensionality reduction method [16]. (B) Determination of the viscosity of different liquids from tactile feedback using an active sequential framework based on Gaussian approximation and Monte Carlo sampling method [17]. (C) Object shape estimation using the Gaussian process classifiers (GPCs) as observation models of both of the object surface and the background [18].

2.3. Tactile Object Learning

We humans use our sense of touch to actively explore our environment and objects through their various physical properties such as surface texture, stiffness, shape, human conductivity, and center of mass. To actively learn about objects through their physical properties and efficiently discriminate among them, humans strategically select tactile exploratory actions to perceive objects' properties (e.g. sliding to sense the textural properties, pressing to estimate the stiffness, and static contact to measure the thermal conductivity). Active tactile exploration is a complex procedure which requires efficient active tactile perception and active tactile learning.

In previous studies mentioned above and also other work [13, 65–70], the roboticists used a predefined number of exploratory movements to sense physical properties of objects having fixed positions and orientation in a known workspace. Therefore, the autonomy of the robot is limited. In this sense, active tactile exploration has shown great potential for enabling the robotic system with more human-like strategies [17]. The autonomous robot should be able to select and execute the exploratory actions that provide the robotic system with the maximum amount of information (see Fig. 2.5-B). In this regard, several approaches were proposed to actively discriminate among objects using their physical properties. For instance in [71], Xu *et al.* used the index finger of the Shadow Hand with the BioTac sensor to collect training data by executing three different exploratory actions five times on each experimental object (pressing for stiffness, sliding for surface texture, and static contact for thermal conductivity). In their study, they placed objects under the index finger, and apply a sequence of exploratory movements to construct observation models. The base and wrist of the dexterous robotic hand were fixed on a table, and all joints in the hand and wrist were deactivated (except two joints of the index finger). These physical constraints therefore resulted in an approach which is un-

scalable for robotic tactile exploration. In [72], a biomimetic fingertip was controlled to slide along ten different surfaces to perceive their textural properties. In this work, the measurement of surfaces' positions were noisy. In order to actively discriminate among the surfaces under position uncertainty, the authors constructed the observation models as well as the position of the surfaces offline by uniformly sampling the collected training data of each surface texture and each possible surface position under a range of contact depths. In another study [73], the Weiss Robotics sensor was mounted on the end-effector of a robot arm to classify 21 objects. They created a database of tactile observations offline by grasping each object with a pre-designed trajectory. The authors managed to actively recognize objects task using tactile images, which were produced by strategically selecting the height of the robot finger and grasping the objects. In [74], Matrins *et al* aimed at developing a general active haptic exploration and recognition strategy for heterogeneous surfaces. The experiments were conducted to search and follow the discontinuities between regions of surfaces with two different materials. However, the experiments were only carried out in simulation using uniformly collected data offline.

An active sequential framework based on Gaussian approximation and Monte Carlo sampling method have been used to determine the viscosity of different liquids from tactile feedback in [75]. In their study, the entire training trials were collected offline. Tanaka *et al.* in [16] combined Gaussian process latent variable and nonlinear dimensionality reduction method to actively discriminate among four cups (paper cup, steel cup, disposal cup, and ceramic cup) (see Fig. 2.5-A). The authors collected 400 training data uniformly using three fingers with a Shadow hand. In this study, the Shadow hand was fixed and the objects were placed on a turntable. The observation model was constructed with action features using the index finger with 2-DOF to generate inflective and horizontal movements on the objects. The authors could discriminate four cups in real experiments and 10 different cups in simulation. Since the proposed method requires a huge amount of training data, the high dimensional action space makes the optimal action search and model learning intractable.

In the above-mentioned work, the location and orientation of the experimental objects in the workspace were known. Moreover, in order to construct the observation models, the training samples were collected uniformly and offline.

To increase the autonomy of a robotic system for the tactile-based object recognition, the robot should be able to autonomously explore an unknown workspace, actively detect the number of objects, as well as estimate their positions and orientations in the workspace. Furthermore, the informativeness of the training data collected with each object is different. Some objects have distinctive tactile properties, which makes it easy to discriminate them among each other.

Therefore, collecting too many training samples with such objects is redundant; whereas for objects, whose physical properties are similar and thus can be easily confused with other objects' properties, it is necessary to collect sufficient samples to construct reliable and robust observation models. Moreover, in order to efficiently discriminate among objects, the autonomous robot should strategically select and execute the exploratory action that provides the robot with the maximum amount of information.

However, in all proposed methods, the observation models were constructed by the predefined number of training samples for each object which were collected offline during tactile exploration. For instance, [16] collected 100 training samples for each experimental object offline. However, the informativeness of training data from each object is different. For *easy* objects which have tactile properties that are discriminative from the others, collecting too many training samples is redundant, whereas for *difficult* objects which are easily confused with each other, their observation models could be insufficiently trained. Therefore, it is necessary to collect training samples efficiently. Moreover, to increase the autonomy of a robotic system during the tactile exploration, the robot should autonomously explore unknown workspace to actively detect the number of objects as well as their corresponding locations and orientations in the workspace. Afterward, it should learn about the objects via their physical properties in online manner in order to construct the reliable object models with a small number of training samples.

In order to tackle the above mentioned issues I propose an active pre-touch approach and a touch-based algorithms to enable autonomous robots efficiently explore the unknown workspace to calculate the number of objects, find their location, and estimate their orientation.

Moreover, taking advantage of my proposed active tactile learning method the robotic systems can efficiently learn about objects based on their physical properties with the least possible number of tactile exploratory actions. In addition, I propose a touch-based probabilistic methods consisting of an active touch workspace exploration, active object discrimination, and active target object search. Following my proposed touch-based active workspace exploration, robots autonomously explores an unknown workspace to captured tactile point cloud (TPC), which are then clustered to determine the number of objects in the workspace and estimate their poses. Taking advantage of the prior constructed observation models and my active object discrimination algorithm, the robotic system efficiently distinguishes between objects via their physical properties and searches to find specified target objects by strategically selecting the optimal exploratory actions to apply on objects to perceive the corresponding physical property (sliding to sense textural properties, pressing to measure stiffness, lifting to determine center of mass).

2.4. Tactile Transfer Learning

Most of the supervised learning algorithms assume that the training data and the test data share the same feature representations and are drawn from the same distributions. Moreover, the performance of learning algorithms is highly dependent on the quality and the number of training samples [76]. In real world applications, however, collecting training samples is costly and there may not be always sufficient training data available. This problem has hindered the applicability of learning methods in practice. For instance, in order to train a classifier to discriminate among objects via their textural properties, the robot needs to collect sufficient training samples by sliding its tactile sensors on the surface of the objects. On the one hand, executing too many sliding actions on the surface of objects to collect training samples is time and memory consuming. On the other hand, sliding many times on the surface of the objects may defect the tactile sensors or robotic skin.

To tackle above mentioned problem, many methods have been developed aiming at using only a small number of training samples. For instance, the *active learning strategy* usually assumes that data samples a machine learner will learn can be strategically selected in order to avoid collecting redundant and non-informative training data [77]. Although active learning methods enable robotic systems to efficiently learn about tasks by strategically collecting training samples, in case of learning new task these learning method need to be re-trained from scratch. Instead, *transfer learning* aims at leveraging the prior knowledge from the related tasks which the robotic systems have learned previously, in order improve the performance for the current task. The previous tasks may come from different domains and have different data distribution or feature representations with the current task. In general, while designing transfer learning algorithms, several issues need to be addressed; (1) what to transfer as a prior knowledge, (2) from where to transfer (2) how to transfer the prior knowledge, (3) how much prior knowledge should be transferred.

(1) *What to transfer* tackles with the issues of which part of knowledge can be transferred from the source domain to the task domain [78]. The prior knowledge can be represented by the training instances (instance-based transfer), common features across domains (feature-based transfer), the parameters in the models (parameter-based transfer) or the relationships between samples (relational-information-based transfer), to name a few.

(2) *From where to transfer* deals with finding the relevant prior knowledge or sources to new task. If two tasks are irrelevant or dissimilar, brute force transfer hurts the performance producing the so called negative transfer [79]. Therefore, knowledge transfer should be beneficial between appropriately related tasks while preventing negative transfer when the tasks are ir-

relevant.

(3) *How to transfer* asks how to use the obtained prior knowledge while learning new tasks. A large variety of strategies have been proposed to integrate in different ways the source knowledge and new information for instance LS-SVM [80], Gaussian process approach, KNN [81], Markov logic [82], boosting approaches [83, 84], graphical models [85].

(4). *How much to transfer* asks how much of the prior knowledge can be transferred to the target domain. Since the *relatedness* (or *transferability*) between sources and targets are different, more knowledge should be transferred when sources are highly related to the target.

In general, while designing transfer learning algorithms, several issues need to be addressed;

(1) what to transfer as a prior knowledge, (2) from where to transfer (2) how to transfer the prior knowledge, (3) how much prior knowledge should be transferred.

(1) *What to transfer* tackles with the issues of which part of knowledge can be transferred from the source domain to the task domain [78]. The prior knowledge can be represented by the training instances (instance-based transfer), common features across domains (feature-based transfer), the parameters in the models (parameter-based transfer) or the relationships between samples (relational-information-based transfer), to name a few.

(2) *From where to transfer* deals with finding the relevant prior knowledge or sources to new task. If two tasks are irrelevant or dissimilar, brute force transfer hurts the performance producing the so called negative transfer [79]. Therefore, knowledge transfer should be beneficial between appropriately related tasks while preventing negative transfer when the tasks are irrelevant.

(3) *How to transfer* asks how to use the obtained prior knowledge while learning new tasks. A large variety of strategies have been proposed to integrate in different ways the source knowledge and new information for instance LS-SVM [80, 86], Gaussian process approach, KNN [81], Markov logic [82], boosting approaches [83, 84], graphical models [85].

(4). *How much to transfer* asks how much of the prior knowledge can be transferred to the target domain. Since the *relatedness* (or *transferability*) between sources and targets are different, more knowledge should be transferred when sources are highly related to the target.

The transfer learning algorithms and active learning strategies aim at learning a reliable model for the tasks of classification or regression with minimal necessary training samples. It is a direct idea to combine active learning with transfer learning to further reduce training samples or human supervision effort. For example, both Shi *et al.* [87] and Saha *et al.* [88] proposed active transfer learning framework in which the classifier in the source domain was first adapted to the target domain. Then a hybrid oracle was constructed which could either directly label the new unlabelled instance by the adapted source classifier, or use generic active learning

methods to quest the human oracle. In the active class selection scenario, Wu *et al.* [89] proposed a method that can leverage the instances from the other tasks to boost the active learning procedure to construct brain-computer interface (BCI) system. The instances from the previous tasks were selected and help the new BCI system to find optimal hyper-parameters.

In this thesis, I present an online tactile transfer learning (OTTL) algorithm to enable robotic systems to re-use their constructed prior learning models while learning about new objects via their textural properties with a few numbers of training samples or even one (one-shot learning). However, using my OTTL the robot constructs prior knowledge with tactile data that was uniformly collected.

To improve my OTTL algorithm, I propose a probabilistic tactile-based active transfer learning method that enables robotic systems to autonomously selects and exploits their relevant prior tactile knowledge while learning about new objects via their physical properties (surface textures, stiffness, and thermal conductivity) with a few number of tactile exploratory actions (sliding, pressing, and static contact) or training samples.

Although there are many research work proposing various transfer learning strategies in visual categorization [78, 90–96], reinforcement learning [97], data mining [98–100], brain computer interface (BCI) [101], and deep learning [102], to the best of my knowledge there is no representation except my works in tactile learning domain.

2.5. Tactile-based slip detection and object manipulation

Slip signals can be detected in several ways. One common approach is to detect vibration signals on the contact surface. Engeberg *et al.* [103] filtered force signals from strain gauges through several band-pass filters with different frequencies and then transformed using FFT. Teshigawara *et al.* [104] have developed a novel sensor which can detect slip by sensing high-frequency signal components above 1kHz. Schoepfer *et al.* [105] used piezo resistive tactile sensor and a frequency-domain approach for incipient slip detection. Although vibration based methods are useful for detecting slip signals, their effectiveness could be gravely impaired due to the vibration generated by robotic systems, especially in the case of manipulating/rotating objects with dynamic centers of mass. Slip signals can also be detected by estimating friction cone, i.e. by following Coulomb's law of friction. This requires the calculation of friction coefficient μ on the contact surface. In order to maintain a stable grasp, the ratio of exerted tangential force to normal force should be maintained within the friction cone [106]. Kobayashi *et al.* [107] used force/torque sensors to measure pressure distribution to detect slip. Instead

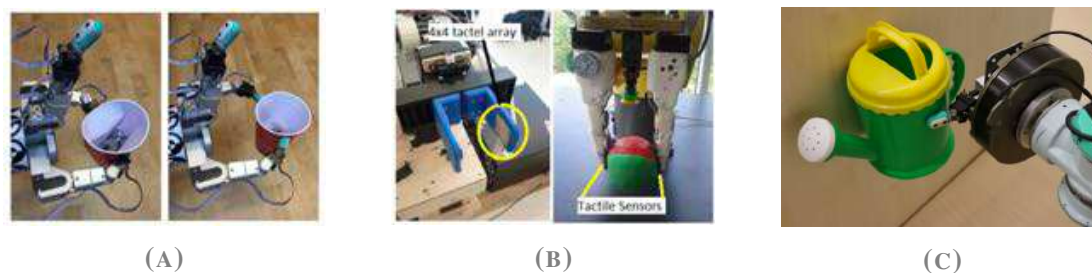


FIGURE 2.6. (A) Grasping deformable objects by measuring the reduction of normal force as well as detecting micro-vibration on the BioTac sensors [19]. (B) Precision grasps, consisting of a slip signal detector and a grasping force set points generator [20]. (C) Utilizing a slip classification result in the feedback loop of an object stabilization controller [21].

of increasing grasping force, they propose to increase the number of applied fingers to stop slip. However, this method is not adaptable for dynamic manipulation of objects, and the relationship of multi-fingers was not considered, which may largely influence the grasping stability. Tada et al. [108] detected macro slip by sensing relative motion using vision sensor firstly, and then they trained a sensor network in order to detect the micro slip using tactile sensors. Some related studies also include approach to distinguish linear slip and rotational slip [109], and approach to discriminate between finger/object and object/world slip events, relying on multidimensional coherence measuring [110]. The performance of slip detection methods, including band pass filter, friction cone, and learned signal are compared in [111]. Since slip signal reflects the stability of grasping on the contact surface, it plays the role of error feedback for the robotic system [26] in manipulation tasks. The robotic system should react promptly to slip signals in order to maintain a stable manipulation.

Su et al. [19] detected slip using two methods, including measuring the reduction of normal force as well as detecting micro-vibration on the sensor skin (see Fig. 2.6-A). A slip-detection based controller was proposed for simple pick-and-place tasks. Taking advantages of the vibrations during slip, which can be detected by PVDF films, Shirafuji et al. [112] trained an artificial neural network (ANN) to output signals for controlling the grasp force. However, training the ANN requires large number of training data, which is also time and memory consuming.

Wettels et al. [118] employed the BioTac multi-modal tactile sensors to detect slips to maintain a stable grasping by controlling the force within the friction cone. De Maria et al. [130] proposed a slip avoidance approach, taking advantage of a tactile exploration phase to estimate the friction coefficient before grasping, using a customized center of pressure (CoP) sensor introduced in [131]. The authors also applied a Kalman filter to track the tangential component in order to regulate the applied grip force. Romano et al. [132] proposed a high-level framework for grasp tasks, based on finger-mounted pressure arrays and a hand-mounted accelerometer,

TABLE 2.2. SUMMARY OF EXISTING SLIP DETECTION METHODS

Study	Slip Detection Method	Control/Learning Method
Shirafuji et al. [112]	Detecting micro-vibrations	Artificial Neural Network (ANN)
Reinecke et al. [111]	Friction Cone/Bandpass Filter/Learning Algorithm	-
Kobayashi, et al. [107]	Detecting micro-vibrations (torque signal)	-
Kanno et al. [113]	Detecting micro-vibrations (torque signal)	-
Engeberg et al. [103]	Detecting micro-vibrations (FFT)	Sliding mode control
Zhang et al. [114]	Measuring center of pressure (CoP)	-
Jamali et al. [115]	Analyzing sensor output	Hidden Markov Model (HMM)
Shirafujiet al. [116]	Detecting micro-vibrations	ANN
Roberts et al. [117]	Optical tracking	-
Teshigawara et al. [104]	Detecting micro-vibrations (DWT)	-
Wettels et al. [118]	Calculating frictional coefficient μ	-
Gunji et al. [119]	Measuring center of pressure (CoP)	PD force control
Engeberg et al. [120]	Analyzing sensor output	Force-Velocity sliding mode control
Engeberg et al. [121]	Detecting micro-vibrations	Adaptive control
Tada et al. [108, 122]	Detecting micro-vibrations	ANN
Cotton et al. [106]	Detecting micro-vibrations (FFT)	-
Birglen et al. [123]	Analyzing sensor output	Fuzzy control
Tsujiuchi, et al. [124]	Measuring center of pressure (CoP)	-
Maeno et al. [125]	Analyzing stick/slip conditions	-
Yamada et al. [126]	Analyzing sensor output	-
Yamada et al. [127]	Analyzing sensor output	-
Maeno et al. [128]	Analyzing stick/slip conditions	-
Veiga et al. [21]	Supervised learning method to create generalizable slip predictors	Random forest
Su et al. [19]	Reduction of normal force and micro-vibration detection	-
Tremblay al. [129]	Open-loop force control	-

which are able to mimic tactile signals provided by human mechanoreceptors. In order to grasp crushable objects, the recent study [20] presents a force regulation approach for precision grasps, consisting of a slip signal detector and a grasping force set points generator (see Fig. 2.6-B). However, in these studies, only one or two fingers of the robotic hands/grippers were employed to stop slip, thus they were incapable of manipulating deformable objects. Table 2.2 summarizes the existing slip detection methods.

In this thesis, I present a novel tactile-based framework for correcting slips and regulating grasping forces in dynamic manipulation tasks. This framework consists of a tangential-force based slip detection method to correct slip and a deformation prevention approach to regulate grasping force, which adjusts the relative positions of fingers in real time, and is realized by estimating the weight of the grasped object. Moreover, I propose a new strategy for manipulating deformable heavy objects by changing their poses. My approaches proposed in this thesis have several advantages over prior work. My proposed framework does not rely on frequency analysis, it is unsusceptible to the vibration signals generated by the robotic system during manipulation, and also robust to external disturbances. In addition, my proposed framework is able to control multiple-fingers of the gripper individually in real time, and is independent of the properties of the grasped object, such as stiffness, surface texture, and center of mass.

2.6. Tactile Human-Robot Interaction

Recent advances in tactile sensing for robotics have opened up new pathways for humanoids to more accurately communicate with humans [133]. Through tactile interaction, various touch modalities may be carried out; a robot may be patted, slapped, punched, or tickled, with each action representative of a separate communicative intent. For any robotic system that is to work closely with humans, evaluation and classification of these touch modalities is vital. Humanoids should understand, just as humans do, that a slap is a form of negative feedback, that a pat is one of encouragement and so on [134]. To achieve this, combination of several layers of technology is required. A significant focus of the field has been on developing and extending tactile sensors utilized to collect and record tactile data. Less focus has been applied on the topic of processing and interpreting this data so as to provide meaningful and helpful information to the humanoid [26]. In this paper, I address the need for robust signal processing methods for tactile data.

As well as facilitating organic human-robot communication [135], the classification and modeling of touch modalities has particular importance in applications such as disabled and aged care, nursing, and caring for patients with mild mental impairment, where a significant amount of communication is non-verbal. In particular, the use of both humanoid and non-humanoid robots have shown to significantly improve outcomes in remedial practice for children with autism [136]. Augmenting such robots with the ability to recognize and respond to social touch would further improve these outcomes.

TABLE 2.3. Summary of the existing touch classification approaches

Study	Touch modalities	Sensing	Features	Learning Method
Naya [1]	Slap, Pat, Scratch, Stroke, Tickle	Ink-sheet force array	<ol style="list-style-type: none"> 1. Max total intensity 2. Max contact area 3. Temporal difference of total intensity at peak 4. Temporal difference of contact area at peak 	K-NN and LDA
Silvera-Tawil [2]	Tap, Pat, Push, Stroke, Scratch, Slap, Pull, Squeeze	EIT force array	<ol style="list-style-type: none"> 1. Max intensity 2. Min intensity 3. Spatial resolution 4. Mean intensity 5. Contact time 6. Rate of change 7. Displacement 8. Location x and y 9. Max potential joint value 10. Min potential joint vale 	Logitboost
Koo [3]	Hit, Beat, Push, Rub	Low-resolution force array and accelerometer	<ol style="list-style-type: none"> 1. Total Force 2. Contact time 3. Contact area change 	Decision tree

2.6.1. Touch identification

Among many sensing methods suitable for touch modality recognition, in humanoid robots, artificial skins could be an appropriate choice. This is due to the high level of bio-mimicry they offer by providing sufficient resolution. While there is no well-accepted definition of what constitutes an artificial skin however, in general an artificial skin is a flexible, interlinked array of individual sensing elements capable of detecting external contact at a medium to high resolution [137]. Traditionally such skins are capable of detecting normal pressure/force, with more advanced skins possessing the capabilities to record sheer force, acceleration, temperature and/or proximity. Kim *et al.* [138] developed such a skin using silicon micro-machining, allowing for the detection of normal and shear forces at high resolution. This skin was shown to be able to effectively measure normal force, hardness, slip, and touch. Such a sensor is ideal for touch classification since movements such as tapping and rubbing can be easily differentiated via the applied shear force. Restricting measurement to only force allows for a higher resolution, however it limits the ability to collect vibro-tactile data. RI-Man [8] is one of the few humanoid robots capable interacting through whole-body contact, and is able to perform complex movements such as lifting a human with its arms. Semiconductor pressure sensors are placed in multiple sections of the robot body, providing tactile feedback on the position and orientation of the human subject. CB2 [139] is another example of full-body interaction,

having a piezoelectric pressure sensitive layer embedded within its silicon covering. Here the goal was to develop a teaching by touching ability, where the robot learns basic movements through tactile interactions. Tajika *et al.* [140] developed a method for characterizing full-body human-robot haptic interaction via hierarchical clustering. Data was recorded from 256 piezoelectric tactile sensors embedded within a child-sized robots skin, and 27 haptic interactions, such as shaking hands and holding up arm, were accurately differentiated using unsupervised learning methods. Interactions were classified based on contact location and the manner of touching, however as only normal force data was collected, sliding movements were not considered, limiting the system. Iwata *et al.* [141] used the structural extension of self-organizing maps (SOMs) technique to classify touch modalities. A fur-based touch sensor used by Flagg *et al.* [142] to recognize three gestures. Gastaldo *et al.* [143] recently could discriminate paintbrush brushing, finger sliding and washer rolling touch modalities from each other using a piezoelectric sensor arrays (PVDF). In [143], the authors offered a new pattern-recognition system, so called tensor-SVM and tensor-RLS in order to differentiate between rolling, sliding, and brushing. To the best of my knowledge there is only a few research that have addressed the problem of touch modality classification. There are three papers, in that they provide replicable, high-accuracy methodologies. In order to evaluate the effectiveness of the method presented in these papers, these methods which are summarised in table are adapted to my data, and evaluated in the paper [1–3]. The table 2.3 shows the summary of the existing touch classification approaches.

In this thesis, I propose a novel approach for touch modality identification via tactile sensing on humanoid robots. Using my proposed approach humanoids with the sensitive body can distinguish between different touch actions are enacted simultaneously on a different body part. Moreover, they precisely can differentiate between touch modalities regardless of the location or orientation of the interaction.

CHAPTER 3

Robust Tactile Descriptors

Touch comes before sight, before speech. It is the first language and the last, and it always tells the truth.

(Margaret Atwood: Der blinde Mörder)

3.1. Introduction

For robotic systems, interact with dynamic environments, recognizing object properties is a challenging task even with advanced vision techniques due to occlusion and poor lighting situations. Tactile sensing instead can provide a rich and direct feedback to the robotic systems from multiple simultaneous contact points and a large tactile sensing area. The objects' material can be characterized and identified with respect to textural properties by moving fingertips on the surface of the objects or moving objects on the sensitive skin area. In order to enable the robotic systems to perceive the textural properties of objects, the robots are equipped with the sense of touch with different sensing technologies. Several tactile feature extraction techniques are proposed to abstract reliable tactile information from the output of the tactile sensors. However, the performance of the proposed tactile descriptors is dependent on particular experimental setup (such as specific tactile sensor technology, well-controlled tools, predefined exploratory movements with constant applied force, etc.).

In this chapter, I propose a set of novel tactile descriptors to enable robotic systems to extract robust tactile information during exploration of objects via their surfaces. I evaluated the performance of the proposed tactile descriptors by employing different robotic platforms, tactile sensing technologies, different exploratory movements and a large number of objects and materials with regular and irregular textural properties. Taking advantage of my proposed descriptors, a robotic hand with multimodal robotic skin on the fingertips performed a set

of active human-like exploratory movements on the surface of materials and in-hand objects, from simple sliding to complex sliding exploratory movements, in order to discriminate among a large number of materials and in-hand objects. Moreover, I observed a humanoid robot with a large-scale artificial robotic skin on its upper body to classify objects, while a large objects were held by the hands, arms, and chest of the robot during sliding ¹.

3.2. Proposed robust tactile descriptors

In earlier studies, researchers employed different signal processing techniques for interpreting tactile signals. The Fourier transform in the frequency domain along with magnitude, skewness, and kurtosis in the time domain have been mostly employed to interpret vibro-tactile signals. The magnitude of the signal is highly sensitive to noise. Thus, it is necessary to design an appropriate filter or filter bank to remove interference from tactile signals, which is a computationally costly procedure.

The Fourier transform presents the relative power of each frequency and calculates frequency responses based on specific time. The Fourier transform is therefore not suitable for analyzing non-stationary signals, particularly in the case of surface texture recognition in which the texture has non-uniform (irregular) properties. In this case, the wavelet transform (DWT) and short-time Fourier transform (STFT) may be the best techniques for analyzing non-stationary signals. They analyze a localized signal by windowing in the time/frequency domain. However, these methods deal with large data vectors (a large feature vectors) causing difficulties at the classification phase. More features require more training samples, which result in rising of computational complexity as well as the risk of over-fitting. To overcome these issues, I propose a set of fundamental tactile descriptor inspired by the Hjorth parameters [147], which were presented for real-time biological signal analyses (Electroencephalography/EEG). My proposed tactile descriptors represent the statistical properties of the tactile signals in the time domains, *Activity*, *Mobility*, and *Complexity*.

The *Activity* (Eq.(3.1)) is the total power of a signal. The *Mobility* parameter (Eq.(3.2)) is the square root of the ratio of the variance of the first derivative of the signal to that of the signal. The *Complexity* (Eq.(3.3)) is the second derivative of the variance and shows how the shape of the signal is similar to a pure sine wave. If the signal is more similar to the sine wave, the complexity value converges to 1.

¹The content of this chapter has been published in [144–146], IEEE©

$$Act(\mathbf{S}) = \frac{1}{N} \sum_{n=1}^N (S_n - \bar{S})^2. \quad (3.1)$$

$$Mob(\mathbf{S}) = \left(\frac{Act(\frac{dS_n}{dn})}{Act(\mathbf{S})} \right)^{-1/2}. \quad (3.2)$$

$$Com(\mathbf{S}) = \frac{Mob(\frac{dS_n}{dn})}{Mob(\mathbf{S})}. \quad (3.3)$$

In above equations, \mathbf{S} is a tactile data vector with N data samples ($n \in \{1, \dots, N\}$) and $\bar{S} = \frac{1}{N} \sum_{n=1}^N S_n$ is the average value, or mean, of \mathbf{S} . Tactile object exploration first requires an initiation of a static contact with the surface of objects by a hand or a sensitive skin area, and then sliding the hand or body part/s (with sensitive skin) over the surface of objects (dynamic motion). The transition from the static state to the dynamic state (and vice-versa) during tactile object exploration depends very much on the frictional properties of the surface texture of objects. Robotic systems (for instance a robotic hand) need to apply more force to transit from the static state to the dynamic state in order to explore the surface of objects with a high friction coefficient. Such a transition affects the outer layer of the robotic skin (it is usually made of soft materials such as silicon). This results in deformation of the outer layer of the robotic skin, which generates linear or/and non-linear correlation between outputs of tactile sensors in the soft skin.

In previous work the starting as wells as the ending parts of the exploratory actions were eliminated [10–12]. In contrary, in this study, I use the entire tactile information perceived during tactile object exploration. Therefore, I propose to use the linear correlation (Eq.(3.4)) and non-linear correlation coefficients (Eq.(3.5)) between tactile signals/sensors as additional tactile features. These features indirectly provide information about the frictional properties of the surface of objects with the robotic systems during the exploratory procedure.

$$L_{\mathbf{S}, \mathbf{V}}^{cor} = \frac{\sum_{n=1}^N (S_n - \bar{S}) \cdot (V_n - \bar{V})}{\sigma(\mathbf{S}) \cdot \sigma(\mathbf{V})}. \quad (3.4)$$

$$N_{\mathbf{S}, \mathbf{V}}^{cor} = 1 - \frac{6 \sum_{n=1}^N (R_k)_n^2}{N(N^2 - 1)}. \quad (3.5)$$

In the above equations, \mathbf{S} and \mathbf{V} are vectors of data over time (input tactile signals) with N samples, and R_k is the difference between the rank of \mathbf{S} and the rank of \mathbf{V} .

In (3.9) and (3.10), $L_{S,V}^{b_i}$ and $N_{S,V}^{b_i}$ are total linear and non-linear correlations between the output of various tactile sensors/tactile signals, respectively. These parameters are averaged over each axis of the tactile sensors as well as entire skin modules ($n_c = 1, \dots, N_c$) in each body part $b_i \in \mathcal{B}$. The proposed final feature descriptors for one body part of a robotic system or one limb of a humanoid robot ($b_i = b_1$) covered with a large number of multi-modal tactile sensors $n_c = 1, \dots, N_c$ with multiple axes $n_s = 1, \dots, N_s$ can be defined as Eq. (3.11).

Eq.(3.11) is the concatenation of total Activity, Mobility, Complexity parameters together with the total linear and non-linear correlation coefficients as one feature vector with 24 data points. The proposed tactile descriptor for a robotic system or a humanoid which its N body parts ($b_n = 1, \dots, b_i, \dots, b_N$) with a large number of multi-modal tactile sensors contributed in the the tactile exploration can be written as Eq. (3.11). The tactile feature vector computed from N body parts ($D_{total}^{1:b_N}$) includes $N \times 24$ data samples.

3.2.1. Proposed tactile descriptors for a large skin area

In this study, I used my proposed fundamental parameters to construct a novel set of tactile descriptor to extract robust tactile information from a large number of tactile sensors or a large robotic skin area. My proposed feature descriptor includes the computed mean value of the Activity, Mobility, and Complexity of the tactile sensor's output over entire signal axes as well as tactile sensors/skin modules in one body part of the robotic system. In addition, my proposed descriptor includes the mean value of the linear and non-linear correlation coefficients between tactile signals. More formally, suppose a body part/limb ($b_i \in \mathcal{B}$) of a robotic system/humanoid (for instance a forearm or an upper arm of a humanoid) is covered with N_c skin cells/modules (one skin cell or skin module can have several tactile sensors with multiple sensing technologies). Each cell/module consists of N_s tactile sensors $(S_{n_c, n_s})^{b_i}$ with multiple axes, $(S_{n_c, n_s}^x)^{b_i}$, $(S_{n_c, n_s}^y)^{b_i}$, and $(S_{n_c, n_s}^z)^{b_i}$ in which $n_c = 1, \dots, N_c$, $n_s = 1, \dots, N_s$, and $b_i \in \mathcal{B}$. More general, each skin cell/module includes multi-modal tactile sensors $(S_{n_c, n_s})^{b_i}$, $(V_{n_c, n_r})^{b_i}$, $(U_{n_c, n_p})^{b_i}$, and etc., where $n_c = 1, \dots, N_c$, $n_r = 1, \dots, N_r$, and $n_p = 1, \dots, N_p$.

The total Activity, Mobility, and Complexity of a large number of multi-modal tactile sensors or a large skin area over each body part ($b_i \in \mathcal{B}$) are described in Eq.(3.6), (3.7), and (3.8), respectively. Using the proposed descriptor (Eq.(3.12)), a robotic system or a humanoid robot can extract robust tactile information when exploring objects or surfaces with each body part or multiple body parts (even whole body tactile exploration), as a human does.

$$\mathbf{A}_S^{b_i} = \left[\frac{\lambda_{n_c}}{N_c N_s} \sum_{n_c=1}^{N_c} \sum_{n_s=1}^{N_s} \text{Act}(S_{n_c, n_s}^x)^{b_i}, \frac{\lambda_{n_c}}{N_c N_s} \sum_{n_c=1}^{N_c} \sum_{n_s=1}^{N_s} \text{Act}(S_{n_c, n_s}^y)^{b_i}, \frac{\lambda_{n_c}}{N_c N_s} \sum_{n_c=1}^{N_c} \sum_{n_s=1}^{N_s} \text{Act}(S_{n_c, n_s}^z)^{b_i} \right]. \quad (3.6)$$

$$\mathbf{M}_S^{b_i} = \left[\frac{\lambda_{n_c}}{N_c N_s} \sum_{n_c=1}^{N_c} \sum_{n_s=1}^{N_s} \text{Mob}(S_{n_c, n_s}^x)^{b_i}, \frac{\lambda_{n_c}}{N_c N_s} \sum_{n_c=1}^{N_c} \sum_{n_s=1}^{N_s} \text{Mob}(S_{n_c, n_s}^y)^{b_i}, \frac{\lambda_{n_c}}{N_c N_s} \sum_{n_c=1}^{N_c} \sum_{n_s=1}^{N_s} \text{Mob}(S_{n_c, n_s}^z)^{b_i} \right]. \quad (3.7)$$

$$\mathbf{C}_S^{b_i} = \left[\frac{\lambda_{n_c}}{N_c N_s} \sum_{n_c=1}^{N_c} \sum_{n_s=1}^{N_s} \text{Com}(S_{n_c, n_s}^x)^{b_i}, \frac{\lambda_{n_c}}{N_c N_s} \sum_{n_c=1}^{N_c} \sum_{n_s=1}^{N_s} \text{Com}(S_{n_c, n_s}^y)^{b_i}, \frac{\lambda_{n_c}}{N_c N_s} \sum_{n_c=1}^{N_c} \sum_{n_s=1}^{N_s} \text{Com}(S_{n_c, n_s}^z)^{b_i} \right]. \quad (3.8)$$

$$\mathbf{L}_{S,V}^{b_i} = \left[\frac{\lambda_{n_c}}{N_c N_s N_r} \sum_{n_c=1}^{N_c} \sum_{n_s=1}^{N_s} \sum_{n_r=1}^{N_r} L^{\text{cor}}(S_{n_c, n_s}^x, V_{n_c, n_r}^x)^{b_i}, \frac{\lambda_{n_c}}{N_c N_s N_r} \sum_{n_c=1}^{N_c} \sum_{n_s=1}^{N_s} \sum_{n_r=1}^{N_r} L^{\text{cor}}(S_{n_c, n_s}^y, V_{n_c, n_r}^y)^{b_i}, \right. \\ \left. \frac{\lambda_{n_c}}{N_c N_s N_r} \sum_{n_c=1}^{N_c} \sum_{n_s=1}^{N_s} \sum_{n_r=1}^{N_r} L^{\text{cor}}(S_{n_c, n_s}^z, V_{n_c, n_r}^z)^{b_i} \right]. \quad (3.9)$$

$$\mathbf{N}_{S,V}^{b_i} = \left[\frac{\lambda_{n_c}}{N_c N_s N_r} \sum_{n_c=1}^{N_c} \sum_{n_s=1}^{N_s} \sum_{n_r=1}^{N_r} N^{\text{cor}}(S_{n_c, n_s}^x, V_{n_c, n_r}^x)^{b_i}, \frac{\lambda_{n_c}}{N_c N_s N_r} \sum_{n_c=1}^{N_c} \sum_{n_s=1}^{N_s} \sum_{n_r=1}^{N_r} N^{\text{cor}}(S_{n_c, n_s}^y, V_{n_c, n_r}^y)^{b_i}, \right. \\ \left. \frac{\lambda_{n_c}}{N_c N_s N_r} \sum_{n_c=1}^{N_c} \sum_{n_s=1}^{N_s} \sum_{n_r=1}^{N_r} N^{\text{cor}}(S_{n_c, n_s}^z, V_{n_c, n_r}^z)^{b_i} \right]. \quad (3.10)$$

$$\mathbf{D}^{b_i} = \left[\mathbf{A}_S^{b_i}; \mathbf{M}_S^{b_i}; \mathbf{C}_S^{b_i}; \mathbf{L}_{S,V}^{b_i}; \mathbf{N}_{S,V}^{b_i} \right]. \quad (3.11)$$

$$\mathbf{D}_{\text{total}}^{b_N} = \left[\mathbf{D}^{b_1}; \mathbf{D}^{b_2}; \mathbf{D}^{b_3}; \dots; \mathbf{D}^{b_i}; \dots; \mathbf{D}^{b_{N-2}}; \mathbf{D}^{b_{N-1}}; \mathbf{D}^{b_N} \right]. \quad (3.12)$$

3.2.2. *Properties of the proposed tactile descriptors*

3.2.2.1. Pre-processing of tactile signals

Pre-processing of each measured signal is required to maximize useful information and minimize the effect of artifacts. It is also important when the tactile signals perceived during texture explorations are correlated to each other and adjacent data samples in the data matrix contain similar related signals. However, in this work, there is no need of further pre-processing or filtering of measured tactile signals before extracting tactile features. In fact, my proposed tactile descriptors automatically remove unimportant baseline offset signals from the signal samples by taking derivatives (first and second order derivatives) of the signals during tactile feature extraction part (Eq.(3.1) and Eq.(3.3)).

3.2.2.2. The proposed tactile descriptors in frequency domain

The state-of-the-art tactile descriptors were defined either in the time domain or in the frequency domain. Although, my proposed tactile descriptors are defined in the time domain, they can be interpreted in the frequency domain as well. The *Activity* (Eq.(3.1)) is the total power of a signal, which also can be interpreted as the surface of the power spectrum in the frequency domain (Parseval's relation). The *Mobility* parameter in (Eq.(3.2)) is the mean frequency estimation with a proportion of standard deviation of the power spectrum. The *Complexity* (Eq.(3.3)) as the second derivative of the power parameter estimates the bandwidth of the signal.

3.2.2.3. Computational complexity

The calculation of the proposed tactile descriptors is based on the variance of the received tactile signals with $\mathcal{O}(N^2)$ computational complexity (N is the number of data samples in Eq.(3.1)). Moreover, there is no need of further pre-processing and filtering of tactile signals. Therefore, the computational cost of extracting robust tactile information using my proposed tactile descriptors is sufficiently low. In other words, calculation of the Mobility and Complexity does not increase the computational complexity. This makes my proposed tactile descriptors an appropriate method for the real-time task. Moreover, tactile descriptor with low computational complexity is particularly necessary for extracting tactile features from a large number of tactile sensors of a robotic system or a large skin area of a humanoid robot during tactile exploration.

3.2.2.4. Built-in tactile sensor selection

The contact may occur at any arbitrary location along with the skin of a robotic system with the surface of objects during the tactile object/surface exploration. Only those tactile sensors or skin modules that are in contact with the surface of the object need to be considered in the feature space. The key result of this inclusion is the decrease in computational cost and energy consumption. This is especially important when a large number of tactile sensors or a large skin area are used. My proposed feature descriptor contains a built-in tactile sensor or skin module selection λ_{n_c} in Eq.(3.6), (3.7), (3.8), (3.9), and (3.10). By thresholding of the force signals (Eq.3.13) to detect contact during tactile exploration, only those tactile sensors or skin cells/modules in a body parts ($b_i \in \mathcal{B}$) being interacted with the surface of the object will contribute in the feature vector.

$$\lambda_{n_c} = \begin{cases} 1 & \text{if } \frac{1}{N_r} \sum_{n_r=1}^{N_r} F_{n_c, n_r} \geq F_t & \text{Contact} \\ 0 & \text{O.W.} & \text{No - contact} \end{cases} \quad (3.13)$$

3.3. System description

3.3.1. Robotic Skin: BioTac[®]

BioTac² is a multi-modal electronic skin (see Fig. 3.1). When it moves over the surface of an object, the generated vibration can be measured by an embedded dynamic pressure sensor (\mathbf{P}_{AC}) with the sampling rate of a 2.2 KHz. The BioTac has 19 impedance-sensing electrodes ($\mathbf{E}_1, \dots, \mathbf{E}_{19}$) distributed over the surface of the rigid part (see Fig. 3.4-E). These electrodes are capable of measuring the deformation that arises when normal forces are applied to the surface of the skin with the sampling rate of 50 Hz. Moreover, the BioTac can measure low frequency pressure (\mathbf{P}_{DC}).

3.3.2. Robotic Skin: Cellular Skin

In order to emulate a human sense of touch, I have designed and manufactured multi-modal tactile sensors called Cellular skin [148] to provide robotic systems with the ability to sense the touch. Each skin cell has one micro controller on the back and one set of multi-modal tactile sensors on the front, including one *three-axis accelerometer*; one *proximity sensor*;

²<http://www.syntouchllc.com/>

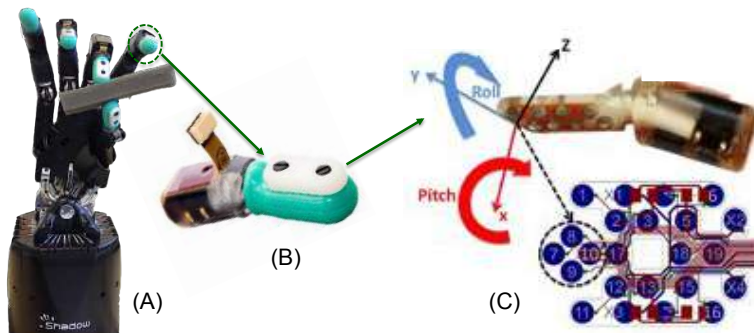


FIGURE 3.1. (A) The Shadow Hand with five BioTac on fingertips. (B) The BioTac[®] multimodal tactile sensor. (C) The BioTac[®] sensors with its 19 impedance electrodes and one pressure sensor (The figure is adapted from [22]).

three *normal-force sensors*, and one *temperature sensor* (see Table 3.1). Skin cells are directly connected with each other via bendable and stretchable inter-connectors. A unique cell ID is assigned to each skin cell within a network of skin patches to efficiently handle a large number of skin cells (see Fig. 3.2-B and Fig. 3.2-C).

3.3.3. The Shadow Hand

The Shadow Hand is an advanced robotic hand system with five fingers equipped with the BioTac $f_i \in \mathcal{F} = \{\text{thumb, index finger, middle finger, ring finger, little finger}\}$. It has 20 actuated degrees of freedom and a further 4 under-actuated movements for total of 24 joints. Each joint has a movement range again the same as or very close to that of a human hand, including the thumb and even the flex of the palm for the little finger. The Shadow Hand is fully integrated with the BioTac through ROS (see Fig. 3.4).

3.3.4. NAO Humanoid Robot

NAO is a small humanoid with 25 degrees of freedom, a 1.6 GHz Intel Atom Central Processing Unit, and height and weight of 58 cm and 4.3 kg respectively. I covered upper body of the NAO with a thin layer of a flexible and stretchable material. In order to provide the humanoid with the sense of touch I mounted 116 Cellular skin on the upper body of NAO: including 32 skin cells on the chest and 14, 12, and 16 skin cells on each hand, forearm, and upper arm respectively (see Fig. 3.2-A). In total, all seven body parts of NAO $b_i \in \mathcal{B} = \{\text{left hand, right hand, left forearm, right forearm, left upper arm, right upper arm, chest}\}$ were equipped with 348 *normal-force sensors*, 116 *three-axis accelerometer sensors*, 116 *proximity sensors*, and 116 *temperature sensors*. I fully integrated all skin cells with NAO via ROS (see Fig. 3.2-D).

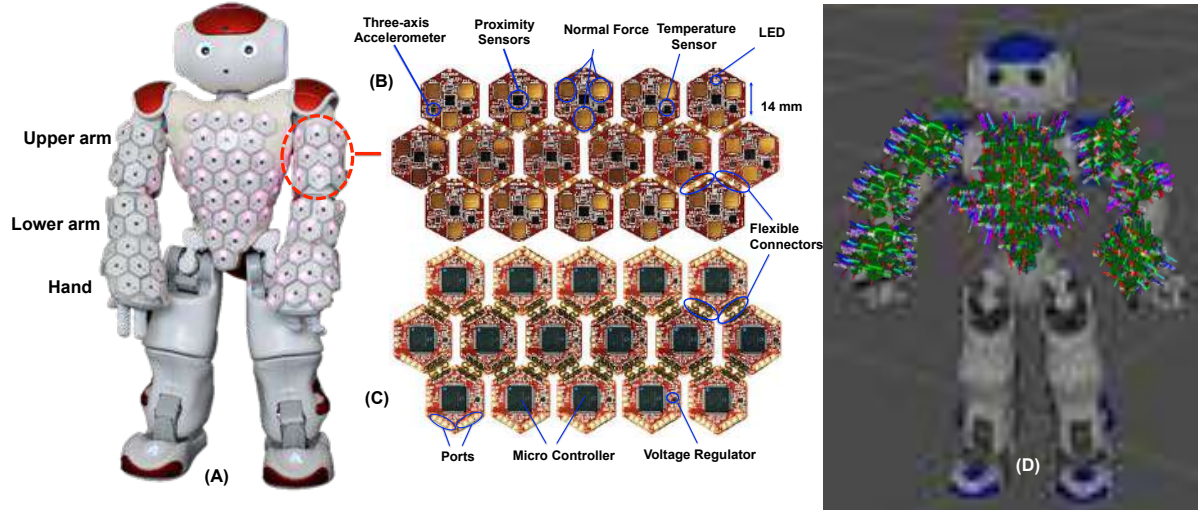


FIGURE 3.2. (A) NAO is equipped with 116 multi-modal artificial skin (Cellular skin) including: 32 skin cells on the chest and 14, 12, and 16 skin cells on each hand, fore arm, and upper arm respectively. (B) and (C) show the front and back of the Cellular skin. (D) shows the skin cells and NAO in rviz. I integrated skin cells with NAO via ROS.

TABLE 3.1. The Cellular skin characteristics.

Modality	Acceleration	Force	Proximity	Temperature
Sensor	BMA250	Customized	VCNL4010	LM71
Per Cell	1	3	1	1
Range	$\pm 2g$	0 – 10 N	1 – 200 mm	$-40 - 150^{\circ}\text{C}$
Resolution	10 bit	12 bit	16 bit	14 bit
Bandwidth	0 – 1 kHz	0 – 33 kHz	0 – 250 Hz	0 – 7 Hz

3.4. Robust feature extraction

3.4.1. Tactile descriptors for the Shadow Hand

While the Shadow Hand with the BioTac on the fingertips was executing sliding movements, the exploratory action generated two types of tactile data which were measured by the pressure sensor $\mathbf{P}_{AC}^{f_i}$ (with the sampling rate of 2.2 KHz) and the impedance sensing electrode array $\mathbf{E}_{nr}^{f_i}$ (with the sampling rate of 50 Hz). In order to extract the robust tactile data, I assumed that the tactile information measured by $(\mathbf{P}_{AC}^{f_i})$ corresponded to high-frequency texture information and the tactile data sensed by $(\mathbf{E}_{nr}^{f_i})$ related to the lower frequency changes in the texture especially about non-uniform or transitional periods in the overall surface texture structure.

My proposed feature descriptors were applied to the collected training and test data set to extract robust tactile information. More formally, the robust tactile feature was computed by substituting each of $(\mathbf{P}_{AC}^{f_i})$ and $(\mathbf{E}_{nr}^{f_i})$ for \mathbf{S} separately, in (3.6), (3.7), and (3.8). Each

finger of the Shadow Hand was considered as one body part $b_i = f_i \in \mathcal{F}$ ($f_i = 1, 2, \dots, 5$) and one skin module $N_c = 1$. Each finger with one BioTac has one ($N_s = 1$) single-axis ($\mathbf{P}_{AC}^{f_i}$) and $N_r = 19$ single-axis impedance electrodes ($\mathbf{E}_{n_r}^{f_i}$). The linear and non-linear correlations between ($\mathbf{P}_{AC}^{f_i}$) and ($\mathbf{E}_{n_r}^{f_i}$) in each finger ($f_i \in \mathcal{F}$) were computed using (3.14) and (3.15). The total feature descriptor for one finger ($f_i \in \mathcal{F}$) includes: $\mathbf{A}_{PAC}^{f_i} = \lambda_{f_i}(Act(\mathbf{P}_{AC}^{f_i}))$, $\mathbf{M}_{PAC}^{f_i} = \lambda_{f_i}(Mob(\mathbf{P}_{AC}^{f_i}))$, and $\mathbf{C}_{PAC}^{f_i} = \lambda_{f_i}(Com(\mathbf{P}_{AC}^{f_i}))$ which are the computed mean value of Activity, Mobility, and Complexity of the output of the dynamic pressure sensor ($\mathbf{P}_{AC}^{f_i}$), respectively and $\mathbf{A}_E^{f_i} = \frac{\lambda_{f_i}}{N_r} \sum_{n_r=1}^{N_r} Act(E_{n_r}^{f_i})$, $\mathbf{M}_E^{f_i} = \frac{\lambda_{f_i}}{N_r} \sum_{n_r=1}^{N_r} Mob(E_{n_r}^{f_i})$, and $\mathbf{C}_E^{f_i} = \frac{\lambda_{f_i}}{N_r} \sum_{n_r=1}^{N_r} Com(E_{n_r}^{f_i})$ which are mean values of the Activity, Mobility, and Complexity of each impedance sensing electrode ($\mathbf{E}_{n_r}^{f_i}$). The mean value of the linear and non-linear correlation coefficients between each impedance sensing electrode, and the dynamic pressure sensor were calculated with (3.14) and (3.15), respectively as additional tactile features.

$$\mathbf{L}_{PAC,E}^{f_i} = \frac{\lambda_{f_i}}{N_r} \sum_{n_r=1}^{N_r} L^{cor}(\mathbf{P}_{AC}, \mathbf{E}_{n_r}^{f_i}). \quad (3.14)$$

$$\mathbf{N}_{PAC,E}^{f_i} = \frac{\lambda_{f_i}}{N_r} \sum_{n_r=1}^{N_r} N^{cor}(\mathbf{P}_{AC}, \mathbf{E}_{n_r}^{f_i}). \quad (3.15)$$

in which

$$\lambda_{f_i} = \begin{cases} 1 & \text{if } \mathbf{P}_{DC}^{f_i} \geq 0.2N \quad \text{Contact} \\ 0 & \text{O.W.} \quad \text{No-Contact} \end{cases} \quad (3.16)$$

$F_t = 0.2N$ in Eq.3.16 is the minimum stable contact force that can be measured by the sensor and was determined during the experiments.

The final proposed feature descriptor for one finger $i = 1$ ($f_i \in \mathcal{F}$) is the concatenation of the total descriptors which can be written as:

$$\mathbf{D}^{f_1} = [A_{PAC}^{f_1}; A_E^{f_1}; M_{PAC}^{f_1}; M_E^{f_1}; C_{PAC}^{f_1}; C_E^{f_1}; L_{PAC,E}^{f_1}; N_{PAC,E}^{f_1}]. \quad (3.17)$$

The total tactile descriptors of five fingers contributed in the tactile object/surface exploration can be written as:

$$\mathbf{D}_{total}^{Shadow} = [\mathbf{D}^{f_1}; \mathbf{D}^{f_2}; \mathbf{D}^{f_3}; \mathbf{D}^{f_4}; \mathbf{D}^{f_5}]. \quad (3.18)$$

In the above equations, \mathbf{D}^{f_1} and $\mathbf{D}_{total}^{Shadow}$ include 8 and 8×5 data samples respectively.

$$\mathbf{A}_{\mathbf{F}}^{b_i} = \left[\frac{\lambda_{n_c}}{N_c N_s} \sum_{n_c=1}^{N_c} \sum_{n_r=1}^{N_r} Act(F_{n_c, n_r})^{b_i} \right]. \quad (3.19)$$

$$\mathbf{M}_{\mathbf{F}}^{b_i} = \left[\frac{\lambda_{n_c}}{N_c N_r} \sum_{n_c=1}^{N_c} \sum_{n_r=1}^{N_r} Mob(F_{n_c, n_r})^{b_i} \right]. \quad (3.20)$$

$$\mathbf{C}_{\mathbf{F}}^{b_i} = \left[\frac{\lambda_{n_c}}{N_c N_r} \sum_{n_c=1}^{N_c} \sum_{n_r=1}^{N_r} Com(F_{n_c, n_r})^{b_i} \right]. \quad (3.21)$$

$$\mathbf{A}_{\mathbf{a}}^{b_i} = \left[\frac{\lambda_{n_c}}{N_c} \sum_{n_c=1}^{N_c} Act(a_{n_c}^x)^{b_i}, \frac{\lambda_{n_c}}{N_c} \sum_{n_c=1}^{N_c} Act(a_{n_c}^y)^{b_i}, \frac{\lambda_{n_c}}{N_c} \sum_{n_c=1}^{N_c} Act(a_{n_c}^z)^{b_i} \right]. \quad (3.22)$$

$$\mathbf{M}_{\mathbf{a}}^{b_i} = \left[\frac{\lambda_{n_c}}{N_c} \sum_{n_c=1}^{N_c} Mob(a_{n_c}^x)^{b_i}, \frac{\lambda_{n_c}}{N_c} \sum_{n_c=1}^{N_c} Mob(a_{n_c}^y)^{b_i}, \frac{\lambda_{n_c}}{N_c} \sum_{n_c=1}^{N_c} Mob(a_{n_c}^z)^{b_i} \right]. \quad (3.23)$$

$$\mathbf{C}_{\mathbf{a}}^{b_i} = \left[\frac{\lambda_{n_c}}{N_c} \sum_{n_c=1}^{N_c} Com(a_{n_c}^x)^{b_i}, \frac{\lambda_{n_c}}{N_c} \sum_{n_c=1}^{N_c} Com(a_{n_c}^y)^{b_i}, \frac{\lambda_{n_c}}{N_c} \sum_{n_c=1}^{N_c} Com(a_{n_c}^z)^{b_i} \right]. \quad (3.24)$$

$$\mathbf{L}_{\mathbf{a}, \mathbf{F}}^{b_i} = \left[\frac{\lambda_{n_c}}{N_c N_s N_r} \sum_{n_c=1}^{N_c} \sum_{n_s=1}^{N_s} \sum_{n_r=1}^{N_r} L^{cor}(a_{n_c, n_s}^x, F_{n_c, n_r})^{b_i}, \frac{\lambda_{n_c}}{N_c N_s N_r} \sum_{n_c=1}^{N_c} \sum_{n_s=1}^{N_s} \sum_{n_r=1}^{N_r} L^{cor}(a_{n_c, n_s}^y, F_{n_c, n_r})^{b_i}, \right. \\ \left. \frac{\lambda_{n_c}}{N_c N_s N_r} \sum_{n_c=1}^{N_c} \sum_{n_s=1}^{N_s} \sum_{n_r=1}^{N_r} L^{cor}(a_{n_c, n_s}^z, F_{n_c, n_r})^{b_i} \right]. \quad (3.25)$$

$$\mathbf{N}_{\mathbf{a}, \mathbf{F}}^{b_i} = \left[\frac{\lambda_{n_c}}{N_c N_s N_r} \sum_{n_c=1}^{N_c} \sum_{n_s=1}^{N_s} \sum_{n_r=1}^{N_r} N^{cor}(a_{n_c, n_s}^x, F_{n_c, n_r})^{b_i}, \frac{\lambda_{n_c}}{N_c N_s N_r} \sum_{n_c=1}^{N_c} \sum_{n_s=1}^{N_s} \sum_{n_r=1}^{N_r} N^{cor}(a_{n_c, n_s}^y, F_{n_c, n_r})^{b_i}, \right. \\ \left. \hat{\mathbf{E}} \frac{\lambda_{n_c}}{N_c N_s N_r} \sum_{n_c=1}^{N_c} \sum_{n_s=1}^{N_s} \sum_{n_r=1}^{N_r} N^{cor}(a_{n_c, n_s}^z, F_{n_c, n_r})^{b_i} \right]. \quad (3.26)$$

$$\lambda_{n_c} = \begin{cases} 1 & \text{if } \frac{1}{N_r} \sum_{n_r=1}^{N_r} F_{n_c, n_r} \geq 0.2 N \quad \text{Contact} \\ 0 & \text{O.W.} \quad \text{No-Contact} \end{cases} \quad (3.27)$$

3.4.2. Tactile descriptors for the NAO

NAO perceived tactile signals related to textural properties of objects through their electronic skin. The tactile information corresponding to high frequency texture information as well as low frequency changes in the overall structure of the texture were measured by each three-axis accelerometer sensor (\mathbf{a}_{n_c, n_s}) and single-axis force sensors (\mathbf{F}_{n_c, n_r}) in each skin cell/module. The proposed tactile feature descriptors (3.6), (3.7), (3.8), (3.14), and (3.15) were used to extract the robust tactile information from the output of each axis of accelerometer sensors ($a_{n_c, n_s}^x, a_{n_c, n_s}^y, a_{n_c, n_s}^z$) as well as force sensors (\mathbf{F}_{n_c, n_r}). The computed features were then averaged over entire skin cells on each body part ($b_i \in \mathcal{B}$) of NAO. More formally Activity, Mobility, and Complexity of accelerometers were computed by (Eq. 3.22), (Eq. 3.23), and (Eq. 3.24), respectively. The robust tactile features were extracted from each of the force sensors by (3.19), (3.20), and (3.21). The final proposed feature descriptor for one body part of NAO ($b_i \in \mathcal{B}$) is the concatenation of the all descriptors which can be written as:

$$\mathbf{D}^{b_1} = [\mathbf{A}_a^{b_1}; \mathbf{A}_F^{b_1}; \mathbf{M}_a^{b_1}; \mathbf{M}_F^{b_1}; \mathbf{C}_a^{b_1}; \mathbf{C}_F^{b_1}; \mathbf{L}_{a,F}^{b_1}; \mathbf{N}_{a,F}^{b_1}] . \quad (3.28)$$

The proposed tactile descriptors of upper body of NAO $b_i \in \mathcal{B} = \{\text{left hand, right hand, left forearm, right forearm, left upper arm, right upper arm, chest}\}$ contributed in the tactile texture exploration can be defined as:

$$\mathbf{D}_{total}^{NAO} = [\mathbf{D}^{b_1}; \mathbf{D}^{b_2}; \mathbf{D}^{b_3}; \mathbf{D}^{b_4}; \mathbf{D}^{b_5}; \mathbf{D}^{b_6}; \mathbf{D}^{b_7}] . \quad (3.29)$$

In this experiment N_c is the number of the skin cell in one body part ($b_i \in \mathcal{B}$). $N_s = 1$, and $N_r = 3$ are the number of existing three-axis accelerometers and force sensors in one skin cell, respectively. In Eq. (3.27), $F_t = 0.2N$ is the minimum stable contact force.

The linear and non-linear correlations between each axis of the accelerometer ($a_{n_c, n_s}^x, a_{n_c, n_s}^y, a_{n_c, n_s}^z$) and force sensors (\mathbf{F}_{n_s, n_r}) were calculated with (3.25) and (3.26) which were then averaged over all skin cells in a body part ($b_i \in \mathcal{B}$).

In the above equations, the feature vectors \mathbf{D}^{b_1} and \mathbf{D}_{total}^{NAO} include 18 and 7×18 data samples respectively.

3.5. Tactile exploration with a robotic hand

Humans can discriminate among objects by means of their textural properties whilst sliding fingertips on the surface of the objects. The exploratory behaviors can be either a simple lateral/medial sliding movement or a complex full hand circular motion in which the fingertips rotate to slid on the surface of the objects. Furthermore, we can discriminate among different hand-held objects by sliding our fingertips on their surfaces without consideration of their shape [149]. In this study, a set of active human-like exploratory movements, from simple sliding to complex exploratory movements, carried out by the robotic hand to perceive the relevant tactile information about the textural properties of materials and objects (active exploration). Moreover, to compare the performance of my proposed tactile feature descriptors with the existing state-of-the-art feature extraction methods, a rotational stage was designed to move experimental materials underneath of the robotic hand to sense the corresponding tactile information of the materials (passive exploration).

3.5.1. Material exploration with the Shadow Hand

3.5.1.1. Properties of experimental materials

The experimental materials consist of 120 various natural and synthetic surface textures with uniform and non-uniform textural structures (textures with different densities and sparsities). The difference in textural properties of experimental materials varied from relatively similar to quite different. The experimental materials include: Papers and vinyl wallpapers, textiles, carpets and mats, foams and sponges, fibers, PVC and rubber type surfaces, leathers and furs, wooden surfaces, metal surfaces, fibreglass and glass surfaces, and carbon sheets (see Fig. 3.3). Here, the Shadow Hand with all five fingers open established a static contact (see Fig. 3.4-A) with each of the experimental materials by moving its wrist toward their surfaces along Z-axis (rotating WR1 joint around X-axis) (see Fig. 3.3). Then each finger was individually controlled to move around Z-axis via FF3, MF3, RF3, LF3, and TH4 joints (see Fig. 3.5) until each of them detected the minimum contact force $P_{DC}^{f_i} = 0.2N$ ($f_i \in \mathcal{F}$). The value of $P_{DC}^{f_i} = F_{min}^{f_i} = 0.2N$ is the minimum stable contact force that can be measured by the sensor and was determined during the experiments which I consider it as a "light contact of the Shadow Hand with a surface". The values of maximum force $F_{max}^{f_i} = 3N$ applied from each finger to the surface of the materials and maximum sliding velocity $v_{max} = 4cm/s$ were selected to avoid any damages to the tactile sensors as well as the robotic hand.



FIGURE 3.3. The selected experimental materials consist of 120 different natural and synthetic textures with uniform (regular) and non-uniform (irregular) structures including: Papers and vinyl wallpapers (Tex.#1-Tex.#37), Textiles (Tex.#38-Tex.#57), Carpets and mats (Tex.#58-Tex.#78), Foams and sponges (Tex.#79-Tex.#82), Fibers (Tex.#83, Tex.#84), PVC and rubber type surfaces (Tex.#85-Tex.#95), Leathers and furs (Tex.#96-Tex.#100), Wooden surfaces (Tex.#101-Tex.#109), metal surfaces (Tex.#110-Tex.#113), Fibreglass and glass surfaces (Tex.#114-Tex.#118), and Carbon sheets (Tex.#119, Tex.#120). All materials acquired from Bauhaus (www.bauhaus.info).

3.5.1.2. Lateral sliding exploratory movement

Training data collection:

To collect training samples the Shadow Hand executed a lateral sliding motion by moving its wrist from right to left and vice-versa for $4cm$ (by rotating WR2 joint around Z-axis). The tactile signals perceived during the exploratory movements were measured by dynamic pressure sensors $P_{AC}^{f_i}$ with a $2.2KHz$ sampling rate and an impedance sensing electrode array $E_{n_r}^{f_i}$ in which $n_r = 1, 2, \dots, 19$ with a $50 Hz$ sampling rate (in total 100 tactile signals from the output of five BioTac sensors). In order to ensure unbiased and fair training data collection, the same sliding velocity $V_{train} = v_{max}/2 = 2cm/s$ and applied force $F_{train}^{f_i} = F_{max}/2 = 1.5N$ as well as exploration time $t = 2s$ were applied across all fingers. The applied force value $F_{train}^{f_i} = 1.5N$ for all fingers was kept constant during each exploration round by continuously measuring $P_{DC}^{f_i}$ ($f_i \in \mathcal{F}$) and controlling each finger via FF3, MF3, RF3, LF3, and TH4 joints (see Fig. 3.5). The orientation of the experimental materials at each round varied by $\pi/4$ along the Z-axis. The exploratory action carried out at each round once with each of 120 materials. The entire data collection procedure was repeated 20 times. At the end of each data collection round, the BioTac sensors were calibrated by measuring $P_{DC}^{f_i}$, $P_{AC}^{f_i}$, and $E_{n_r}^{f_i}$ and setting their outputs to zero when the sensors were not in contact with the materials.

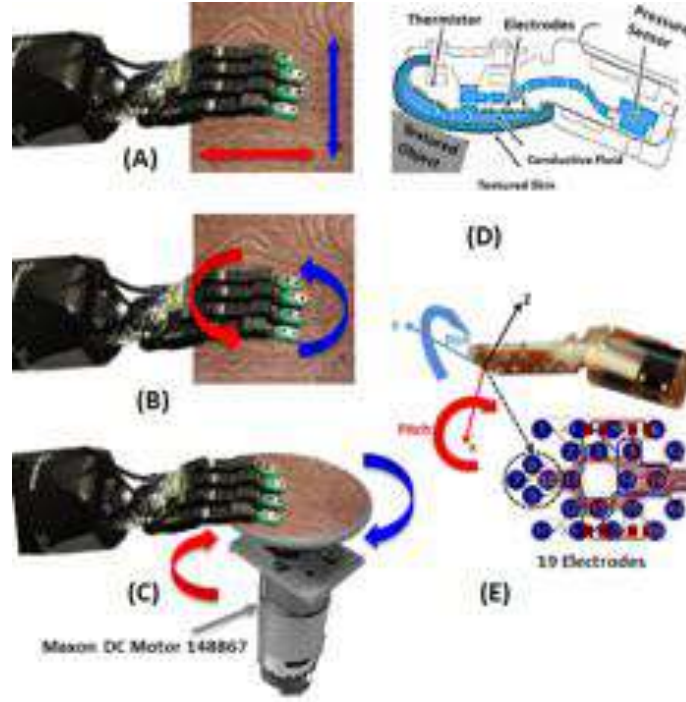


FIGURE 3.4. The Shadow Hand is exploring the textural properties of materials. (A) shows the execution of the lateral and medial exploratory movements. In (B), the Shadow hand performs human-like circular exploratory motion. In (C) an experimental material rotates underneath of the fingertips of the Shadow hand with a constant velocity. (D) and (E) demonstrate the BiTac sensors with its 19 impedance electrodes and one pressure sensor (The figures are adapted from [22]).

Test data collection:

To evaluate the performance of the proposed descriptor as well as the robot tactile learning, test data was collected separately. Unlike the training phase, at each test data collection round, the applied force value for each finger f_i was chosen uniformly at random from $F_{test}^{f_i} \in \{F_{min}^{f_i}, F_{min}^{f_i} + \Delta f_{test}, F_{min}^{f_i} + 2\Delta f_{test}, \dots, F_{max}^{f_i}\}$ in which $F_{min}^{f_i} = 0.2N$, $F_{max}^{f_i} = 3N$, and $\Delta f_{test} = 0.4N$. The applied force was then chosen for each finger f_i from $F_{test}^{f_i} \in \{0.2, 0.6, 1, 1.4, 1.7, \dots, 3\}$. The velocity of the lateral sliding movement V_{test} (the velocity of hand or WR2 joint) was selected uniformly at random from $V_{test} \in \{v_{min}, v_{min} + \Delta v_{test}, v_{min} + 2\Delta v_{test}, \dots, v_{max}\}$, in which $v_{min} = 0.5cm/s$, $v_{max} = 4cm/s$, $\Delta v_{test} = 0.5cm/s$, and $V_{test} \in \{0.5, 1, 1.5, 2, 2.5, \dots, 4\}$. Contrary to the training part, the exploration time, at each round, was selected uniformly at random from $T_{test} \in \{t_{min}, t_{min} + \Delta t, t_{min} + 2\Delta t, \dots, t_{max}\}$ in which $t_{min} = 2s$, $t_{max} = 10s$, $\Delta t = 1s$, $T_{test} \in \{2, 3, 4, \dots, 10\}$. At each round, test data was collected with each of 120 surfaces once. The orientation of the experimental materials varied by $\pi/6$ along the Z-axis. The entire test data collection was repeated 100 times. All data was

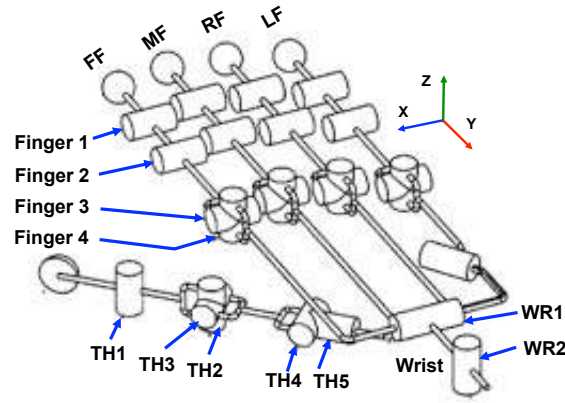


FIGURE 3.5. Kinematics Diagram of the Shadow Hand.

collected over a time period of three weeks to take into account any changes in environmental condition during the experiment. The values of $\Delta f_{test} = 0.4N$ and $\Delta v_{test} = 0.5cm/s$ were determined during the experiment based on the sensitivity and stability of the sensors and also hardware constrain of the robot.

3.5.1.3. Medial sliding exploratory movement

The Shadow Hand, with all fingers open, initiated a static contact (light touch) with the surface of the experimental materials by rotating the WR1 joint around X-axis (see Fig. 3.5). In order to perceive the tactile properties, the Shadow Hand slid all five fingers medially from up to down and vice-versa (see Fig. 3.4-A) for $4cm$. The medial motion looked like the Shadow Hand closed and opened (and vice-versa) its fingers on the experimental surface.

Training data collection:

Here, the position and velocity of WR2, FF3, MF3, RF3, LF3, and TH3 joints (see Fig. 3.5) were controlled to generate the medial sliding movement. The exploratory motion parameters such as sliding velocity and applied force were kept constant along all fingers $V_{train} = 2cm/s$ and $F_{train}^{fi} = 1.5N$. The exploration time at each round was $t = 2s$. The rest of data collection was identical to the training data collection procedure described for the lateral sliding movement.

Test data collection:

The medial exploratory movement was performed by the Shadow Hand to collect the test data. The exploratory parameters such as sliding velocity, applied force values, and exploration time were chosen from V_{test} , $F_{test}^{f_i}$, and T_{test} respectively. The rest of the procedure was identical to the test data collection with the lateral sliding movement.

3.5.1.4. Circular sliding exploratory movement

One of the most complex human hand exploratory motion is the sliding all five fingers circularly along the surface of an object. The aim of this part of study was to examine the performance of my proposed descriptors by executing human-like complex exploratory motions. Since the hard coding of the Shadow Hand to generate such a motion was time consuming, I used the CyberGlove³. The CyberGlove is fully integrated to the Shadow Hand via ROS. When a human wearing a CyberGlove moves fingers, the Shadow Hand can imitate the same movements. All kinematics values of the joints of the robotic hand while imitating the human hand motions such as position, orientation, and velocity of FF2, FF3, MF2, MF3, RF2, RF3, LF2, LF3, TH2 and TH3 joints were recorded and then saved in a rosbag file. By playing back the rosbag files, the Shadow Hand could re-produce the same hand movements.⁴ In this study, the exploratory motions of 11 human adults as subjects (6 females and 5 males) were captured. Each participant h_i was asked to wear the CyberGlove. Then each subject established a static contact with the surface of a material and then moved fingers circularly on the surface of the material for $T_{max} = 10s$. At the same time, the Shadow Hand connected to the CyberGlove was generating the same movements. The entire procedure was repeated 20 times with each subject and with a 15 min resting pause between each round. All recorded kinematics data was then added to a dataset $H \in \{h_1^{20}, h_2^{20}, \dots, h_{11}^{20}\}$ in which h_i^{20} includes 20 separate rosbag file for subject h_i . It is noteworthy to mention that there was no tactile feedback available for the robot.

Training data collection:

To collect training data, one h_i^{20} was randomly selected from $H \in \{h_1^{20}, h_2^{20}, \dots, h_{11}^{20}\}$. In order to have fair data collection procedure identical to the lateral and medial training phase, the position and orientation values of some joints such as FF3, MF3, RF3, LF3, and TH4 in each rosbag file of h_i^{20} were modified. By playing back each modified rosbag file h_i^{20} , the

³<http://www.cyberglovesystems.com/>

⁴www.wiki.ros.org/cyberglove/Tutorials/.

Shadow Hand with all five fingers open was establish a static contact (see Fig. 3.4-B) with each of the experimental surfaces until each of the finger detected $P_{DC}^{f_i} = 0.2N$. The applied force value for all fingers was chosen from F_{train} . The rest of the procedure was the same as described for lateral and medial training data collection parts.

Test data collection:

The Shadow Hand randomly selected 10 exploratory motions from each of the 10 remaining human subjects $H_{test} \in \{h_1^{10}, h_2^{10}, \dots, h_{10}^{10}\}$. Using the information related to these exploratory motions, the Shadow Hand reproduced 100 circular exploratory movements to collect test data. The value of applied force for each finger f_i was selected individually from $F_{test}^{f_i}$. The selected applied force value $F_{test}^{f_i}$ for each finger f_i was kept constant during each exploration. The exploration time, at each round, was selected uniformly at random from T_{test} . The rest of test data collection remained identical to the previous test data collection parts.

In order to collect fair training data and to evaluate my proposed descriptors systematically with the test data, the kinematics information (position, orientation, and velocity) of FF3, MF3, RF3, LF3, and TH4 in each rosbag were modified. However, this modification was less time consuming than hard coding of the robot to generate the human-like movements.

3.5.1.5. Combined exploratory movement

Training data collection:

The combined exploratory movement was the combination of three exploratory actions *lateral + medial + circular*. At each round, the Shadow Hand executed sequentially lateral, medial, and circular sliding movements ($S_{train}^{comb} = S_{LMC}$) on the surface of each material to collect training tactile data. The exploration time, at each round was $t = 3s$. The rest of the procedure remained identical to the previous training data collection parts.

Test data collection:

To collect test data, at each round, the exploratory action was uniformly selected at random from $S_{test}^{comb} \in \{S_L, S_M, S_C, S_{LMC}, S_{LCM}, S_{MLC}, S_{MCL}, S_{CLM}, S_{CML}\}$ and then was executed by the robot. The action set included the combination of lateral, medial, and circular motions with different sequences. For instance, S_{CML} means the Shadow Hand performed,



FIGURE 3.6. In-hand uniform shaped objects.

in order, circular, medial, and lateral actions. The velocity of sliding and applied normal force were selected from V_{test} and $F_{test}^{f_i}$ respectively. The exploration time was chosen from T_{test} in which $t_{min} = 3s$, $t_{max} = 10s$, $\Delta t = 1s$, and $T_{test} \in \{3, 4, 5, \dots, 10\}$. The rest of the procedure was the same as the previous test data collection parts.

3.5.1.6. Rotational stage

Previously, researchers have used well-controlled experimental devices to validate their proposed tactile descriptors. Therefore, to compare the performance of my proposed tactile feature extraction technique with the state-of-the-art I have designed a well-controlled rotational stage Fig. 3.4-C. The system consists of a Maxon DC motor (GEARHEAD MAXON 203114, PLANETARY, 42MM, 4.3/1) and a 3D printed plate made of poly lactic acid (PLA) material with a radius of $r = 70mm$. A Maxon motor control and an encoder HEDS5540 are used to control the velocity of the motor.

Training data collection:

Each experimental material was attached firmly to one 3D printed plate. The velocity of the motor was kept constant with a frequency of $f_{train}^M = 0.1011Hz$ during training data collection. The Shadow Hand established a light contact with the experimental surface $P_{DC}^{f_i} = 0.2N$. The applied force value for all fingers were kept constant at each data collection round $F_{train}^{f_i} = 1.5N$. The attached material was rotated underneath of all five fingertips for $t = 2s$. The rest of the procedure was identical to the previous training data collection parts. In order to have fair data collection, each surface texture was attached to one plate.



FIGURE 3.7. In-hand complex shape objects.

Test data collection:

In order to collect test data similar to previous studies, the velocity of the motor and the applied force value were deliberately chosen to be the same as in the training part $V_{test} = V_{train} = 2\text{cm/s}$ and $F_{test}^{f_i} = F_{train}^{f_i} = 1.5\text{N}$. The exploration time was selected from $T_{test} \in \{3, \dots, 10\}$. The rest of the procedure was identical to the previous test data collection parts.

3.5.2. In-hand object exploration with the Shadow Hand

3.5.2.1. Properties of In-hand Objects

In this study, 32 natural and synthetic everyday objects with uniform (regular) and non-uniform (irregular) textural properties were selected. Fourteen objects with an identical geometrical shape (in this case a spherical shape) were chosen, including a tomato, apple, pomegranate, kiwi, orange, a pine cone textured ball with an irregular texture, a mirror texture ball, two plastic balls with almost similar smooth surface texture, rough textured ball, colorful ball with a smooth surface, a rough spherical sponge, and string ball with an irregular texture (see Fig. 3.6). Additionally, eighteen objects with different complex shapes including a banana, zucchini, carrot, cucumber, a peeled banana, pine cone, a toothbrush, a floor brush, a soap, a memory sponge, a cardboard box, a rough textured star, a coffee capsule, a spray bottle, and a plastic baby feeder (see Fig. 3.7). In both sets of objects, the difference in the surface texture properties varied from relatively similar to quite different. Humans can discriminate among in-hand objects by perceiving their textural properties whilst sliding fingertips on their surfaces regardless of the objects' shape.

Training data collection:

Each experimental object was placed between thumb (TH), little (LF), and ring (RF) fingers of the robot (see Fig. 3.5). Then the Shadow Hand started closing its fingers to hold the object. The tactile feedbacks from P_{DC}^{LF} , P_{DC}^{RF} , and P_{DC}^{TH} were utilized to refine the current pose of the object and stabilize the current grasp. The grasp force values of each experimental object (with different stiffness and friction coefficient) were determined individually during the experiment. The grasp force were kept constant during each exploration by measuring continuously the outputs of P_{DC}^{LF} , P_{DC}^{RF} , P_{DC}^{TH} and by controlling the position of (LF2, LF3), (RF2, RF3), and (TH2, TH3, TH4, TH5) joints. However, this can be done autonomously by the robot by implementing a slip detection and deformation prevention method. I will consider this improvement as a future work by implementing my recently proposed slip detection and deformation prevention strategy to the Shadow Hand [150]. In order to perceive textural properties of each in-hand object, the robot used its index (FF) and middle (MF) fingers to establish a light contact with the surface of each object $P_{DC}^{FF} = 0.2N$ and $P_{DC}^{MF} = 0.2N$. Afterwards, the Shadow Hand slid each index and middle finger 2 cm on the surface of the in-hand object by rotating FF2 and MF2 around X-axis. Tactile data was measured by the BioTac sensors using the impedance electrodes ($\mathbf{E}_{n_r}^{FF}$ and $\mathbf{E}_{n_r}^{MF}$) and the pressure sensors (P_{AC}^{FF} and P_{AC}^{MF}), in total 40 tactile signals from the output of two BioTac sensors. The maximum applied force ($F_{max}^{f_i} = 2N$) as well as the maximum sliding velocity $v_{max} = 4cm/s$ were selected to avoid any damages to the in-hand objects. The sliding velocity $V_{train} = V_{max}/2 = 2cm/s$ and the applied normal force $F_{train}^{f_i} = F_{max}^{f_i}/2 = 1N$ at each round were kept identical in both fingers. At each round, the training data was collected once with each of the experimental object. The entire data collection repeated 20times. At each round, the experimental objects were held with $\pi/4$ perturbation in pose around X-axis. At the beginning of each round, the BioTac sensors were calibrated.

Test data collection:

Here, the robotic hand used its little (LF), ring (RF), and middle (MF) fingers to grasp each object. Afterwards, the robot with its thumb (TH) and Index (FF) established a light contact with the surface of the hand-held object ($P_{DC}^{FF} = 0.2N$ and $P_{DC}^{MF} = 0.2N$). Then the robot slid its thumb (TH) and index (FF) 1cm on the surface of object by rotating (TH3, TH4) and FF2 joints around X-axis. The velocity of the sliding movement V_{test} and the value of the applied force F_{test} for the thumb (TH) and Index finger (FF) were chosen separately from $V_{test} \in \{v_{min}, v_{min} + \Delta v_{test}, v_{min} + 2\Delta v_{test}, \dots, v_{max}\}$, $F_{test}^{f_i} \in \{F_{min}^{f_i}, F_{min}^{f_i} + \Delta f_{test}, F_{min}^{f_i} +$

$2\Delta f_{test, \dots, F_{max}^i}$. In this scenario, $v_{min} = 0.5\text{cm/s}$, $v_{max} = 4\text{cm/s}$, $\Delta v_{test} = 0.5\text{cm/s}$, $F_{min}^i = 0.2\text{N}$, $F_{max}^i = 2\text{N}$, $\Delta f_{test} = 0.4\text{N}$ ($V_{test} \in \{0.5, 1, 1.5, \dots, 4\}$ and $F_{test} \in \{0.2, 0.6, 1, \dots, 2\}$). At each exploration round, the velocity and applied force values were kept constant by measuring P_{DC}^{TH} and P_{DC}^{FF} and controlling the position of TH3 and Th4 joints for thumb and FF2 and FF3 for the index finger. The exploration time was chosen from $T_{test} \in \{t_{min}, t_{min} + \Delta t, t_{min} + 2\Delta t, \dots, t_{max}\}$ in which $t_{min} = 2\text{s}$, $t_{max} = 10\text{s}$, and $T_{test} \in \{2, 3, \dots, 10\}$. At each round, test data was collected once with each of 32 experimental in-hand objects. The orientation of the hand-held objects varied by $\pi/4$ around X-axis. The entire test data collection was repeated 100 times.

3.6. Tactile exploration with a humanoid

Humans can sense the textural properties of objects by sliding the sensitive body parts with large skin area (such as hand, lower arm, upper arm, etc.) on the surface of the objects. In order to grasp and lift an unknown large object we utilize our both hands and arms and even upper part of our body such as chest. In this case, a large area of our skin are in contact with the surface of the large object. As the large object starts sliding between our hands and arms, we can recognize the physical properties of the large object. In this part of the study, a set of active human-like exploratory movements carried out by NAO equipped with large-scale artificial skin to perceive the textural properties of 120 materials and 120 large objects with different weights W_i . In addition, a rotational stage was used to move the experimental materials underneath the NAO's hand.

3.6.1. Material surface exploration with NAO

3.6.1.1. Lateral sliding exploratory movement

NAO initiated a static contact with the surface of the material by moving its either right hand via RShoulderPitch joint or the left hand using LShoulderPitch joint until the average of total normal force sensors on the hand reached $\frac{1}{N_r N_c} \sum_{n_c=1}^{N_c} \sum_{n_r=1}^{N_r} F_{n_c, n_r} = 0.2\text{N}$ (light contact); in which $N_r = 3$ is the number of the normal force sensor in each skin cell and $N_c = 14$ is the number of the skin cell mounted on one hand. Afterwards, NAO explored the textural properties of the materials by sliding its hand laterally “ d ” cm on the surface of the material by moving the RShoulderRoll or LShoulderRoll joint (see Fig. 3.8). Tactile information was measured by the force sensors F_{n_c, n_r} with a 250 Hz sampling rate and three-axis accelerometer sensors \mathbf{a}_{n_c, n_s} with a 1 KHz sampling rate, in which $n_s = 1, 2, 3$ ($N_s = 3$) is the number of

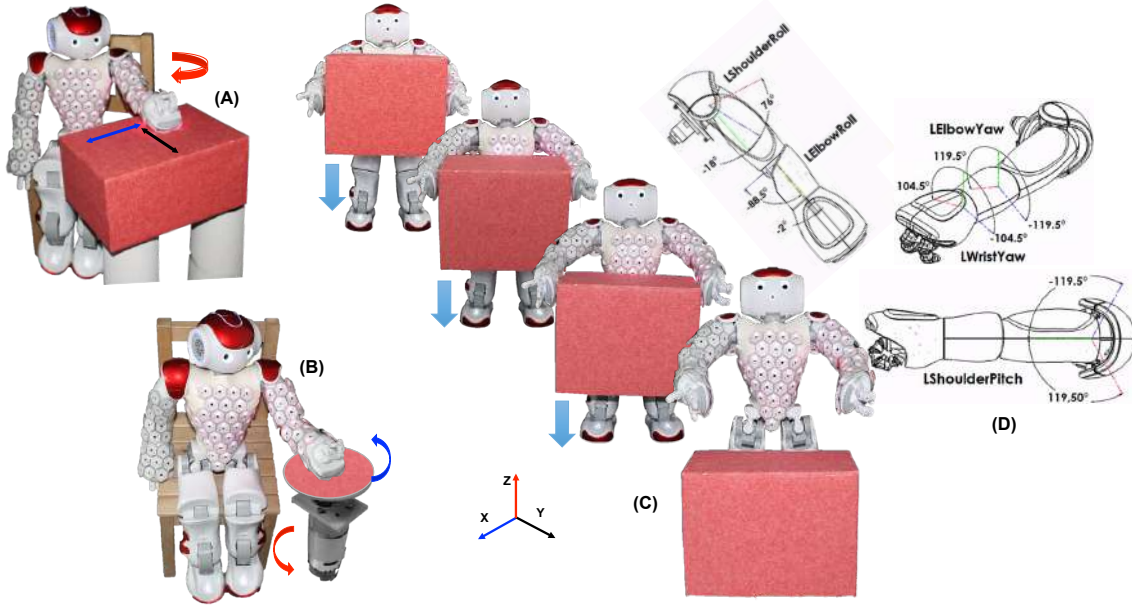


FIGURE 3.8. (A) NAO executes lateral, medial, or circular exploratory movements to sense the textural properties of the object (active exploration). (B) The experimental material/texture rotates underneath of NAO's hand with a constant velocity (passive exploration). (C) The large object was held by NAO with its upper body slides gradually between its hands, arms, and chest (passive exploration). (D) The kinematics of NAO's arm which is adapted from www.doc.aldebaran.com.

the axis of the accelerometer (in total 84 tactile signals from the output of 14 skin cells on the hand). The maximum force that NAO applied with its hand to the surface of the materials was $F_{max}^{hand} = \frac{1}{N_r N_c} \sum_{n_c=1}^{N_c} \sum_{n_r=1}^{N_r} F_{n_c, n_r} = 3N$ and the maximum velocity of the sliding was $v_{max} = 4cm/s$.

Training data collection:

In order to collect training samples, NAO slid its right hand $2cm$ on the surface of each 120 materials once which was then repeated 20 times. The velocity of the sliding movement $V_{train} = v_{max}/2 = 2cm/s$ and the value of the applied force $F_{train}^{hand} = F_{max}^{hand} = 1.5N$ were kept constant across all trials. The exploration time of each round was $t = 2s$. The orientation of the experimental materials, at each round, varied by $\pi/4$ around the Z-axis. At the end of each exploration, each skin cell was calibrated by measuring the outputs of the sensors F_{n_c, n_r} , \mathbf{a}_{n_c, n_s} and removing their biased signals (offset) when the skin cells were not in contact with the materials.

Test data collection:

Humanoid robots should be able to recognize textural properties of the objects with both left and right hand, even though only one of them was used in the training phase. In this experiment, NAO used its left hand to collect test data by sliding 1cm on the surface of the materials.

The velocity of the sliding movement and the value of the applied force were chosen from $V_{test} \in \{v_{min}, (v_{min} + \Delta v_{test}), (v_{min} + 2\Delta v_{test}), \dots, v_{max}\}$, $F_{test}^{hand} \in \{F_{min}^{hand}, (F_{min}^{hand} + \Delta f_{test}), (F_{min}^{hand} + 2\Delta f_{test}), \dots, F_{max}^{hand}\}$ respectively, in which $v_{min} = 0.5cm/s$, $\Delta v_{test} = 0.5cm/s$, $F_{min}^{hand} = 0.2N$, $\Delta f_{test} = 0.4N$. For instance $V_{test} \in \{0.5, 1, 1.5, 2, \dots, 4\}$ and $F_{test}^{hand} \in \{0.2, 0.6, 1, 1.4, \dots, 3\}$. The exploration time, at each round, was chosen from T_{test} with $t_{min} = 2s$, $t_{max} = 10s$, $\Delta t = 1$. Therefore, the exploration time set was $T_{test} \in \{2, 3, \dots, 10\}$. At each round, the orientation of the experimental materials varied by $\pi/6$ around the Z-axis. The entire data collection procedure was repeated 100 times. The rest of the procedure was the same as in the training data collection. The values of $\Delta f_{test} = 0.4N$ and $\Delta v_{test} = 0.5s$ were determined based on sensitivity and stability of the skin cells and NAO's hardware constrain.

3.6.1.2. Medial exploratory sliding movement

In order to generate the medial exploratory movement, NAO moved its hand forward and backward (along Y-axis). NAO executed the medial movement with its right hand to collect training data by controlling the positions and velocities of RShoulderPitch, RElbowRoll, and RElbowYaw joints in order to slide its hand 2 m on the surface of the materials. The test data was collected with the left hand using LShoulderPitch, LElbowRoll, and LElbowYaw joints while sliding 1cm on the materials' surfaces (see Fig. 3.8). The rest of training and test data collection procedure remained the same as described above.

3.6.1.3. Circular sliding exploratory movement

NAO explored the textural properties of the materials and collected training data by sliding its right hand circularly (clockwise) on the materials' surfaces. The robot was programmed to move its hand circularly by controlling the positions and velocities of the RShoulderRoll, LShoulderPitch, RElbowRoll, and RElbowYaw (see Fig.3.8). To collect test data, the circular motion was generated with the left hand (counter clockwise) via LShoulderRoll, LShoulderPitch, LElbowRoll, and LElbowYaw joints. The rest of training and test data collection process remained the same as explained in previous parts.

3.6.1.4. Combined exploratory movements

All three exploratory movements were combined as one motion (lateral+medial+circular). Here, at each round, NAO continuously slid its hand laterally, medially, and circularly to explore textural properties of each object. The data collection procedures remained identical to the previous parts. However, the exploration time in the training data collection phase, at each round was $t = 6s$ and for the test data collection was selected from T_{test} in which $t_{min} = 3s$, $t_{max} = 15s$, $\Delta t = 3s$ or $T_{test} \in \{3, 6, 9, 12, 15\}$.

3.6.1.5. Combined exploratory movement

Training data collection:

The combined exploratory movement was performed with the right hand of NAO to collect training data. At each round, NAO sequentially performed the lateral, medial, and circular sliding movements ($S_{train}^{comb} = S_{LMC}$) on the surface of each material for $t = 3s$. The rest of the procedure remained identical to the previous training data collection parts.

Test data collection:

The test data was collected, at each round, with the NAO's left hand. Contrary to the training part, the exploratory action was uniformly selected at random from $S_{test}^{comb} \in \{S_L, S_M, S_C, S_{LMC}, S_{LCM}, S_{MLC}, S_{MCL}, S_{CLM}, S_{CML}\}$. The exploration time was selected from T_{test} in which $t_{min} = 3s$, $t_{max} = 10s$, $\Delta t = 1s$, and $T_{test} \in \{3, 4, 5, \dots, 10\}$. The rest of the procedure was the same as the previous test data collection parts.

3.6.1.6. Rotational stage

In this part of the experiment the same experimental set up as in section 3.5.1.6 was used to collect tactile data by NAO's hands (see Fig.3.8-B). The rest of the experiment remained identical to the training and test data collection explained earlier.

3.6.2. Large object exploration with NAO

3.6.2.1. Properties of the large objects

Taking into account NAO's size and weight, I created 360 large objects with the same dimension $32 \times 22 \times 14 \text{ cm}^3$ (see Fig. 3.8) and three different weight categories: 120 objects weighing 500 g, 120 objects weighing 1000 g, and 120 objects weighing 1500 g. I then covered the surface of each set of the object with 120 different surface textures (see Fig. 3.3).

Training data collection:

Here, NAO was standing in front of a table. Its both arms were straight and parallel to each other and were able to open and close them in the horizontal direction (X-axis) using LShoulderRoll and RShoulderRoll joints. The experimental object was placed between NAO's arms. Afterwards, NAO slowly closed its arms to grasp the object. However, the position of the object between the NAO's arm could vary slightly along the arms or Y-axis (see Fig. 3.3-C). To be sure that all 14 skin cells on each hand will be in contact with the surface of the object during the grasp, NAO used the feedback from proximity sensors (\mathbf{P}_{n_c}). Proximity sensors give a measurement of the closeness corresponding to each skin cell with an experimental object's surface (which is called pre-contact or pre-touch). If a skin cell is close to the surface of an object ($d_{n_c} < 3\text{cm}$), in which d_{n_c} is the distance of one cell n_c from the surface), the normalized output of the proximity sensor is equal to one $\mathbf{P}_{n_c} = 1$, otherwise $\mathbf{P}_{n_c} = 0$. As soon as NAO realized its hands were close enough to the surface of the object via proximity ($d_{n_c} < 3\text{cm}$), it moved its arms n steps ($n = 1, \dots, 5$ and at each step 0.5cm) forward or backward along Y-axis using LShoulderRoll, LElbowRoll and LElbowYaw joints of the left hand and RShoulderRoll, RElbowRoll, and RElbowYaw joints of the right hand until it was sure that all skin cells on each hand will be in contact with the surface of the object. Afterwards, it started closing the arms to grasp the object. As soon as the average of total force sensors on the hand exceeded the grasping force value $\frac{1}{N_r N_c} \sum_{n_c=1}^{N_c} \sum_{n_r=1}^{N_r} F_{n_c, n_r} > f_{o_i}^{grasp}$, it lifted the large object for 10cm from the table using LShoulderPitch and RShoulderPitch joints. The value of the force to grasp an object firmly $f_{o_i}^{grasp}$ within NAO's arm was determined during the experiments based on the objects' weights as I did not implement any slip detection and deformation prevention methods on NAO ($f_{500}^{grasp} = \frac{1}{N_r N_c} \sum_{n_c=1}^{N_c} \sum_{n_r=1}^{N_r} F_{n_c, n_r} = 2N$, $f_{1000}^{grasp} = 2.7N$, and $f_{1500}^{grasp} = 3.5N$). Afterwards, NAO pulled the large object (o_i) towards its chest by moving its arms backward along Y-axis until the large object was in contact with its chest and NAO detected $\frac{1}{N_r N_c} \sum_{n_c=1}^{N_c} \sum_{n_r=1}^{N_r} F_{n_c, n_r} = 0.2N$ via the skin cells of the chest ($N_c = 32$ skin cells). As the experiment proceeded, NAO slowly opened its arms until the object started to slide

between its arms and chest. When the object was sliding, it generated vibrations on the large skin area. The caused vibro-tactile signals were measured by accelerometers (\mathbf{a}_{n_c, n_s}) and force sensors (\mathbf{F}_{n_c, n_r}) on the hands, fore arms, upper arms, and chest (in total 696 tactile signals from 116 skin cells). At each round, the exploration carried out once with each of 120 objects weighing 1000 g, which was repeated 20 times. It is noteworthy to mention that in this experiment, the exploration time (sliding time), velocity of sliding, and value of applied normal force were dependent on the large objects' weights. In other words, objects with different weights slide with different velocities. Moreover, the robot needs to apply different force values by its hand to the surface of the object in order to grasp and then lift them up.

Test data collection:

The test data collection was carried out as described for training data collection (see Fig.3.8-C). The test exploration was repeated 100 times; 50 times for each large object weighing 500g and 50 times for objects weighing 1500g and 120 different surface textures. The exploration or sliding time, velocity of sliding, and the amount of applied force were different from the training data collection part as they varied depending on the objects' weights. The entire procedure was carried out over a time period of three weeks. This experiment was designed to evaluate the performance of the proposed tactile descriptor among different sliding time and velocity (exploration time and velocity) during passive object exploration. Moreover, by this experiment I can examine the robustness of the proposed descriptor against external noises generated due to the vibration or motion of the humanoid during passive exploration.

3.6.2.2. Support Vector Machine (SVM)

The Support Vector Machine (SMV) [151] was used to construct tactile object classification models from the extracted tactile features received during the training phase. While giving labeled training data (supervised learning) the algorithm constructs a hyper-plane or set of hyper-planes in a high dimensional space in order to classify new objects from their textural properties.

3.6.2.3. Expectation Maximization (EM)

The Expectation Maximization (EM) algorithm [152] for Gaussian Mixture Models (GMM) with a spherical covariance matrix was employed to categorize objects via their textures. Given a Gaussian mixture model, the goal is to maximize the likelihood function with respect to the parameters (comprising the means and covariances of the components and the

mixing coefficients). EM is an unsupervised and iterative algorithm that generalizes k-means to a probabilistic setting in four steps. First to initialize the means, covariances, mixing coefficients and evaluate the initial value of the log likelihood in order to select K data points uniformly at random as initial means and select the covariance matrix of the whole data set for each of the initial K covariance matrices. Expectation step (E step) computes the cluster probability of each data sample and the Maximization step (M step) uses these probabilities to estimate the gaussian distribution parameters. In step four, EM evaluates the log likelihood and checks for convergence of either the parameters or the log likelihood. If the convergence criterion is not satisfied, it returns to step two (E step). Convergence is ensured since the algorithm is guaranteed to enhance the log likelihood at each iteration. The Normalized Mutual Information method (NMI) [153] was used to measure the quality of the clustering results.

3.7. Experimental results

3.7.1. *Experimental evaluation with the Shadow Hand*

3.7.1.1. Supervised Material Discrimination

An SVM classifier [151] with linear kernel was employed by the robotic hand to discriminate among materials/objects via their textural properties. To obtain the best learning parameters and the regularizer value C , 5-fold cross validation (CV) was carried out on entire training data set. In this regard, the collected training set was randomly split into 5 folds; 4 of those for training and one for evaluation. The procedure was repeated 10 times to obtain an average performance on the evaluation sets. The entire process was repeated 20 times with different values for $C \in \{10^{-4}, 5^{-4}, 3^{-4}, 2^{-4}, \dots, 2^4, 3^4, 5^4, 10^4\}$ to find the one with the lowest cross validation error. After this process, the SVM with the optimal parameters was re-trained with the entire training set to construct the learning models which were then used by the Shadow Hand for the prediction of the unseen separately collected test set.

If a robot uses its full hand to learn about the textural properties of materials, it should be able to discriminate among materials (during the evaluation phase) with each of its finger or different combination of two, three, four, or five fingers.

In this experiment, the SVM was trained with the training data collected with all five fingers (full hand) of the Shadow Hand to construct learning texture models. To evaluate the robustness of my proposed tactile descriptors the constructed tactile learning models were evaluated to predict with the test data $S_{test}^{1:100} \in \{S_f^1, S_f^2, \dots, S_f^{100}\}$ in which f was uniformly selected at random from $f \in \{f_{FF}, f_{MF}, \dots, (f_{FF}f_{MF}), (f_{MF}f_{RF}), \dots, (f_{FF}f_{MF}f_{RF}), \dots,$

$(f_{FF}f_{MF}f_{RF}f_{LF}f_{TH})$. For instance in $S^1_{(f_{FF}f_{MF})}$ includes only the contribution of the index finger (FF) and middle finger (MF) during text data collection. Table 3.2 shows that the robotic hand successfully discriminated among 120 materials with 100% recognition rate when it performed each of five exploratory motions while sliding with different combination of its fingers.

Exploratory Behavior	Training with	Test with	SVM
Lateral sliding	(five fingers)	Combination of different (from one finger to five fingers)	100%
Circular sliding			100%
Combination of Lateral, Medial, and Circular			100%
Rotational sliding			100%

TABLE 3.2. Surface textures classification by Shadow Hand. The best regularizer value that was found by CV for all experiments is $C = 0.001$.

3.7.1.2. On-line material discrimination

There is a trade off between complexity of learning algorithms and power of tactile descriptors in tactile object and material discrimination domains. Using the state-of-the-art feature extraction techniques (see Table 2.1), the robotic systems needed to store a large number of samples (as a batch of data) in memory during training. The growth of object classes results in a memory explosion, making the state-of-the-art feature descriptors unfit for real-time robotic systems. In this experiment, I investigated whether it is possible for the robots to discriminate materials and objects with an on-line learning algorithm (low memory consumption) while utilizing my proposed descriptors. To evaluate this, the Shadow Hand employed the PA algorithm to classify 120 experimental materials online. Using my proposed descriptors, the robotic hand constructed texture models whilst receiving training samples sequentially and over time ($t = 1, \dots, 20$). In this experiment, the learning parameter η was fixed to 1. The recognition rates at each time t were computed by using the currently constructed learning models to predict test data. Fig. 3.9 shows the averaged classification rate at each training step ($t = 1, \dots, 20$) with the lateral, medial, circular, and rotational exploratory behaviors. Fig. 3.9 illustrates that the Shadow Hand achieved 100% recognition accuracy after training with 15 samples with each of the exploratory movements. Fig. 3.9 demonstrates that the Shadow Hand with circular sliding exploratory movements and 10 training samples ($t = 10$) obtained 100% classification accuracy. Furthermore, I evaluated the performance of tactile material discrimination with the combination of all test dataset $S^{1:100}_{LMC_{test}} \in \{S^{1:100}_{L_{test}}, S^{1:100}_{M_{test}}, S^{1:100}_{C_{test}}\}$. To do this, I combined all test data collected by executing the lateral ($S^{1:100}_{L_{test}}$), medial ($S^{1:100}_{M_{test}}$), and circular ($S^{1:100}_{C_{test}}$) sliding actions (300 samples in total). Afterwards, 100 samples were

selected uniformly at random from the combined data set $S_{LMC_{test}}^{1:100} \in \{S_{L_{test}}^{1:100}, S_{M_{test}}^{1:100}, S_{C_{test}}^{1:100}\}$. The constructed texture models were then evaluated to predicting test samples in $S_{LMC_{test}}^{1:100}$. Fig. 3.9 shows that the Shadow Hand obtained 96% discrimination accuracy with 15 trials with the lateral and medial exploratory actions, which is slightly lower than when it was evaluated with the test data collected either with lateral ($S_{L_{test}}^{1:100}$) or medial ($S_{M_{test}}^{1:100}$) sliding movement. Moreover, Fig. 3.9 illustrates that the robotic hand successfully achieved 100% classification accuracy with 7 training samples with circular sliding motion. This is due to the fact that some of the experimental materials, such as carpets and textiles, have multidirectional textures. In this case the circular sliding motion provide rich tactile information in all directions (X-Y direction). In other words, the circular exploratory action helped the robot to learn about the textural properties of the materials with a few samples and quicker than when it explores the materials with either medial or lateral sliding motion. However, the robotic system receiving a few more training samples achieved the same recognition performance as obtained with the circular sliding motion. In another experiment, the PA algorithm sequentially received 20 training samples that were obtained by the robot during performing the combined exploratory action ($S_{train}^{comb} = S_{LMC}$) on the surface of the materials. The constructed texture models at each time t were evaluated to predicting the test data collected with different combination of the exploratory actions $S_{test}^{comb} \in \{S_L, S_M, S_C, S_{LMC}, S_{LCM}, S_{MLC}, S_{MCL}, S_{CLM}, S_{CML}\}$. The combination of lateral, medial, and circular motions as one motion, (S_{train}^{comb}) provided the richest tactile information with the robotic hand. In this case the Shadow Hand achieved 100% classification accuracy with only 6 training samples. Let us consider the circular exploratory movement as the combination of the lateral and medial movements. Then, the combined exploratory motion is the combination of two times lateral movements and two times medial movements. Therefore, at each time, it provides more tactile information with the robotic hand at each exploration.

3.7.1.3. Supervised In-hand object discrimination

This experiment scrutinized whether the tactile in-hand object recognition performance depends only on how well and robustly the robotic hand could interpret the perceived tactile surface texture information of the held objects regardless of their shapes. The Shadow Hand should be able to discriminate in-hand objects via their textural properties without considering the geometrical properties of the in-hand objects (proprioceptive information) while moving its fingers slightly on the surface of in-hand objects. To evaluate this capability, the Shadow Hand used the SVM with the linear kernel method. To construct the tactile learning models, the SVM with the optimal learning parameters was trained by tactile features generated from

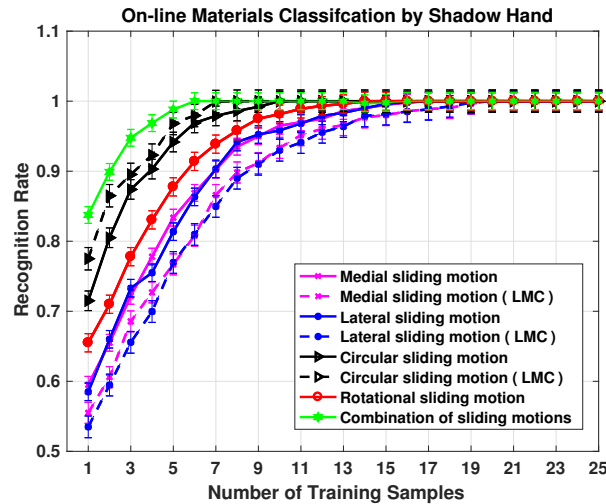


FIGURE 3.9. Results of On-line Material Classification by the Shadow Hand

the collected training set with uniform shaped objects (see Fig. 3.6). The constructed tactile models were then evaluated to predict the corresponding test set. The learning procedure was repeated with training and test sets of the complex shape objects (see Fig. 3.7). Table 3.3 shows the Shadow Hand classified in-hand objects with uniform shapes from each other via their texture properties with 98.5% recognition accuracy. Moreover, it discriminated among in-hand complex shape objects with 98.7% recognition accuracy.

Furthermore, an additional experiment was carried out. The Shadow Hand was trained with the combined training sets of uniform and complex shape objects. Using constructed tactile object models, the robot successfully distinguished 30 multiple shape in-hand objects from each other with 98.3% recognition accuracy. Table 3.3 illustrates that using the proposed robust tactile descriptors, the Shadow Hand successfully classified in-hand objects with multiple shapes via their textural properties (cutaneous information) regardless of their shapes (proprioceptive information) similar to humans.

3.7.1.4. On-line In-hand objects discrimination

In this experiment, the Shadow Hand used the on-line PA algorithm. The same learning procedure as described before were performed with each of trial samples of the identical shape, complex shape, and multiple shape in-hand objects separately. The constructed texture models at each time step ($t = 1, \dots, 20$) were evaluated using entire corresponding test sets. Fig. 3.10 shows the classification accuracy rate corresponding to Identical Shape Objects, Complex Shape Objects, and Multiple Shape Objects. The experimental outcomes (see Fig. 3.10) show that the Shadow Hand successfully recognized identical, complex, and multiple shape objects

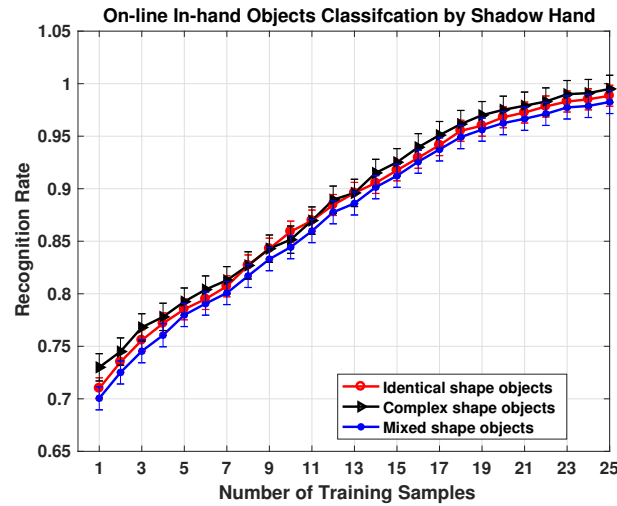


FIGURE 3.10. Results of On-line In-Hand Objects Classification by Shadow Hand

In-Hand Objects	Training with	Test with	SVM
Identical Shape Objects	Index finger	Thumb	98.5%
Complex Shape Objects	&	&	98.7%
Mixed Shape Objects	Middle finger	Index finger	98.3%

TABLE 3.3. In-Hand objects classification with SVM by Shadow Hand. The best regularizer value that was found by CV for all experiments is $C = 0.003$.

via their surface textures with a high average recognition rate substantially better than chance. The robotic hand achieved an average recognition rate of 96% with only 20 training samples online. Fig. 3.10 illustrates that the Shadow Hand, when receiving a few samples in sequence ($t = 21, \dots, 25$) could achieved 100% recognition rate.

3.7.1.5. Unsupervised materials and In-hand objects categorization

In this experiment, the robotic systems employed the EM algorithm as an unsupervised learning approach to categorize materials/objects via their textural properties. In this way, the EM was trained with the entire unsupervised data set in all scenarios. The EM algorithm was initialized by the k-means clustering. The number of cluster k was set to be equal to the number of class of the experimental materials or objects. The k-means algorithm was repeated 20 times at each time and the EM algorithm iterated 100 times. The Normalized Mutual Information (NMI) was used to evaluate the clustering results. Table (3.4) shows that the Shadow Hand successfully categorized among the experimental materials and clustered the in-hand objects via their textural properties in all schemes. The discrimination performance of In-hand object

in all scenarios is a bit lower than the performance of materials classification. The reduction in accuracy for in hand object discrimination is due to the variations in the contact positions occurred during exploration as there was no active slip detection and prevention method implemented in the robotic hand.

Exploratory Behavior	NMI
Lateral sliding motion	0.92
Medial sliding motion	0.91
Circular sliding motion	0.92
Combination of Lateral, Medial, and Circular sliding motions	0.95
Rotational sliding	0.93
In-hand Identical Shape Objects	0.87
In-hand Complex Shape Objects	0.84
In-hand Mixed Shape Objects	0.85

TABLE 3.4. Results of Materials and In-hand Objects Categorization by the Shadow Hand.

3.7.2. Experimental results with NAO

3.7.2.1. Supervised Material Discrimination

NAO used the SVM to classify 120 materials via their textural properties. In order to construct learning models, the SVM with the optimal learning parameters was trained with the training data (collected with the right hand). The constructed learning models then was evaluated to predict the test data (collected with the left hand). Table 3.5 shows that NAO classified 120 materials with higher than 97% accuracy in all schemes.

3.7.2.2. Supervised large object discrimination

The main goal of this experiment was to evaluate the performance of the proposed tactile descriptor while extracting tactile features from a large number of tactile sensors (a large skin area). The other goal was to investigate if discrimination of objects along surface texture properties is independent of an object's weight during the passive exploration. The velocity of an object sliding between NAO's arms and chest relates directly to the object's weight, any variation in the object's weight should not affect on texture perception. In other words, NAO should recognize large objects sliding between its arms and chest (passive exploration) via their textural properties regardless of their weights.

In this regard, SVM was trained with a training set collected with objects having the same 1000g weight and 120 various surface textures. The constructed texture models were examined using test sets including objects with 500g and 1500g weights. Table 3.6 that shows NAO successfully classified large objects with 90.6% recognition accuracy.

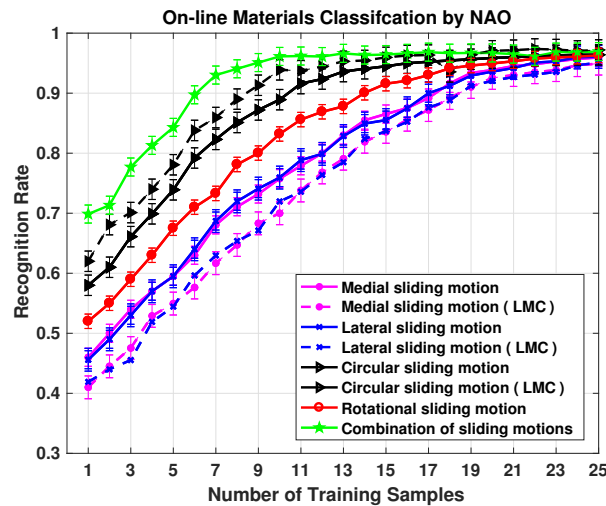


FIGURE 3.11. Results of On-line Material Texture Classification by NAO

In order to assess the efficiency of the proposed tactile descriptors across various objects' weights, the experiment was repeated with different training and test sets. In this regards, NAO was trained with a training set of the large objects with $500g$ and then examined using test sets including objects with $1000g$ and $1500g$ and 120 different textures. The same procedure was performed with training sets of objects of $1500g$ and test set of objects of $500g$ and $1000g$. The final experiment in this context was conducted with a training set of objects of $500g$, $1000g$, and $1500g$, and the robot learning system was evaluated using an unseen test set separately collected with objects of $500g$, $1000g$, and $1500g$.

Table 3.6 demonstrates the classification performance in which NAO discriminated 120 large objects through their surface properties regardless of any variation in objects' weights during the experiment. Objects with various weights but the same surface texture properties tend to be recognize as same class of object. The reduction in discrimination performance is due to some variation with the position of the large object during sliding between the robot's arms and chest.

Exploratory Behavior	Training with	Test with	SVM
Lateral sliding	Right Hand	Left Hand	97.1%
Medial sliding			97.3%
Circular sliding			98.2%
Combination of Lateral, Medial, and Circular			98.5%
Rotational sliding			97.9%

TABLE 3.5. Surface textures classification by NAO. The best regularizer value that was found by CV for all experiments is $C = 0.005$.

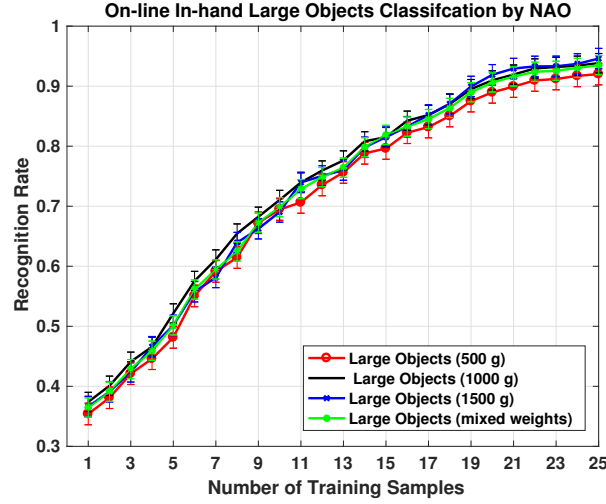


FIGURE 3.12. Results of On-line Large objects Classification by NAO

3.7.2.3. On-line material discrimination

NAO used the PA algorithm in order to learn about textural properties of 120 materials on-line. The same learning procedure as described before was performed with the training and test data. Fig. 3.11 displays that NAO obtained higher than 93% recognition with each of the exploratory movements with only 20 training samples. Moreover, NAO with circular exploratory movement and 10 training samples ($t = 10$) obtained 90% classification accuracy.

Furthermore, the performance of the materials exploration with each of the lateral, medial, and circular sliding movements was separately evaluated with the combination of all test data ($S_{LMC_{test}}^{1:100}$). Fig. 3.11 illustrates that NAO achieved 93% classification accuracy with 24 training sample using either lateral or medial exploratory action. As a result, the humanoid obtained 90% recognition rate with only 9 training samples. Fig. 3.11 also displays that NAO obtained 95% recognition rate when it received 10 trials with the combined exploratory movement ($S_{train}^{comb} = S_{LMC}$). The constructed texture models at each time t were evaluated to predicting the test data collected with different combination of the exploratory actions $S_{test}^{comb} \in \{S_L, S_M, S_C, S_{LMC}, S_{LCM}, S_{MLC}, S_{MCL}, S_{CLM}, S_{CML}\}$.

Large Objects	Training with	Test with	SVM
Large Objects with 500 g weight	Upper Body (large skin area)	Upper Body (large skin area)	90.6%
Large Objects with 1000 g weight			90.9%
Large Objects with 1500 g weight			91%
Large Objects with Mixed weight			90.5%

TABLE 3.6. Large objects discrimination with SVM by NAO. The best regularizer value that was found by CV for all experiments is $C = 0.003$.

Exploratory Behavior	NMI
Lateral sliding motion	0.88
Medial sliding motion	0.89
Circular sliding motion	0.91
Combination of Lateral, Medial, and Circular motions	0.93
Rotational sliding	0.92
In-hand Large Objects (500g)	0.81
In-hand Large Objects (100g)	0.83
In-hand Large Objects (1500g)	0.85
In-hand Large Objects (Mixed weights)	0.87

TABLE 3.7. Results of Materials Categorization by NAO.

3.7.2.4. On-line large objects discrimination

Fig. 3.12 shows that NAO successfully discriminated large objects using its large-scale skin with very high recognition rates online. The obtained classification performance is comparable with the performance NAO that achieved with the SVM (batch learning). However, using the on-line learning method the robot consumed much less memory to store data. This is due to the power of my proposed tactile descriptors which provided the robot with the rich tactile information.

3.7.3. Unsupervised materials and large objects categorization

The EM algorithm as an unsupervised learning approach was used to categorize materials and large objects via their textural properties. The same procedure as described before was performed with the entire unsupervised data collected by NAO. Table (3.7) shows that the NAO successfully clustered all 120 experimental materials and also 120 large objects via their textural properties in all schemes.

3.8. Summary and discussion

In order to evaluate the performance of my proposed tactile descriptors, I conducted an extensive experiment with multiple robotic systems, various tactile sensing technologies, and a large number of natural and synthetic objects and materials. In this experiment, the Shadow Hand and NAO with artificial skin successfully classified 120 various materials with regular and irregular structures while executing active human-like exploratory movements. The experiment was extended to the in-hand object discrimination, in which the robotic hand discriminated 30

uniform and complex shaped objects with regular and irregular textural properties. Moreover, the robustness and computational efficiency of the proposed descriptors were assessed with a humanoid and a large sensing area. The achieved high recognition rate by NAO shows that my tactile descriptors provided robust tactile information from the large number of tactile signals for discriminating among large objects via their surface texture regardless of their weight. The experimental results show that the Shadow Hand obtained higher tactile discrimination accuracy than NAO in all scenarios. It is due to the fact that the BioTac has high spatial resolution and the existing ridges on its outer layer help to better sense the textural properties of the objects/materials. The Cellular Skin used on NAO has a comparatively low spatial resolution. Although this was compensated by my proposed feature descriptors, which provided information-rich tactile features, reducing the size of the skin cells will increase the spatial resolution. Moreover, in order to increase the sensitivity of the Cellular Skin, I will consider to re-design its outer silicone layer and will add micro-ridges to it.

In all robot learning processes, the texture models constructed with the training samples, which were collected uniformly with all objects and materials. However, the information richness of training samples is different. For instance, some objects have discriminant textural properties that make them easy to discriminate from others. In the future, I will improve my tactile learning method to enable the robotic systems to efficiently collect training samples by strategically selecting objects and executing the exploratory actions. This tactile learning process can be further improved by enabling the robots to leverage the obtained prior tactile knowledge while actively learning new objects or materials via their textural properties (active tactile transfer learning).

CHAPTER 4

Active Pre-touch and Touch for Object Learning in an Unknown Workspace

Science is about knowing; engineering is about doing.

(Henry Petroski)

4.1. Introduction

In previous studies, researchers have used passive learning methods with pre-defined number of training samples in order to learn about objects via their physical properties (see Sec. (2.3)). However, the informativeness of training data obtained with each object is different. Some objects have discriminant tactile properties that make them easily to be identified from the others. Therefore, collecting too many training samples with these objects is redundant, whereas for objects, which are easily confused with each other due to their similar properties, it is necessary to collect sufficient numbers of samples to construct reliable and robust observation models. Moreover, in these studies, the location and orientation of the experimental objects in the workspace were known. To increase the autonomy of a robotic system during the tactile-based object learning, the robot should be able to autonomously explore unknown workspace, actively detect the number of objects as well as estimate their positions in the workspace. In this chapter, I propose a complete probabilistic tactile-based framework which consists of two parts: (I) an active pre-touch strategy to efficiently explore unknown workspaces; (II) an active learning algorithm to learn about objects' physical properties with the least number of training samples. Following the active pre-touch strategy, the robotic systems with multimodal artificial skin efficiently explore unknown workspaces in order to estimate the number of objects, their location, and their orientation. By taking advantage of my proposed robust tactile

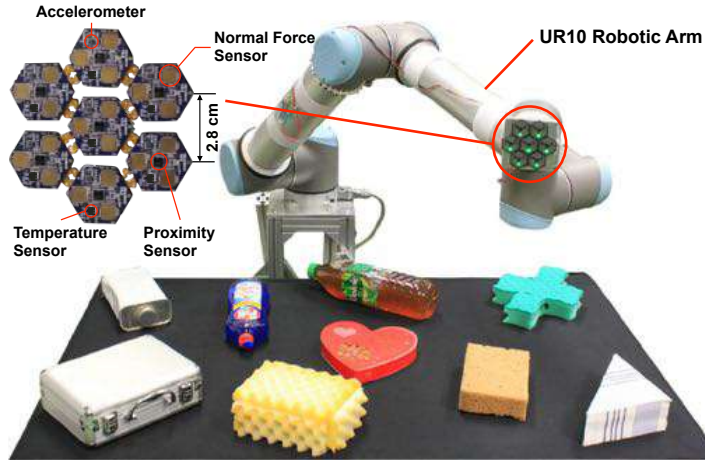


FIGURE 4.1. Experimental setup. The UR10 robotic arm mounted with the multi-modal artificial skin on its end-effector.

descriptors presented in chapter 3 and my probabilistic active tactile learning algorithm, the autonomous robots were able to learn about physical properties of the objects (such as surface texture, stiffness, and thermal conductivity) with the lowest possible number of samples by strategically selecting the next object to learn next physical property ¹.

4.2. Active pre-touch for workspace exploration

I propose an active pre-touch probabilistic approach for robotic systems with the proximity sensors to efficiently explore an unknown workspace. This method reduces the number of exploratory movements and measurements required to localize objects in the workspace. Then, the robot is able to estimate the number of objects, their poses, and their geometric centroids.

4.2.1. Problem Definition

The workspace W_{XYZ} is defined as a discretized 3D grid bounded by the reaching capabilities of the robot (see Fig. (4.3)). The artificial skin of the robot has an array of N_c proximity sensors with known locations $l_{1:N_c}^n$ with respect to the end-effector position l^n at each observation n . The sensor array outputs a set of measurements $z_{1:N_c}^n$. To take into account the non-linearities and the uncertainty associated with those measurements, I compute the distance d^n between the skin cells and the object as the probability $p(d^n | z_i^{1:n}, l^{1:n})$ (for i th proximity sensor given all previous measurements).

¹The content of this chapter has been published in [154], IEEE©

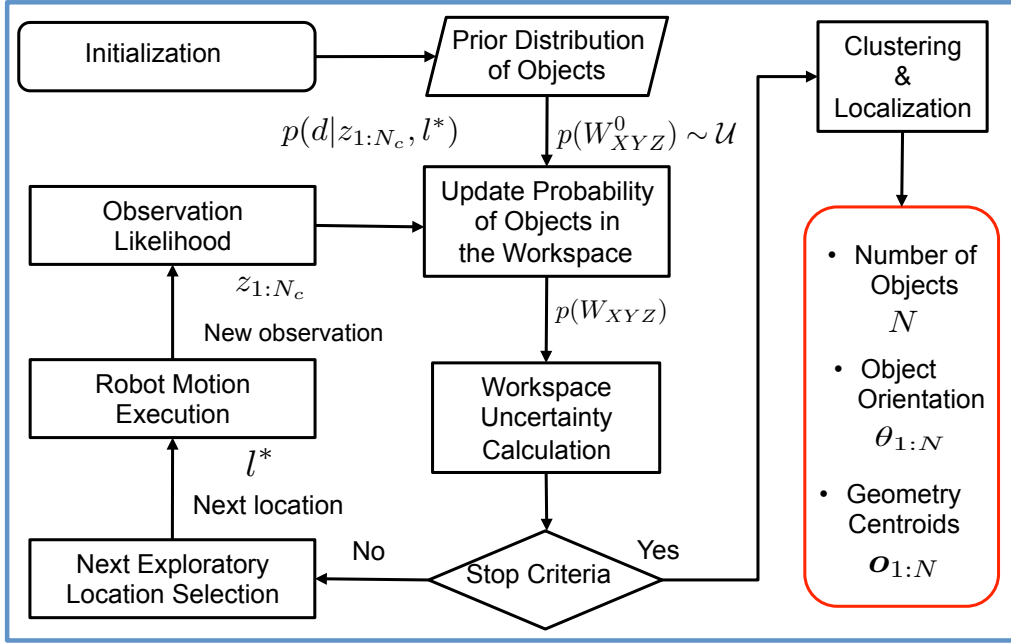


FIGURE 4.2. Proposed Active Pre-Touch Algorithm for Workspace Exploration.

Finally, I define $p(W_{XYZ}^n)$ as the probability of the presence of an object in every cell of the workspace at the n th observation. The initial $p(W_{XYZ}^0)$ is a uniform distribution that will be updated using the new measurements. I assume that the robot's end-effector is horizontal to the X-Y plane of the workspace.

4.2.2. Robotic system with multimodal robotic skin

In order to evaluate the performance of my proposed active pre-touch workspace exploration and active tactile object learning I mounted one skin patch (see Sec. (3.3.2)) on the end-effector of the 6-DoF industrial robot called UR10 (Universal Robots)². The skin patch consists of 7 skin cells including: 7 proximity sensors, 7 three-axis accelerometer sensors, 7 temperature sensors, and 21 normal-force sensors (see Fig. (4.1)). The information measured by the proximity sensors are used to explore the workspace. The normal force sensors are used to measure the stiffness of the objects. The textural properties of objects are sensed via accelerometers and force sensors.

²www.universal-robots.com

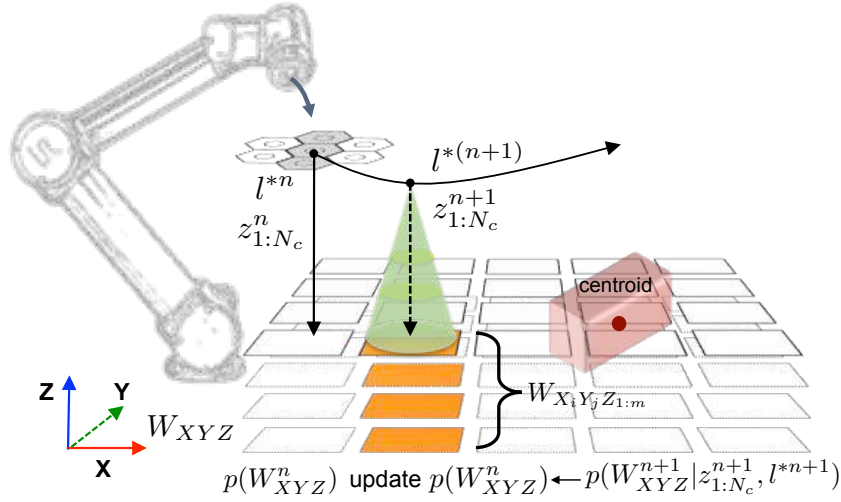


FIGURE 4.3. An illustration of active pre-touch process.

4.2.3. Methodology

First, the robot starts the exploration from a fixed location corresponding to a grid edge. Then, it generates a set of potential next end-effector locations $l^{n+1} \in L^{n+1}$, i.e., the centre of each neighbouring grid cell. Afterwards, it selects the one that maximizes the probability of detecting an object. The robot performs the next movement and uses the new sensor measurements $z_{1:N_c}^n$ to update $p(W_{XYZ}^n)$. This process will be iteratively executed until the robot is certain about the workspace, e.g., the entropy of $p(W_{XYZ}^n)$ is below 1%. In order to fuse the measurements taken from all sensors of the array I assume that their readings are independent of each other. The joint probability distribution is given by:

$$p(d^n | z_{1:N_c}^{1:n}, l^{1:n}) \propto \prod_{i=1}^{N_c} p(z_i^n | l^n, d^n) p(d^{n-1} | z^{1:n-1}, l^{1:n-1}) \quad (4.1)$$

Where $p(z_i^n | l^n, d^n)$ is the likelihood of having measurement z_i^n given that the object is at distance d^n and the end-effector is at l^n . This is obtained experimentally (see 4.5.2.1). As the end-effector is moving on X-Y plane, d^n corresponds to the cells of $W_{X_i Y_j Z_{1:m}}$, where i and j are defined by the end-effector's location l^n and $Z_{1:m}$ are the cells below l^n (m is the number of cells in Z direction, the orange colored cells in Fig. (4.3)).

4.2.3.1. Selection of the next exploratory location

In order to compute the next best location l^{*n+1} of the end-effector, I employ a method based on [155] proposed for air vehicles with radar, which in this study I modified it to be used with an array of proximity sensors. Considering that the end-effector is moving on X-Y plane, I define the current estimate of the 2D workspace as $p(W_{XY}^n)$. The best next end-effector location l^{*n+1} is the one that maximizes the probability of detecting an object in the workspace:

$$l^{*n+1} = \arg \max_{l^{n+1} \in L^{n+1}} \sum_{W_{XY}} p(z_{1:N_c}^{n+1} = D|l^{n+1}, W_{XY}^{n+1}) p(W_{XY}^n) \quad (4.2)$$

where $p(z_{1:N_c}^{n+1} = D|l^{n+1}, W_{XY}^{n+1})$ is the probability of detecting an object given the next location l^{n+1} , which for every proximity sensor i (for the skin patch $i = 1, \dots, 7$) is modelled using the following exponential function:

$$p(z_i^{n+1} = D|l^{n+1}, W_{XY}^{n+1}) = P_{max} e^{-\sigma \left(\frac{\|l^{n+1} - W_{X_i Y_j}^n\|}{d_{max}} \right)^2} \quad (4.3)$$

where $\|\cdot\|$ is the Euclidean distance and $W_{X_i Y_j}$ defines the center position of each grid cell in X-Y plane. $P_{max} \in (0, 1)$ (in this study $P_{max} = 0.9$) is the maximum probability of detecting an object with the proximity sensor, and d_{max} ($d_{max} = 5$ cm) and σ ($\sigma = 0.6$) shape the maximum coverage of the sensor cone in the workspace grid (green cone in Fig. 4.3). In order to update $p(W_{XY}^n)$, via recursive Bayesian estimation, I assume that the observations $z_{1:N_c}^n$ are "non-object detection" (Fig. 4.3).

4.2.3.2. Estimation of number of object and their geometry centroids

First, the final $p(W_{XYZ}^n)$ is thresholded (e.g. 0.9 probability) obtaining a binary 3D matrix where 0 is a no-object and 1 is an object. Then, I estimate the number of objects k using a three dimensional connected-labelling algorithm and removing the small clusters (one grid cell) that are unconnected regions of objects. The cells are considered connected if they are adjacent following the 26-connected neighborhood pattern. In order to include all the occupied regions and not only the connected ones, the number of objects found is used to initialize the k-means algorithm that computes the 3D bounding box of each object. Finally, the pose and the geometric centroid of each object are extracted by means of its bounding box.

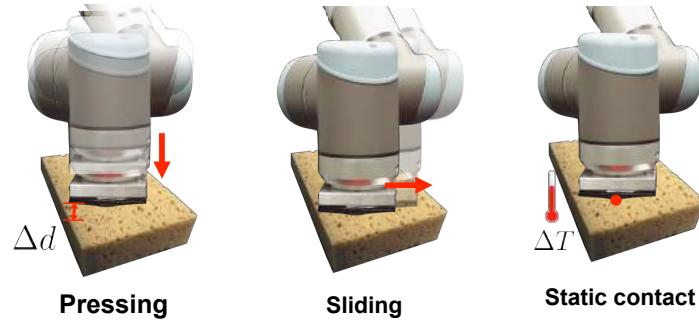


FIGURE 4.4. Exploratory actions: pressing, sliding, and static contact

4.3. Objects' physical properties perception

A robotic system with the sense of touch needs to execute various exploratory actions on the objects to perceive their physical properties as a human does. For instance, a robot slides its sensitive area on the object's surface to sense its textural property, presses on an object to measure its stiffness, and performs static contact with an object to estimate its thermal conductivity.

4.3.0.1. Stiffness estimation

The robot measures the stiffness of an object by pressing on the object (see Fig. 4.4). To do this, UR10 with artificial skin on its end-effector first establishes a light contact with the objects. The light contact is detected as soon as the measured normal force averaged over all sensors F_{av} exceeds a threshold f_ϵ , i.e. $F_{av} > f_\epsilon$ ($N_c = 7$ is the number of skin cell and $N_r = 3$ is the number of normal force sensors in each skin cell).

$$F_{av} = \frac{1}{N_c N_r} \sum_{n_c=1}^{N_c} \sum_{n_r=1}^{N_r} F_{n_c, n_r} \quad (4.4)$$

Afterwards, the UR10 with its sensitive end-effector presses the top surface of the object. For all normal force sensors F_{n_c, n_r} , the difference between the forces recorded before and after pressing ($\Delta F_{n_c, n_r}$) is used as an indication of the stiffness on the local contact area. The averaged difference value over all force sensors serves as a measurement of stiffness of the object which can be formally written as:

$$\mathcal{S} = \frac{1}{N_c N_r} \sum_{n_c=1}^{N_c} \sum_{n_r=1}^{N_r} \Delta F_{n_c, n_r}. \quad (4.5)$$

4.3.0.2. Thermal conductivity measurement

A robotic system with tactile sensing can identify objects through thermal cues by applying static contact on them. When measuring the object's thermal conductivity, the robot contacts its sensitive part with the object surface for a certain time period $t_{contact}$, during which the average temperature time series of the contacted area is recorded by temperature sensors:

$$T_{total} = \left\{ \frac{1}{N_c N_T} \sum_{n_c=1}^{N_c} \sum_{n_T=1}^{N_T} T_{n_c, n_T}^i \right\}_{i=1}^{t_{contact}} \quad (4.6)$$

where N_T is the number of temperature sensors in each skin cell, and T_{n_c, n_T} represents the recordings of a temperature sensor. The final thermal feature (TF) is the combination of the average temperature time series and its gradient at each time step $TF = [T_{total}, \Delta T_{total}]$. I reduce the dimension of TF vector to 10 dimensions via Principle Component Analysis (PCA) method which was then used as the final thermal conductivity feature vector of each object.

4.3.0.3. Textural properties perception

To perceive textural properties of objects, the robotic system equipped with the artificial skin slides its sensitive part on the surface of objects. The vibrations generated during the sliding movement are measured by the three-axis accelerometer in each skin cell. The proposed tactile feature descriptors described in Sec. (3.4.2) used to extract the robust tactile information from the output of each axis of accelerometer sensors ($a_{n_c, n_s}^x, a_{n_c, n_s}^y, a_{n_c, n_s}^z$) and force sensors (\mathbf{F}_{n_c, n_r}). The robust tactile feature was extracted by Eq.(4.7).

$$\mathbf{D}^{UR10} = [\mathbf{A}_a; \mathbf{M}_a; \mathbf{C}_a; \mathbf{L}_a; \mathbf{N}_a; \mathbf{A}_F; \mathbf{M}_F; \mathbf{C}_F; \mathbf{L}_F; \mathbf{N}_F] . \quad (4.7)$$

In this experiment $N_c = 7$ is the number of the skin cell. $N_s = 1$, and $N_r = 3$ are the number of existing three-axis accelerometers and force sensors in one skin cell, respectively.

4.4. Active touch for physical properties learning (AT-PPL)

In this section, I describe my proposed probabilistic method for active tactile object learning (see Fig.4.5). My proposed algorithm enables a robotic system to efficiently learn about objects via their physical properties and to correspondingly construct the observation models of the objects. I start with formalizing the active tactile learning problem. Then, I describe in detail my proposed algorithm called Active Touch for Learning Physical Properties (AT-PPL).

4.4.1. Problem definition

Suppose that there are N objects ($\mathcal{C} = \{c_i\}_{i=1}^N$) in the workspace with the known poses. I denote the physical properties of objects by $\mathcal{K} = \{k_j\}_{j=1}^K$. These objects may have similar physical properties, for instance similar surface textures, while some might have quite different properties, such as different stiffness and thermal conductivity. In this scenario, the task of the robot is to efficiently learn about objects by means of their physical properties with as few training samples as possible and to efficiently construct the reliable observation models of the objects. Since the objects with the similar properties cannot be easily distinguished from each other, the robot should autonomously collect more training samples with these objects. The active tactile learning problem is formulated as a standard supervised learning problem for multi-class classification, where each object is regarded as a class; for each tactile property, a probabilistic classifier is efficiently constructed by iteratively selecting the *next object to explore* and the *next physical property to learn*, in order to collect the next training sample. In my proposed active learning algorithm the one versus all (OVA) Gaussian Process Classifier (GPC) is employed to construct observation models of objects. GPC trains the function $\mathcal{X} \xrightarrow{f} \mathcal{Y}$, where \mathcal{X} is the observation set and \mathcal{Y} is the target set which contains integers indicating the labels of the input data, $\mathcal{Y} = \{1, 2, 3, \dots, N\}$. Given a new sample \mathbf{x}^* , the observation probability of a class $p(y|\mathbf{x}^*)$ can be estimated by $f(\mathbf{x}^*)$. In this paper I used the radius basis function RBF kernel [156] as the covariance function.

4.4.2. Methodology

The robot starts the learning process by building a training dataset with a small number of samples ($\mathcal{T} = \{\mathcal{T}_{k_j}\}_{j=1}^K$, where k_j represents a physical property of objects). Then the robot iteratively collects new training data. At each iteration, the AT-PPL algorithm updates GPCs with the training data set collected thus far, and estimates the uncertainty in the constructed observation models (classification competence estimation) which guide to next round of tactile data collection. Using AT-PPL the robot enlarges the training dataset by greedily sampling the

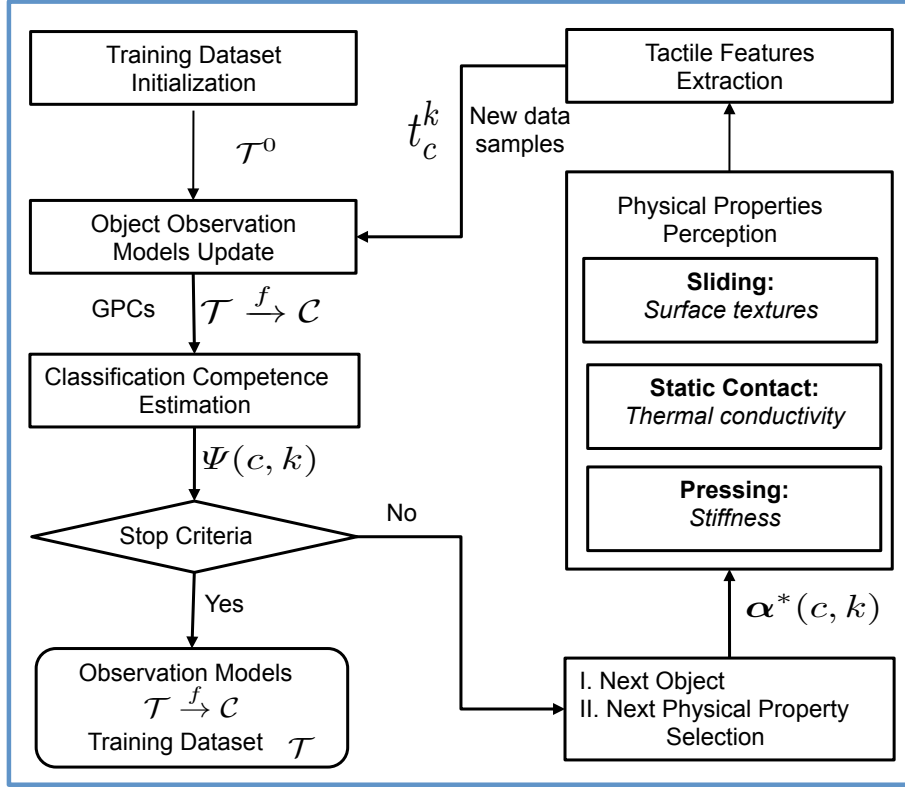


FIGURE 4.5. Proposed Active Touch for Learning about Objects via their Physical Properties (AT-PPL).

next object and the next property which may bring the largest improvement to the performance of GPCs. The learning process is repeated until a target criteria is satisfied, in my case, when there is no improvement of the uncertainty of GPCs. Finally, the robotic system constructs reliable observation models of the objects by using the efficiently collected training dataset. In order to estimate the GPCs competence, AT-PPL measures the Shannon entropy of each training sample $\mathbf{t} \in \mathcal{T}$: $\mathcal{H}(c|\mathbf{t}) = -\sum_{c \in \mathcal{C}} p(c|\mathbf{t}) \log(p(c|\mathbf{t}))$. Then the training dataset of one property \mathcal{T}_k will be divided into categories $\mathcal{T}_k = \{\mathcal{T}_{c_i}^k\}_{i=1}^N$, in which \mathcal{T}_c^k contains N_c^k number of samples. The GPCs competence $\Psi(c, k)$ is estimated as the mean value of the Shannon entropy:

$$\Psi(c, k) = \frac{1}{N_c^k} \sum_{\mathbf{t}_c^k \in \mathcal{T}_c^k} \mathcal{H}(c|\mathbf{t}_c^k). \quad (4.8)$$

Higher the $\Psi(c, k)$ is, more uncertain the robot is about the object.

4.4.2.1. Next object to explore and next physical property to learn

Let us define the object-property pair, $\alpha(c, k)$ as a function of the object c ($\mathcal{C} = \{c_i\}_{i=1}^N$) and physical property $k \in \{\text{texture, stiffness, thermal conductivity}\}$ ($\mathcal{T} = \{\mathcal{T}_{k_j}\}_{j=1}^3$). After selecting $\alpha(c, k)$, the robot moves to the object c and executes the corresponding exploratory action to perceive the physical property k . In order to learn about objects efficiently, the robot can greedily sample the next object and the next property which maximize $\Psi(c, k)$ of GPCs (exploitation). In order to avoid being trapped in the local maxima, I added an exploration rate so that the robot can randomly select $\alpha(c, k)$ by following the uniform distribution (exploration). I denote p_α as a probability, which is uniformly generated at each iteration in the AT-PPL. Then the next object c^* and next physical property s^* is determined by:

$$\alpha^*(c, k) = \begin{cases} \arg \max_{c_i \in \mathcal{C}, k_j \in \mathcal{K}} \Psi(c_i, k_j), & \text{if } p_\alpha > \epsilon_\alpha \\ c = \mathcal{U}\{c_1, c_2, \dots, c_N\}, k = \mathcal{U}\{k_1, k_2, k_3\}, & \text{otherwise} \end{cases} \quad (4.9)$$

where ϵ_α is the parameter to control the exploration-exploitation trade-off.

4.5. Experimental results

In order to evaluate in real time the performance of my proposed framework which consists of active pre-touch and active touch, I designed two experimental scenarios. In the first scenario, the robotic system was asked to autonomously and efficiently learn about the experimental objects based on their physical properties (stiffness, surface textures, and thermal conductivity). In the second scenario, the task of the robot was to actively discriminate among objects, taking advantage of the prior knowledge of the objects obtained during the active learning process. In both scenarios, the workspace was unknown, and the robot had no knowledge about the number of objects and their positions in it. It is noteworthy to mention that I arbitrarily changed the light intensity when conducting the experiments, in order to show that my framework works well under different light conditions (please watch the video to this study).










S: --	T: +	C: --	S: --	T: ++	C: --	S: +	T: --	C: ++
 Sponge			 Soft sponge			 Toolbox		
S: O	T: ++	C: O	S: O	T: --	C: O	S: -	T: O	C: +
 Ice-tea bottle			 Tableware detergent			 Chocolate box		
S: O	T: +	C: -	S: +	T: --	C: +	S: ++	T: O	C: +
 Damp sponge			 Metal bottle			 Toy block		

FIGURE 4.6. Experimental objects. The physical properties are evaluated subjectively by human subjects and are indicated in the panel to the upper right of each object (S: stiffness, T: roughness of surface textures, C: thermal conductivity. ++: very high; +: high; O: middle; -:low; --: very low).

4.5.1. Properties of experimental objects

To assess my proposed framework, I deliberately selected nine objects with different materials (glass, metal, cardboard, and plastic) with regular and irregular textures, and various shapes (triangular, rectangular, cross, and heart shape) (Fig. 4.6). The physical properties of the objects varied from relatively similar to quite different.

4.5.2. Active learning about objects' physical properties

In the first scenario, the robotic system used my proposed active pre-touch method to efficiently explore the unknown workspace. Then, it actively learned about objects by means of their physical properties.

4.5.2.1. Active Pre-touch for Workspace Exploration

Fig. (4.8) illustrates the workspace, which is a cuboid of $110cm \times 64cm \times 10cm$ ($L \times W \times H$). A corresponding Cartesian coordinate frame (world coordinate frame) was defined along its length edge (X-axis), width edge (Y-axis), and height edge (Z-axis). This workspace was discretized into $27 \times 24 \times 10$ grid cells. The likelihood of the proximity sensors $p(z_i^n | l^n, d^n)$ was modelled as a Gaussian distribution $\mathcal{N}(\mu, \sigma)$ at each discretized distance

$$d = [5, 4, 3, 2, 1.5, 1, 0.8, 0.5, 0.2, 0]cm, \text{ in which}$$

$$\mu = [0.008, 0.015, 0.028, 0.065, 0.11, 0.25, 0.38, 0.76, 0.93, 0.98],$$

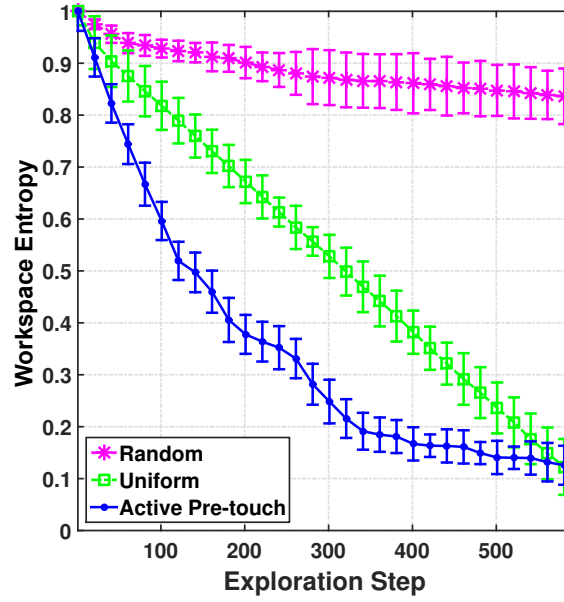


FIGURE 4.7. Statistical evaluation of the active pre-touch method with random and uniform strategies. The horizontal axis shows the number of movements the robot has when exploring the workspace. The vertical axis shows the Shannon entropy in the workspace.

$\sigma = [0.03, 0.04, 0.06, 0.1, 0.28, 0.7, 1.2, 1.6, 0.18, 0.09] \cdot 10^{-1}$. During the exploration, the sensor array (the end-effector of the robot) was held at the maximum height of the workspace and horizontal to the X-Y plane. The performance of my proposed active pre-touch method was compared with the random and uniform strategies which served as baselines. Using the random pre-touch exploration strategy, at each exploration step, the robot randomly selects the next location by following the uniform distribution. I calculated the grid entropy to measure the uncertainty of the workspace during the exploration. To perform the statistical study, each strategy was repeated 10 times. In each experiment the maximum number of robot movements was set to 600. Fig. (4.7) illustrates that using the proposed active pre-touch strategy, the robot reduced its uncertainty about the workspace drastically compared to random and uniform approaches. This is due to the fact that with my proposed method, the robot explored the locations with the higher probability of observing an object. Fig. (4.8) illustrates the results of workspace exploration after 300 steps. Fig. (4.8-B) shows that using my active pre-touch strategy, all of the nine objects were successfully clustered and localized, whereas uniform and random strategies suffered from insufficient exploration of the workspace, yielding either wrong determination of the objects' number or wrong geometry estimation Fig. (4.8-C) and (4.8-D).

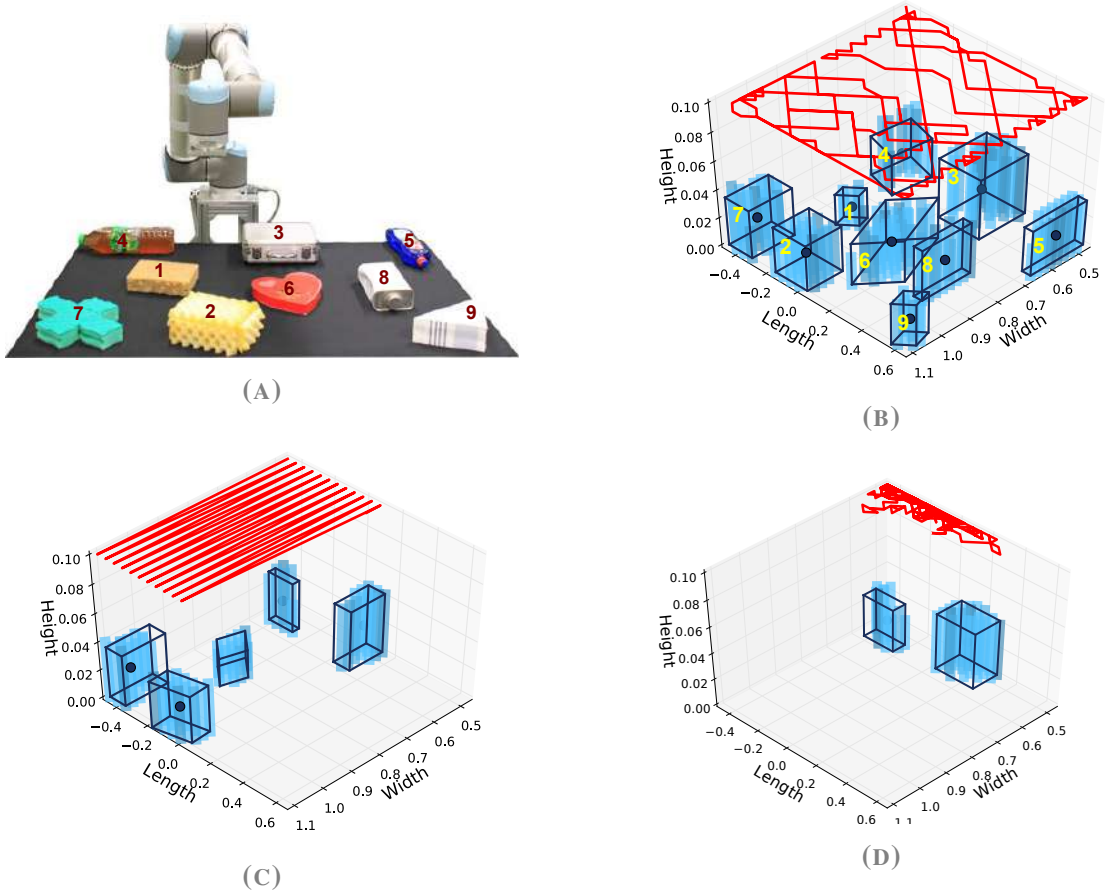


FIGURE 4.8. (A) The unknown workspace which the robot explored. (B)-(D): Trajectories of the robot's end-effector during the exploration of the workspace and the localization results using three methods. (B): Active pre-touch strategy. (C): Uniform strategy. (D): Random strategy. (E): Statistical evaluation of the active pre-touch method with random and uniform strategies. The horizontal axis shows the number of movements the robot has when exploring the workspace. The vertical axis shows the Shannon entropy in the workspace.

4.5.2.2. Active touch for learning physical properties

4.5.2.3. Test Data Collection

I evaluated my proposed active learning algorithm with a test database, which was constructed automatically by the robot by performing the three exploratory movements 20 times on each object (pressing, sliding, and static contact). The robot started each exploratory action with light contact with the objects, with the minimum stable contact force that can be measured by the artificial skin ($F_{av} = 0.05N$). The pressing movement consisted of pressing the end-effector with skin cells $2mm$ on the surface of the objects and measuring the total normal force for $3s$. For sliding, the robot slid its artificial skin on the surface of the objects with the constant velocity of $1cm/s$ for $3cm$. To measure the thermal conductivity of objects, the

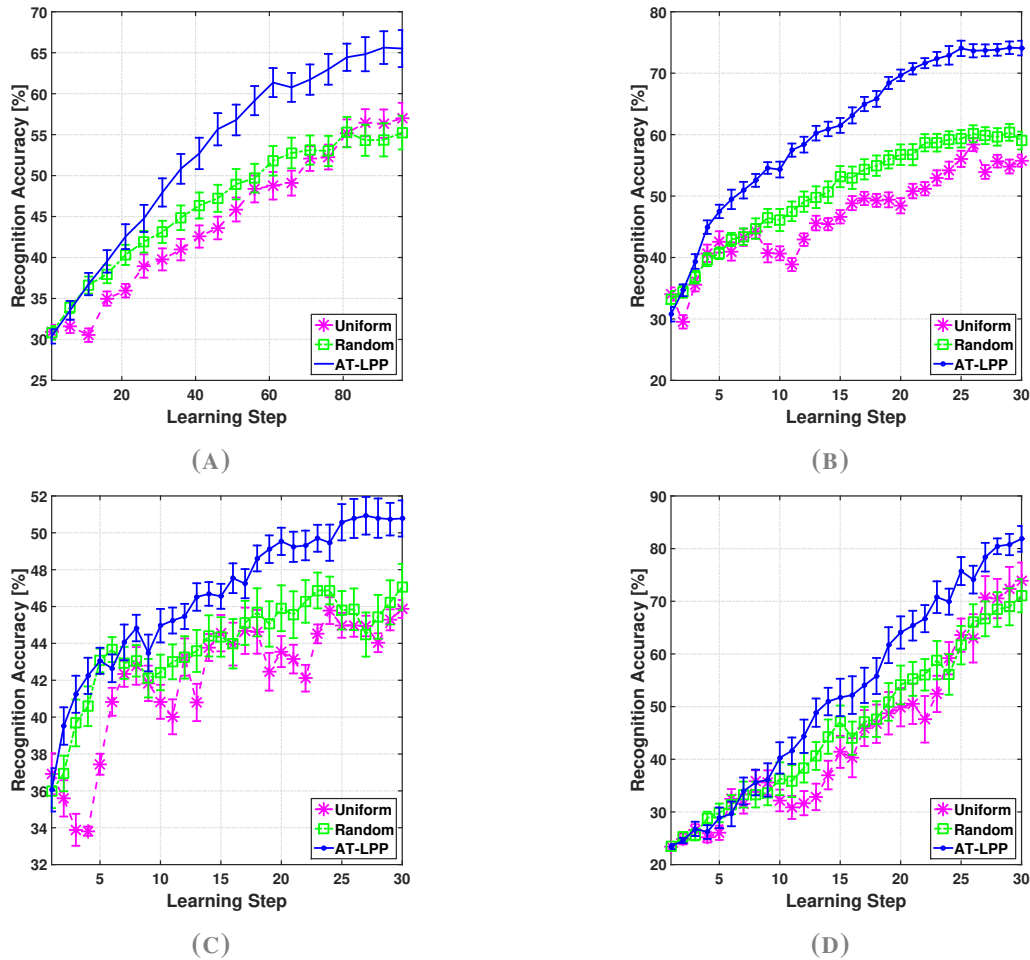


FIGURE 4.9. (A): Evaluation of AT-PPL with three physical properties (stiffness, surface textures, and thermal conductivity). (B)-(D): Evaluation of AT-PPL by learning about the experimental objects via one physical property (B): Surface textures. (C): Stiffness. (D): Thermal conductivity. The horizontal axis represents the learning steps (at each step a new training sample is collected), and the vertical axis represents the value of recognition accuracy on the test dataset averaged over 30 runs.

robot made a static contact with the objects, including a light contact and pressing its sensitive part 1mm on the the surface for 15s . Then robot raised its end-effector for 30s in order to restore the sensors to ambient temperature. In this way the artificial skin had a similar initial temperature condition in all trials.

4.5.2.4. Active learning about objects via three physical properties

To initialize the active learning process, the robot collected small training samples by performing each of three exploratory actions once on each object. Each step when the robot sampled a new training instance, the recognition accuracy of GPCs was measured with the test dataset. The performance of the AT-PPL was compared with the random and uniform strategy. In this regard, the entire experiment was repeated 30 times using each approach. Fig. (4.9) shows

that AT-PPL consistently outperforms the other methods by obtaining the same recognition accuracy with fewer training samples. For instance, the robot had in average 50% fewer training samples compared to the other methods, when the recognition accuracy reached 55% (see Fig. (4.9-A)). Therefore, the robot following AT-PPL method can construct reliable observation models of objects with efficient training samples.

4.5.2.5. Active Learning about Objects via One Physical Property

In order to assess further the performance of the AT-PPL algorithm, the robot was additionally asked to learn about objects via one of the three tactile properties individually. Fig. (4.9-B), (4.9-C), and (4.9-D) indicate that the learning progress was dependent on the distributions of the extracted features of the physical properties. Fig. (4.9-C) shows that learning about objects via their stiffness is more difficult, whereas the learning process for object surface texture and thermal conductivity were faster and resulted in higher recognition accuracy (see Fig. (4.9-A) and (4.9-D)). In all three cases, AT-PPL performs better than random and uniform methods. It can be concluded that using my proposed method (AT-PPL), the robot can efficiently learn about objects even with one modality of its artificial skin.

4.6. Summary

In this chapter, my proposed a probabilistic tactile-based framework consisting of active pre-touch and active touch methods for robotic systems with multi-modal artificial skin. Using my proposed framework, the robot performed a complete series of tasks, i.e., the exploration of unknown workspaces based on active pre-touch approach, active touch-based learning of object's physical properties, and the active object discrimination task. The effectiveness of my proposed framework was evaluated through online experiments and statistical analysis. Results show that the framework outperforms baseline uniform and random strategies in all the tasks. The active pre-touch strategy presents a maximum entropy reduction of 30%, and 70% compared to uniform and random respectively, as well as achieving better estimation of the objects poses. The active touch learning provides high recognition accuracy with fewer samples, reaching 50% of fewer samples than the baseline strategies. Due to the low spatial resolution provided by the proximity sensors on the artificial skin array, objects which are close to each other in the workspace can hardly be clustered after the exploration. In order to tackle this problem, the spacial resolution of the sensor array can be increased by fusing the proximity information and force signals while contacting the objects.

CHAPTER 5

Active Touch for IObject Discrimination and Target Object Search

Statistics is the grammar of science.

(Karl Pearson)

5.1. Introduction

In the previous chapter, I introduced an active touch strategy to enable robotic systems to strategically learn about physical properties of the object. In this regard, the robots with small numbers of training data constructed a reliable observation models using the Gaussian process for stiffness, surface texture, and thermal conductivity. In this chapter, I propose an active tactile object discrimination method and an active target object search strategy. By taking advantage of the constructed observation models via my proposed active tactile learning method, the robotic system can efficiently discriminate among objects and search for specified target objects by strategically selecting the optimal exploratory actions to apply on objects to perceive the corresponding physical property (sliding to sense textural properties, pressing to measure stiffness, lifting to determine center of mass) in an unknown workspace. My proposed probabilistic touch-based framework consists of four parts: (I) an active touch approach for exploring the unknown workspace (Fig. (5.2)), (II) an active touch method for efficiently learning about objects' physical properties (surface texture, stiffness, and center of mass) (Fig. (5.7)), and (III) an active object discriminating strategy (Fig. (5.8)) and (IV) an active target search method (Fig. (5.9))¹.

¹The content of this chapter has been submitted to [157, 158].

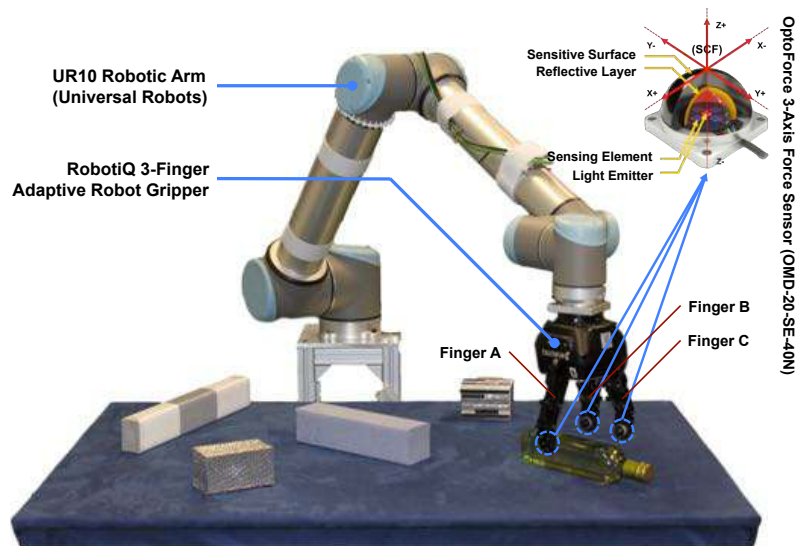


FIGURE 5.1. The experimental setup. A Robotiq three-finger adaptive robot gripper is equipped with OptoForce sensors and mounted on a UR10 robotic arm

First, taking advantage of the Gaussian process regression (GPR), the robot efficiently explores the workspace from different directions, by strategically selecting the most informative position to explore, so that the total uncertainty of the workspace can be reduced as quickly as possible. The tactile data captured during exploration are then clustered in order to determine the number of objects in the workspace. For each cluster, a minimum bounding box is calculated to estimate the location, orientation, and geometric center of each object. After that, the robot starts learning about objects via their physical properties by strategically selecting the objects to explore and the physical properties to perceive. In this regard, the robot moves to the selected object and applies the exploratory action on the object to perceive the selected object property (sliding to sense the textural properties, pressing to estimate the stiffness, lifting to determine the center of mass (CoM)). Afterwards, the robot exploits the perceived physical property of the explored objects and constructs observation models using the Gaussian process classification (GPC). The built observation models will then be used as constructed robot's prior knowledge for actively discriminating among objects. By strategically selecting a sequence of exploratory actions, the robot efficiently searches for target object/s in a workspace that contains both known and unknown objects. Furthermore, for the first time, the center of mass of rigid objects is considered as an intrinsic property for object learning and discrimination. In this regard, I propose a tactile-based algorithm to enable robotic systems to estimate the center of mass of rigid objects.

5.2. System description

In this study, I used different experimental setup than previous work described previous chapters (see chapter 3 and 4) in order to assess the robustness of my proposed AT-LPP as well as active object discrimination and search methods across different tactile sensors and robotic platforms.

5.2.1. Robotic gripper

I used the Robotiq 3-Finger Adaptive Robot Gripper which is an under-actuated industrial gripper with three fingers (A, B, and C) (see Fig. 5.1). Finger B and C were aligned on the same side of the gripper, and they moved in the opposite direction as finger A. The position range of each of the gripper's fingers was divided into 255 counts, with 0 indicating fully open, and 255 fully closed. Thus, the position of the finger was represented using position counts in this paper. I mounted the gripper at the end of the UR10 (Universal Robots) robotic arm (6-DoF) (see Fig. 5.1), which was controlled to collaborate with the gripper, in order to explore the workspace and interact with objects.

5.2.2. Tactile sensors

Three channels of the OptoForce ² OMD-20-SE-40N 3D tactile sensor set were installed on each fingertip of the gripper. The OptoForce sensor can measure forces in three directions, using infrared light to detect small deformation in the shape of the outer sensor surface. It has a nominal capacity of 40N in Z_{SCF} direction, and ± 20 N in both X_{SCF} and Y_{SCF} directions. In this paper, I discuss forces in two coordinate frames: world coordinate frame (WCF) (see Fig. 5.3) and sensor coordinate frame (SCF) (see Fig. 5.1), both of which are standard Cartesian coordinate systems. In SCF, I discuss the tangential force vector \mathbf{f}_{T_i} and the normal force vector \mathbf{f}_{N_i} exerted on the grasped object. The value of tangential force exerted by the i^{th} finger is calculated as:

$$|\mathbf{f}_{T_i}| = \left(|\mathbf{f}_{x_i}|^2 + |\mathbf{f}_{y_i}|^2 \right)^{-1/2} \quad (5.1)$$

The force vectors in SCF are represented as \mathbf{f}_{x_i} , \mathbf{f}_{y_i} , and \mathbf{f}_{z_i} with the subscript i denoting the index of the finger, $i = 1, 2, 3$, correspond to Finger A, B, and C, respectively.

²www.optoforce.com/

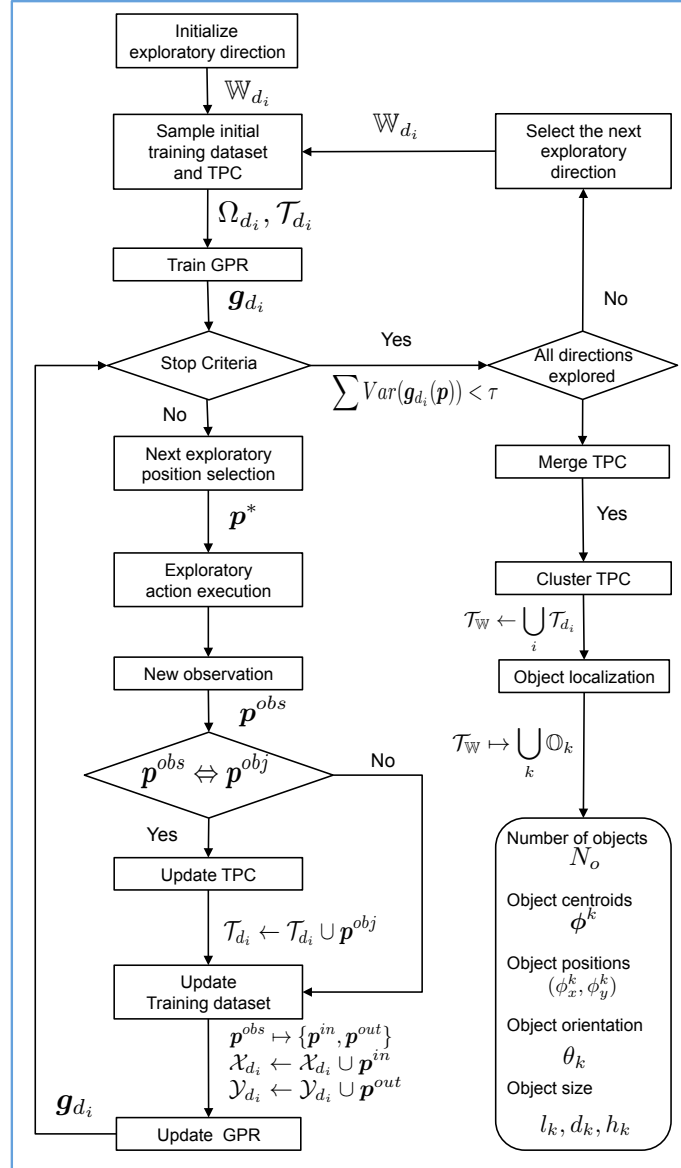


FIGURE 5.2. My proposed probabilistic active touch method for workspace exploration.

5.3. Active touch for unknown workspace exploration

In this section, I propose a probabilistic active touch method for robotic system with the sense of touch to efficiently explore an unknown workspace. Taking advantage of the proposed approach, the robot strategically executes translational movements from each direction into the workspace, in order to efficiently detect contact with objects via the tactile sensors that installed on the fingertips.

The sampled points obtained during each movement are used to construct the probabilistic observation model (constructed using the GPR) of the workspace from the current exploratory direction. Among the collected sampled points, the ones that are detected on the object surface (i.e. the robot contacted the object before it reached the target position of the movement), are registered into the tactile point cloud (TPC) dataset, which is clustered and used to localize objects after exploration.

The GPR model guides the exploration by predicting the next exploratory position, which is the position that has the maximum uncertainty in the current explored workspace. Consequently, the total uncertainty of the workspace can be reduced as quickly as possible during exploration.

After the explorations from all possible directions are completed, the entire TPC dataset is clustered, and then the clustering result is used to localize and map the experimental objects in the workspace.

5.3.1. Tactile point cloud construction

The workspace is defined as a discretized 3D mesh-grid within the reaching capabilities of the robotic hand. Spatial point in the workspace is denoted as $\mathbf{p}_n = (x_n, y_n, z_n)$, $\mathbf{p}_n \in \mathbb{R}^3$, $n \in \mathbb{N}^3$, which lies in predefined boundaries in the WCF: $x_n \in [\underline{x}, \overline{x}]$, $y_n \in [\underline{y}, \overline{y}]$, and $z_n \in [\underline{z}, \overline{z}]$ with the underline and overline of x , y , and z denoting the lower and upper boundaries of the corresponding axis of the WCF, respectively. The workspace can be explored from multiple directions d_i , $i \in \mathcal{I}_{DIR}$. In this work, the workspace is explored from four directions: $\{d_i\} \equiv \{X_+, Y_-, X_-, Y_+\}$, $\mathcal{I}_{DIR} = \{1, 2, 3, 4\}$ with the subscript “+” and “-” representing the positive and negative directions of the X and Y directions of the WCF (see Fig. 5.3). The workspace in the direction d_i is denoted as \mathbb{W}_{d_i} . For the exploration in each direction, the start plane and the target plane are one pair of opposite side faces of the workspace, and they are perpendicular to the exploratory axis. In the exploration process, the n^{th} action $\mathbf{t}_n \in \mathbb{R}^3$ is a translational movement from one position on the start plane \mathbf{p}_n^{start} to the corresponding position on the target plane \mathbf{p}_n^{start} , and the trajectory of \mathbf{t}_n is parallel to the exploratory direction. After executing the action \mathbf{t}_n , an observation \mathbf{p}_n^{obs} is obtained.

A light contact is detected as soon as the resultant force $|\mathbf{f}^{RES}|$ on the surface of the exploratory finger exceeds a threshold, i.e. $|\mathbf{f}^{RES}| > \delta$. The resultant force on the exploratory finger is calculated as:

$$|\mathbf{f}^{RES}| = \left(|\mathbf{f}_x|^2 + |\mathbf{f}_y|^2 + |\mathbf{f}_z|^2 \right)^{-1/2} \quad (5.2)$$

³ \mathbb{R} is the set of real numbers, \mathbb{N} is the set of natural numbers.

with f_x , f_y , and f_z being the force components in the X -axis, Y -axis, and Z -axis of the SCF, respectively.

During the movement, if the sensor on the exploratory finger has detected a light contact before reaching to \mathbf{p}_n^{start} , indicating the robot has touched an object on its surface, then the current 3D coordinates of the contact position, $\mathbf{p}_n^{obs} = \mathbf{p}_n^{object}$, will be recorded. However, if no light contact is detected until the movement is completed, the target position will be returned as the obtained observation, i.e. $\mathbf{p}_n^{obs} = \mathbf{p}_n^{target}$.

The TPC dataset \mathcal{T}_{d_i} is the set of all the \mathbf{p}_n^{object} collected during the exploration of \mathbb{W}_{d_i} . The complete TPC of the workspace is denoted as $\mathcal{T}_{\mathbb{W}} = \cup_i \mathcal{T}_{d_i}$.

Here I take the exploration of \mathbb{W}_{d_4} as an example to clarify this procedure (see Fig. 5.3). In this case, the exploratory direction is $d_4 = Y_+$, thus the y coordinates of the spacial points increase along the exploratory direction. The start plane is the X - Z plane that passes through the positions with minimum Y coordinates (points satisfy $y = \underline{y}$), while the target plane is parallel to the start plane and passes through positions with maximum Y coordinates (points satisfy $y = \bar{y}$). Thus \mathbf{t}_n starts from $\mathbf{p}_n^{start} = (x_n, \underline{y}, z_n)$ and points towards $\mathbf{p}_n^{target} = (x_n, \bar{y}, z_n)$. If an observation $\mathbf{p}_n^{obs} = \mathbf{p}_n^{object}$ is obtained, it will be added into \mathcal{T}_{d_4} . Otherwise, \mathcal{T}_{d_4} will not be updated.

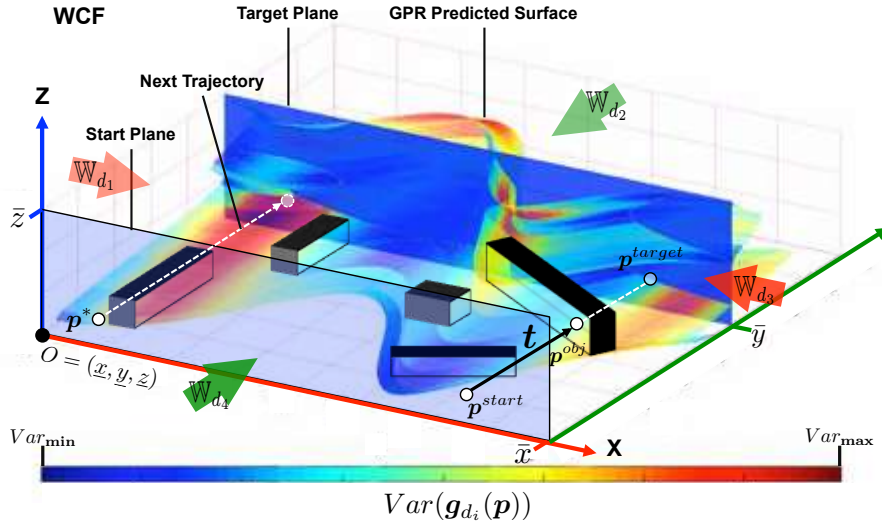


FIGURE 5.3. The illustration of the active exploration process of an unknown workspace \mathbb{W}_{d_4} (workspace in $d_4 = Y_+$ direction). The uncertainties (variance) at different positions are revealed by the color. Red color represents high uncertainty, while blue color represents low uncertainty.

5.3.2. Workspace modeling

I use Gaussian Process Regression approach to construct a probabilistic model of the workspace in the current exploratory direction to guide the exploratory process. A brief introduction of the Gaussian Process (GP) method [156] is provided in appendix B.

I explain the application of GP in exploration task through the example introduced in Sec. (5.3.1).

For the exploration of \mathbb{W}_{d_4} , all points that trajectory \mathbf{t}_n passes through have the same x_n and z_n coordinate, and \mathbf{p}_n^{obs} returns the y_n coordinate, i.e. the depth of the object surface from the start point \mathbf{p}_n^{start} in this direction.

I considered the single training input of the GPR model \mathbf{g}_{d_4} , $\mathbf{p}_n^{in} = (x_n, z_n)$, $\mathbf{p}_n^{in} \in \mathcal{X}_{d_4}$, $\mathcal{X}_{d_4} \subseteq \mathbb{R}^2$, $n \in \mathbb{N}$, and the corresponding training label (output): $\mathbf{p}_n^{out} = (y_n)$, $\mathbf{p}_n^{out} \in \mathcal{Y}_{d_4}$, $\mathcal{Y}_{d_4} \subseteq \mathbb{R}$, $n \in \mathbb{N}$, with (x_n, y_n, z_n) being the coordinates of the observed point \mathbf{p}_n^{obs} of the trajectory \mathbf{t}_n .

The entire training dataset of \mathbf{g}_{d_i} is denoted as $\Omega_{d_i} = \{\mathcal{X}_{d_i}, \mathcal{Y}_{d_i}\}$. Represent the universal set of the 2D coordinate \mathbf{p}_n all over the corresponding start plane as \mathbb{X}_{d_i} ; and $\mathbf{p}_n = (y_n, z_n)$ for $i = 1, 3$, whereas $\mathbf{p}_n = (x_n, z_n)$ for $i = 2, 4$.

Given N pairs of training data $\{\mathcal{X}_{d_4}, \mathcal{Y}_{d_4}\} = \{\mathbf{p}_n^{in}, \mathbf{p}_n^{out}\}_{n=1:N}$, the predicted distribution of target function $\mathbf{g}_{d_4}(\mathbf{p})$, $\mathbf{p} \in \mathbb{X}_{d_4}$ is denoted as $\hat{\mathbf{g}}_{d_4}(\mathbf{p}) \sim \mathcal{GP}(\hat{\mu}(\mathbf{p}), \hat{\nu}(\mathbf{p}))$, and the corresponding mean function and variance function are calculated as:

$$\hat{\mu}(\mathbf{p}) = \tilde{\mathbf{k}}^T (\mathbf{K} + \sigma_n^2 \mathbf{I})^{-1} \mathbf{y}, \quad (5.3)$$

$$\hat{\nu}(\mathbf{p}) = k(\mathbf{p}, \mathbf{p}) - \tilde{\mathbf{k}}^T (\mathbf{K} + \sigma_n^2 \mathbf{I})^{-1} \tilde{\mathbf{k}}. \quad (5.4)$$

where $k : \mathcal{X} \times \mathcal{X} \mapsto \mathbb{R}$ is the covariance function, $\tilde{\mathbf{k}}$ is the covariance vector with its n^{th} element indicating the covariance between the test input \mathbf{p} and the n^{th} training data point \mathbf{p}_n^{out} , and $\mathbf{y} \in \mathbb{R}^N$ is a vector of training outputs \mathbf{p}_n^{out} . The (i, j) entry of the matrix \mathbf{K} represents the covariance between i^{th} and j^{th} training inputs, i.e. $K_{i,j} = k(\mathbf{p}_i^{in}, \mathbf{p}_j^{in})$.

The predicted target $\hat{\mathbf{p}}^{out}$ for the test input $\hat{\mathbf{p}}^{in}$ subjects to the Gaussian distribution: $\hat{\mathbf{p}}^{out} \sim \mathcal{N}(\hat{\mu}(\hat{\mathbf{p}}^{in}), \mathbf{K} + \sigma_n^2 \mathbf{I})$, and the probability of predicted $\hat{\mathbf{p}}^{out}$ is denoted as $p(\hat{\mathbf{p}}^{out})$.

5.3.3. Next exploratory position selection

The contact positions $\mathbf{p}^{obs} \in \mathcal{T}$ are discretely distributed points in the workspace. Hence, a large number of exploratory movements are required to obtain an authentic estimation of the workspace, which is not data-efficient and also time consuming.

A strategy for selecting the next exploratory position is necessary to reduce the total number of non-informative exploratory samples. In order to select the next sample position, several approaches are used, such as [18, 159]. These approaches explore the unknown area and exploit the information from the known region in the workspace. In this paper, I focus on the uncertain region of the workspace during exploration in order to reduce the total uncertainty of the workspace model as soon as possible. Considering the example discussed in Sec. (5.3.2), a GPR model \mathbf{g}_{d_4} is trained to make a prediction of $\mathbf{p}_n^{out} = y_n$, given input $\mathbf{p}_n^{in} = (x_n, z_n)$.

I propose using the variance predicted by the GPR model, $Var(\mathbf{g}_{d_i}(\mathbf{p}))$, since it indicates the uncertainty in the current model at input position \mathbf{p} , $\mathbf{p} \in \mathbb{X}_{d_i}$. In addition, the uncertainty of the workspace \mathbb{W}_{d_i} modeled by the GPR model \mathbf{g}_{d_i} can be measured by its total variance, defined as $\sum_{\mathbf{p} \in \mathbb{X}_{d_i}} Var(\mathbf{g}_{d_i}(\mathbf{p}))$.

To reduce the total variance as soon as possible, I select the next exploratory position $\mathbf{p}^* = (x_{n+1}, z_{n+1})$ as the one with the largest variance in the present GPR model:

$$\mathbf{p}^* = \underset{\mathbf{p} \in \mathbb{X}_{d_i}}{\operatorname{argmax}} Var(\mathbf{g}_{d_i}(\mathbf{p})). \quad (5.5)$$

In other words, the robot explores the position \mathbf{p}^* , which the current trained workspace model is mostly uncertain of.

5.3.4. One-shot data collection for initializing the GPR

At the beginning of the exploration process of one direction, the robot first samples a few uniformly located points on the start plane to initialize the GPR model. For example, the training dataset of the GPR model \mathbf{g}_{d_4} is denoted as $\Omega_{d_4} = \{\mathcal{X}_{d_4}, \mathcal{Y}_{d_4}\}$, which can be initialized by sampling $M \times N$ points on the start plane, these points are represented as $(\underline{x} + \frac{m}{M-1}(\bar{x} - \underline{x}), \underline{z} + \frac{n}{N-1}(\bar{z} - \underline{z}))$, $m = 0, 1, \dots, M-1$, $n = 0, 1, \dots, N-1$. In the meantime of collecting Ω_{d_4} , sampled points which satisfy $\mathbf{p}^{obs} = \mathbf{p}^{object}$ are registered to the TPC dataset \mathcal{T}_{d_4} . Then \mathbf{g}_{d_4} is trained using the dataset Ω_{d_4} , as described in Sec.(5.3.2).

5.3.5. Updating the total uncertainty of TPC

After initialization, the robot selects the next exploration position based on the GPR prediction. As soon as the next exploratory position $\mathbf{p}^* = (x_{n+1}, z_{n+1})$ is determined, the robot moves to the start position $\mathbf{p}_{n+1}^{start} = (x_{n+1}, \underline{y}, z_{n+1})$ on the start plane and then executes an exploratory movement towards the corresponding target position $\mathbf{p}_{n+1}^{target} = (x_{n+1}, \bar{y}, z_{n+1})$. During the movement, the robot maintains the orientation of the tactile sensor in the d_4 direction.

If a contact on the object surface is detected during this motion, i.e. $\mathbf{p}_{n+1}^{obs} = \mathbf{p}_{n+1}^{object}$, the current 3D position of the sensor, $\mathbf{p}_{n+1}^{object} = (x_{n+1}, y_{n+1}, z_{n+1})$, is registered to \mathcal{T}_{d_4} , and the robot immediately retreats back to the start position. If no contact is detected, the observation $\mathbf{p}_{n+1}^{obs} = \mathbf{p}_{n+1}^{target}$ is returned ($y_{n+1} = \bar{y}$).

The coordinate of the sampled point along the exploratory direction is used as the training output (i.e. label set), while the other two dimensions are used as training input. The observation \mathbf{p}_{n+1}^{obs} is added into the training set Ω_{d_4} by appending $\mathbf{p}_{n+1}^{in} = (x_{n+1}, z_{n+1})$ into \mathcal{X}_{d_4} and appending $\mathbf{p}_{n+1}^{out} = (y_{n+1})$ into \mathcal{Y}_{d_4} . The GPR model is updated using the updated Ω_{d_4} , and then the next exploratory position is selected according to Eq. 5.5.

5.3.6. Stop criteria

The exploratory process in the current direction continues until a stop criterion is satisfied. For example, when the total uncertainty of the model, $\sum_{\mathbf{p} \in \mathbb{X}_{d_i}} Var(\mathbf{g}_{d_i}(\mathbf{p}))$, reduces below a tolerable threshold τ . When the exploration process terminates in one direction (d_i), the robot starts the new exploration in the next exploratory direction d_{i+1} by following the same procedure. The entire unknown workspace is completely explored when the exploratory processes are finished for all \mathbb{W}_{d_i} .

5.3.7. Object localization and mapping

When the exploration of the unknown workspace is completed, the TPC of the entire workspace, $\mathcal{T}_{\mathbb{W}}$, can be constructed by merging all the TPCs collected in different directions: $\mathcal{T}_{\mathbb{W}} = \cup_i \mathcal{T}_{d_i}$. I cluster all the data points in $\mathcal{T}_{\mathbb{W}}$ to obtain the points that belong to the same object into one category, so as to localize each object in the workspace.

5.3.7.1. Clustering of tactile point cloud

In order to cluster the constructed tactile point clouds I use the Mean-Shift clustering method [160], which is non-parametric and application-independent. The Mean-Shift clustering approach does not require prior knowledge of the number of categories, and its performance is independent of the shape of the data clusters. After clustering, $\mathcal{T}_{\mathbb{W}}$ is divided into N_o mutual exclusive subsets, denoted as $\mathcal{T}_{\mathbb{W}} \mapsto \cup_k \mathbb{O}_k, k = 1, 2, \dots, N_o$, where N_o is the estimated number of objects, and \mathbb{O}_k contains all the points in the k^{th} cluster, i.e. belong to the k^{th} object. For the sake of increasing robustness against the noise, a minimum number of data points contained in one category is assigned. If a cluster \mathbb{O}_k contains fewer data points than this lower limit, points in this cluster are considered as noise and this cluster will be discarded.

Algorithm 5.1 Active unknown workspace exploration**Input** : $[x, \bar{x}], [y, \bar{y}], [z, \bar{z}]$

▷ workspace description

Output: $\mathcal{B}_k, \theta_k, l_k, d_k, h_k$
 $\{\mathbf{v}_i^k\}, \boldsymbol{\phi}^k = (\phi_x^k, \phi_y^k, \phi_z^k)$ **Tactile Point Cloud Construction****for** $\mathbb{W}_{d_i}, i \in \mathcal{I}_{DIR}$ **do**Initialization: \mathcal{T}_{d_i} ▷ $\mathcal{T}_{d_i} \subseteq \Omega_{d_i}$ Initialization: train GPR $\mathbf{g}_{d_i} : \mathcal{X}_{d_i} \mapsto \mathcal{Y}_{d_i}$ using Ω_{d_i}

▷ Sec. (5.3.2)

Initialization: $\sum_{\mathbf{p} \in \mathbb{X}} \text{Var}(\mathbf{g}_{d_i}(\mathbf{p}))$

▷ initialize total uncertainty

while $\sum_{\mathbf{p} \in \mathbb{X}_{d_i}} \text{Var}(\mathbf{g}_{d_i}(\mathbf{p})) > \tau$ **do** $\mathbf{p}^* \leftarrow \underset{\mathbf{p} \in \mathbb{X}_{d_i}}{\text{argmax}} \text{Var}(\mathbf{g}_{d_i}(\mathbf{p}))$

▷ Sec. (5.3.3)

 $\mathbf{p}^{obs} \leftarrow$ execute action following t **if** \mathbf{p}^{obs} is \mathbf{p}^{object} **then**| collected on the object surface $\mathcal{T}_{d_i} \leftarrow \mathcal{T}_{d_i} \cup \mathbf{p}^{obs}$

▷ update TPC

end $\mathcal{X}_{d_i} \leftarrow \mathcal{X}_{d_i} \cup \mathbf{p}^{in}, \mathcal{Y}_{d_i} \leftarrow \mathcal{Y}_{d_i} \cup \mathbf{p}^{out}$ ▷ update $\Omega_{d_i}, \Omega_{d_i} = \mathcal{X}_{d_i}, \mathcal{Y}_{d_i}$ ▷ train \mathbf{g}_{d_i} ▷ using Ω_{d_i} ▷ update the GPR model \mathbf{g}_{d_i} ▷ calculate $\sum_{\mathbf{p} \in \mathbb{X}_{d_i}} \text{Var}(\mathbf{g}_{d_i}(\mathbf{p}))$

▷ update total uncertainty

end**end****Objects Localization** $\mathcal{T}_{\mathbb{W}} = \bigcup_i \mathcal{T}_{d_i}$

▷ merge TPC

 $\bigcup_k \mathbb{O}_k, k = 1, 2, \dots, N_o \leftarrow \text{cluster}(\mathcal{T}_{\mathbb{W}})$

▷ cluster TPC, Sec. (5.3.7.1)

for $k = 1 : N_o$ **do**

▷ Sec. (5.3.7.2)

 \mathcal{B}_k

▷ construct bounding box

 $\{\mathbf{v}_i^k\}, i = 1, 2, \dots, N_v$

▷ construct set of vertices

 $\boldsymbol{\phi}^k = (\phi_x^k, \phi_y^k, \phi_z^k)$

▷ estimate center of object

 l_k, d_k, h_k

▷ estimate object shape

 θ_k

▷ estimate object orientation

end

5.3.7.2. Object localization

For estimating the location and geometric measurement of each clustered object, a 3D minimum bounding box \mathcal{B}_k is calculated for each point set \mathcal{O}_k , $k = 1, 2, \dots, N_o$. The minimum bounding box is the smallest enclosing volume that contains all the points in the data set. The vertices of each \mathcal{B}_k are represented as: $\mathbf{v}_i^k = (v_{i_x}^k, v_{i_y}^k, v_{i_z}^k)$, $i = 1, 2, \dots, N_v$, where $N_v = 8$ in this work. The geometric center of the k^{th} object, $\phi^k = (\phi_x^k, \phi_y^k, \phi_z^k)$, is calculated as: $\phi^k = (\sum_i v_{i_x}^k / N_v, \sum_i v_{i_y}^k / N_v, \sum_i v_{i_z}^k / N_v)$, therefore the object is located at (ϕ_x^k, ϕ_y^k) on the reference plane (the X - O - Y plane) of the workspace.

The geometric measurement of the object, i.e. length l_k , width d_k , and height h_k can be roughly estimated by calculating the Euclidean distance between vertices on the reference plane (for l_k and d_k , $l_k > d_k$) and in the Z direction (for h_k). The orientation of the k^{th} object is $\theta_k \in [0, \pi]$, defined as the angle that is included between its long edge (the l_k edge) and the positive direction X axis of the WCF. As soon as the geometric information (l_k , d_k , and h_k) of the k^{th} object is determined, an Object Coordinate Frame (OCF) can be defined with respect to the object. As an example, to defined the OCF for a cuboid object, the origin can be assigned as one vertex of the object, and the X , Y , and Z axes of the OCF can be defined as along the length (l_k), depth (d_k), and height (h_k) edge of the object's bounding box.

5.4. Objects' physical properties perception

In tactile object recognition problem, the physical properties of objects are perceived by executing various exploratory actions on the objects. For instance, a robotic system with tactile sensing presses an object to obtain its stiffness, slides on the object's surface to perceive its textural property, and lifts the object at several positions to determine its center of mass. If various exploratory actions are executed on the same objects, multiple physical properties can be sensed by the robot. In this part, I introduce my approaches to perceive the physical properties of the objects, namely stiffness, surface texture, and center of mass.

5.4.1. Stiffness property

The robot perceives the stiffness of objects by pressing the tactile sensors against the objects' surfaces (see Fig. 5.4-A). In this study, by exploiting the geometric information of target object computed during workspace exploration (Sec. (5.3)), the robot first moves to the target object and adjusts the orientation of the gripper to keep the finger facing the object's surface. Then, the gripper establishes a light contact with the object by all three fingertips. The light contact

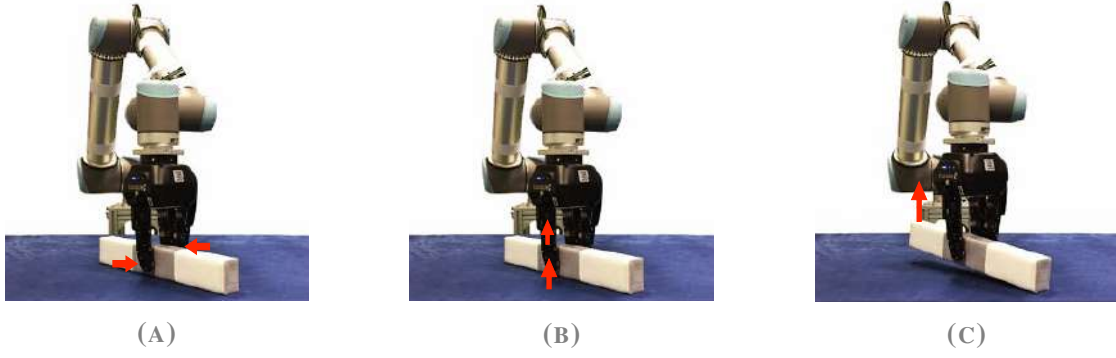


FIGURE 5.4. (A) Pressing, to measure the stiffness. (B) Sliding, to perceive the textural property. (C) Lifting, to check if the current position is the CoM.

is detected as soon as the measured resultant forces (f_r^{RES}) of all tactile sensors exceed a threshold (f_t), i.e. $f_r^{RES} > f_t$, $r = 1, 2, 3$. Afterwards, the gripper presses the object by closing all its fingers simultaneously for N_ϵ extra position counts. For each finger r , the difference in its resultant forces recorded before and after pressing, Δf_r^{RES} , is used as an indication of the stiffness on the local contact area. The difference value averaged over all fingers serves as a measurement of stiffness of the object.

$$S_{O_i} = \sum_r^{N_r} \Delta f_r^{RES}. \quad (5.6)$$

with the subscript O_i indicating the i^{th} object, and N_r the total number of tactile sensors in contact with the object.

5.4.2. Surface texture property

When the robot slides its fingertips on the surface of an object, it generates vibration (see Fig. 5.4-B). The caused vibration can be measured by each tactile sensor on the fingertip f_{n_v} ($n_v = 1, 2, \dots, N_v$, is the number of output signals from one tactile sensor) to sense the textural property of the object. I adapted my proposed tactile descriptors to extract robust tactile information from the output of the three-axis OptoForce tactile sensor (Eq. (3.6), (3.7), (3.8)), and (Eq. (3.9), (3.10)). The final proposed feature descriptors for the robotic system with three fingers (F_A, F_B , and F_C) and each fingertip with a three-axis tactile sensor ($n_v = 1, 2, 3$; $N_v = 3$ is the number of output signal from one tactile sensor) can be written as:

$$\mathbf{D}_{total}^{grip} = [\mathbf{A}_{grip}; \mathbf{M}_{grip}; \mathbf{C}_{grip}; \mathbf{L}_{grip}; \mathbf{N}_{grip}] \quad (5.7)$$

The final feature descriptor (Eq. (5.7)) is the concatenation of all extracted features as one feature vector. The final feature vector D_{total}^{grip} has 15 data samples.

5.4.3. Center of mass property

The CoM of a rigid body is a constant position with respect to the object. In this work, I present a tactile-based approach to determine the CoM of the target object via lifting actions.

Think of the process of lifting an object, for example, a steelyard. The steelyard can only maintain its balance (in the equilibrium state) during lifting, if and only if the resultant force's line of application passes through its CoM. In this case, two conditions should be satisfied, i.e. the force condition and the torque condition, which state that both resultant force and resultant torque applied on the lifted object are zero.

I show that in a three-contact-point case, both force and torque conditions can be verified via tactile-based approaches by taking advantage only of the force signals measured on the contact surfaces, and the determination of the CoM of the target object (here I take the 1D CoM as an example) can be formulated as the problem of searching for a lifting position on the object, at which the conditions for equilibrium are satisfied.

5.4.3.1. Linear slip detection for force condition verification

Consider a target object that lying on the reference plane is grasped by the robotic gripper on its side faces and then slowly lifted up for a distance Δh . The applied lifting force (the force component in the gravitational direction) balances the object's weight and the other applied external forces (e.g. support force from the reference plane, if exists). When the object is lifted up and stays at a target height, it will not slip out of the gripper (linear slip does not happen on the contact surface), as long as the resultant force applied on the object is zero, i.e. the force condition is satisfied. The force condition should be satisfied to guarantee that the object can be stably lifted to a target height.

I verify the force condition by detecting linear slip of the object, which can be realized by measuring the increasing rate of lifting force on the contact point (see chapter refsec:chap:MDO:Integration). The lifting force f_L on one contact point is the component of the applied result force that decomposed in the Z direction of the WCF. A linear slip is detected as soon as the value of lifting force applied on the contact surface f_L has increased by a percentage ϵ within a short time period of Δt :

$$|f_L(t + \Delta t) - f_L(t)| > \epsilon \cdot |f_L(t)|. \quad (5.8)$$

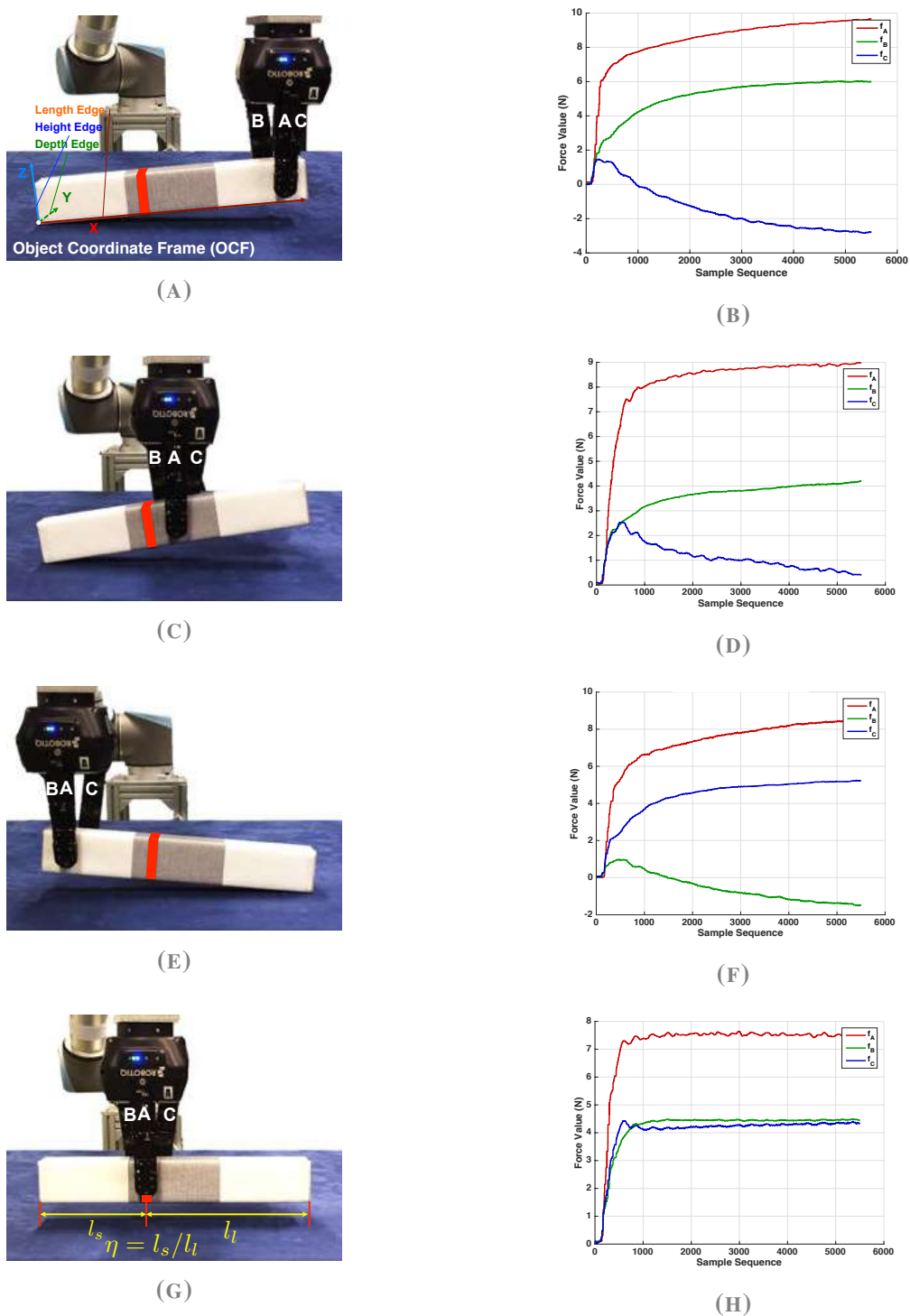


FIGURE 5.5. The analysis of lifting forces (i.e. frictions) at different lifting positions along the length edge of a target object. (A),(C),(E),(G): The robot lifts object at different positions. The real CoM of the object is marked by the red ribbon in each figure. A),(C),(E),(G): The sequence of corresponding lifting force signals from each contact point during lifting process. If the object is lifted almost at its CoM (D), the frictions measured on the contact points on the same side are almost the same (H), owe to the positional symmetry.

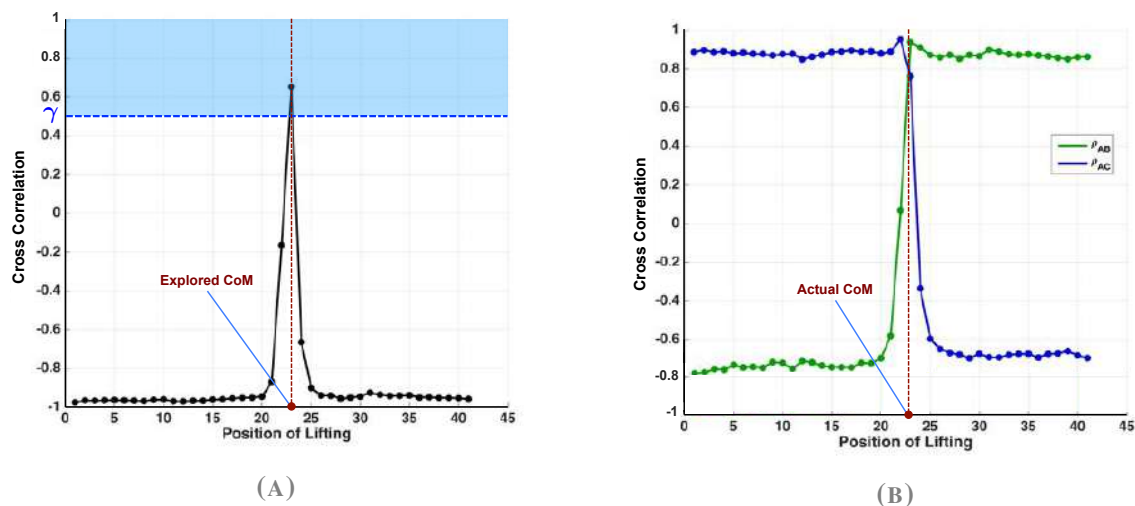


FIGURE 5.6. The target object was lifted up at 41 sequential positions along its length edge, and at each lifting position, the measured sequences of frictions from contact points A , B , and C , were recorded during the lifting process. The abscissa scale denotes the lifting positions sequentially distributed along the object, from one tail (1) to the other tail (41). The ordinate scale represents the calculated cross-correlation of signal sequences. (A) The cross-correlation ρ_{BC} is used to determine if the corresponding lifting position can be determined as the real CoM. (B) The relationship of ρ_{AB} and ρ_{AC} is used to guide the selection of the next lifting position.

The robotic gripper regulates its applied force by detecting linear slips during the lifting process, in order to satisfy the force condition. In application, the gripper first closes its fingers compliantly until all the fingertips are in light contact with the object's surface. Then the robot slowly lifts the object to a target height. If the object has slid out of the gripper during this process, or if a linear slip is detected after the object has been lifted to the target height, the grasping force is considered insufficient. Then the robot lays down the object, opens the gripper, re-grasps the object with an increased grasping force, and then lifts up the object again. The robot repeats this procedure until the grasped object can be lifted up to the target height and held stably (no linear slip is detected). Then the force condition is considered satisfied, and the robot proceeds to check the torque condition.

5.4.4. Object rotation detection for torque condition verification

If the applied resultant torque is not zero, the grasped object will rotate as it is being lifted up, i.e. rotational slip happens on the contact points. However, to the best of my knowledge, rotational slip on one single contact point can hardly be detected based solely on the force signal. Thus, in a two-contact-point grasp case, the rotation of the grasped object cannot be

detected based on rotational slips on the contact area. I show that based on force signals, it is possible to detect the rotation of the lifted object with at least three contact points (denoted as A, B, and C), among which two contact points (e.g. B and C) are aligned on the same side of the grasped object and close to each other, while opposite to the other one (e.g. A).

I propose to detect the rotation of the object by measuring the similarity between frictions measured on different contact points during lifting.

The cross-correlation of two jointly stationary series \mathbf{x} and \mathbf{y} is defined as

$$\rho_{\mathbf{x}\mathbf{y}} = \frac{\text{cov}(\mathbf{x}, \mathbf{y})}{\sigma_{\mathbf{x}}\sigma_{\mathbf{y}}} \quad (5.9)$$

with $\text{cov}(\mathbf{x}, \mathbf{y}) = \mathbb{E}[(\mathbf{x} - \bar{\mathbf{x}})(\mathbf{y} - \bar{\mathbf{y}})^T]$ being the cross-covariance of \mathbf{x} and \mathbf{y} , $\bar{\mathbf{x}}$ and $\bar{\mathbf{y}}$ being the vectors composed of expected values of \mathbf{x} and \mathbf{y} , respectively; $\sigma_{\mathbf{x}}$ and $\sigma_{\mathbf{y}}$ to denote the standard deviation of \mathbf{x} and \mathbf{y} . The cross-correlation $\rho_{\mathbf{x}\mathbf{y}}$ is a normalized value within $[-1, 1]$, thus it can also be applied on objects of different textures and stiffness, even if the change of contact properties may result in different absolute values of the friction. The closer $\rho_{\mathbf{x}\mathbf{y}}$ to 1, the higher the similarity between \mathbf{x} and \mathbf{y} .

In this case, I focus on rigid objects, and I assume that during the lifting process, the three contact positions satisfy the symmetry property that B and C are symmetrical with respect to A, i.e. A, B, and C formulate an isosceles triangle. As a result, same lifting forces should be applied on B and C (or in other words B and C should have balanced the same linear frictions) if the object is lifted at its CoM. I represent the time series of frictions recorded on each contact points of A, B, and C as \mathbf{f}_A , \mathbf{f}_B , and \mathbf{f}_C , respectively. The lifting position is represented by position A. The torque condition is considered to be satisfied if ρ_{BC} is higher than an expected similarity level γ (see Fig. 5.6a):

$$\rho_{BC} \geq \gamma, \gamma \in (0, 1]. \quad (5.10)$$

If both force and torque conditions are satisfied, the current lifting position can be estimated as the CoM.

5.4.5. CoM Exploration

The CoM is a constant 3D position in the corresponding OCF. Here I explain the exploration of the 1D CoM component along the X -axis of the OCF (referred to as the exploratory axis) as an example.

For searching the 1D CoM component, I propose to use the binary search algorithm, which is the 1D optimal search algorithm with a computational complexity of $\mathcal{O}(\log_2 N_s)$ for maximum N_s sampling points.

I denote the cross-correlation of f_A and f_B as ρ_{AB} , the cross-correlation of f_A and f_C as ρ_{AC} . At different side of the real CoM, ρ_{AC} and ρ_{AB} show the contrary numerical relationship (see Fig. 5.6b). It reveals the fact that between two adjacent contact points (B and C), the one that is closer to the real CoM balances larger friction. According to this relationship, the robot determines the exploratory range of the next lifting, thus the sequence of lifting positions is guaranteed to converge to the real CoM of the object. For example, if $\rho_{AB} > \rho_{AC}$, according to the binary search algorithm, the exploratory range of the next action is determined as one of the bisected ranges, which is closer to B while further away from C. The robot then lifts the object at the middle of this exploratory range.

5.4.5.1. Center of mass feature

The length of the object along the exploratory axis can be segmented by the corresponding CoM component into two parts. In order to extract the CoM as an object feature that is independent of the position and orientation of the object, I represent the CoM feature as a ratio of the shorter segment (indicated by the subscript s) to the longer part (indicated by the subscript l) (see Fig. 5.5g). For example, the CoM property of a 3D object can be formulated in the length-depth-height order:

$$\eta = (l_s/l_l, d_s/d_l, h_s/h_l). \quad (5.11)$$

Therefore, η is constant for rigid objects, and each component of η lies in the range of $(0, 1]$. In this paper, only the CoM component along the length edge (1D, along the X -axis of the OCF) is considered. To explore the CoM, the robot moves its end-effector above the centroid of the target object, adjusts its orientation, and lifts the object at determined positions sequentially along its length edge. The robot first regulates its grasping force to satisfy the force condition. As long as the object can be lifted and held stably without linear slip, the robot records the force signals while lifting the object for a distance Δh , and analyzes the cross-correlation of signal sequences to determine if the current lifting position can be estimated as the CoM. If not, the robot selects the next lifting position based on the relationship of signals ((Sec. 5.4.5)). In this work, the explored CoM feature η is denoted as one single scalar: $\eta = l_s/l_l$.

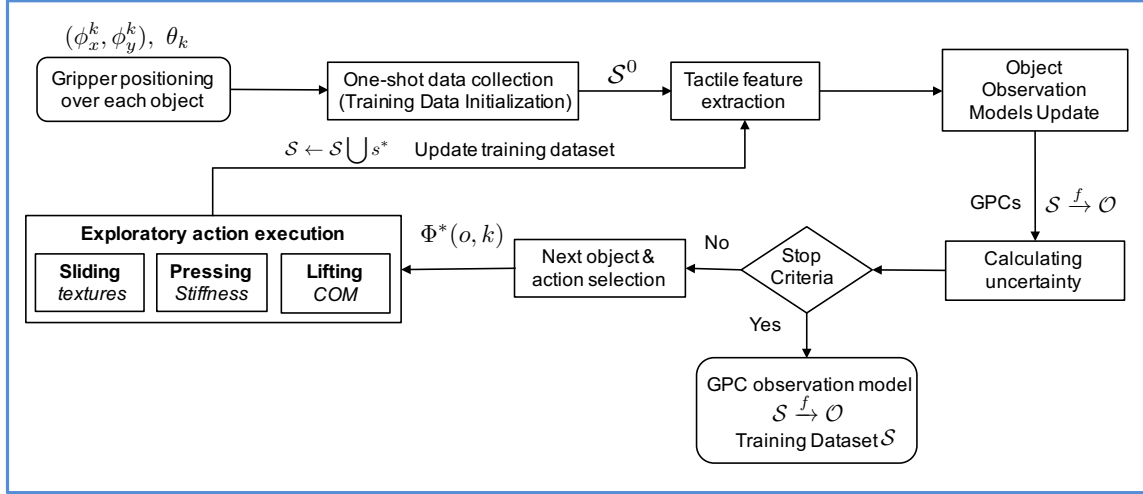


FIGURE 5.7. my proposed probabilistic active touch algorithm for efficient learning about objects' physical properties (texture, stiffness, center of mass)

5.5. Active touch for learning physical properties

In this section, I recall my proposed probabilistic method for active touch object learning method chapter 4.4 (AT-PPL). My proposed algorithm enables robotic systems to efficiently learn about objects via their physical properties such as surface texture, stiffness, and the center of mass properties and to correspondingly construct the observation models of the objects (see Fig.5.7).

5.5.1. Problem definition

Suppose the robot have explored the unknown workspace and found N objects $\mathcal{O} = \{o_i\}_{i=1}^N$ and then determined their poses. Now, the robot is asked to learn about the objects via their physical properties. I denote the physical properties of objects by $\mathcal{K} = \{k_j\}_{i=j}^K$. These objects might have similar physical properties, for instance similar stiffness, while some might have quite different properties, for example different center of mass and /or texture.

In this situation, the robot's task is to efficiently learn about objects by means of their physical properties with as few training samples as possible and to efficiently construct the reliable observation models of the objects. Since the objects with the similar properties cannot be easily discriminated among each other, the robot should autonomously collect more training samples with these objects.

The active touch-based object learning problem (AT-LPP) is formulated as a standard supervised learning problem for multi-class classification, where each object o_i is considered as a class; for each physical property k_j , a probabilistic classifier is efficiently constructed by

iteratively selecting the “*next object to explore*” and the “*next physical property to learn*”, in order to collect the next training sample.

In AT-LPP algorithm the one versus all (OVA) Gaussian Process Classifier (GPC) is used to construct observation models of objects. In this case, the target (or label) set \mathcal{Y} contains integers indicating the labels of input data, i.e. $\mathcal{Y} = \{1, 2, \dots, N\}$, for N possible target classes in total. Each target label is mapped to a vector $\mathbf{v}_y \in \mathbb{R}^N$. In the vector \mathbf{v}_y , all entries are set to -1 except the y^{th} entry which is set to 1. Then the function relation that maps the input data \mathcal{X} into the classes \mathcal{Y} is learned as: $\mathbf{f} : \mathcal{X} \mapsto \mathcal{Y}$.

GPC estimates the probability of each target label $p(y|\tilde{\mathbf{x}})$ for a test data point $\tilde{\mathbf{x}}$ by $\mathbf{f}(\tilde{\mathbf{x}})$, and then assigns it to the class with the largest predicted probability:

$$\tilde{y} = \arg \max_{y \in \mathcal{Y}} \mathbf{f}(\tilde{\mathbf{x}}) \quad (5.12)$$

In this study, I used the RBF as kernel function Eq.(B.6) in appendix B, and the hyper-parameters are selected by cross-validation.

5.5.2. Methodology

5.5.2.1. One-shot tactile data collection

To start learning about objects via their physical properties, the robot first constructs a small set of training data $\mathcal{S} = \{\mathcal{S}_{k_j}\}_{j=1}^K$ by executing each of the three actions $\mathcal{A} = \{a_{k_j}\}_{j=1}^K$ once on each object (One-shot tactile data collection), in order to perceive the object physical property denoted as $k_j \in \{\text{texture, stiffness, center of mass}\}$, $K = 3$ and $a_{k_j} \in \{\text{sliding, pressing, lifting}\}$.

Then the autonomous robot iteratively collects new training samples \mathcal{S}_{k_j} . At each iteration, AT-LPP algorithm updates GPCs with the training data set collected hitherto, and estimates the uncertainty in the constructed observation models which guide to next round of tactile data collection.

5.5.2.2. Objects’ Uncertainty Estimation

In order to estimates the uncertainty in the objects’ observation models the AT-LPP measures the Shannon entropy of each training samples. In this regard, the training dataset of one physical property \mathcal{S}_k is divided into categories $\mathcal{S}_k = \{\mathcal{S}_{o_i}^k\}_{i=1}^N$, where each category $\mathcal{S}_{o_i}^k$ has M_i^k number of samples. For each set of training samples, the mean value of the Shannon entropy is measured:

Algorithm 5.2 Active touch for object learning

Input : $\mathcal{O} = \{o_i\}_{i=1}^N$ ▷ N objects to learn, each is regarded as a class
 $\mathcal{L} = \{l_i\}_{i=1}^N$ ▷ The locations of the objects
 K ▷ object physical properties

Output: GPCs, \mathcal{S} ▷ observation models, training dataset,
initialization: \mathcal{S} ▷ one-shot tactile data collection

initialization: GPCs $\mathbf{f} : \mathcal{S} \mapsto \mathcal{O}$ ▷ Gaussian Process Classifiers. Sec. (5.5.2)

for $r = 1 : R$ **do**

$p(o|\mathbf{s}) \leftarrow \mathbf{f}(\mathbf{s})$ ▷ class predictions for training data
 $E[\mathcal{H}_{t+1}(k)] \leftarrow \sum_{o \in \mathcal{O}} p(o) \mathcal{H}_{t+1}(o, k)$ ▷ object uncertainty, Sec. (5.5.2.3)
 $\Phi^*(o, k) \leftarrow \underset{o_i \in \mathcal{O}, k \in K}{\operatorname{argmax}} E[\mathcal{H}_{t+1}(k)]$ ▷ Next object and next physical property selection.

Sec. 5.5.2.3

$Move_robot(l_i)$ ▷ move the robot to the object o_i
 $Execute_action(a_k)$ ▷ Sec. (5.5.2.3)
 $\mathcal{S} \leftarrow \mathcal{S} \cup \mathbf{s}^*$ ▷ update training dataset with new samples

end

$$\mathcal{H}(o_i, k) = \frac{1}{M_i^k} \sum_{\mathbf{s}_{o_i}^k \in \mathcal{S}_{o_i}^k} \mathcal{H}(\mathbf{s}_{o_i}^k) \quad (5.13)$$

$$\mathcal{H}(\mathbf{s}_{o_i}^k) = - \sum_{o \in \mathcal{O}} p(o|\mathbf{s}_{o_i}^k) \log(p(o|\mathbf{s}_{o_i}^k)) \quad (5.14)$$

with the $p(o|\mathbf{s}_{o_i}^k)$ being the observation probability predicted by the GPC model. The higher the $\mathcal{H}(o_i, k)$ is, the more uncertain the robot is about the object.

5.5.2.3. Next object to explore and next physical property to learn

I define the object-property pair, $\Phi(o_i, k)$ as a function of the object $\mathcal{O} = \{o_i\}_{i=1}^N$ and the physical property k . After selecting $\Phi(o_i, k)$, the robot moves to the object o_i and executes the action a_k to perceive the physical property k . In order to reduce the entropy of the observation models as quickly as possible, the next training sample is generated from the pair $\Phi(o_i, k)$ with the largest entropy. In order to learn about objects efficiently, the robot can greedily sample the next object and the next property which maximize $\mathcal{H}(o_i, k_j)$ of GPCs (exploitation). In this way, the robot autonomously collects more training samples from the objects based on their physical properties which are easily confused. At the end of each iteration, the new training sample will be added to the entire dataset $\mathcal{S} := \mathcal{S} \cup \mathbf{s}^*$.

The active learning process is repeated until a target criterion is reached, in my case, when there is no perceived reduction of the entropy for the observation models, or the robot collects a certain number of training samples. In order to avoid being trapped in the local maxima, I add an exploration rate so that the robot can randomly select $\Phi(o, k)$ by following the uniform distribution (exploration). I denote p_Φ as a probability, which is uniformly generated at each iteration in the AT-LPP. Then the next object o^* and next physical property k^* is determined by:

$$\Phi^*(o, k) = \begin{cases} \operatorname{argmax}_{o_i \in \mathcal{O}, k_j \in K} \mathcal{H}(o_i, k_j), & \text{if } p_\Phi > \epsilon_\Phi \\ o = \mathcal{U}\{o_1, o_2, \dots, o_N\}, k = \mathcal{U}\{k_1, k_2, k_3\}, & \text{o.w.} \end{cases} \quad (5.15)$$

In Eq.5.15, the parameter ϵ_Φ controls the exploration-exploitation trade-off.

5.6. Active touch for object discrimination

Assuming the observation models with the efficient training dataset are constructed during the active learning process (see Fig.5.7), the autonomous robot is faced with the task of identifying objects from each other in an unknown workspace. In this scenario (see Fig.5.8), the robot is asked to discriminate among objects which have already been learned. However, in this scenario, each object can have various orientations and positions in the workspace.

5.6.1. Problem definition

The task of the robot is to perform a sequence of exploratory actions ($\mathcal{A} = \{a_k\}_{k=1}^K$) to efficiently discriminate among objects which have already been learned. However, the objects can have different positions and orientations in the unknown workspace. Therefore, using the proposed active touch workspace exploration method the robot first localize the objects in the workspace (see Sec. (5.3)). Then the robot exploits the objects' prior knowledge that efficiently obtained by my proposed active object learning strategy (the observation models and training dataset of objects) (see Fig.5.7), in order to iteratively execute exploratory actions on objects. In this part of study, I propose a method to enable the robotic system to determine the most informative exploratory action at each step, such that the objects can be distinguished with the fewest exploratory actions possible (see Fig.5.8).

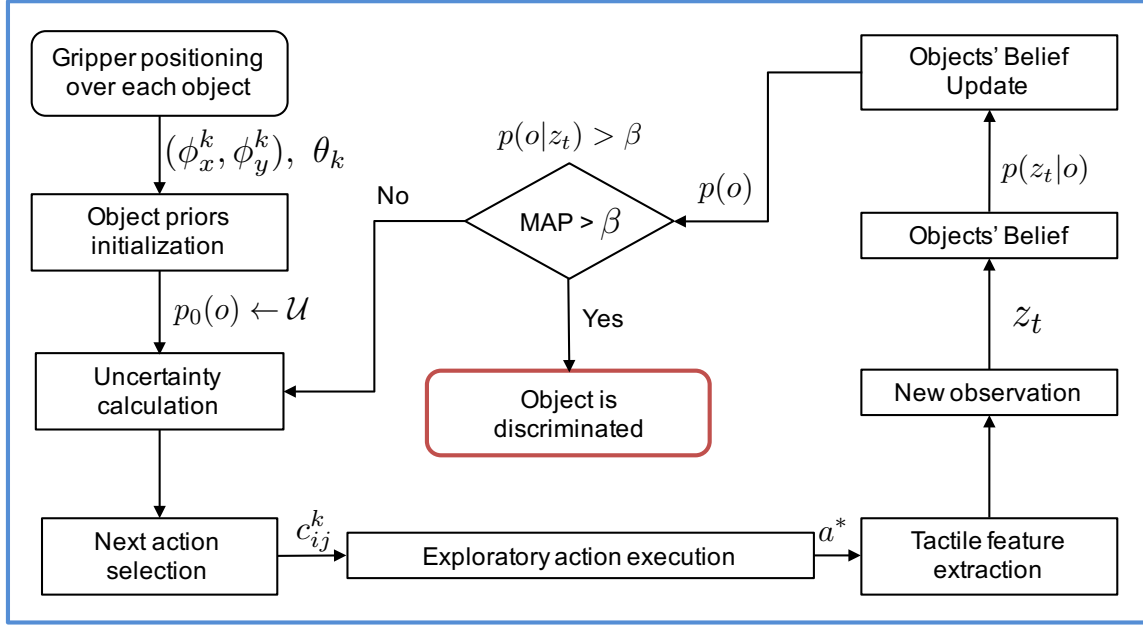


FIGURE 5.8. My proposed probabilistic active touch for discrimination among objects based on their physical properties.

my

5.6.2. Methodology

The object discrimination task is achieved through sequentially executing the exploratory actions on the objects. Firstly, the object's belief $p(o)$ is initialized as being uniformly distributed. Next, an exploratory action is executed on the object in order to perceive an observation z_t . Then, the object's belief is updated which helps to determine the next exploratory movement a^* . This process is repeated until a target criterion is reached: for example, until the Maximum A Posteriori (MAP) exceeds a probability threshold, or the maximum times to update the procedure is reached.

5.6.2.1. Objects' Belief Updating

Once an action a_k has been performed and the corresponding observation z_t is obtained at time step t , the object posterior distribution can be updated using Bayes' rule:

$$p_t(o|z_t) \propto p(z_t|o)p_{t-1}(o) \quad (5.16)$$

with $p_{t-1}(o)$ being the posterior distribution from the previous time step, and $p(z_t|o)$ being the observation probability calculated by the observation models.

Algorithm 5.3 Active touch for object discrimination

Input : $\mathcal{L}_{\mathcal{M}} = \{l_m\}_{m=1}^M$ \triangleright The locations of M objects in the workspace
GPCs, $\mathcal{S} = \{\mathcal{S}_n\}_{n=1}^N$ \triangleright observation models, training data for N classes of objects

Output: $o_{1:M}$

for $m = 1 : M$ **do**

$p_0(o) \leftarrow \mathcal{U}$ \triangleright initialize object priors

$Move_robot(l_m)$ \triangleright move the robot to another object

while $\nexists n | (p(o_n | z_t^k) > \beta)$ **do**

$a^* \leftarrow Select_action(p(o))$ \triangleright Sec. (5.6.3)

$Execute_action(a^*)$

$p_t(o | z_t) \propto p(z_t | o)p_{t-1}(o)$ \triangleright get observation z_t , update object priors: Sec. (5.6.2.1)

end

$o_m \leftarrow \underset{o_n \in \mathcal{O}}{\operatorname{argmax}}(p(o))$ \triangleright object identified

end

5.6.3. Next optimal exploratory action selection

When selecting which exploratory action is optimal to recognize objects, I need to predict the benefit of the movement based on the updated object priors $p(o)$ and the prior knowledge (observation models and training dataset). In this work, I propose a method to estimate the expected benefit of a movement, which guides the next action selection called Confusion Matrix-based Uncertainty Minimization (CMUM). My proposed method predicts the benefit of an exploratory action by inferring the resulting confusion between objects. If a movement produces tactile information which is most easily discriminated among objects, then objects can be recognized more quickly by executing such a exploratory action. Conversely, exploratory actions which generates confused observations are not helpful. Therefore, the advantage of selecting a particular exploratory action can be inferred by how much confusion the action results in. To do this, I measure the confusion of an exploratory action by calculating the objects' similarity, and use it to guide the next action selection. Similar work has been done by Fishel et al. in [12]. However, their method suffered from the curse of dimensionality and their method could only be tractable with low-dimensional features. In contrast, my proposed method is unrestricted by the feature dimensions, and thus can be applied to high dimensional features, such as surface texture property.

5.6.3.1. Proposed confusion matrix-based uncertainty minimization (CMUM)

When predicting the confusion c_{ij}^k between objects o_i and o_j for the tactile property k , I calculated the observation probability $p(o_j|\mathbf{s}_{o_i}^k)$ for each training sample, which belongs to the object o_i , but is misclassified to the object o_j . Then c_{ij}^k is estimated by the average value of $p(o_j|\mathbf{s}_{o_i}^k)$:

$$c_{ij}^k = \frac{1}{M_i^k} \sum_{\mathbf{s}_{o_i}^k \in \mathcal{S}_{o_i}^k} p(o_j|\mathbf{s}_{o_i}^k) \quad (5.17)$$

with M_i^k being the number of training data for object o_i and tactile property k . c_{ij}^k ranges between 0 and 1, where 0 refers to no confusion, and 1 means total confusion.

After obtaining a new observation \mathbf{z}_t^k at time step t , the expected confusion $J_{o_i,k}$ between the object o_i and the others is measured:

$$J_{o_i,k} = \frac{\sum_{o_j \in \mathcal{O}, o_j \neq o_i} p(o_j|\mathbf{z}_t^k) c_{ij}^k}{\sum_{o_j \in \mathcal{O}} p(o_j|\mathbf{z}_t^k) c_{ij}^k}. \quad (5.18)$$

The expected confusion $E[J_k]$ for property k can be estimated by considering all objects:

$$E[J_k] = \sum_{o \in \mathcal{O}} p(o|\mathbf{z}_t^k) J_{o,k}. \quad (5.19)$$

This value predicts the confusion between objects after executing an exploratory movement. In other words, it measures the expected uncertainty of an action. The next action a^* is selected in order to bring the maximum benefit. In my case, this means minimizing the expected uncertainty:

$$a^* = \underset{k}{\operatorname{argmin}} (E[J_k])^{\beta_k} \quad (5.20)$$

where the discount factor β_k is used to control the exploration-exploitation trade-off. It is inversely proportional to the number of times an action has been taken.

5.7. Active touch for target object search

The task of the robot is to recognize a target object/s in the unknown workspace includes both known and unknown objects with different orientations and locations. In this scenario the robot should efficiently search for a object in this workspace. Different from the object discrimination task in which all objects in the workspace should be distinguished (see Fig. 5.8), in the problem of target object search (see Fig. 5.9), the robot only needs to recognize the

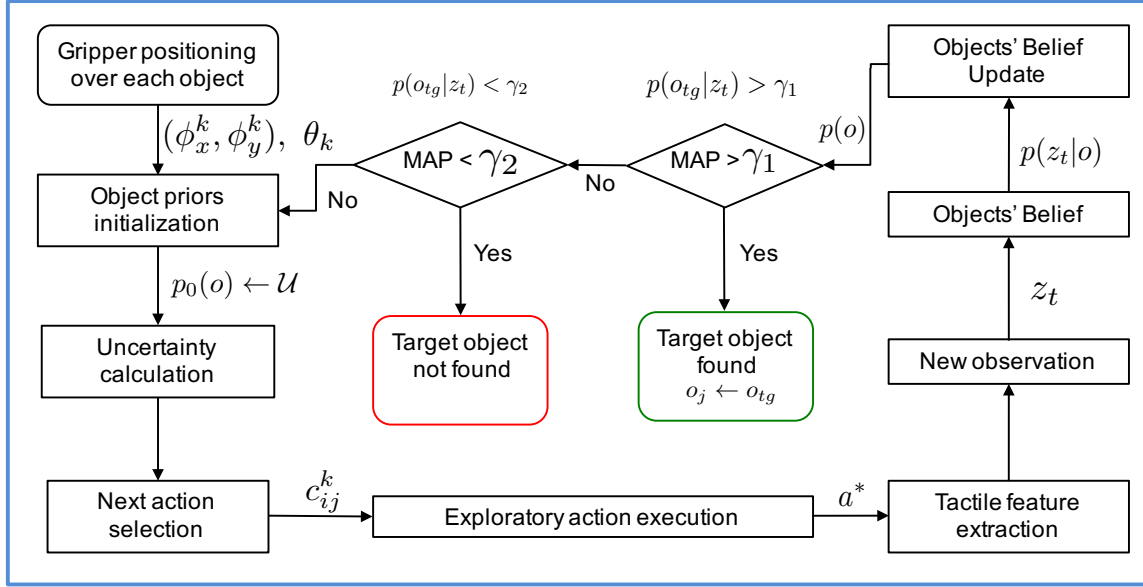


FIGURE 5.9. My proposed probabilistic active touch strategies for searching a target object/s in the workspace that contains unknown objects.

target objects. To do this, I divided the objects which are explored in the active learning into categories of target object and non-target objects $\mathcal{O} = \mathcal{O}_{tg} \cup \mathcal{O}_{non-tg}$, and divide the training dataset correspondingly $\mathcal{S} = \mathcal{S}_{tg} \cup \mathcal{S}_{non-tg}$. Then the multi-class GPCs are reduced to binary classifiers which give the observation probability $p(o \in \mathcal{O}_{tg} | \mathbf{z})$.

$$p_t(o_{tg} | \mathbf{z}_t) \propto p(\mathbf{z}_t | o_{tg}) p_{t-1}(o_{tg}) \quad (5.21)$$

in which $p_t(o_{tg} | \mathbf{z}_t)$ being the posterior distribution from the previous time step, and $p(\mathbf{z}_t | o_{tg})$ being the observation probability calculated by the observation models. The optimal exploratory action is selected by the robot following the procedure described in Sec. (5.6.3). The similarity between object pares is calculated by my proposed CMUM method explained in Sec. (5.6.3.1). The Algorithm 5.4 show the proceder of my proposed active target search more in detail.

5.7.1. Baseline: Expected Entropy Reduction (EER)

I used expected entropy reduction (EER) method as a baseline to compare with my proposed CMUM method. The EER is an approach for estimating the expected benefit of a exploratory action by predicting its entropy [73, 161]. The exploratory action which produces lower entropy can better discriminate among objects. To do the comparison, I measured the expected entropy reduction for different action to perceive different physical properties of an object.

Algorithm 5.4 Active touch for target object search

Input : $\mathcal{L}_{\mathcal{J}} = \{l_j\}_{j=1}^J$ ▷ The locations of J objects in the workspace
 $o_{tg} \in \mathcal{O}$ ▷ define which object to find

Output: l_{tg}

initialization: $\mathcal{S} = \{\mathcal{S}_{tg}, \mathcal{S}_{non-tg}\}$ ▷ divide training data
initialization: binary GPCs ▷ Sec. (5.6.2.1)

$p(o_{tg}) \leftarrow \frac{1}{2}$ ▷ initialize target object priors

for $j = 1 : J$ **do**

$Move_robot(l_j)$

while $p(o_{tg}) > \tau_1$ or $p(o_{tg}) < \tau_2$ **do**

$a^* \leftarrow Select_action(p(o_{tg}))$ ▷ select next exploratory movement

$Execute_action(a^*)$

end

if $p(o_{tg}|z_t^k) > \gamma_1$ **then**

$o_j \leftarrow o_{tg}$ ▷ target object found

$l_{tg} \leftarrow l_j$

end

if $p(o_{tg}|z_t^k) < \gamma_2$ **then**

continue ▷ leave the robot to another object

end

end

Let us denote $\mathcal{H}_{t+1}(k)$ the entropy at the next time step $t + 1$ from the action a_k taken to obtain an observation \mathbf{z}_{t+1}^k , where k refers to the object property. I measure $\mathcal{H}_{t+1}(k)$ by:

$$\mathcal{H}_{t+1}(k) = - \sum_{o \in \mathcal{O}} p_{t+1}(o|\mathbf{z}_{t+1}^k) \log(p_{t+1}(o|\mathbf{z}_{t+1}^k)). \quad (5.22)$$

Since I do not know which measurements \mathbf{z}_{t+1}^k the robot will obtain at time $t + 1$, I need to integrate all possible observations. This is approximated through summing up all the samples in the training dataset \mathcal{S}_k for tactile property k , weighted by the object priors $p(o)$:

$$E[\mathcal{H}_{t+1}(k)] = \sum_{o \in \mathcal{O}} p(o) \mathcal{H}_{t+1}(o, k) \quad (5.23)$$

where $\mathcal{H}_{t+1}(o, k)$ is the mean value of the entropy for an object o :

$$\mathcal{H}_{t+1}(o_i, k) = \frac{1}{M_i^k} \sum_{\mathbf{s}_{o_i}^k \in \mathcal{S}_{o_i}^k} \mathcal{H}_{t+1}(o_i, k | \mathbf{s}_{o_i}^k) \quad (5.24)$$

$$= -\frac{1}{M_i^k} \sum_{\mathbf{s}_{o_i}^k \in \mathcal{S}_{o_i}^k} \sum_{o \in \mathcal{O}} p_{t+1}(o | \mathbf{s}_{o_i}^k) \log(p_{t+1}(o | \mathbf{s}_{o_i}^k)) \quad (5.25)$$

with M_i^k being the number of training data for object o_i and tactile feature k . $p_{t+1}(o | \mathbf{s}_{o_i}^k)$ is the object posterior at $t + 1$, updated by the training sample $\mathbf{s}_{o_i}^k$. Actions have more benefit when the expected entropy is minimized:

$$a^* = \underset{k}{\operatorname{argmin}} E[\mathcal{H}_{t+1}(k)] \quad (5.26)$$

5.8. Experimental results

To evaluate the performance of my proposed framework in real time, as well as experimentally validate the efficiency of the suggested approaches for active object learning and active object recognition in an unknown workspace, the robotic system performed experiments in three different scenarios.

At the beginning of all scenarios, the robot did not have any prior knowledge about the location, orientation, and the number of objects. Thus it is necessary for the robot to first explore the entire workspace to gather information about target objects located inside. After exploration, the robot was able to address each object in the workspace and to perform different tasks.

The first task of the robot was to actively and autonomously learn the physical properties of experimental objects in the workspace, i.e. their stiffness, textural properties, and CoM (see Fig. 5.11). In the second scenario (see Fig. 5.17), the task of the robot was to efficiently discriminate among the objects, taking advantage of the knowledge of objects that was learned in the previous scenario. The objects had different locations and orientations in the workspace to the first scenario.

In the last scenario (see Fig. 5.19), the robot was asked to search for a specified target object in an unknown workspace that contains objects, some of which were already learned by the robot previously, and some were not (new objects).

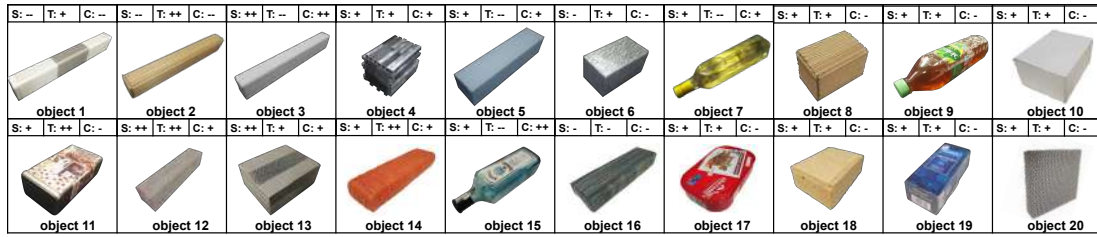


FIGURE 5.10. Experimental objects. The physical properties are evaluated subjectively by human subjects and are indicated in the panel to the upper right of each object (S: stiffness, very soft (-) and very hard (++) T: roughness of surface textures, very smooth (-) and very rough (++) C: center of mass, far from the centroid (-), close to the centroid (++)).

In these experiments, the robotic system, i.e. the UR10 robotic arm, the Robotiq gripper, and the OptoForce sensors, was controlled in the framework of ROS. Tactile signals were sampled at a frequency of 333Hz, and the gripper was controlled at 50Hz.

5.8.1. Properties of experimental objects

In order to evaluate the performance of my proposed framework, I deliberately selected 20 objects (see Fig. 5.10), made of various materials, such as wood, glass, metal, and plastic. The physical properties of these experimental objects vary from relatively similar to quite different. Since the focus of this work is object recognition via surface texture, stiffness, and CoM, the geometrical properties of the objects are out of my scope. Due to the constraints from my hardware (e.g. size of sensor, width and length of robotic fingers), I selected cuboids and objects of bar shape, so that these constraints can be satisfied.

5.8.2. Active Touch for Object Learning in Unknown Workspace

In the first scenario (see Fig. 5.11(WS-1)), the robot started with the active exploration of the unknown workspace to determine the number of objects, as well as their positions, sizes, and orientations. After this, it actively learned about each object using my proposed approach.

5.8.2.1. Active touch for exploration of unknown workspace

The unknown workspace (see Fig. 5.3) is a cuboid with the size of $1000mm(\text{Length}) \times 640mm(\text{Width}) \times 100mm(\text{Height})$, and the world coordinate frame is defined along its width edge (X), length edge (Y), and height edge (Z). Five objects were selected randomly at uniform from object list in Fig.5.10 and put in the workspace⁴. Starting from the origin position,

⁴Due to the constraints of the workspace, it is difficult for the UR10 robot to explore more than five objects. Therefore, five out of 20 objects were selected randomly at uniform for the evaluation.

the workspace is discretized by a step size of 40 *mm* in both *X* and *Y* directions, and 15 *mm* in *Z* direction, according to the width (40 *mm*) of the finger and the distance from fingertip to the center of sensor (15 *mm*). Therefore, the allowed number of sampling points is 25 along the *Y* axis, 16 along the *X* axis, and 4 in *Z* axis, thus the maximum number of sampling for the entire workspace of all four directions counts up to 328 (the total number of mesh grids on four start planes of the workspace). The robot performed exploration clockwise around the workspace, i.e. from \mathbb{W}_{d_1} to \mathbb{W}_{d_4} in sequence.

5.8.2.2. Tactile point cloud construction

I take the exploration of \mathbb{W}_{d_4} as an example, as explained in Sec. 5.3.1. During the exploration process, fingers of the gripper were controlled individually and only one finger was stretched out for exploration. The gripper first stretched out finger A while maintained finger B and finger C closed, and then the UR10 moved its end-effector (the gripper) to the start position on the start plane with the tactile sensor (the fingertip) orienting the d_4 direction, and then started exploration. A contact was detected as soon as the resultant force (Eq. 5.2) measured on the fingertip of A exceeds $\delta = 0.5 N$, then the current position of the finger A was returned as an observation point. The observation point is added into the training dataset of the GPR g_{d_4} . If this light contact is detected before the robot reached the target point, it is also added to the TPC dataset \mathcal{T}_{d_4} .

In order to initialize the GPR model, the robot first uniformly sampled 6 ($M = 3, N = 2$) equally spaced points in total on the start plane as training dataset Ω_{d_4} . After the GPR model was trained, the robot selected the next sampling position according to the predicted variance. The robot continued sampling until the stop criteria is satisfied, which is $\sum_{\mathbf{p} \in \mathbb{X}_{d_i}} Var(g_{d_i}(\mathbf{p})) < \tau$. Then it started the exploration in the next directions. The entire TPC dataset $\mathcal{T}_{\mathbb{W}} = \cup_i \mathcal{T}_{d_i}, \mathcal{I}_{DIR} = \{1, 2, 3, 4\}$ was fully constructed (see Fig. 5.11(a-1)) after the exploration of the entire workspace was completed.

5.8.2.3. Baseline strategies for comparison

In order to evaluate my proposed active workspace exploration strategy, I selected the uniform sampling strategy and the random sampling strategy as baselines for evaluating the performance. For both baseline strategies, the robot sampled exactly the same initialization dataset as for the active exploration strategy at the beginning of the exploration.

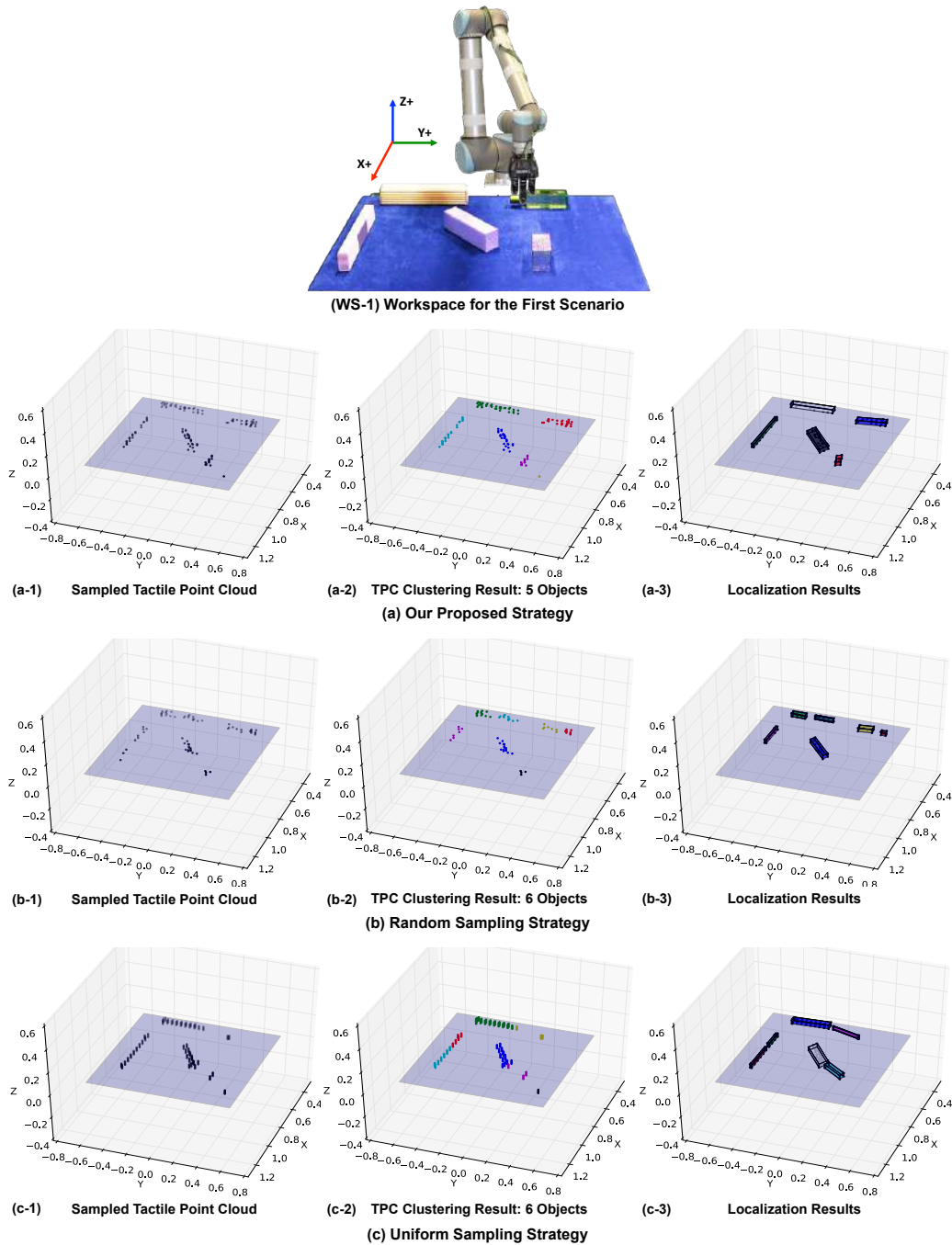


FIGURE 5.11. The active exploration results of the unknown workspace in the first scenario (see Sec. 5.8.3). (WS-1) The layout of the workspace in the first scenario. From left to right, each one of the three sub-figures aligned in a row illustrates the constructed TPC, clustering result of TPC, and result of object localization. (a) The active exploration results of the unknown workspace by applying my proposed strategy. (b) The active exploration results of the unknown workspace by applying random sampling strategy. (c) The active exploration results of the unknown workspace by applying uniform sampling strategy.

Following the uniform sampling strategy, the robot started from one corner of the start plane, and then sampled over all of the start points on the start plane column-wise. For example, the robot started from one corner (e.g. $(\underline{x}, \underline{z})$) of the start plane of \mathbb{W}_{d_4} . The robot sampled from (x_i, \underline{z}) to (x_i, \bar{z}) , and then moved horizontally to the next column (start with (x_{i+1}, \underline{z})).

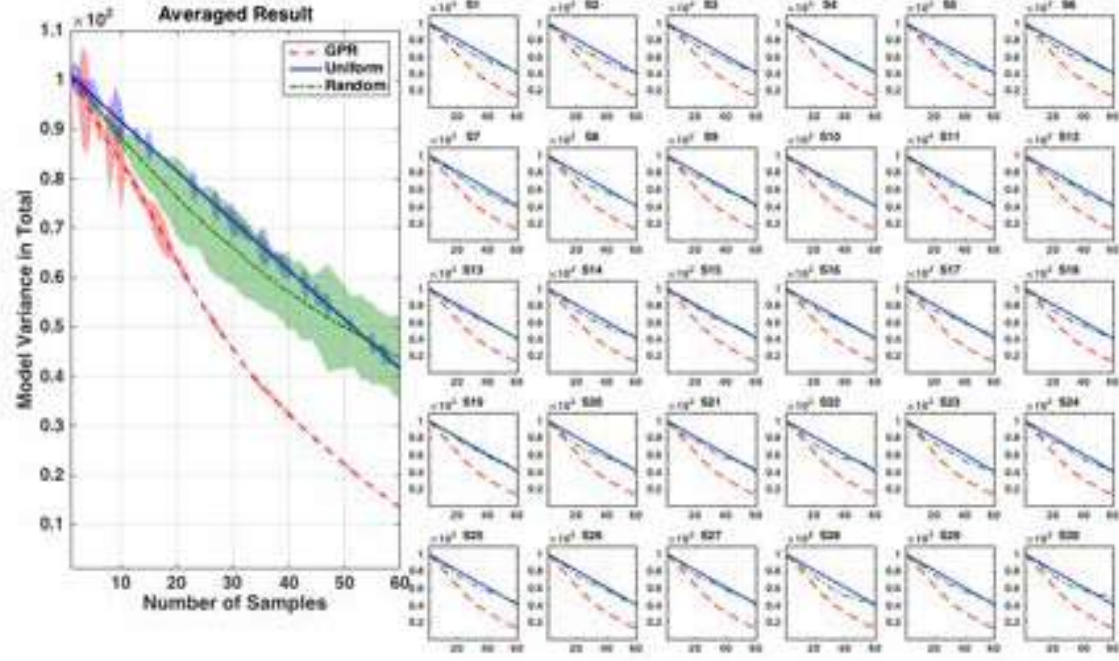


FIGURE 5.12. The statistical comparison of the performance of the proposed active exploration strategy (GPR), uniform strategy, and random strategy for exploring the unknown workspace. Each small sub-figure on the right side named $S1 - S30$ corresponds with one experimental scenario and illustrates the change of total variance in one exploratory direction (here I take $X+$ direction as an example) as the number of samples increases, by applying different exploratory strategies. The large sub-figure on the left side shows the averaged total variance over all the 30 scenarios with the shadowed area denoting the standard deviation.

When applying the random sampling strategy, all of the points $\mathbf{p} \in \mathbb{X}$ on the start plane have the same probability to be selected, and the robot arbitrarily chose a start point on the start plane, and then executed the translational movement.

Since by following my proposed active exploration strategy, the average value of required sample steps for satisfying the stop criteria ($\sum_{\mathbf{p} \in \mathbb{X}_{d_i}} Var(\mathbf{g}_{d_i}(\mathbf{p})) < \tau$) is 60 for \mathbb{W}_{d_1} , \mathbb{W}_{d_3} and 40 for \mathbb{W}_{d_2} , \mathbb{W}_{d_4} , I set these number of sample steps as the stop criteria for both uniform sampling and random sampling in the experiment.

The constructed TPC by following the random and uniform strategies are plotted in Fig. 5.11(b-1) and Fig. 5.11(c-1), respectively.

5.8.2.4. Statistical evaluation of exploration strategies

To statistically compare the performance of three different strategies, the robot explored the unknown workspace in total 30 different scenarios.

TABLE 5.1. Evaluation of clustering performance based on the normalized mutual information (NMI).

Group	1	2	3	4	5	6	7	8	9	10	11	12	13	14	15
NMI	1.00	0.94	0.84	0.80	0.86	0.93	0.96	1.00	0.90	0.91	0.87	1.00	1.00	0.91	0.82
Group	16	17	18	19	20	21	22	23	24	25	26	27	28	29	30
NMI	1.00	0.85	0.87	1.00	0.95	1.00	0.85	0.91	0.83	0.88	0.90	1.00	1.00	0.93	0.90

For each strategy, a GPR model with the same parameters is trained and updated after each observation point is obtained. When applying the active exploration strategy, the GPR model is used to select the next sample position, as well as measure the uncertainty of the workspace (total variance); while applying uniform and random strategies, the GPR models are trained only to calculate the uncertainty (total variance) of the workspace after each sampling.

In each scenario and for every strategy, the robot first sampled 6 positions ($M = 3$, $N = 2$) for \mathbb{W}_{d_1} , \mathbb{W}_{d_3} (4 for \mathbb{W}_{d_2} , \mathbb{W}_{d_4} , $M = 2$, $N = 2$) to initialize the GPR model at the beginning. Then the robot sampled 60 steps for \mathbb{W}_{d_1} , \mathbb{W}_{d_3} and 40 steps for \mathbb{W}_{d_2} , \mathbb{W}_{d_4} , and recorded the value of the total variance predicted by the trained GPR model after each sample step. A small total variance $\sum_{\mathbf{p} \in \mathbb{X}_{d_i}} \text{Var}(\mathbf{g}_{d_i}(\mathbf{p}))$ indicates that the GPR model, which is trained with the dataset sampled so far, can accurately describe the workspace; in other words, the exploration strategy is data-efficient.

The statistical comparison of the results is illustrated in Fig. 5.12. Since the exploration processes in each direction are independent, here I only compared the exploration performance of \mathbb{W}_{d_1} . The result shows that for all the strategies, the uncertainty of the workspace reduces as the number of samples increases. At each sample step, the workspace has the minimal total variance by following the active exploration strategy, and its uncertainty reduces faster than either uniform or random strategy, indicating that the workspace can be much more efficiently sampled by applying the proposed active exploration strategy than the baseline strategies.

5.8.2.5. Object localization and mapping

The sampled TPC in each scenario is clustered using the Mean-Shift approach (see Fig. 5.11(a-2), Fig. 5.11(b-2), and Fig. 5.11(c-2)). Clusters with less than 5 data points were considered noise points and therefore discarded. After this, the minimum bounding box was calculated for each cluster to estimate the location, orientation, and geometric center of each object (see Fig. 5.11(a-3), Fig. 5.11(b-3), and Fig. 5.11(c-3)). As Fig. 5.11 shows, all of the experimental objects were successfully clustered (see Fig. 5.11(a-2)) and correctly localized (see Fig. 5.11(a-3)) by employing my proposed strategy. However, by applying random sampling strategy, some regions of the workspace were not sufficiently explored, thus the TPC was incorrectly clustered into 6 objects (see Fig. 5.11(b-2)) and the estimated geometric information

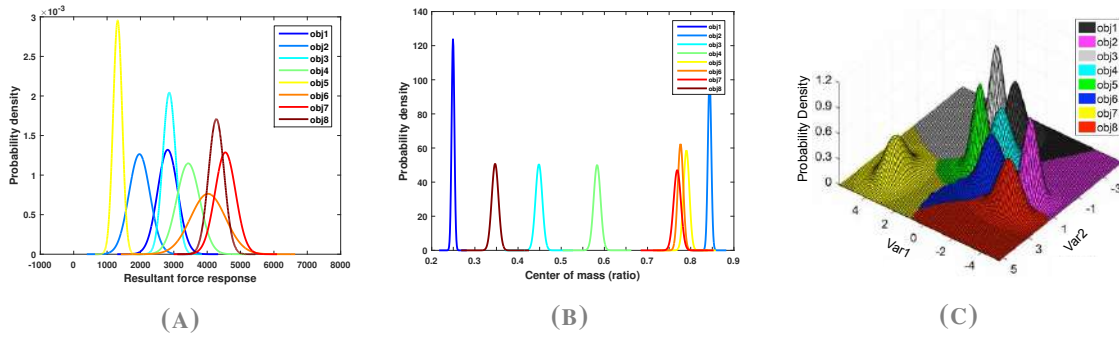


FIGURE 5.13. Distributions of the features extracted from the test dataset. (A) The resultant force response for stiffness. (B) CoM. (C) Robust textural descriptors. The observation distributions for object stiffness and CoM are modeled by univariate Gaussian distribution. To visualize the distribution of textures, I first reduce the 12 dimensional texture descriptor to 2D vector via Principle Component Analysis (PCA). Then I model the distributions of features by multivariate Gaussian distribution.

of the objects was fallacious as a result (see Fig. 5.11(b-3)). While using the uniform sampling approach, because of the constraints of sample steps, the robot was not able to complete the exploration. Therefore, only part of the workspace was fully explored. As a result, the TPC dataset was not complete (see Fig. 5.11(c-2)) and objects were not able to be correctly localized (see Fig. 5.11(c-3)).

I evaluated the performance of Mean-Shift clustering approach in all 30 scenarios based on the normalized mutual information (NMI). Table 5.1 shows the NMI values of the clustering result in each scenario. The average NMI of all 30 scenario is 0.92.

In 9 out of 30 scenarios, the TPC data were perfectly clustered ($NMI = 1.00$). In 16 out of 30 scenarios, the sampled data points were clustered ($NMI < 1.00$) followed by a successful localization and mapping of the experimental objects. Although some points were wrongly clustered, due to either the noise data or the connection of adjacent objects; however, by filtering out the noise clusters and constructing the bounding boxes, the localization and mapping results were acceptable for the robot to execute the subsequent tasks. The clustering failed in the remaining 5 scenarios, either because a large part of the TPC dataset were wrongly clustered, or the number of clusters does not match the number of real objects (object number is wrongly estimated). The reason is, multiple experimental objects were densely placed in these scenarios, some of them even connected to each other, thus these objects are occluded and cannot be fully explored.

The active exploration process of the unknown workspace was carried out at the beginning of each scenario, and the obtained information of objects was used for the subsequent procedures.

5.8.3. Evaluation of active tactile object learning (AT-LPP)

5.8.3.1. Test Data Collection

The performance of my proposed active object learning was evaluated with a test dataset. The dataset was collected by the robot autonomously, by performing three exploratory actions (pressing, sliding, and lifting) on 20 experimental objects (Fig.5.10). The data collection procedure was repeated 20 times for each object and each exploratory action. During executing all exploratory actions, the gripper is controlled in "pinch" mode, i.e. finger B and finger C of the gripper were arranged next to each other and are controlled to have the same positions. Finger B and finger C move simultaneously and are opposite to the moving direction of finger A. In this configuration, these three contact positions (fingertips) form an isosceles triangle with B and C symmetric with respect to A.

For pressing action, the robot first moved to the object (i.e. let the geometric center of three fingers coincides the geometric center of the target object), it then closed all fingers for $N_\epsilon = 3$ extra position counts after a light contact of $f_t = 0.5 N$ on each fingertip. When sliding on the surface of objects, the robot slid for 30 mm vertically after contacting the object (light contact force: $f_t = 0.5 N$). In order to lift the object, the robot exerted an initial contact force of 0.5 N to grasp the object and then lifted it up for $\Delta h = 30 mm$. A linear slip was detected, if the tangential force had increased more than 25% within $\Delta t = 1 s$ after the object being lifted to the target height. The expected similarity level for the CoM was set as $\gamma = 0.9$; however, considering the time consumption, the process of exploring the CoM would also be terminated if the distance between two successive lifting positions was less than 0.5 mm.

5.8.3.2. Baselines

The performance of my proposed active learning strategy (AT-LPP) was evaluated with both random and uniform sampling strategies.

B.1. Random Learning Strategy:

While applying the random learning strategy, both of the next object $o = \mathcal{U}\{o_1, o_2, \dots, o_N\}$ and the next physical property $k = \mathcal{U}\{k_1, k_2, k_3\}$ subject to uniform distribution ($o \sim \mathcal{U}(1, N)$ and $k \sim \mathcal{U}(1, 3)$), i.e. all of the o s (and k s) have the same probability to be selected. The robot arbitrarily determines the next object $o \in \{o_1, o_2, \dots, o_N\}$ and the next physical property to learn $k \in \{\text{surface texture, stiffness, center of mass}\}$.

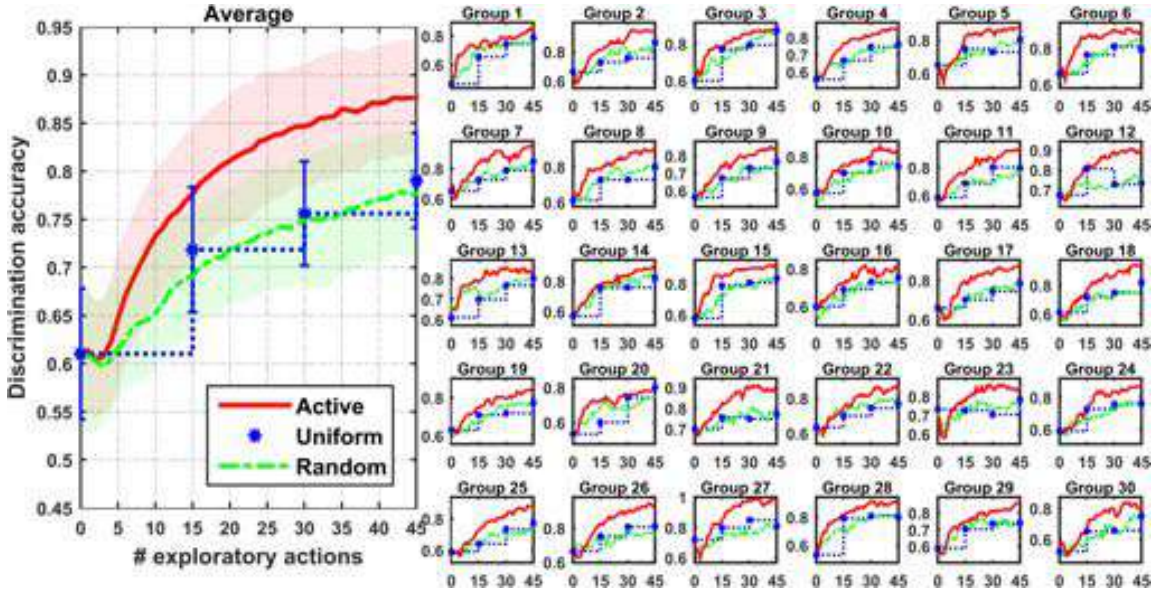


FIGURE 5.14. Active learning about objects based on their physical properties. The horizontal axis represents the number of training data collected thus far. The vertical axis shows the mean value of the classification accuracy of evaluation dataset averaged over 30 runs.

B.1. Uniform Learning Strategy:

Using the uniform learning approach, at each round of the exploration, the robot learned about all three physical properties of each object in the workspace. In other words, the robot moved to each of five object $\{o_1, o_2, \dots, o_N\}$ and executed all three exploratory actions $\{a_1: \text{sliding}, a_2: \text{pressing}, a_3: \text{lifting}\}$ on each object in order to learn about $\{k_1: \text{texture}, k_2: \text{stiffness}, k_3: \text{center of mass}\}$.

5.8.3.3. Evaluation of active tactile object learning via all physical properties

In this scenario, the task of the robot was to learn five objects in the workspace based on their physical properties (stiffness, surface textures, CoM). To initialize the active learning process, the robot collected small training samples by performing each of three exploratory actions once on each object. Each step when the robot sampled a new training instance, the recognition accuracy of GPCs was measured with the test dataset.

Fig. 5.13 illustrates the distributions of the tactile features extracted from the eight objects (as an example) in test dataset. On the one hand, depending on the physical properties, objects have different degrees of confusion. For instance, Fig. 5.13c shows that although some objects have similar surface structures, they can be discriminated by their textural property, thanks to my proposed robust tactile descriptors. In contrast, it is difficult to distinguish objects using

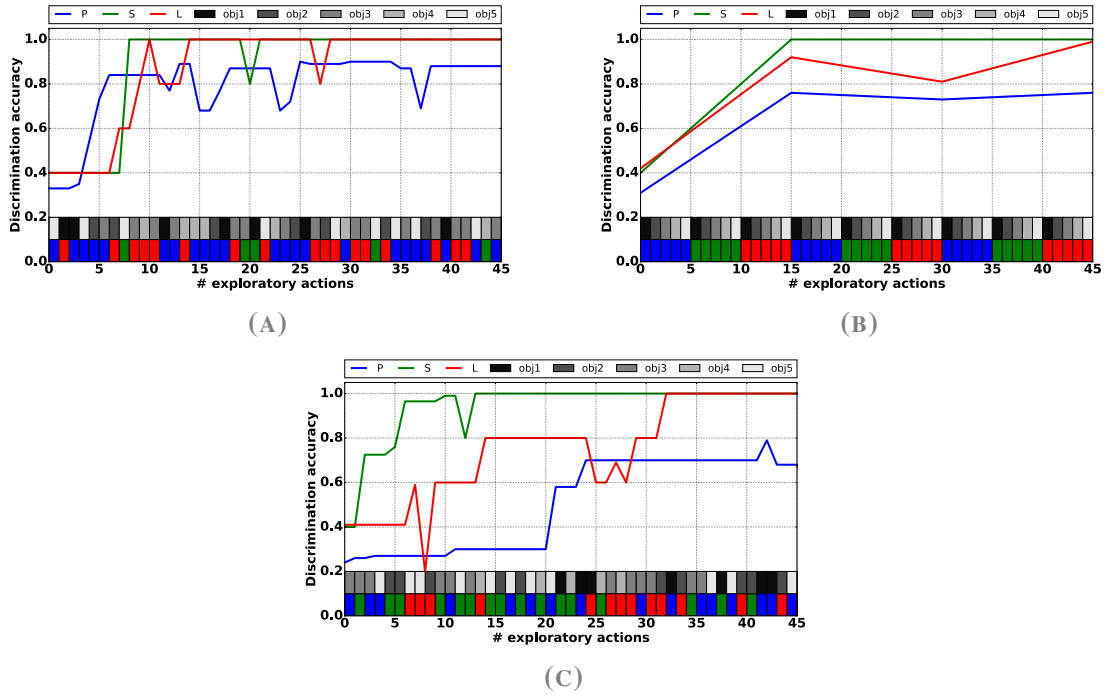


FIGURE 5.15. An example of learning five objects with three physical properties. Three object and exploratory action selection methods are compared. (a) Proposed active learning method AT-LPP, (b) Uniform sampling method, (c) Random sampling method. The lower bar shows the exploratory actions at each time step (“P” for pressing, “S” for sliding, “L” for lifting). The upper bar shows the object to explore at each step. The vertical axis shows the classification accuracy on the test database.

stiffness, because the stiffness of the objects are very similar (see Fig. 5.13a). On the other hand, for the same physical property, objects’ confusion are different from each other. For example, Fig. 5.13b clearly shows that objects 1, 2, 3, 4, and 8 can be easily recognized via their CoM, whereas objects 5, 6, and 7 are confused with each other.

At each object learning round 5 objects $\{o_1, o_2, \dots, o_5\}$ were randomly selected out of 20 objects $\mathcal{O}_{1:20}$ (see Fig. 5.10). Then, the robot learned about objects via their physical properties. In order to have a fair comparison between my AT-LPP method and the baseline learning strategies the robot executed 45 exploratory actions in total during learning process. This process is repeated 30 times for 30 groups of objects, each group is repeated 5 times.

Fig. 5.14 shows the robot’s learning progress measured by the classification accuracy on the test dataset each of 30 groups of experiments as well as the classification accuracy averaged over all 30 groups. Fig. 5.14 demonstrate that AT-LPP consistently outperforms the baseline methods by obtaining the higher recognition accuracy while performing fewer exploratory

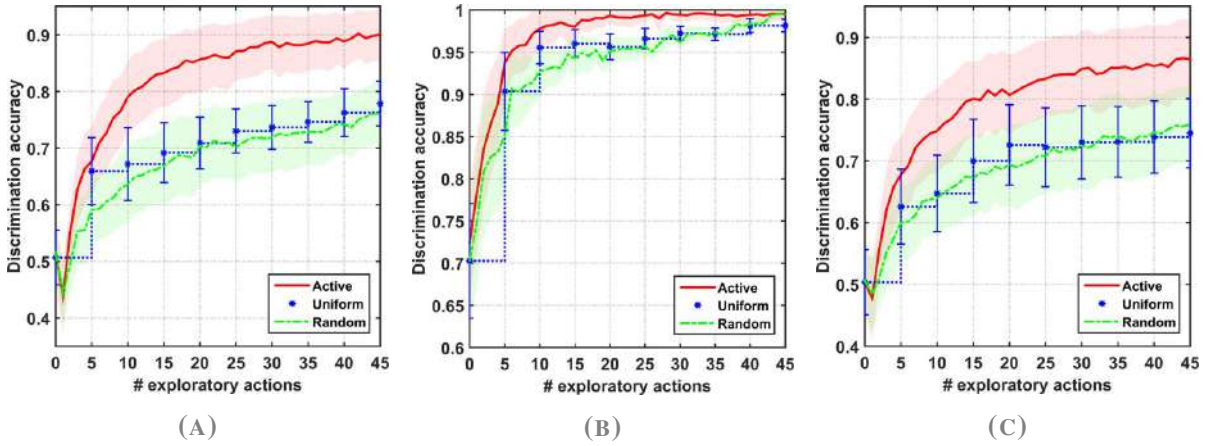


FIGURE 5.16. Active learning each object physical property individually. (A) Learning object’s stiffness. (B) Learning object’s surface textures. (C) Learning object’s CoM. The horizontal axis represents the growing number of training data, and the vertical axis represents the value of classification accuracy on the test data averaged over 30 runs.

actions. For instance, the robot obtained in average more than 81% recognition accuracy when it performed 20 exploratory actions. However, using random and uniform strategies the robot achieved 71% recognition rate with the same number of actions. Obviously, the active learner learns about the object more quickly than uniform and random sampling strategies.

Apart from a numerical evaluation of the performance of the proposed method, I also investigated the learning process and decision of the strategy over time. Fig. 5.15 demonstrates one exemplifying result of the learning progress following three aforementioned strategies to select next object and next physical property. The bottom rows with a color code illustrate the selected object and action to perceive physical property at each decision step. Fig. 5.15a shows that following my proposed learning method AT-LPP, the robot focused on collecting more training samples for the objects’ physical properties that make objects to be more confused (such as stiffness). Moreover, using AT-LPP the robot sampled less data to obtain the observations with which objects can be quickly recognized (such as surface texture). Conversely, since uniform (see Fig. 5.15b) and random learning strategies (see Fig. 5.15c) collected training samples without exploiting their informativeness, the “difficult” objects were insufficiently learned, while the “easy” objects were redundantly observed.

5.8.3.4. Evaluation of active tactile object learning via single physical property

In order to evaluate the robustness of my active learning algorithm, the robotic system was asked to learn about objects via only one of the three tactile properties (stiffness, surface texture, and CoM). Random sampling and uniform sampling serve as baseline. Each method was run 30 times by the autonomous robot. Fig. 5.16 shows the learning performance of

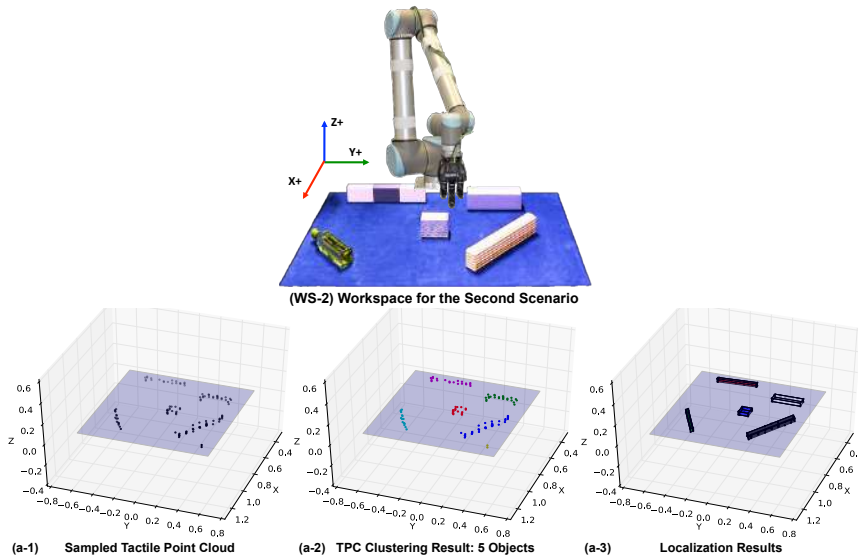


FIGURE 5.17. The active exploration results of the unknown workspace in the second scenario (see Sec. 5.8.4) by applying my proposed strategy. (WS-2) The layout of the workspace in the second scenario. (a-1) The constructed TPC. (a-2) Clustering result of TPC. (a-3) Object localization result.

the robotic system when it explored the objects. It is evident that the learning progress was dependent on the distributions of the tactile features. For instance, Fig. 5.16a shows that learning objects via their stiffness led to low classification accuracy, because object's were confused by their stiffness. It is the same situation for learning objects via their CoM (see Fig. 5.16c). On the contrary, objects were easily distinguished by using my proposed robust tactile descriptors (see Fig. 5.16b). Therefore, the learning process for object surface texture was faster and ended with higher recognition rate. In all cases (see Fig. 5.16), the entropy reduction method outperforms the other two methods by up to 30% of the recognition accuracy with the same number of training samples. Therefore, my active learner is robust to different distributions of the tactile features.

5.8.4. Evaluation of Active Object Discrimination

With the reliable observation models constructed by my proposed active touch learning method (AT-LPP) with 30 groups of objects previously, I evaluated my proposed active object discrimination and action selection strategy. To do this, I compute the decision steps using my CMUM, the expected entropy reduction (EER) (Sec. 5.7.1) and random strategy $a^* \in \mathcal{U}(1, 3)$, $a^* \in \{a_1 : \text{sliding}, a_2 : \text{pressing}, a_3 : \text{lifting}\}$ approaches to discriminate among objects in the workspace (see Fig. 5.17(WS-2)).

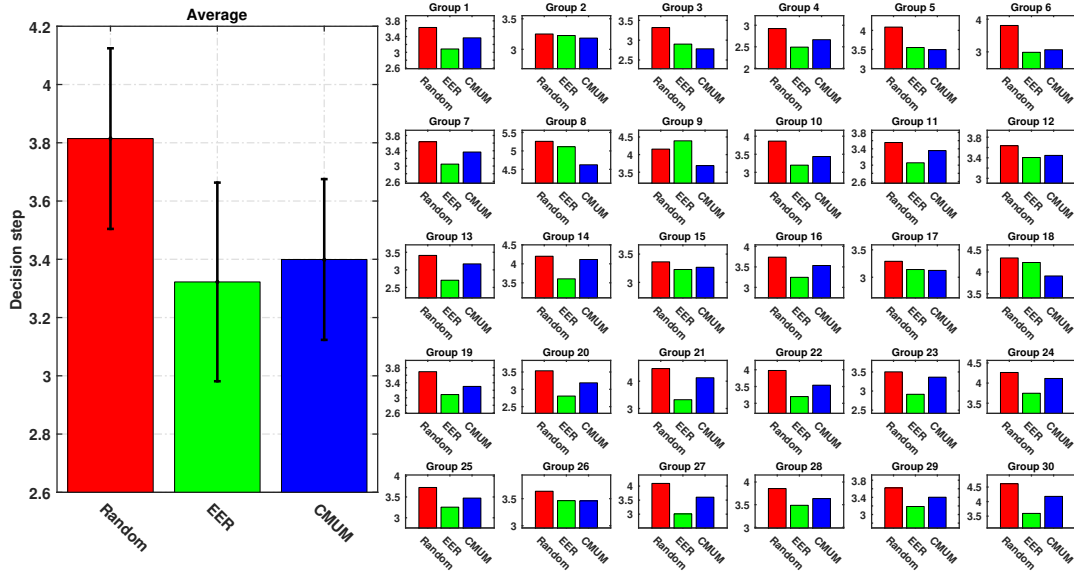


FIGURE 5.18. Evaluating active object discrimination and target object search. Average decision steps the robot takes to discriminate objects.

In this regard, the robot first explored the workspace following the procedure as described in Sec. 5.8.2. The constructed TPC, clustering results, and localization results are illustrated in Fig. 5.17.

The robotic system executed a sequence of exploratory movements on an object, until the object MAP exceeded 90%, or the iterations reached seven times. Then, I measured the number of decision steps and compared the MAP results to the true object class. The experiment was repeated 30 times. In each experiment, the robot used three methods to explore each object five trails.

Fig. 5.18 shows the average number of decision steps. The robot discriminated among objects by CMUM and EER more quickly than the random method. Furthermore, the decision accuracy from CMUM are higher than EER and random (CMUM: 99.9%, EER: 92.4%, Random: 93.2%). Therefore, I can conclude that a robotic system that uses my proposed CMUM can discriminate objects quickly and correctly.

5.8.5. Evaluation of active target object search

When evaluating the robot's competence of searching for the target objects, I randomly replaced two known objects in the workspace at each of 30 groups of objects with two randomly selected unknown objects (see Fig. 5.19).

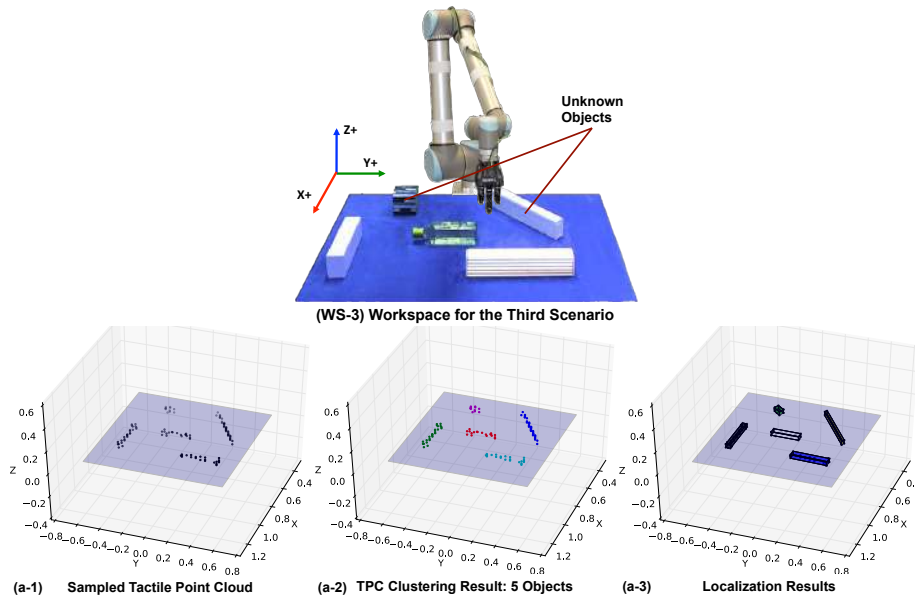


FIGURE 5.19. The active exploration results of the unknown workspace in the third scenario (see Sec. 5.8.5) by applying my proposed strategy. (WS-3) The layout of the workspace in the third scenario. (a-1) The constructed TPC. (a-2) Clustering result of TPC. (a-3) Object localization result.

Now the task of the robot is to find the targeted object, or leave the non-targeted object as quickly as possible while taking the advantage of its already constructed observation models in Sec. as prior knowledge.

To do this, the robotic system explored each of the object in the workspace using my proposed CMUM strategy and the EER and random strategies as baselines. Each strategy was run 30 times with 30 groups of randomly selected objects. In each round, the robot explored each object in the workspace five times. The exploration was run until the object MAP is larger than 90%, or until seven exploratory movements were conducted. As a result, the robot either detected the target object (when $p(o = o_{tg}) > p(o \neq o_{tg})$) or the non-target object (when $p(o = o_{tg}) < p(o \neq o_{tg})$). I recorded the number of exploratory movements the robot executed in order to make a decision, as well as the decision accuracy.

Fig. 5.20 illustrates average decision steps over 30 groups of objects which robot takes to find the target objects. Fig. 5.20 shows that both CMUM and EER take fewer steps than random method to recognize all target objects. The decision accuracy from CMUM is higher than EER and the random selection (CMUM: 99%, EER: 87%, Random: 90%). Fig. 5.21 shows the average decision step the robot leaves the non-target objects. Fig. 5.21 demonstrates the similar results using CMUM, EER, and random strategies, the robotic system efficiently leave the non-target objects with almost the same decision accuracy (CMUM: 97%, EER: 92%, Random: 94%).

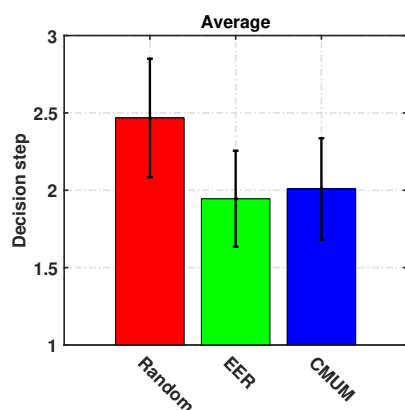


FIGURE 5.20. Evaluating active object discrimination and target object search. Average decision steps the robot takes to find the target objects.

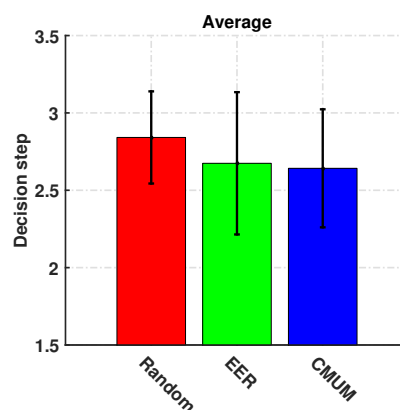


FIGURE 5.21. Evaluating active object discrimination and target object search. Average decision steps leave the non-target objects.

5.9. Summary and discussion

I proposed a probabilistic strategy to enable the autonomous robot to explore its surroundings with high efficiency, in order to localize and estimate the geometric information of the objects in its perimeter. Taking advantage of GP regression, the robotic system explored the workspace so that more tactile points were sampled on the objects and around their perimeter. At each phase, the tactile data already collected were used to construct a probabilistic model to guide the next step of workspace exploration. The experimental results show that my proposed approach outperforms both random and uniform data selection. The robotic system then clustered the captured tactile data points to ascertain the number of objects in the workspace. The minimum bounding box was calculated for each cluster to estimate the location, orientation, and geometric center of each object. After object localization and workspace mapping, the autonomous robot actively discriminated them from each other based on their physical properties. In this regard, the robot used my proposed GP classification based method to efficiently learn the physical properties of objects. It used the extended version of my previously proposed tactile descriptor to perceive the textural properties of objects by sliding its fingertips on the surface of the objects (objects with either regular or irregular textural properties). Moreover, the robot employed my suggested tactile-based approach to estimate the CoM of rigid objects. It measured the stiffness of each object by pressing against them with its three fingertips.

In previous studies, the observation models were constructed by the predefined number of training samples for each object, which were collected offline during tactile exploration. Contrary to previous works, using my proposed algorithm, the robotic system sampled the objects such that with a smaller number of exploratory actions it constructed reliable object observa-

tion models online. The robot collected more training samples from “difficult” objects which had fewer discriminative tactile properties and thus were confused with other objects. In other words, the robot did not deposit any redundant tactile information. The experimental results illustrate that the robotic system learned about objects based on their physical properties efficiently and achieved higher classification accuracy by using my proposed approach. It proves that my proposed method outperforms random and uniform sampling strategies.

After object learning phase, the autonomous robot efficiently distinguished experimental objects with arbitrary location and orientation from each other. It also found the target object in the workspace quickly. To do this, it used my proposed strategies for active object discrimination and target object search and took the advantage of the reliable observation models constructed during the object learning phase.

In this regard, the robotic system predicted the benefit of each of the exploratory actions (pressing, sliding, and lifting) and executed the one that would obtain the most discriminative properties. The performance of my proposed method was compared with both EER and random exploratory action selection strategies. The experimental results show that by using my proposed method, the robotic system discriminated among objects faster than by using random strategy, and reached higher recognition rate than the EER.

When estimating the benefit of an exploratory movement, CMUM inferred the dissimilarity between objects by building a probabilistic confusion matrix.

The most computational intensive part of the task is the Gaussian process; its computational complexity is $\mathcal{O}(N^3)$ with N being the number of training data. The computational complexity of the active touch for unknown workspace exploration is the same as the GPR model, i.e., $\mathcal{O}(N^3)$, since the exploration processes of each direction are independent. The computational complexity of active touch learning is $N_p \times N_o \times \mathcal{O}(N^3)$, where N_p is the number of object physical properties, N_o is the number of objects, and N is the number of training data points. The complexity active object discrimination is $\mathcal{O}(N_o)$, comes from the updating of the object belief. For active target object search, the complexity is $\mathcal{O}(N^3)$ for training the binary GPCs, then it becomes $\mathcal{O}(N_o)$ for the update of object belief during the online experiment.

The computation of action selection was proportional to the square of the number of objects ($\mathcal{O}(N_o^2)$). However, EER integrated all the training samples to predict the benefit of an exploratory action. As the number of training samples grew, the computation became costly. In this case, for example instead of GPs, the sparse approximation of Gaussian processes [162] can be used.

Furthermore, it was found that compared to CMUM, EER would more frequently converge to an incorrect decision when the probability threshold was not set high enough. Its performance could be improved when the threshold was set higher, and more exploratory movements were required.

Moreover, due to the constraints of my hardware, such as the size of robotic fingers and the spatial resolution of the tactile sensor, I selected cuboid objects to satisfy these constraints.

In the future, in order to evaluate my proposed framework with complex shapes and deformable objects, I will equip a humanoid robot with the sense of touch and will extend my framework for dual hand workspace exploration and tactile object recognition. I will also generalize my proposed algorithm for the estimation of the center of mass of objects with complex shape. Moreover, a fascinating future work would be enabling the autonomous robot to learn about unknown objects while searching for the known target object in a workspace (life-long active object learning).

CHAPTER 6

Online Tactile Transfer Learning

The art and science of asking questions is the source of all knowledge.

(Thomas Berger)

6.1. Introduction

The performance of tactile object learning algorithms depends heavily on the quality and the number of training samples. In real-world applications, however, collecting training samples is costly and there may not always be an adequate amount of training data available. In chapter 3, we proposed a set of robust tactile descriptor for the robotic system to discriminate among objects via their textural properties. The robots uniformly collected sufficient training samples by sliding their tactile sensor/s or skin area on the surface of the objects to construct robust learning models of the objects. On the one hand, collecting many training data is memory and time-consuming. On the other hand, executing many exploratory actions on the surface of the objects may damage tactile sensors. Moreover, in case of learning a new set of objects the learning algorithms need to re-trained from scratch. In other words, the robots are still unable to re-use their tactile knowledge that was previously obtained when they learn about new objects.

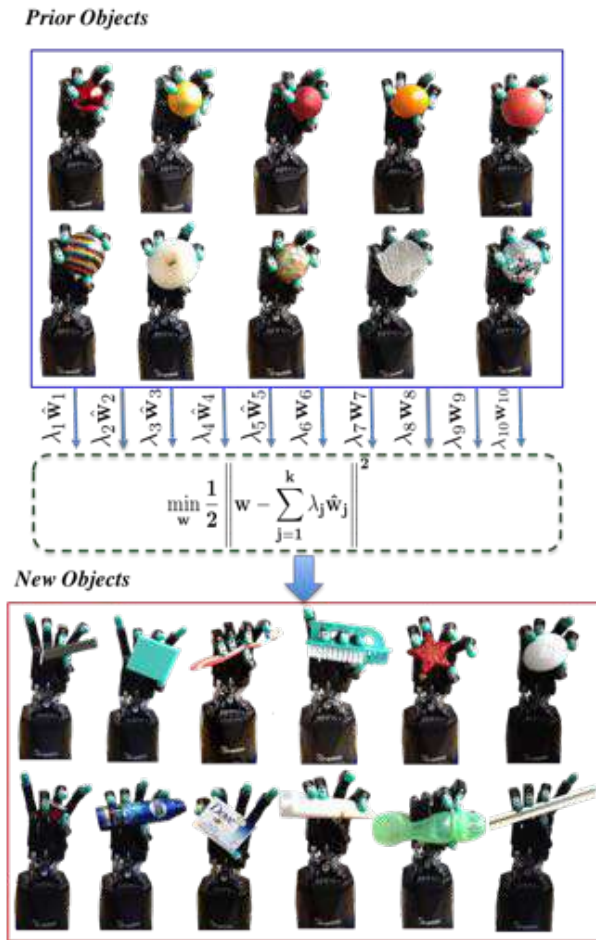


FIGURE 6.1. The Shadow Hand with BioTac robotic skin. Employing the proposed tactile transfer learning method the Shadow Hand could re-use its prior knowledge while discriminating new objects from their texture with a very few trials. The illustrated formula is the regularizer term of the adapted LS-SVM in (6.2). The weight assigned to each prior knowledge λ was found by minimizing Eq.(6.2). K is the number of prior knowledge.

To tackle the above-mentioned problem, in this chapter, we propose an online tactile transfer learning algorithm to enable robotic systems to autonomously select and exploit their previously constructed objects' model while learning about new objects with using the fewer training samples. The performance of our proposed method was experimentally evaluated by the Shadow Hand equipped with multimodal robotic skin. Furthermore, we evaluated the robustness of the algorithm with negative tactile knowledge.¹

¹The content of this chapter has been submitted to [86, 163]. The initial idea comes from [80, 164] which we re-designed and extensively improved it for the tactile data.

6.1.1. Problem definition

Lets consider a scenario where the Shadow Hand has already constructed a set of tactile learning models to discriminate $k = 10$ different surface textures (see Fig.6.1-Prior Objects) with sufficient enough available training samples. Now the task of the Shadow Hand is to classify $M = 12$ new surface textures (see Fig.6.1-New Objects) with only one or a very few available training samples while re-using the previous learned texture models (Prior texture models) in an online manner. Our proposed hybrid tactile transfer learning method has four main steps. (1) Constructing Prior Texture Models (2) Autonomously selecting the most relevant multiple texture models for the new texture recognition (Prior Texture Model Selection) (3.1) Initializing the online learning algorithm with the constructed prior models (3.2) Constructing the new texture models while receiving new textures/objects (4) Updating And Re-weighting the Prior Textures Models. The initial idea comes from our method in [80, 164] which we re-designed and extensively improved it for the tactile data.

6.2. Prior tactile knowledge construction

The Shadow Hand employed the Least Squared Support Vector Machine (LS-SVM) [165] to construct several prior texture models. In this case the LS-SVM was trained with $k = 10$ prior textures (see Fig. 6.1-Prior Objects). More formally, consider a classification scenario with an entire available set of training data $\{\mathbf{z}_\ell, y\}_{\ell=1}^{N_k}$ where $\ell = 1, \dots, N_k$, $k = 10$ is the number of prior objects/textures, N_k is a number of training samples of each prior object, $\mathbf{z} \subset \mathbb{R}^d$ is an input vector describing the ℓ^{th} sample and $y \in \mathbb{Y}$ is the corresponding objects' label. The main purpose is to construct a function, $g_j(\mathbf{z}) = \hat{\mathbf{w}}_j \cdot \mathbf{z}$ ($j = 1, \dots, k$) that can divide the unseen test data. In this respect, $\phi(\mathbf{z})$ is utilized to map the input trial samples to a higher dimensional feature space, in our case, radial basis kernel. In LS-SVM the texture model parameters (\mathbf{w}, b) are obtained by solving

$$J^{\mathbf{w}} = \min_{\mathbf{w}, b} \frac{1}{2} \|\mathbf{w}\|^2 + \frac{C}{2} \sum_{\ell=1}^N [y - \mathbf{w} \cdot \phi(\mathbf{z}_\ell) - b]^2 . \quad (6.1)$$

where C is a regularization parameter that controls the bias-variance trade-off. N is the number of the training samples collected with each prior objects (in our case $N = 30$).

6.3. Prior tactile knowledge selection

By slightly modifying the regularization term in LS-SVM (6.1) [166], it is possible to construct new discriminating texture models for the new objects (see Fig.6.1-New Objects) close to the already constructed prior models (see Fig.6.1-Prior Objects):

$$J^{\mathbf{w}\hat{1}:k} = \min_{\mathbf{w}, b} \frac{1}{2} \left\| \mathbf{w} - \sum_{j=1}^k \lambda_j \hat{\mathbf{w}}_j \right\|^2 + \frac{C}{2} \sum_{\ell=1}^N [y - \mathbf{w} \cdot \phi(\mathbf{z}_\ell) - b]^2. \quad (6.2)$$

where $\hat{\mathbf{w}}$ is the parameter describing the prior texture models and λ is a scaling factor corresponding to ranking the prior models and decides how much and from where to transfer the prior tactile knowledge. In other words λ controls to what degree the new texture models are close to the prior texture models. The optimization problem (6.2) has the same cost function as LS-SVM in which the regularizer term has been modified to impose closeness between the new texture models and a linear combination of prior texture models. The weight factor λ assigned to each prior texture model was found by minimizing $\sum_{t=1}^k \ell_t(\tilde{y}, y)$ subject to $\|\boldsymbol{\lambda}\|_2 \leq 1$ where \tilde{y} is the leave one out prediction for the t -th sample and $\boldsymbol{\lambda} = (\lambda_1, \dots, \lambda_k)$. With this formulation the final prediction function for the collected testing data is:

$$g(\mathbf{z}) = \mathbf{w} \cdot \mathbf{z} + b = \left(\sum_{j=1}^k \lambda_j \hat{\mathbf{w}}_j + \sum_{t=1}^T \alpha_t \mathbf{z}_t \right) \cdot \mathbf{z} + b. \quad (6.3)$$

In (6.3) α_t are the coefficients of the support vectors for the new textures classification problem.

6.4. Online learning methodology

The robotic systems employed the cost-sensitive multi-class Passive Aggressive (PA) method to discriminate among M classes of objects or materials while receiving samples continuously over time. The passive aggressive is as a margin based online or open-ended learning technique in order to construct and update learning models continuously [167]. Using PA, at each time step, the robot constructed texture models to generate the corresponding prediction for the current received samples. The received true label was then used as a feedback in order to update the texture models for the next coming new samples. More formally, PA estimates the model parameters $\mathbf{w}_t \in \mathbb{R}^d$ at every time $t = 1, 2, \dots, T$ receives new data samples $\{\mathbf{z}_m, y_m\}_{m=1}^M$ where $\mathbf{z}_m \in \mathbb{R}^m$ are sequential samples with $y_m \in \mathbb{Y}$ as their corresponding labels. Assume that the PA is provided with a set of d features ϕ_1, \dots, ϕ_d where each feature ϕ_i is a mapping

from $\mathbb{Z} \times \mathbb{Y}$ to the reals. We denote by $\Phi(\mathbf{z}_m, y_m) = (\phi_1(z_m, y_m), \dots, \phi_d(z_m, y_m))$ the vector formed by concatenating the outputs of the features. At $t = 1$, the PA starts with the model parameters having values equal to zero. It means at $t = 1$, $\mathbf{w}_1 = (0, \dots, 0)$, then the value of confidence on prediction was then computed with

$$\hat{y}_t = \arg \max_{\mathbf{y} \in \mathbb{Y}} (\mathbf{w}_t \cdot \Phi(\mathbf{z}_{m,t}, y_{m,t})). \quad (6.4)$$

Afterwards, PA updates the models when receives new samples by solving Eq.(6.5).

$$\mathbf{w}_{t+1} = \min_{\mathbf{w} \in \mathbf{R}^d} \frac{1}{2} \|\mathbf{w} - \mathbf{w}_t\|^2 + \eta \xi. \quad (6.5)$$

which results in Eq.(6.7).

$$\mathbf{w}_{t+1} = \mathbf{w}_t + \theta_t (\Phi(\mathbf{z}_{m,t}, y_{m,t}) - \Phi(\mathbf{z}_{m,t}, \hat{y}_{m,t})), \quad (6.6)$$

$$\theta_t = \min \left\{ \eta, \frac{\max\{0, 1 + \mathbf{w}_t \cdot (\Phi(\mathbf{z}_{m,t}, y_{m,t}) - \Phi(\mathbf{z}_{m,t}, \hat{y}_{m,t}))\}}{\|\Phi(\mathbf{z}_{m,t}, y_{m,t}) - \Phi(\mathbf{z}_{m,t}, \hat{y}_{m,t})\|^2} \right\}. \quad (6.7)$$

In Eq.(6.5), η is a positive value that governs the influence of the slack terms. This technique is known as a PA-I cost sensitive multi-class classification with prediction-based update (PB) [167]. ξ is a non-negative scaling factor of the objective cost function. In Eq.(6.6), $\mathbf{z}_{m,t}$ is a current received sample at time t and $y_{m,t}$ is the label of the received samples.

6.5. Tactile transfer learning methodology

This is a hybrid algorithm [80, 164] in which the adapted LS-SVM provides autonomously the most relevant prior models $k = 10$ to the new texture models $M = 12$. This results in constructing an initial new texture models:

$$\mathbf{w}_1 = \sum_{s=1}^k \lambda_s \hat{\mathbf{w}}_s + \sum_{t=1}^T \alpha_t \mathbf{z}_t. \quad (6.8)$$

The (6.8) is composed of two parts. The first part is the linear combination of the weighted prior texture models where \mathbf{w}_s is the prior model, λ_s is the scaling factor (needs to be updated at each time t), and k is the number of prior models. The second part represents the received new training texture samples (T is the number of the samples). Now, the PA algorithm uses the new initial models \mathbf{w}_1 in (6.8) instead of the $\mathbf{w}_1 = (0, \dots, 0)$ to learn from the $(t+1) - th$ new incoming texture samples.

6.5.1. Updating and re-weighting the prior textures models

So far, we initialized the PA learning algorithm by integrating the prior and new texture models. But, still, the prior texture models are not directly re-weighted during the on-line learning process. We describe here how the weights of the prior and new texture models will be updated during the on-line learning progressively in time. In this case, the prediction can be made on each new incoming samples by means of the current constructed texture models in (6.8) as $\mathbf{w}_1 \cdot \mathbf{z}_t$.

The results of the prediction $\sigma_{k,t}$ will be cropped between (-1,1) and will be used as the $(d+k) - th$ element (d is the dimension of a new sample and k is the number of the prior models) in the feature vector of \mathbf{z}_t defined as:

$$\mathbf{z}'_t = (\mathbf{z}_t, \sigma_{1,t}, \dots, \sigma_{k,t}) \in \mathbb{R}^{d+k}, \quad (6.9)$$

where

$$\sigma_{k,t} = \max\{-1, \min\{1, \mathbf{w}_1^k \cdot \mathbf{z}_t\}\}. \quad (6.10)$$

The new samples with such a modified representation enters the online algorithm. At $t = 1$ online algorithm predicts with $sign(\mathbf{w}'_1 \cdot \mathbf{z}'_1)$ in which the $\mathbf{w}'_1 = (\mathbf{w}_1, \mathbf{1}) \in \mathbb{R}^{d+k}$. For the $t+1$ the updating rule in Eq.(6.6) now is

$$\mathbf{w}'_{t+1} = \mathbf{w}'_t + \theta_t y_t \mathbf{z}'_t, \quad (6.11)$$

where

$$\theta_t = \min\left\{C, \frac{\max\{0, 1 - y \mathbf{w}'_t \cdot \mathbf{z}'_t\}}{\|\mathbf{z}'_t\|^2}\right\}. \quad (6.12)$$

and the final predictions are

$$\mathbf{w}'_t \cdot \mathbf{z}'_t = \sum_{i=1}^{t-1} \theta_i y_i \left(\underbrace{\mathbf{z}_i \cdot \mathbf{z}_t}_{\text{New Samples}} + \underbrace{\sigma_{k,i} \sigma_{k,t}}_{\text{Prior knowledge}} \right). \quad (6.13)$$

Algorithm 6.1 Online Tactile Transfer Learning

Input : $\{\mathbf{z}_\ell, y\}_{\ell=1}^{N_k}$, $\ell = 1, \dots, N_k$, $k = 10$ ▷ Prior training data.
 k number of prior knowledge, N_k number of training samples of each prior object
 \mathbf{z}_t new comping samples, $\eta = 1$

Output: $\hat{y}_{m,t}$ ▷ Predicted label of received samples

Prior tactile model construction

for $K = 1 : k$ **do**
 $\mathbf{w}_k \leftarrow \underset{\mathbf{w}, b}{\operatorname{argmin}} \frac{1}{2} \|\mathbf{w}\|^2$ ▷ Prior tactile model construction (Sec. 6.2)
end

for $K = 1 : k$ **do**
 $\lambda_{1:k} \leftarrow \underset{\|\lambda\|_2 \leq 1}{\operatorname{argmin}} \sum_{t=1}^k \ell_t(\tilde{y}, y)$
 $\mathbf{w}_k \leftarrow \underset{\mathbf{w}, b}{\operatorname{argmin}} \frac{1}{2} \|\mathbf{w} - \sum_{j=1}^k \lambda_j \hat{\mathbf{w}}_j\|^2$ ▷ How to transfer (Sec. 6.2)
 ▷ Weighting prior models (How much to transfer) (Sec. 6.3)
end

Online Tactile Learning

initialize: $\mathbf{w}'_{k,1} \leftarrow (\mathbf{w}_1, \mathbf{1}) \in \mathbb{R}^{d+k}$

for $t = 1 : T$ **do**
 $\sigma_{k,t} \leftarrow \max\{-1, \min\{1, \mathbf{w}_{k,1} \cdot \mathbf{z}_t\}\} \Rightarrow \sigma_{k,t} \in [-1, 1]$ ▷ Update and re-weight the prior tactile models (Sec. 6.5.1)
 for $m = 1 : M$ **do**
 $\mathbf{z}_{m,t}$ ▷ Get new samples, Compute tactile feature (Sec: 6.6.4)
 $\mathbf{z}'_{m,t} \leftarrow (\mathbf{z}_{m,t}, \sigma_{1,t}, \dots, \sigma_{k,t}) \in \mathbb{R}^{d+k}$ ▷ New augmented samples (Sec. 6.5.1)
 $\hat{y}_{m,t} \leftarrow \underset{y \in \mathbb{Y}}{\operatorname{argmax}} (\mathbf{w}_t \cdot \Phi(\mathbf{z}_{m,t}, y_{m,t}))$ ▷ Predict the label of received samples $y_{m,t} \in \mathbb{Y}$ ▷
 Receive correct label
 $\theta_t \leftarrow \min \left\{ \eta, \frac{\max\{0, 1 + \mathbf{w}_t \cdot (\Phi(\mathbf{z}_{m,t}, y_{m,t}) - \Phi(\mathbf{z}_{m,t}, \hat{y}_{m,t}))\}}{\|\Phi(\mathbf{z}_{m,t}, y_{m,t}) - \Phi(\mathbf{z}_{m,t}, \hat{y}_{m,t})\|^2} \right\}$ ▷ set
 $\mathbf{w}_{t+1} \leftarrow \mathbf{w}_t + \theta_t (\Phi(\mathbf{z}_{m,t}, y_{m,t}) - \Phi(\mathbf{z}_{m,t}, \hat{y}_{m,t}))$ ▷ Update
 end
end

Hence \mathbf{w}'_t is composed of two parts, one part is the knowledge coming from the new instances in sequence and the other part is the prior texture knowledge (see Algorithm 6.1). Hence \mathbf{w}'_t is composed of two parts, one part is the knowledge coming from the new instances in sequence and the other part is the prior texture knowledge (see Algorithm 6.1).

6.6. Tactile perception and data collection

6.6.1. Properties of experimental objects

In this work 22 everyday objects (natural and synthetic) were selected. 10 objects were chosen with an identical geometrical shape property (spherical shape), including a Red and a Yellow ball with almost similar smooth surface texture, a Rough textured ball, an Orange, an Apple, a Colorful ball with smooth and non-uniform texture, a Rough spherical sponge, a Pine apple textured ball (non-uniform texture), a String ball, and a Mirror ball (see Fig.6.1-Prior Objects). Also, 12 objects with different shapes including a Soft sponge, a Memory sponge (non-uniform texture), a Toothbrush (non-uniform texture), a Floor brush, a Rough textured star (non-uniform texture), a Soap, a Spray, a Coffee capsule, a Paper box, a Cream tube, a Plastic baby feeder, and a Metal ruler (see Fig.6.1-New Objects). The first set of the objects was used to construct a prior tactile knowledge and the second set was considered as new objects which the robotic hand should recognize them with the help of its prior tactile knowledge. In both sets of the objects, the difference in the surface texture properties between the selected objects varied from relatively similar to noticeably different.

6.6.2. *Data collection with prior objects*

The Shadow Hand held each of the spherical shaped prior objects (see Fig.6.1-Prior Objects) in palm with three random fingers. Afterwards, the robotic hand explored the texture of each in-hand object by randomly moving the remaining two free fingers to slide over the surface of the in-hand object for 3 seconds. The texture exploration was repeated 50 times for each prior objects with random orientation. The entire collected data (for each object) then randomly divided in two sets, one set for the training purpose with 30 samples and the other set with 20 trials for the testing.

6.6.3. *Data collection with new objects*

In this scenario, the robotic hand used its three fingers to hold each of the complex shaped object (Fig.6.1-New Objects). The surface exploration carried out with the remaining two fingers by sliding over the surface of each object for 3 seconds. The data collection was repeated 30 times for each new object. The entire collected data (for each new object) was divided in two sets, 10 samples for the training and 20 for the testing.

6.6.4. *Feature extraction methodology*

Our proposed tactile descriptors described in chapter 3.4 used to extract robust tactile information from tactile signals that were measured by the BioTac sensor during object surface texture exploration.

6.7. Experimental evaluation and results

In this section we show empirically the effectiveness and consistency of our proposed online tactile transfer algorithm.

6.7.1. *Constructing prior tactile models*

In order to construct 10 prior texture models LS-SVM classifier was employed. The entire training samples (30 training samples for each prior texture) were split in two parts, 70% for training and 30% for the testing. Five-fold cross validation was applied to find the optimal kernel parameter and regularizer value C . LS-SVM was then re-trained with the entire collected training data and the obtained optimal parameters to construct 10 prior texture models. The learned texture models $(\mathbf{w}, \mathbf{b}) \in R^{10}$ were then evaluated by predicting on unseen collected test data (20 test samples for each class of prior texture). The Shadow Hand using LS-SVM could classify successfully 10 prior textures with 100% recognition accuracy.

6.7.2. *Evaluating the performance of Online Transfer Learning*

The Shadow Hand used the proposed tactile transfer learning technique to recognize 12 new objects via their textures. The proposed algorithm enabled the Shadow Hand to re-use $k = 10$ already constructed prior texture models while learning from a very few new training samples. In this scenario, the new textures/objects (see Fig.6.1-New Objects) entered to the proposed hybrid online transfer learning sequentially one after one to construct new hybrid learning models. At each time $t = 1, \dots, 10$, the constructed leaning models were evaluated by predicting on unseen new test data. The prediction results were reported as a recognition rate in Fig. 6.2-(A).

6.7.3. *Baseline*

In order to compare our proposed method with the traditional online learning method, the traditional PA algorithm was employed to construct surface texture models while receiving new training samples continuously over time (one new texture per time ($t = 1, \dots, 10$)). The new constructed learning models at each time t were evaluated by predicting on unseen new test data (20 test samples per new textures). The classification results were reported as a recognition rate in Fig. 6.2-(A). The value for η was fixed to 1 in both hybrid online transfer learning and PA online learning (base line). Fig. 6.2-(A) shows that using our proposed hybrid online transfer learning method the Shadow Hand could discriminate 12 new textures with 97% recognition accuracy while using only one new training sample plus ten prior models. By increasing the number of training samples from one to ten, the Shadow Hand achieved 100% recognition accuracy. The results in Fig. 6.2-(A) illustrates that our proposed method outperforms the traditional online learning.

The computational cost of the online tactile transfer learning approach is $\mathcal{O}(T^2 + N^3 + kN^2)$. In other words, the computational complexity of our proposed algorithm is the sum of the computational cost of the PA algorithm ($\mathcal{O}(T^2)$) and adapted LS-SVM ($\mathcal{O}(N^3) + \mathcal{O}(kN^3)$). T is the total number of new textures, k is the number of the prior texture models, and N is the number of the trials used to construct the hybrid learning models with adapted LS-SVM. In our proposed method only a few number of trials entered to the adapted LS-SVM in order to construct the learning models (6.8). Hence, the term ($\mathcal{O}(N^3) + \mathcal{O}(kN^3)$) in the proposed method is negligible. Therefore, our proposed method and PA online algorithm have similar computational complexity. It is worth to mention that growing the number of prior textures increases the probability to find more useful and related prior models for the new textures. Moreover, it is important to mention that our proposed method will have substantially higher performance if the texture properties of the prior and new objects will be more similar to each other.

6.7.4. *Decreasing number of prior objects*

In this scenario 5 out of 10 prior objects randomly selected to construct the new prior models. All procedure explained in Sec. 6.7.1, 6.7.2, and 6.7.3 was repeated with randomly selected 5 prior objects. Moreover, in order to evaluate the robustness of our proposed tactile learning algorithm, the experiment was repeated 50 more times. Fig. 6.2-(B) illustrates the averaged recognition rate over 50 experiments. The results in Fig. 6.2-(B) shows that our proposed method outperforms the traditional online learning. In this scenario, the Shadow

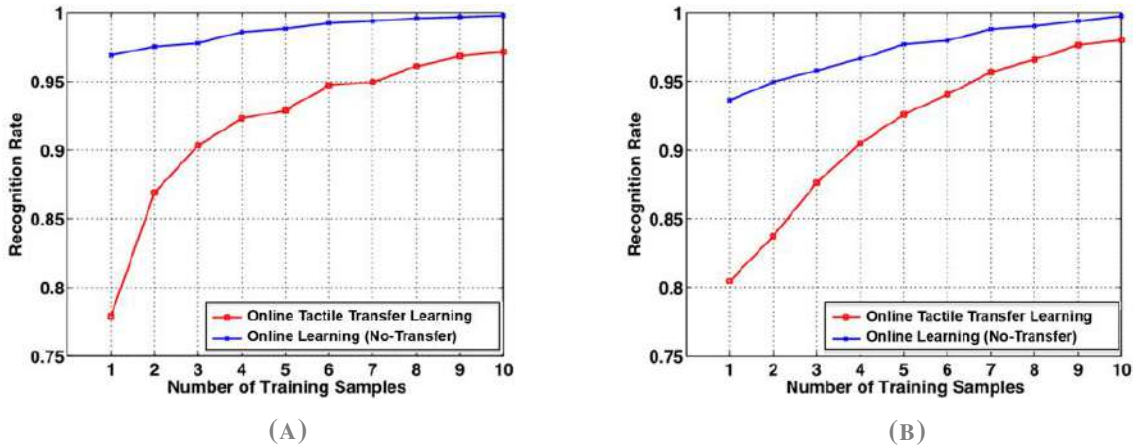


FIGURE 6.2. The figure shows the recognition results on a separate test data for the online tactile transfer learning and PA online learning (No-Transfer) methods. (A)-The robot is re-used the obtained tactile knowledge was constructed with 10 prior objects. (B)-The robot had access to 5 prior knowledge. The recognition results on the new test set were plotted as a function of the number of the training samples.

Hand achieved 94% and almost 100% recognition accuracy with only one and ten trials, respectively. Although having more prior knowledge increases the chance to find more relevant prior information for new tasks (therefore, higher recognition rate), it increases the computational complexity of the transfer learning algorithm. For instance the computation time of our algorithm with 10 and 5 prior knowledge was 360 ms and 330 ms, respectively (PC with Intel(R) Core(TM) i7-4510U CPU@2.00 GHz 2.60 GHz 32 GB Ram). This becomes more serious when the number of prior knowledge will increase to 100,000 or 1,000,000. Solving such a constrain in any transfer learning approach can be a new challenge to tackle for the future research.

6.7.5. *Negative knowledge transfer*

In transfer learning scenario the constructed prior models are not always relevant to new object/texture models. If the prior models are dissimilar to the new models, brute force transfer can degrade the recognition performance, generating so called negative knowledge transfer. Ideally, a transfer learning method should be beneficial between prior and new models while avoiding negative transfer when the object surface textures are not a good match. We show that our proposed tactile transfer learning technique is robust against of the negative knowledge transfer. In this respect, Expectation Maximization algorithm was employed to find out which of the new textures are similar or dissimilar to the prior textures. In this case, the EM was trained with entire training samples (10 samples per each texture) to cluster 20 objects (both prior and new object textures). The EM then was evaluated by unseen test data (20

		Identified As																				
		Red ball	Yellow ball	Rough ball	Orange	Apple	Colorful ball	Spongy ball	Pine ball	String ball	Mirror ball	Soap	Memory Sponge	Tooth brush	Floor brush	Rough star	Metal Ruler	Spray	Paper Box	Cream tube	Baby feeder	
Actual Object	Red ball	14	3	0	0	0	0	0	0	0	0	0	0	0	0	0	0	0	0	0	2	1
	Yellow ball	4	14	0	0	0	0	0	0	0	0	0	0	0	0	0	0	0	0	0	1	1
	Rough ball	0	0	10	0	0	0	3	0	0	0	0	0	1	1	9	0	0	0	0	0	0
	Orange	0	0	0	17	0	0	0	0	0	0	1	2	0	0	0	0	0	0	0	0	0
	Apple	0	0	0	0	18	0	0	0	0	0	2	0	0	0	0	0	0	0	0	0	0
	Colorful ball	0	0	0	0	0	17	0	0	0	0	0	0	0	0	0	0	0	0	0	1	2
	Spongy ball	0	0	3	0	0	0	12	0	0	0	0	0	2	0	3	0	0	0	0	0	0
	Pine ball	0	0	0	0	0	0	0	20	0	0	0	0	0	0	0	0	0	0	0	0	0
	String ball	0	0	0	0	0	0	0	0	20	0	0	0	0	0	0	0	0	0	0	0	0
	Mirror ball	1	1	0	0	0	0	0	0	0	18	0	0	0	0	0	0	0	0	0	0	0
	Soap	0	0	0	1	2	0	0	0	0	0	17	0	0	0	0	0	0	0	0	0	0
	Memory Sponge	0	0	0	3	0	0	0	0	0	0	0	17	0	0	0	0	0	0	0	0	0
	Tooth brush	0	0	0	0	0	0	3	0	0	0	0	0	15	0	2	0	0	0	0	0	0
	Floor brush	0	0	0	0	0	0	2	0	0	0	0	0	0	17	1	0	0	0	0	0	0
	Rough star	0	0	3	0	0	0	3	0	0	0	0	0	1	1	12	0	0	0	0	0	0
	Metal Ruler	0	0	0	0	0	0	0	0	0	0	0	0	0	0	0	18	2	0	0	0	0
	Spray	0	0	0	0	0	0	0	0	0	0	0	0	0	0	0	0	3	17	0	0	0
	Paper Box	0	0	0	0	0	0	0	0	0	0	0	0	0	0	0	0	0	0	20	0	0
	Cream tube	1	1	0	0	0	0	0	0	0	0	0	0	0	0	0	0	0	0	0	17	1
	Baby feeder	2	1	0	0	0	1	0	0	0	0	0	0	0	0	0	0	0	0	0	2	14

FIGURE 6.3. This figure shows the confusion matrix for the clustering of 20 objects via texture properties using EM method.

samples per each texture). Fig. 6.3 illustrates the resulted confusion matrix. Regarding to the obtained confusion matrix, Spray, Metal ruler, Pine apple, and String ball did not have any similarity with the prior object in terms of surface texture properties (see Fig. 6.1-Prior Objects). In this scenario, Spray, Metal ruler, Pine apple, and String ball were selected as a set of new textures while the prior textures were remain same. The hybrid online transfer learning was employed to discriminate the four new textures and traditional PA was used as a base line. The rest of the procedure was the same as describe in Sec. 6.7.2. Fig. 6.2-(C) illustrates the classification results in terms of recognition accuracy. The results clearly show that the obtained recognition performance while using the proposed hybrid online transfer learning is similar to the performance achieved while using the traditional PA. This means that our algorithm stopped transferring irrelevant prior knowledge to new task.

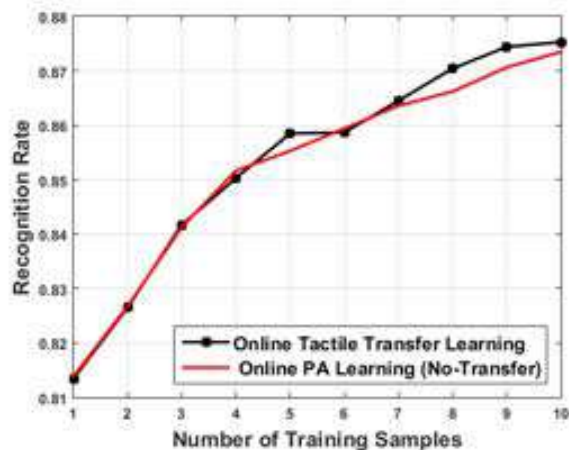


FIGURE 6.4. The figure shows the recognition results corresponding to the hybrid tactile transfer learning and traditional transfer learning (No-Transfer) in which the new surface textures were dissimilar to the prior textures. The recognition results on the new test set were plotted as a function of the number of the training samples

6.8. Summary

In this chapter, we focused on online tactile knowledge transfer across texture categories. We proposed an online tactile transfer learning method to provide the robotic systems with the ability to re-use previously learned tactile models (prior models) to discriminate new textures with a very few available training samples.

In this study, the distribution of the tactile information in both prior knowledge and new tasks were similar. In future, we will solve the problem in which the data distributions (feature space) in both previous and new data are different. It is also interesting if it will be possible to transfer tactile information to new tasks in which prior and new tactile data are measured by different types of tactile sensors (different in character and technology).

CHAPTER 7

Active Tactile Transfer Learning

Science is a way of thinking much more than it is a body of knowledge.

(Carl Sagan)

7.1. Introduction

In the previous chapter, I introduced an online tactile transfer learning (OTTL) algorithm to enable robotic systems to re-use their constructed prior models to learn a new set of objects via their textural properties with a few numbers of training samples or even one (one-shot learning). Using my OTTL strategy, the robot learned about the new objects with the tactile data that was uniformly collected. Moreover, the OTTL helps the autonomous robots to exploit their past tactile experience obtained while learning one physical property.

In order to improve my OTTL, I combined my previously proposed active tactile learning and active tactile object discrimination methods (chapter 4 and 5) with the tactile transfer learning (chapter 6). Here, I present my new active tactile transfer learning method (ATTL) which reduces the number of training samples further. Using the ATTL method, robotic systems strategically select and exploit the most relevant prior tactile knowledge to efficiently learn about new unknown objects via multiple physical properties (surface texture, stiffness, and thermal conductivity) with fewer samples.¹

¹The content of this chapter has been published in [168].

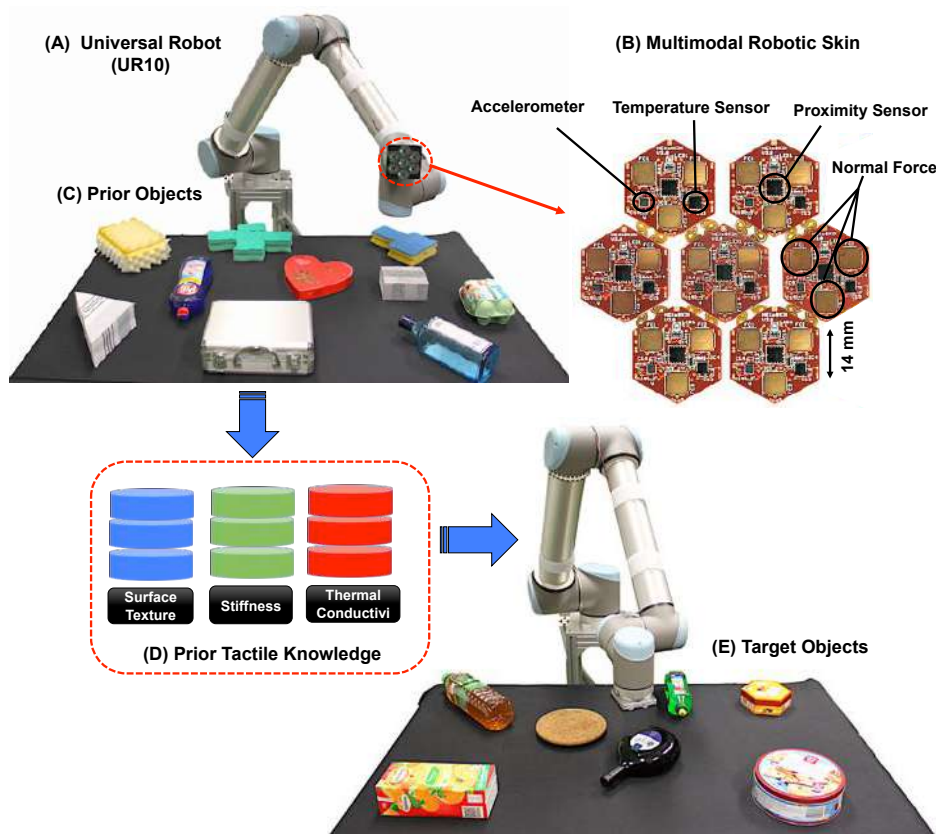


FIGURE 7.1. The scenario of active tactile transfer learning for object discrimination in the unstructured environment. The robotic arm (A) equipped with multimodal artificial skin (B) can actively learn about prior objects (C) in an unstructured environment to build the tactile knowledge of these objects. Then it can leverage this tactile knowledge (D) to actively learn about new objects (E) in another unknown workspace

7.2. Active pr-touch for workspace exploration

In order to perceive the physical properties of the objects in an unknown workspace, the robot should be able to autonomously explore the workspace and locate the objects therein. Here, I use my previously proposed active pre-touch approach (see Sec.4.2) which can reduce the number of exploratory movements and measurements required for unknown workspace exploration. By exploiting my active pre-touch method, the robot is able to autonomously find the number of objects in the workspace, estimate their positions and orientations, and compute their geometric centroids.

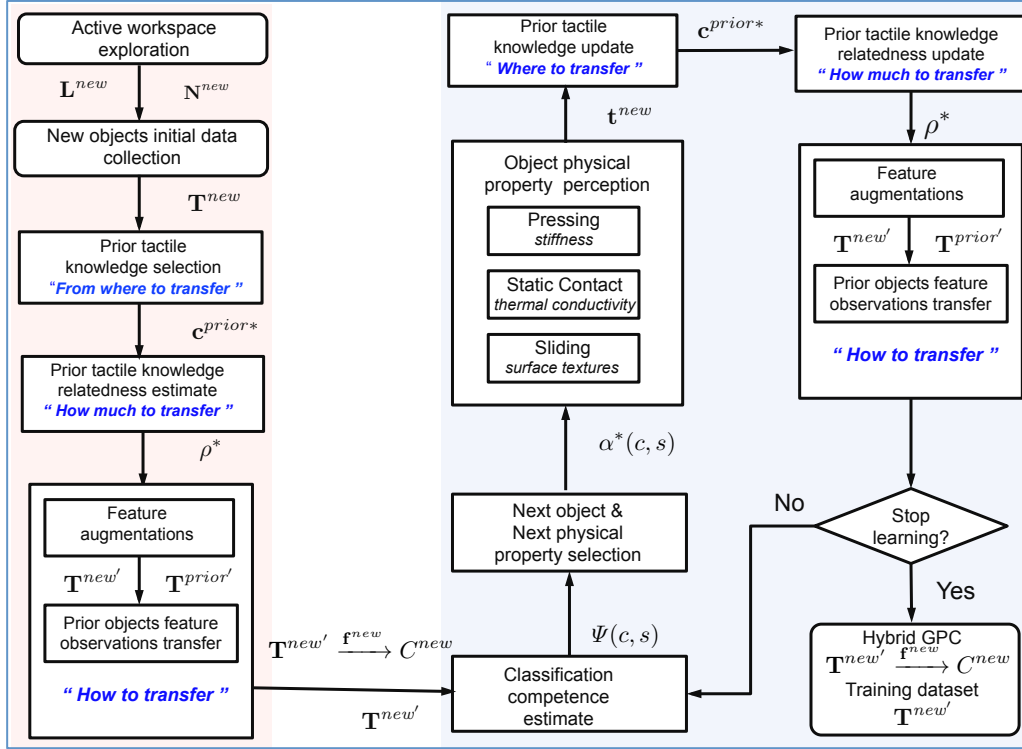


FIGURE 7.2. The proposed method of the probabilistic tactile-based active tactile transfer learning for object discrimination in unstructured environment.

7.3. Active tactile transfer learning (ATTL)

My proposed Active Tactile Transfer Learning (ATTL) algorithm enables the robotic systems to leverage their past tactile experience (prior tactile knowledge) while learning about new objects based on their physical properties with fewer training samples.

7.3.1. Problem definition

Consider a scenario in which the robotic system has already learned N_{prior} number of objects (denoted as $C^{prior} = \{c_j^{prior}\}_{j=1}^{N_{prior}}$) via their physical properties (stiffness, surface texture, and thermal conductivity, denoted as $S = \{s_1, s_2, s_3\}$). The obtained prior knowledge consists of the prior objects' feature observations ($T^{prior} = \{T_{s_1}^{prior}, T_{s_2}^{prior}, T_{s_3}^{prior}\}$) and their reliable observation models denoted by $T^{prior} \xrightarrow{f^{prior}} C^{prior}$ (see Fig. 7.1 (C) and (D)). The task of the robot is to learn about a new set of objects (Fig. 7.1 (E)) via their physical properties. I denote N_{new} number of new objects as $C^{new} = \{c_i^{new}\}_{i=1}^{N_{new}}$. Some of the new objects might share similar physical properties with the prior objects (for instance similar textural properties). Now, the robot is asked to actively learn about the new objects properties while re-using its

past tactile experience. In other words, the robotic system should efficiently construct the observation models $T^{new} \xrightarrow{\mathbf{f}^{new}} C^{new}$ with the feature observations $T^{new} = \{T_{s_1}^{new}, T_{s_2}^{new}, T_{s_3}^{new}\}$ for each of the physical properties perceived during the exploration of the *new objects*, while transferring the obtained tactile knowledge of the *prior objects*.

I formulate the ATTL as a standard supervised learning problem for multi-class classification, where each object is regarded as a class c ; for each tactile property s , a Gaussian Process Classification (GPC) is used to construct the objects' observation models. GPC describes the function $X \xrightarrow{\mathbf{f}} Y$, where X is the observation set and Y is the target set which contains integers indicating the labels of the input data. The model assumes that there is an underlying latent function $X \xrightarrow{\mathbf{h}} \mathbb{R}$, which is sampled by the GP prior [156]: $\mathbf{h}|X \sim \mathcal{GP}(\mathbf{0}, K(X, X))$ with zero mean and kernel function $K : X \times X \rightarrow \mathbb{R}$. The kernel function describes the similarity between two observations. In my work, one-vs-all multiclass GPC is employed. For each object, a binary GPC ($\mathbf{f}_n(\cdot)$) is learned, with its hyper-parameters being optimized through maximizing the log likelihood. Given a new sample \mathbf{x}^* , each binary classifier predicts the observation probability of its label $p(y_n|\mathbf{x}^*)$. The sample is assigned to the class with the largest predicted probability:

$$y^* = \arg \max_{y_n \in Y} p(y_n|\mathbf{x}^*) \quad (7.1)$$

7.3.2. Methodology

My active tactile transfer learning method has three main steps: (1) The robot first executes each of the exploratory actions (sliding, pressing, and static contact) once on each new object to collect a small number of new objects' feature observations T^{new} (one-time data collection). (2) For each new object and each physical property, the robot transfers the prior tactile knowledge consisting of the observation models $\mathbf{f}^{prior}(\cdot)$ and feature observations T^{prior} . To do this, the robot first selects the most relevant prior knowledge, in my case, feature observations to transfer (Sec. 7.3.2.1). Then, it exploits the selected feature observations and the predictions from the prior objects' observation models to improve the new objects' GPC models (Sec. 7.3.2.2). (3) The robot iteratively constructs the new objects' observation models. In each iteration, the robot actively selects the next object and next physical property to explore and collect the new objects' feature observations (Sec. 7.3.2.3). Then, it updates its prior tactile knowledge regarding *only* the selected physical property, including re-selecting the prior tactile knowledge and transferring it to the new objects (Sec. 7.3.2.1 and 7.3.2.2). The learning process is repeated until there is no improvement in the uncertainty of the new objects' observation models. My algorithm is demonstrated by Algorithm 7.1. In the rest of this paper, I refer to j as the prior object c_j^{prior} , and i as the new object c_i^{new} .

7.3.2.1. Prior Tactile Knowledge Selection

When learning about a new object via one physical property, the ATTL selects the most relevant prior object to transfer (from where to transfer), taking advantage of the prediction from the observation models constructed by the prior objects. More formally, consider $p(c_j^{prior} | \mathbf{t}_{s,i}^{new})$ to be as a prediction from the prior object's (c_j^{prior}) observation model with regard to the physical property s . $\mathbf{t}_{s,i}^{new}$ is a feature observation from the new object c_i^{new} . I calculate the average prediction to all $N_{s,i}^{new}$ number of samples that belong to the new object c_i^{new} by $\bar{p}(c_j^{prior} | T_{s,i}^{new}) = \frac{1}{N_{s,i}^{new}} \sum p(c_j^{prior} | \mathbf{t}_{s,i}^{new})$. This value estimates the relatedness of the physical property s between the prior object c_j^{prior} and the new object c_i^{new} . The higher the value is, the more similar two objects are. Thus, the prior object with the largest average prediction value (denoted as $c_{s,i}^{prior*}$) can be selected to transfer its feature observations of the physical property s to the new objects :

$$c_{s,i}^{prior*} = \arg \max_{c^{prior} \in C^{prior}} \bar{p}(c_j^{prior} | T_{s,i}^{new}). \quad (7.2)$$

7.3.2.2. Prior Tactile Knowledge Transfer

Sec. 7.3.2.1 describes “from where” the robot can transfer the prior objects’ feature observations. In this section, I explain “how and how much” the robot can reuse this prior knowledge. While leveraging the prior object's (c_j^{prior}) feature observations $T_{s,j}^{prior}$ of the physical property s to the new object c_i^{new} , I define $\mathbf{h}_{s,j}^{prior}$ and $\mathbf{h}_{s,i}^{new}$ to be the latent functions of the GPC models built by the feature observations from prior objects $T_{s,j}^{prior}$ and new object $T_{s,i}^{new}$ respectively. It is assumed that these two functions are not independent from each other, but are sampled dependently over a Gaussian prior (hybrid GP). I use this hybrid GP as the observation model of the new object: $\mathbf{h}_{s,i}^{new} \leftarrow [\mathbf{h}_{s,j}^{prior}, \mathbf{h}_{s,i}^{new}]$. Its kernel function is defined as:

$$K = \begin{bmatrix} K^t(T_j^{prior}, T_j^{prior}) & \rho K^t(T_j^{prior}, T_i^{new}) \\ \rho K^t(T_i^{new}, T_j^{prior}) & K^t(T_i^{new}, T_i^{new}) \end{bmatrix} \quad (7.3)$$

where K^t is the base kernel function that measures the similarity of training samples. In my case, I use radial basis function (RBF) [156], whose hyper-parameters are found by maximizing the log-likelihood of this hybrid GPC model.

$K^t(T_j^{prior}, T_j^{prior})$ and $K^t(T_i^{new}, T_i^{new})$ measure the similarity for feature observations of the prior object and the new object respectively. $\rho K^t(T_j^{prior}, T_i^{new})$ and $\rho K^t(T_i^{new}, T_j^{prior})$ measure the similarity between the feature observations of the prior object and the new object respectively. The parameter ρ ranges between 0 and 1. As analyzed by Chai et al. [169], ρ controls “how much” the feature observations should be transferred. $\rho = 0$ indicates that the prior object and the new object are irrelevant, whereas $\rho = 1$ indicates that the two objects are regarded to be the same. I estimate ρ by the average prediction probability of the training samples:

$$\rho = \begin{cases} \bar{p}(c_j^{prior} | T_{s,i}^{new}) & \text{if } \bar{p}(c_j^{prior} | T_{s,i}^{new}) > \epsilon_\rho \\ 0 & \text{o.w} \end{cases} \quad (7.4)$$

with ϵ_ρ being the threshold below which a transfer of irrelevant prior tactile knowledge is avoided.

The method introduced above uses the hybrid GP to transfer the prior tactile knowledge. The parameter ρ controls “how much” to transfer. It can also stop transferring irrelevant past tactile experience. However, it does not fully exploit the tactile knowledge from all prior objects, since it combines the feature observations of *one* prior object to *each* new object. In this regard, I use a feature augmentation trick. The prediction outputs from all prior objects’ observation models are employed as auxiliary features to describe the physical property of the objects. The augmented representation of a new sample \mathbf{t} can be defined as:

$$\mathbf{t}' = [\underbrace{\mathbf{t}}_{\text{original feature observation}}, \underbrace{p(c_1^{prior} | \mathbf{t}), p(c_2^{prior} | \mathbf{t}), \dots, p(c_{N_{prior}}^{prior} | \mathbf{t})}_{\text{prior tactile knowledge}}]. \quad (7.5)$$

The augmented feature observations are then used to train the hybrid GPC.

7.3.2.3. Next New Object and Next Physical Property Selection

When the robot iteratively updates the new objects’ observation models, it actively decides which new object to explore and which physical property to perceive in order to collect new feature observations. Here, I use my previously proposed AT-LPP algorithm (see chapter 4).

Algorithm 7.1 Active Tactile Transfer Learning

Input : $C^{new} = \{c_i^{new}\}_{i=1}^{N_{new}}$, $L^{new} = \{\mathbf{l}_{c_i^{new}}\}_{i=1}^{N_{new}} \triangleright N_{new}$ new objects with positions L^{new} , each object is regarded as a class c_i^{new} .

$C^{prior} = \{c_j^{prior}\}_{j=1}^{N_{prior}}$, T^{prior} , $T^{prior} \xrightarrow{\mathbf{f}^{prior}} C^{prior} \triangleright$ Prior knowledge

Output: $T^{new'} \xrightarrow{\mathbf{f}^{new}} C^{new}$, $T^{new'} \triangleright$ New objects' GPCs and feature observations.

Initialization: $T^{new} \triangleright$ One time data collection for the new objects.

Prior tactile knowledge transfer for all new objects & physical properties

for $s = \{s_1, s_2, s_3\}$ **do**

for $i = 1 : N_{new}$ **do**

$c_{s,i}^{prior*} \leftarrow \text{priorKnowledgeSelection}(\bar{p}(c_j^{prior} | T_{s,i}^{new})) \triangleright$ Sec. 7.3.2.1

$\rho_{s,i} \leftarrow \text{correlationEstimate}(c_{s,i}^{prior*}, \bar{p}(c_j^{prior} | T_{s,i}^{new})) \triangleright$ Eq. 7.4

$T_{s,i}^{new'} \leftarrow \text{featureAugmentation}(T_{s,i}^{new}) \triangleright$ Eq. 7.5

$\mathbf{f}_{s,i}^{new'}(\cdot) \leftarrow \text{updateGPC}(T_{s,i}^{new'}, \rho_{s,i}) \triangleright$ Sec. 7.3.2.2

end

end

$T^{new'} = \{T_{s_1,i}^{new'}, T_{s_2,i}^{new'}, T_{s_3,i}^{new'}\}_{i=1}^{N_{new}}$

$\mathbf{f}^{new}(\cdot) = \{\mathbf{f}_{s_1,i}^{new'}(\cdot), \mathbf{f}_{s_2,i}^{new'}(\cdot), \mathbf{f}_{s_3,i}^{new'}(\cdot)\}_{i=1}^{N_{new}}$

while *not stop condition*() **do**

New Feature Observation Collection

$\Psi(s, c_i^{new}) \leftarrow \text{competenceEstimation}(\mathbf{f}^{new}(\cdot)) \triangleright$ Eq. 7.7

$\alpha(s^*, c_i^{new*}) \leftarrow \text{objectPropertySelection}(\Psi(s, c_i^{new})) \triangleright$ Eq. 7.8

$\text{moveTo}(\mathbf{l}_{c_i^{new*}})$

\triangleright Robot moves to the object

$\mathbf{t}^{new} \leftarrow \text{actionExecution}(s^*)$

\triangleright Get new training sample

$T^{new} \leftarrow T^{new} \cup \mathbf{t}^{new}$

\triangleright Update training database

Update prior tactile knowledge

for $i = 1 : N_{new}$ **do**

$c_{s^*,i}^{prior*} \leftarrow \text{priorKnowledgeSelection}(\bar{p}(c_j^{prior} | T_{s^*,i}^{new}));$

$\rho_{s^*,i} \leftarrow \text{correlationEstimate}(c_{s^*,i}^{prior*}, \bar{p}(c_j^{prior} | T_{s^*,i}^{new}))$

$T_{s^*,i}^{new'} \leftarrow \text{featureAugmentation}(T_{s^*,i}^{new})$

$\mathbf{f}_{s^*,i}^{new'}(\cdot) \leftarrow \text{updateGPC}(T_{s^*,i}^{new'}, \rho_{s^*,i})$

end

end

My method estimates the classification competence of the new objects' observation models which guides the robot to the next round of data collection. First, the robot measures the Shannon entropy of each new objects' feature observation that has been collected $\mathbf{t}^{new} \in T^{new}$.

$$\mathcal{H}(\mathbf{t}^{new}) = - \sum_{c_i^{new} \in C^{new}} p(c_i^{new} | \mathbf{t}^{new}) \log(p(c_i^{new} | \mathbf{t}^{new})) \quad (7.6)$$

Then the training data set T^{new} is divided into categories according to the physical property s and object class c_i^{new} . The GPC's classification competence $\Psi(s, c_i^{new})$ is estimated as the mean value of the Shannon entropy:

$$\Psi(s, c_i^{new}) = \frac{1}{N_{s,i}^{new}} \sum_{\mathbf{t}^{new} \in T_{s,i}^{new}} \mathcal{H}(\mathbf{t}^{new}) \quad (7.7)$$

where $N_{s,i}^{new}$ is the number of feature observations from $T_{s,i}^{new}$. The higher $\Psi(s, c_i^{new})$ is, the more uncertain the robot is about the object.

I define $\alpha(s, c_i^{new})$ as a function of the object c_i^{new} and physical property s . After selecting $\alpha(s, c_i^{new})$, the robot moves to the object c_i^{new} and executes the corresponding exploratory action to perceive the physical property s . In order to efficiently collect new feature observations, the AT-LPP algorithm determines the next object c^{new*} and next physical property s^* by:

$$\alpha(s^*, c^{new*}) = \begin{cases} \arg \max_{s \in \{s_1, s_2, s_3\}, c_i^{new} \in C^{new}} \Psi(s, c_i^{new}), & \text{if } p_\alpha > \epsilon_\alpha \\ s^* = \mathcal{U}\{s_1, s_2, s_3\}, c^{new*} = \mathcal{U}\{c_1^{new}, \dots, c_{N_{new}}^{new}\}, & \text{o.w.} \end{cases} \quad (7.8)$$

where ϵ_α is the parameter to control the exploration-exploitation trade-off. p_α is a probability which is uniformly generated with at each learning iteration.

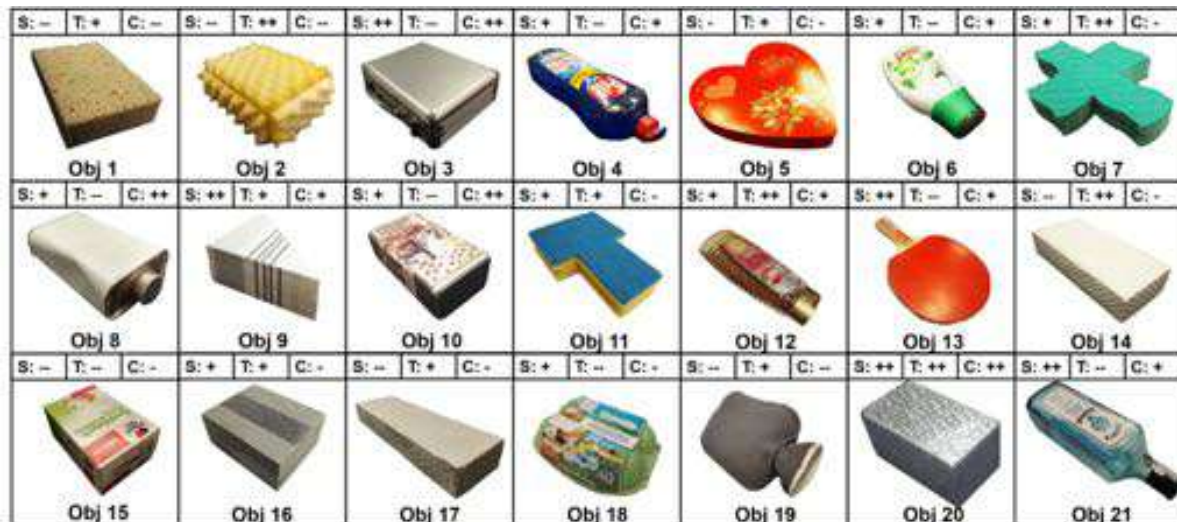


FIGURE 7.3. Prior objects. The physical properties are evaluated subjectively by human subjects and are indicated in the panel to the upper right of each object (S: stiffness, T: roughness of surface textures, C: thermal conductivity. ++: very high; +: high; -: low; --: very low.)

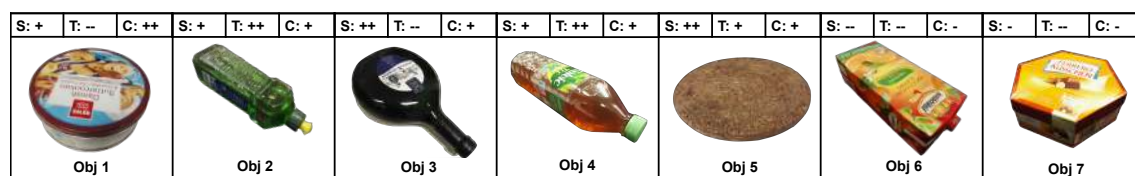


FIGURE 7.4. New objects.

7.4. Experimental evaluation and results

7.4.1. Experimental Objects

To evaluate my proposed active tactile learning method, I deliberately selected two sets of objects, one set with 21 objects as prior objects (Fig. 7.3) and another set with 7 objects as new objects (Fig. 7.4). All experimental objects were made by different materials (such as glass, cardboard, and plastic) with regular and irregular surface textures and various shapes (such as triangular, rectangular, cross, and heart shape). The physical properties of these objects (stiffness, surface textures and thermal conductivity) varied from similar to different.

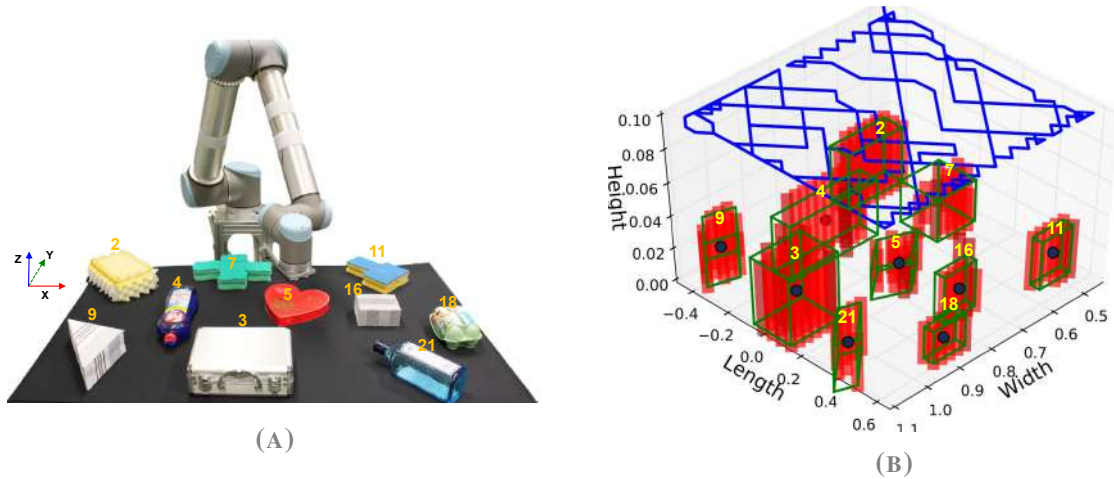


FIGURE 7.5. (A) The unknown workspace which the robot explored. (B) Trajectories of the robot's end-effector during the exploration of the workspace and the localization results using active pre-touch strategy.

7.4.2. Experimental setting

I assessed the performance of my proposed active tactile transfer learning method (ATTL) in real time. The robot was tasked to actively learn about new objects (Fig. 7.4) while reusing the prior tactile knowledge constructed from the prior objects (Fig. 7.3). In each experiment, the workspace was unknown, and the robot had no knowledge about the number of objects and their positions therein. Therefore, before it applied any exploratory actions with objects, the robot used the active pre-touch strategy in chapter 4 to explore the unknown workspace and estimate their positions and the geometrical centroids. Although the objects had random positions and orientations in the unknown workspace, they were fixed to the table in order not to move when the robot slid its end-effector over their surfaces.

7.4.3. Workspace exploration

Fig. 7.5a illustrates the unknown workspace which is a cuboid of $110\text{cm} \times 64\text{cm} \times 10\text{cm}$ ($L \times W \times H$). A corresponding Cartesian coordinate frame (world coordinate frame) was defined along its length edge (X-axis), width edge (Y-axis), and height edge (Z-axis). This workspace was discretized into $27 \times 24 \times 10$ grid cells. During the exploration, the sensor array (the end-effector of the robot) was positioned at the maximum height of the workspace and horizontal to the X-Y plane. Fig. 7.5b shows an example of the exploration result. The robot successfully estimated the number and the positions of ten objects that had been randomly placed on the workspace.

7.4.4. Evaluation of Active Tactile Transfer Learning (ATTL)

7.4.4.1. Prior Tactile Knowledge Construction

The robot first collected the feature observations from prior objects (Fig. 7.3), and then built their GPC observation models. These feature observations and the observation models served as the prior tactile knowledge. To do this, the robot automatically performed each exploratory action 20 trials on the prior objects. The robot began to apply each of the exploratory movement with a light contact with objects with approximately $0.05N$ of the total normal force measured by the artificial skin. For the pressing movement, the robot first pressed the robotic skin $2mm$ on the objects' surface and then recorded the normal force feedback for $3s$. To perceive the surface texture of the objects, the robotic system slid the robotic skin on the objects with constant velocity of $1cm/s$ for $3s$. When measuring the thermal conductivity, the robot pressed its sensitive part $2mm$ on the objects' surface and held for $15s$. Then it raised its end-effector for $30s$ so that the temperature sensor recovered to ambient temperature. In this way, the robot could measure the temperature change during the static contact with a similar initial temperature condition.

7.4.5. Test data collection for new objects

The performance of the proposed ATTL method was evaluated with a test database of the new objects (Fig. 7.4). This was achieved by following the same data collection procedure described in Sec. 7.4.4.1.

7.4.6. Baselines

I compared my proposed ATTL method (with prior tactile knowledge) with the uniform learning method and the active tactile learning (AT-LPP) method as baselines. Using the uniform method, the robot uniformly applied each exploratory action on each new object. Using the ATL method, at each learning step the robot can follow my proposed AT-LPP method in chapter 4 to strategically select the next object to perceive and the next physical property to explore, however, it was unable to exploit its prior tactile knowledge.

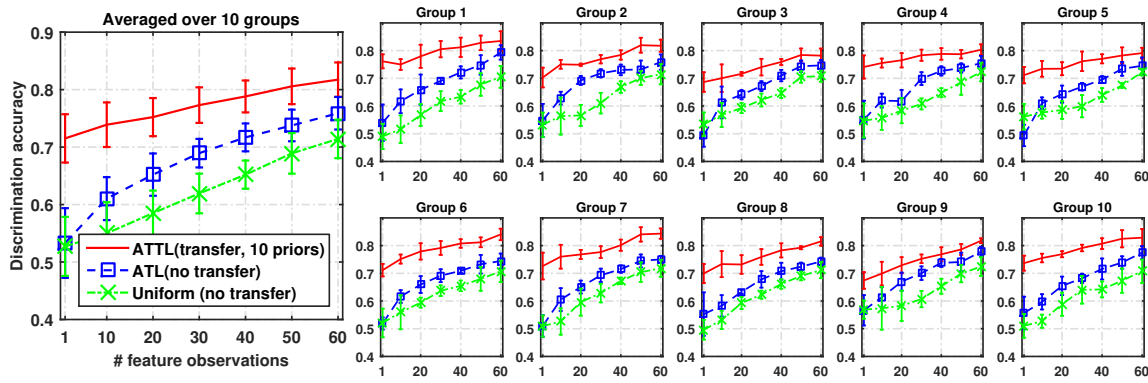


FIGURE 7.6. Evaluation of the active tactile learning performance using ten prior objects. The right small plots show the results from 10 groups of prior objects. Their averaged performance is plotted on the left. The figure illustrates the comparison results between ATTL and ATL (no transfer) as well as uniform (no transfer) methods. The horizontal axis represents the growing number of feature observations, and the vertical axis represents the averaged value of discrimination accuracy on the test data set. The figure illustrates Learning about the new objects based on three physical properties.

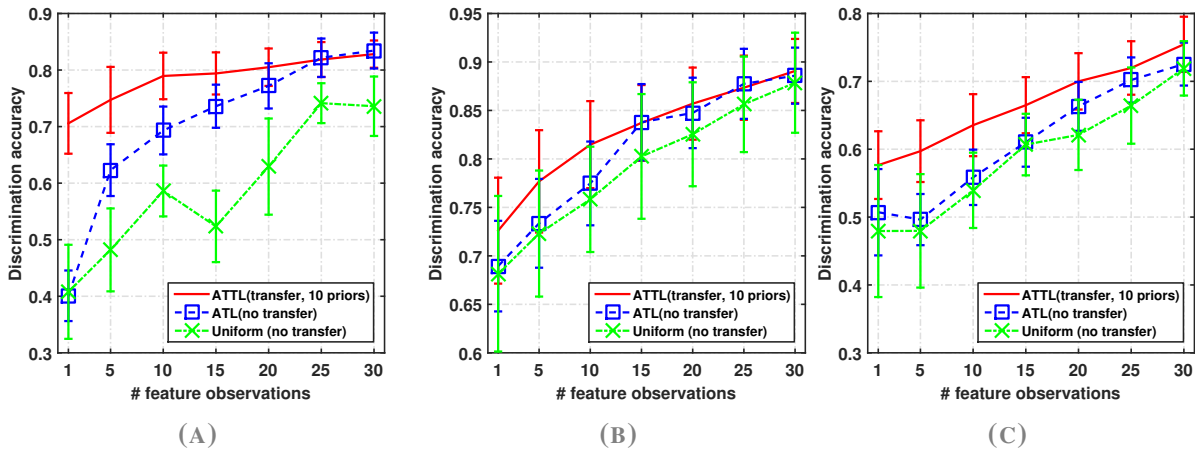


FIGURE 7.7. (A) Evaluation of the active tactile learning performance based on only stiffness property. (B) Evaluation of the active tactile learning performance based on only surface texture. (C) Evaluation of the active tactile learning performance based on only thermal conductivity.

7.4.6.1. Learning about new objects with ten prior objects

I first evaluated the ATTL performance of learning about new objects with the help of 10 prior objects. This experiment was conducted 10 trails. At each trail, the robot first randomly selected 10 prior objects following the uniform distribution in order to construct a group of prior tactile knowledge. Then the robot reused this tactile knowledge to learn about the new objects by following the ATTL, ATL, and uniform methods five times.

To initialize the learning process, the robot collected one feature observation for each new object and each physical property (stiffness, surface texture, and thermal conductivity). At each step when the robot sampled a new feature observation, the new objects' discrimination accuracy of the test data set was measured by the new objects' observation models, which were re-trained by all the feature observations the robot had collected so far. To have a fair comparison between the ATTL and the baseline methods, the robot collected in total 60 feature observations by exploring the new objects.

Fig. 7.6 illustrates that the ATTL method consistently outperforms the ATL and uniform methods by reaching higher discrimination accuracy when collecting the same number of feature observations. For instance, the robot had in average 20% higher discrimination accuracy than the ATL and uniform strategies, when the robot received only one training sample (one-shot learning) (Fig. 7.6). By increasing the feature observations from 1 to 60, the robotic system using my proposed ATTL method leveraged the past tactile experience and achieved a discrimination accuracy of 83%, whereas following the ATL and uniform methods, it only obtained 71% and 76%, respectively.

I also evaluated ATTL when the robot used only one of the physical properties (stiffness, surface texture and thermal conductivity) to learn about new objects. In this instance, the total number of feature observations was set to 30. Fig. 7.7a, 7.7b and 7.7c show that in all three cases, the ATTL outperforms ATL and uniform strategies. Therefore, using my proposed ATTL algorithm, the robot can efficiently construct reliable new objects' observation models with fewer training samples.

7.4.6.2. Decreasing the number of prior knowledge

In this experiment, I decreased the number of prior objects from 7, 5 to 3. The robotic system following the same procedure explained above (Sec. 7.4.6.1) to learn about new objects (Fig. 7.4). The results in Fig. 7.8a, Fig. 7.8b, Fig. 7.8c, and Fig. 7.8d show that when the robot used fewer prior objects, it achieved lower discrimination accuracy. This is due to the fact that reducing the number of prior objects decreases the probability of finding highly-relevant prior tactile knowledge for the new objects. This phenomena became clearer when I decreased the number of priors objects from 10 to 3. In spite of this, using my ATTL method even with 3 prior objects achieved higher discrimination accuracy than the baseline methods.

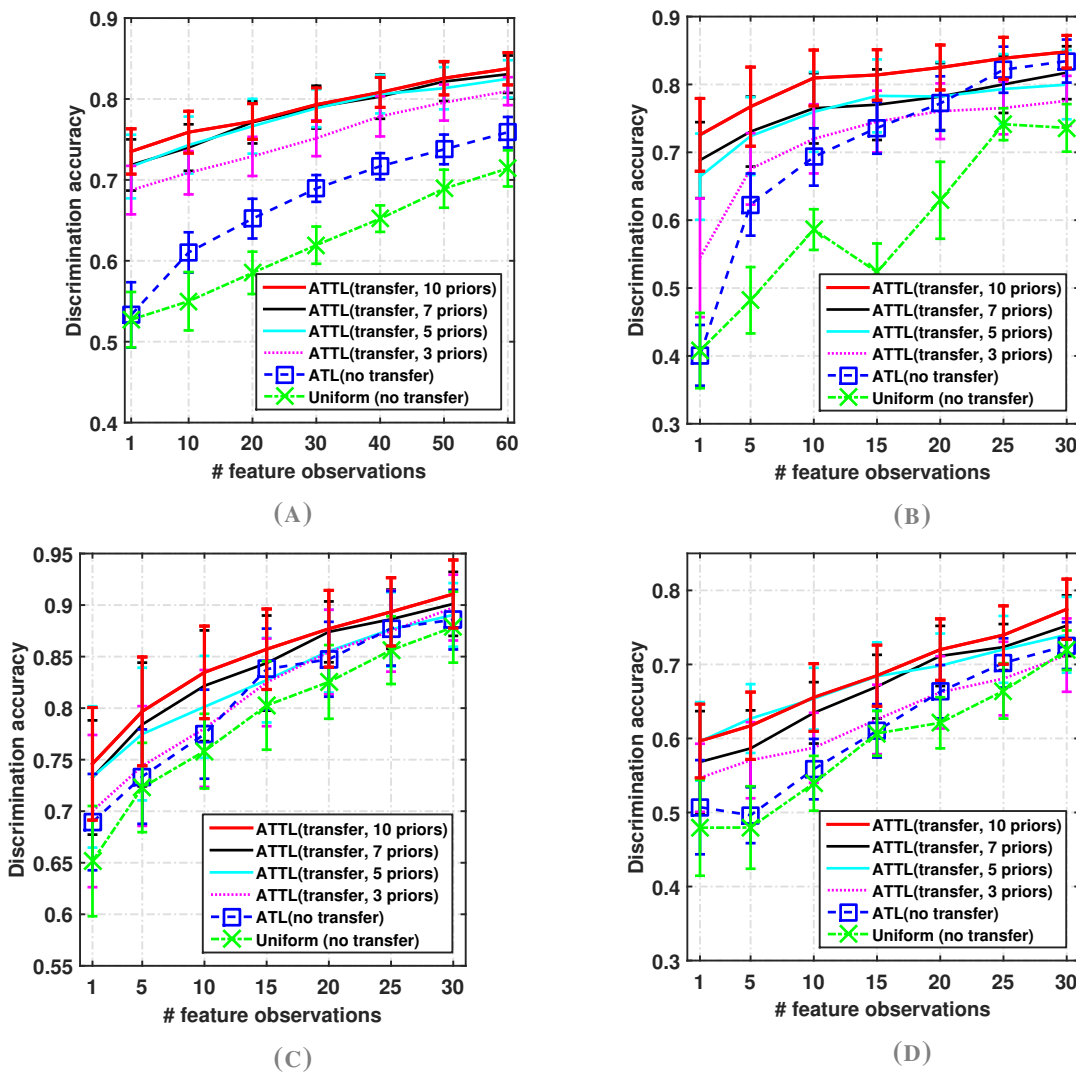


FIGURE 7.8. Evaluation of the ATTL performance using different number of prior objects. (A) Learning about the new objects based on three physical properties; (B) based on only stiffness; (C) based on only surface texture; (D) based on only thermal conductivity.

7.4.6.3. Robustness evaluation of ATTL

So far, the robot was tasked to leverage the prior tactile knowledge constructed by the objects in Fig. 7.3 to learn about objects in Fig. 7.4. To further test the robustness of the ATTL algorithm, in this experiment I randomly selected 7 objects out of all 28 experimental objects as new objects and the rest as prior objects, and conducted the same experiment explained in Sec. 7.4.6.1 for 50 times. The averaged learning performance was illustrated in Fig. 7.9. The

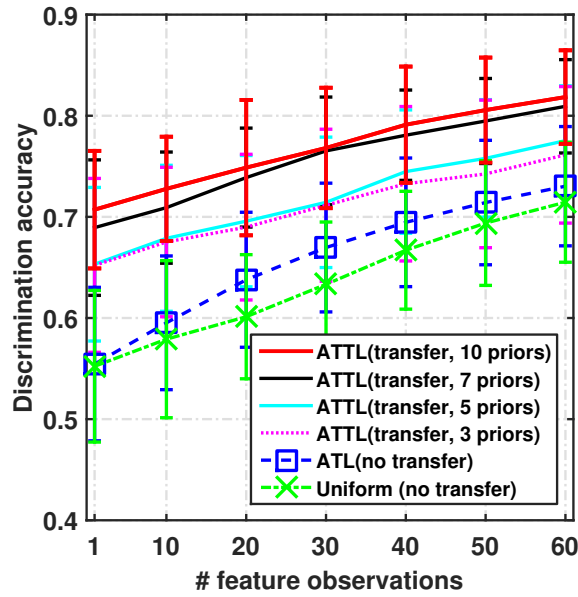


FIGURE 7.9. Learning about new objects with different number of prior objects. The new objects and the prior objects were randomly selected, following the uniform distribution.

results clearly show that the robot using the ATTL method with 3 prior objects consistently outperformed the baseline methods with a discrimination accuracy improvement of 5%. Such improvement increases to over 10% when the robot leveraged 10 prior objects to learn about new objects.

7.4.7. Evaluation of ATTL for negative tactile knowledge transfer

In transfer learning, the constructed prior knowledge is not always relevant to new tactile observation models. In this case, a brute-force transfer may even degrade the learning performance, generating a so called negative knowledge transfer. When the new and the prior objects are not a good match, a transfer learning method should avoid leveraging negative knowledge.

In this experiment, I evaluated my proposed algorithm against the negative tactile knowledge transfer. To do this, I constructed confusion matrices for all 28 experimental objects w.r.t each physical property in order to find out which of the prior objects were similar and dissimilar to the new objects. The confusion matrices were constructed by training the Support Vector Machine (SVM) models for all 28 objects with ten training samples randomly selected for each object, and using the trained SVM to predict ten unobserved data instances. I calculated the average confusion between objects and normalized the values between 0 and 100, with 0 being totally dissimilar and 100 highly similar. Fig. 7.10, Fig. 7.11, and Fig. 7.12

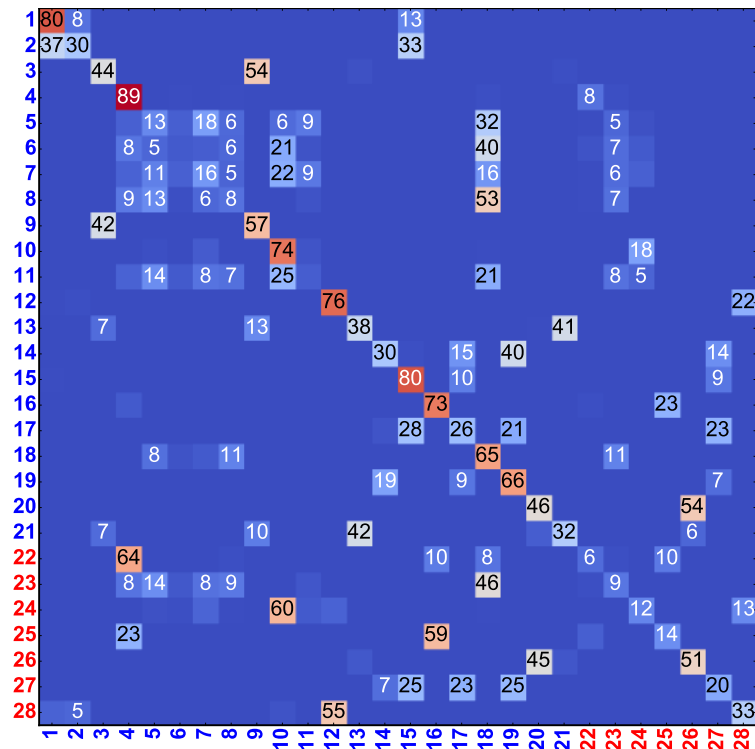


FIGURE 7.10. Confusion matrix for stiffness of 28 objects (prior objects (from 1 till 21) + new objects (22 till 28)). The blue index indicates the prior objects, and the red index new objects.

demonstrate the resulting confusion matrices constructed for stiffness, texture, and thermal conductivity respectively. The blue index indicates the prior objects, and the red index new objects. Regarding stiffness, the prior objects {1, 2, 3, 9, 13} were totally unrelated to the new objects; for surface texture, prior objects {6, 7, 9, 10, 21}; and for thermal conductivity, prior objects {4, 6, 8, 10, 13}. Therefore, I respectively selected these objects to construct prior tactile knowledge and test ATTL performance, when the robot learned about new objects based on each physical property. I also used objects {2, 3, 6, 10, 13} as prior objects for learning based on three properties. The performance of the ATTL method was compared with ATL which served as the baseline. The rest of the procedure was similar to Sec. 7.4.4.

Fig. 7.13 illustrates the recognition performance attained using ATTL and ATL (no transfer). The results show that the recognition performance achieved by ATTL with irrelevant prior objects is similar to the ones obtained with the ATL method (no-transfer) in the case of learning about objects via three physical properties (Fig. 7.13a) and via only one physical property (Fig. 7.13b, 7.13c, and 7.13d). This indicates that my proposed ATTL can stop transferring irrelevant prior knowledge.

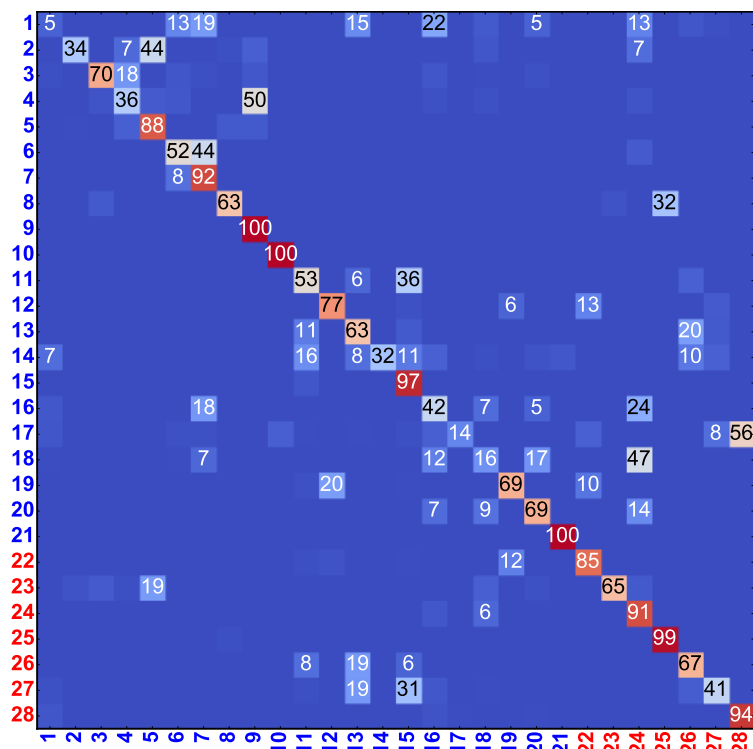


FIGURE 7.11. Confusion matrix for surface texture of 28 objects (prior objects (from 1 till 21) + new objects (22 till 28)). The blue index indicates the prior objects, and the red index new objects.

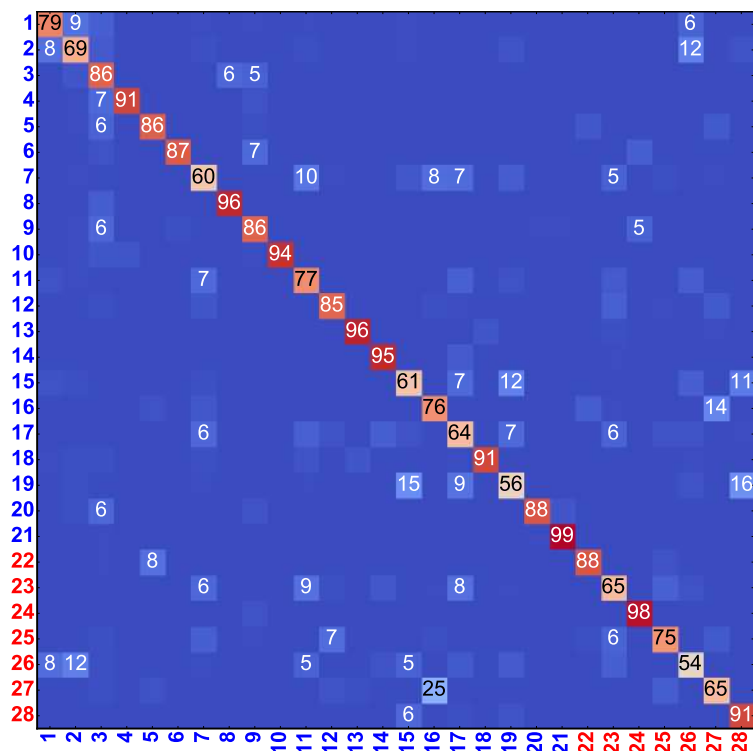


FIGURE 7.12. Confusion matrix for thermal conductivity of 28 objects (prior objects (from 1 till 21) + new objects (22 till 28)). The blue index indicates the prior objects, and the red index new objects.

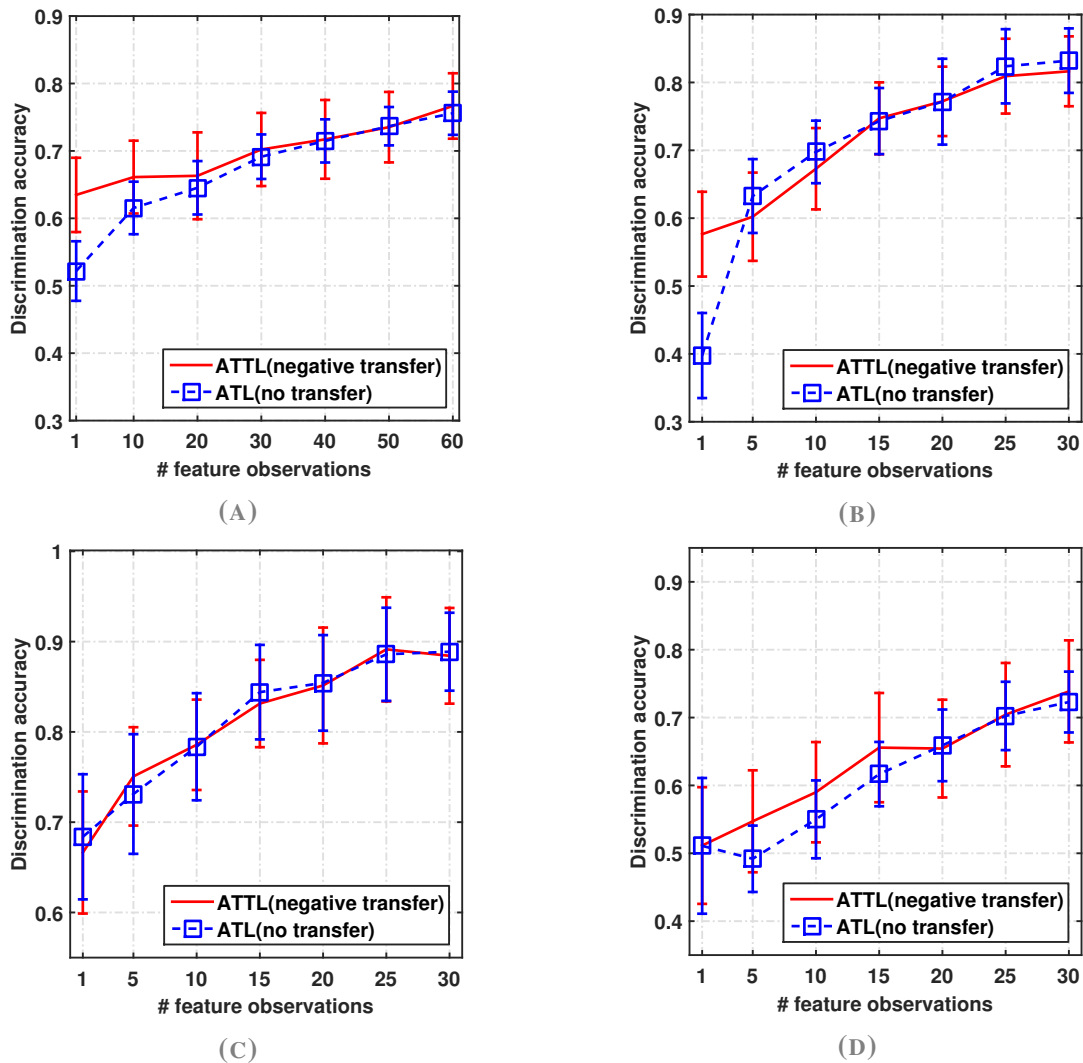


FIGURE 7.13. Evaluation of active tactile learning with negative prior knowledge constructed by deliberately selected five prior objects that were unrelated to the new objects. (A) Learning about the new objects based on three physical properties, prior objects: object {2, 3, 6, 10, 13}; (B) based on only stiffness, prior objects: object {1, 2, 3, 10, 18}; (C) based on only surface texture, prior objects: object {6, 7, 9, 10, 21}; (D) based on only thermal conductivity, prior objects: object {4, 6, 8, 10, 13}.

7.5. Summary and discussion

In this study, I proposed an active tactile transfer learning algorithm to enable a robotic system with multi-modal artificial skin to actively leverage the prior tactile knowledge to learn new objects in the unknown workspace. By taking advantage of my previously proposed pre-touch exploration approach, the robotic system can strategically select the next exploratory location in the workspace to efficiently collect pre-touch information. The attained data were then used to ascertain the number and positions of the objects. Employing my proposed active tactile transfer learning algorithm (ATTL), the robot automatically leveraged the most relevant and

informative prior knowledge to learn about new unknown objects with a few training samples or even one with very high discrimination accuracy. It achieved 72% discrimination accuracy with only one training sample plus 10 prior tactile knowledge (one-shot tactile learning). Besides, the robot was able to automatically decide how much to leverage the prior tactile knowledge or stop transferring the irrelevant one which could degrade the learning performance (Fig. 7.13). Furthermore, the robot attained higher discrimination accuracy, when the number of its prior tactile knowledge increased (Fig. 7.8 and 7.9). It accounts for the fact that increasing the number of prior knowledge also enhances the probability of finding more relevant ones. The experimental results show that in all scenarios, the ATTL outperformed uniform learning strategy in which training data was collected uniformly, and no past tactile experience was leveraged. The ATTL also performed better than the ATL method, because following the ATL the robot was unable to use any prior knowledge, even though it could strategically collect training samples. On the contrary, using the ATTL method the robotic system re-uses its prior tactile knowledge to learn about new objects by strategically selecting the next object and next informative exploratory action. A limiting assumption of my work is that the positions of the experimental objects are fixed and also the objects are placed flat in X-Y plane in the unknown workspace. Moreover, due to the low spatial resolution provided by the proximity sensors on the artificial skin array, objects that are close to each other can hardly be clustered after the robot explores the workspace. In order to tackle this problem, the spatial resolutions of the sensor array can be increased by fusing the proximity information and force signals while the robot touching the objects.

CHAPTER 8

Manipulation of Deformable Objects

The least touchable object in the world is the eye.

(Rudolf Arnheim)

8.1. Introduction

Tactile sensing enables robotic systems to interact safely with humans and objects by providing direct feedback to solve the slip detection problem, which is crucial to regulating grasping force in dexterous robotic manipulation. In this chapter, I present a novel tactile-based framework for detecting/correcting slips and regulating grasping forces to enable robotic gripper or hands with the sense of touch to safely manipulate deformable objects with the dynamic center of mass. My framework consists of three parts; (I) a tangential-force based slip detection method to correct slip; (II) a deformation prevention approach to regulate grasping force, which adjusts the relative positions of fingers in real time, and is realized by estimating the weight of the grasped object; (III) a new strategy for manipulating deformable heavy objects by changing their poses.

My proposed framework has several advantages over prior work. For instance, it does not require any prior knowledge of the contact surface (e.g. friction coefficient). In addition, my proposed framework is able to control multiple-fingers of the gripper individually in real time and is independent of the properties of the grasped object, such as stiffness, surface texture, and center of mass.

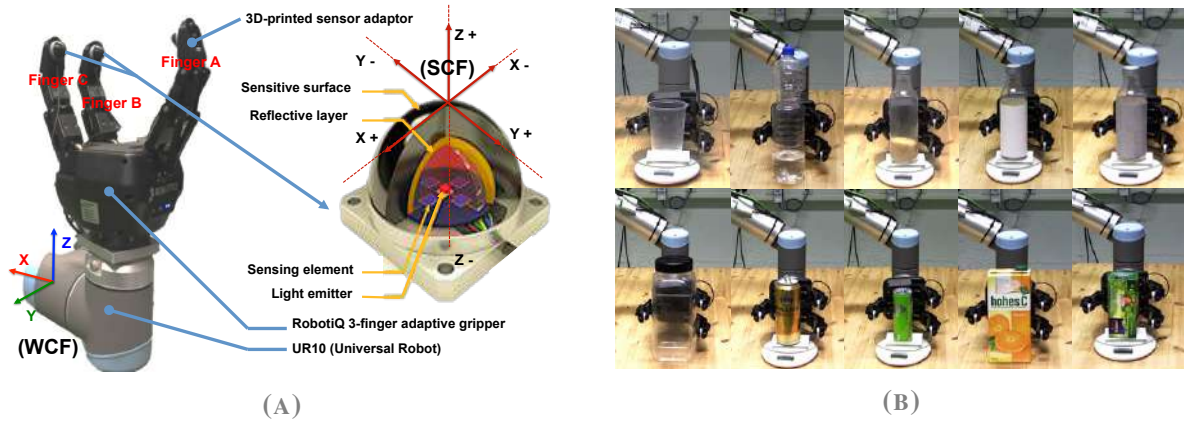


FIGURE 8.1. (A) Three-finger adaptive robot gripper from Robotiq is equipped with OptoForce sensors and mounted on the UR10 robotic arm (B). Experimental objects are shown in (C).

During this chapter, I first propose to use tangential force rather than normal force for slip detection in dynamic manipulation tasks. Then, I describe my approach to reduce the deformation caused by large forces exerted on grasped objects. Furthermore, I suggest a novel strategy for preventing slip of deformable heavy objects.¹

8.2. Methodology

8.2.1. Problem definition

Slip signals are of great significance for manipulation tasks. Previous work shows that both tangential force and normal force on the contact surface can be used for slip detection; however, to the best of my knowledge, no study has compared the slip detection approaches of using tangential force and normal force. In order to investigate which type of force is more informative for detecting slip signals in case of dynamic manipulation, I performed several experiments using different everyday objects (see Fig. 8.1).

Fig. 8.2 shows the changes of tangential force and normal force recorded during the manipulation of the deformable bottle filled with 300mL water. In this experiment, the deformable bottle was first stably grasped by the gripper while applying minimum grip force measured by OptoForce sensors. Then the gripper released its fingers for one position count, and the robotic arm started rotating the gripper at the same time for $\pi/3$ in the direction where finger A moves above fingers B and C. At this moment, a slip happened due to insufficient grasping force. Fig. 8.2 illustrates that both tangential and normal forces increased as the object

¹The content of this chapter has been published in [150].

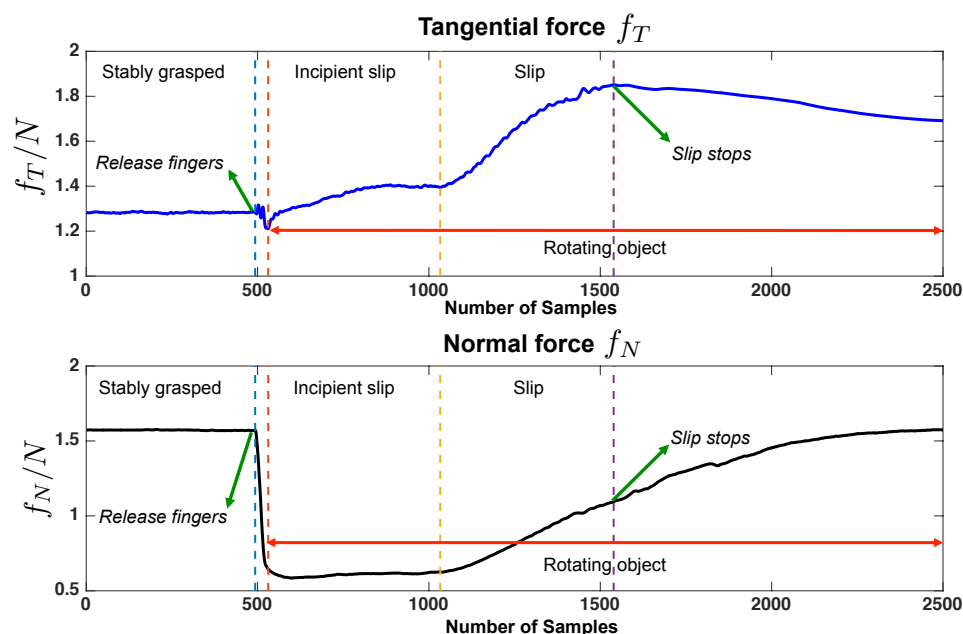


FIGURE 8.2. Tangential force and normal force signals exerted by one of the fingers (here finger B) during rotating a deformable bottle filled with 300g water by $\pi/3$.

slipped. This shows that the normal force cannot be used for slip detection during the dynamic manipulation. The reduction of normal force during the slip event was compensated by the increment of the grasped object's weight component in the identical direction during the rotation/manipulation. Thus, I propose to use tangential force to detect slip signals especially in the case of dynamic manipulation tasks. Exploiting tangential force instead of normal force is important for preventing influences generated by grasping poses and changing of the center of mass of the grasped objects. Based on my finding, in order to design a robust robotic system for object manipulation, I detect slip events by measuring the increasing rate of the tangential force (f_T) in slip direction, i.e. a slip happens as soon as the increment of f_T has exceeded a certain percentage δ within a short time period Δt .

8.2.2. Deformation prevention

A stable grasping can be ensured by detecting slip signals; however, it is also important to protect the grasped object from being damaged during manipulation, which means to reduce the object's deformation caused by the grasping forces as much as possible. I propose a new approach to prevent deformation during manipulating/rotating deformable objects. Grasped object deforms as grip force increases. Since the movement direction of the gripper's fingers is

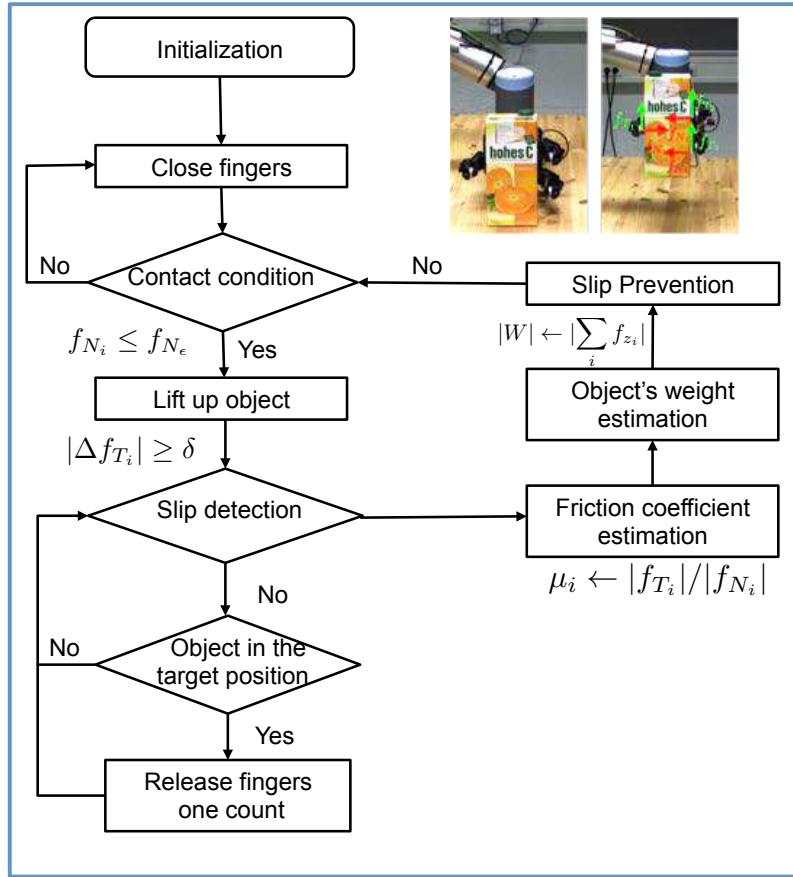


FIGURE 8.3. Estimation of the friction coefficient

perpendicular to the local contact surface, normal force serves as an indicator of deformation extent. Therefore, to avoid any large local deformation of objects, an upper bound for normal force, \bar{f}_N , is required for all fingers according to the stiffness of target object. Moreover, as fingers of the gripper may share different portions of grasping force due to irregularity of the object's shape, it is necessary to adjust the relative positions of the fingers. In this regard, I suggest to estimate the weight of the grasped object. In this scenario, the force exerted by each finger is decomposed in WCF and the resultant force along Z_{WCF} direction, $|\sum_i \mathbf{f}_{z_i}|$, is calculated as an estimation of the grasped object's weight as long as the grasp is stable, i.e. neither slip nor large deformation occurs. I decompose the force exerted by each finger in WCF and calculate the resultant force along Z_{WCF} direction, $|\sum_i \mathbf{f}_{z_i}|$, as an estimation of the grasped object's weight as long as the grasp is stable, i.e. neither slip nor large deformation occurs. In an ideal critical stable state, resultant force in Z_{WCF} direction should exactly balance the object's weight $|W|$; however, considering the impulse generated by the varying center of mass, a margin should be taken into consideration. Hence, if the norm

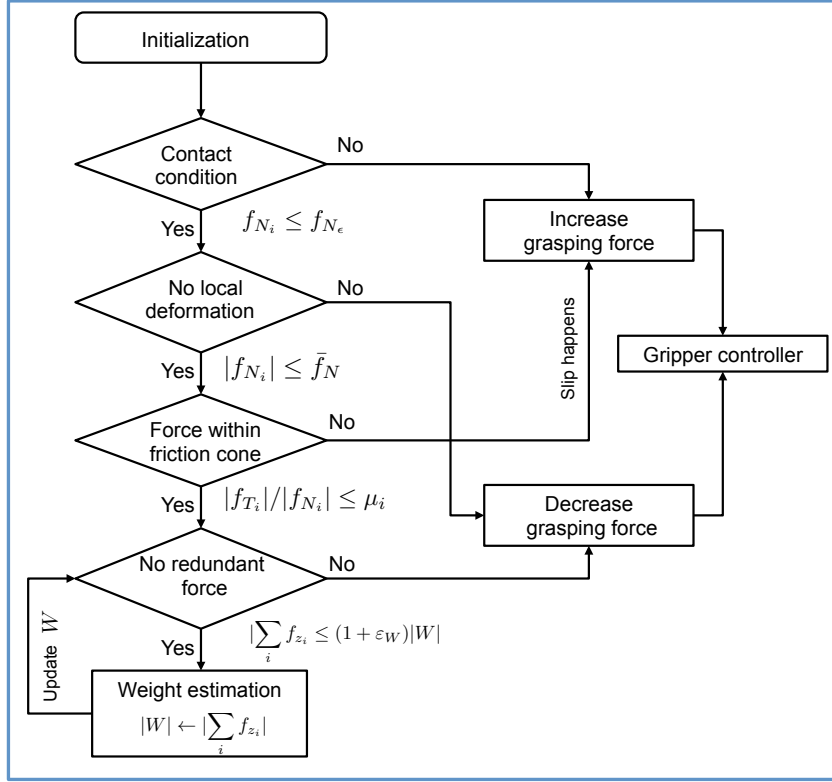


FIGURE 8.4. Slip Correction and Force Regulation

of current resultant force has exceeded a certain percentage over $|W|$, the gripper is considered to have applied redundant forces, which should be reduced. Since the target object's weight is estimated only in stable state, this suggested approach can also be used for object whose weight varies during manipulation.

8.2.3. Slip correction and force regulation

Here I propose a position-level slip correction and grip force regulation framework. On the one hand, it regulates grasping force to prevent objects from sliding. I detect slip when it happens for the first time by measuring the increasing rate of tangential force, i.e. a slip signal is detected as soon as the increment of f_T has exceeded a certain percentage δ within a short time period Δt . As soon as the first slip is detected, the ratio of the tangential force's norm $|f_T|$ to the normal force's norm $|f_N|$ is calculated as an estimation of the friction coefficient μ_i on the corresponding contact area, which will be used to prevent slip during the dynamic manipulation process, i.e. a slip is detected as soon as $|f_{T_i}|/|f_{N_i}| \geq \mu_i$ and then grip force is supposed to be increased to stop slip. On the other hand, large deformation of grasped object is prevented not only by maintaining normal force exerted by each finger within its

Algorithm 8.1 Slip Correction and Grip Force Regulation

 Initialization: Move robots to initial position, Open gripper, Reset sensors

Slip Detection Procedure

initialize the robotic system

while $\exists i : |\mathbf{f}_{N_i}| \leq f_{N_\epsilon}$ **do**| $P_i \leftarrow P_i + 1$ **end** $slip_happens \leftarrow \mathbf{False}$ **Starts Lifting up Object**Repeat $|\Delta \mathbf{f}_{T_i}| \leftarrow |\mathbf{f}_{T_i}(t)| - |\mathbf{f}_{T_i}(t - \Delta t)|, \forall i$ **if** $\exists i : |\Delta \mathbf{f}_{T_i}| \geq \delta$ **then**| $slip_happens \leftarrow \mathbf{True}$ **end**

Until object is lifted up

if $not\ slip_happens$ **then**| Repeat $P_i \leftarrow P_i - 1, \forall i$ | $|\Delta \mathbf{f}_{T_i}| \leftarrow |\mathbf{f}_{T_i}(t)| - |\mathbf{f}_{T_i}(t - \Delta t)|, \forall i$ | Until $\exists i : |\Delta \mathbf{f}_{T_i}| \geq \delta$ **end** $\forall i, \mu_i \leftarrow |\mathbf{f}_{T_i}| / |\mathbf{f}_{N_i}|,$ $|\mathbf{W}| \leftarrow |\sum_i \mathbf{f}_{z_i}|$ $\forall i, P_i \leftarrow P_i + 1,$ $\forall i, (f_{N_i})_{min} \leftarrow |\mathbf{f}_{N_i}|,$ **Gripper Controller****while** $Ture$ **do**| **if** $\exists i : |\mathbf{f}_{N_i}| \leq f_{N_\epsilon}$ **then**| | $P_i \leftarrow P_i + 1$ | **end**| **else**| | **if** $\exists i : |\mathbf{f}_{N_i}| \geq \bar{f}_N$ **then**| | | $P_i \leftarrow P_i - 1$ **else**| | | **if** $\exists i : |\mathbf{f}_{T_i}| / |\mathbf{f}_{N_i}| \geq \mu_i$ **then**| | | | $P_i \leftarrow P_i + 1$ **else**| | | | **if** $|\sum_i \mathbf{f}_{z_i}| > (1 + \epsilon_W) |\mathbf{W}|$ **then**| | | | | $i_m = \arg \max\{|\mathbf{f}_{N_i}|\}$ $P_{i_m} \leftarrow P_{i_m} - 1$ **else**| | | | | | $|\mathbf{W}| \leftarrow |\sum_i \mathbf{f}_{z_i}|$ | | | | **end**| | | **end**| | **end**| **end**| **end**| **end**| **end****end**

corresponding upper bound, but also by adjusting the resultant force in Z_{WCF} direction, w.r.t. the estimated weight. This framework is summarized in Algorithm 8.1. Notice that $|\mathbf{f}_{T_i}(t)|$ denotes the value of \mathbf{f}_{T_i} sensed at time t . After initialization, gripper closes to contact the target object. All fingers are controlled individually, so each finger stops closing as soon as its exerted normal force exceeds $f_{N\epsilon}$. Hence, the grasping gesture can adapt the shape of the target object's surface. Once target object is grasped, the robotic arm starts lifting the grasped object up. In the meantime, if slip happens, μ_i is calculated for each contact area. Then, the gripper closes its fingers for one position count to stop slip and $|\mathbf{W}|$ is estimated. If the target object is lifted up without slip, the gripper will keep releasing all its fingers simultaneously for one position count at each time, until one slip happens and is detected. Afterwards, dynamic manipulation process will start. In each control loop, contact state (touch or not) of each finger will be checked firstly to ensure contact. Then the exerted normal force and force ratio $|\mathbf{f}_{T_i}|/|\mathbf{f}_{N_i}|$ of each finger as well as resultant force $|\sum_i \mathbf{f}_{z_i}|$ are measured for controlling finger positions. $|\mathbf{W}|$ is updated in every stable grasping state.

8.2.4. Manipulation of Deformable Heavy Object

When the weight of grasped deformable object increases (for instance, by pouring water into a grasped container), the robotic gripper should either apply larger force to prevent the object from sliding, which may result in crushing the object; or just release the object immediately. However, humans can still hold the deformable heavy objects (even with dynamic centers of mass) by rotating them and changing their orientations/positions. Although the desired orientation of the grasped object is changed, the object may be safely grasped without increasing the applied force. I have observed from the results of the experiment described in section 8.2.1 that the grasped object stopped sliding and stabilized gradually as being rotated by the UR10 (the object slid between the fingers but did not leave the gripper) without closing fingers (see Fig. 8.2). This phenomenon can be explained by the change of grasping pose, since the object's weight component decreased with rotation in slip direction and became small enough for the contacted fingers to provide enough friction force to compensate. Therefore, using the advantage of my finding during the experimental study in section 8.2.1, I suggest an approach of changing the object's pose to stop slip in order to manipulate deformable heavy objects. In this section, I analyze the grasping model and present a theoretical proof for this proposed strategy.

Considering an object of weight $|\mathbf{W}|$ is grasped stably, and all tangential forces on the contact surface (\mathbf{f}_{T_i}) are directed toward $-Z_{WCF}$, i.e. Z_{WCF} parallels Z_{SCF} , and then the object is rotated by an angle θ ($\theta \in [0, \pi/2]$). If the grasp is stable, exerted force should satisfy:

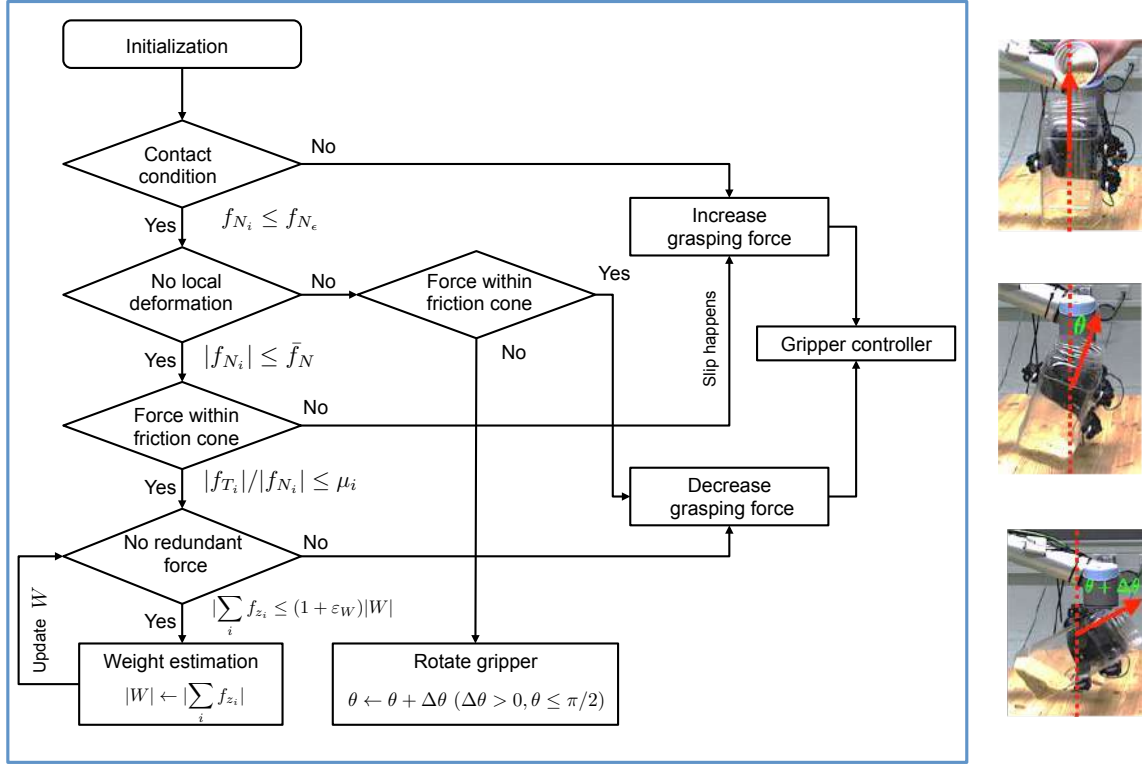


FIGURE 8.5. Human-like Strategy for Manipulating Deformable Heavy Object

$$\sum_i \mathbf{f}_{N_i} + \sum_i \mathbf{f}_{T_i} + \mathbf{W} = \mathbf{0}, \quad (8.1)$$

$$\sum_i |\mathbf{f}_{T_i}| \leq \sum_i \mu_i |\mathbf{f}_{N_i}|. \quad (8.2)$$

As the target object is grasped stably, the resultant force $|\sum_i \mathbf{f}_{T_i}|$ (i.e. the friction) is able to balance the weight component $|\mathbf{W}| \cos \theta$ which is tangential to the contact surface; however, if the resultant tangential force is not able to compensate this weight component (for each finger, the maximum $|\mathbf{f}_{T_i}|$ available is provided by $\mu_i |\mathbf{f}_{N_i}|$, Eq. 8.2), slip occurs. Therefore, slip can be stopped either by increasing $|\sum_i \mathbf{f}_{N_i}|$, i.e. enhancing the upper bound of tangential force, or by reducing $|\mathbf{W}| \cos \theta$, which equals increasing θ in $[0, \pi/2]$. The former approach has been applied for slip prevention in previous research [118]. However, since normal forces should be constrained to prevent large deformation (section 8.2.2), I suggest exploiting the latter strategy, i.e. reducing weight component $|\mathbf{W}| \cos \theta$ by rotating, especially for the manipulation of deformable objects. This approach can be applied to control the gripper by following the procedure in Algorithm 8.2 after the initialization and slip detection procedures in Algorithm 8.1.

Algorithm 8.2 Manipulation of Deformable Heavy Object

```

Gripper Controller while  $Ture$  do
  if  $\exists i : |\mathbf{f}_{N_i}| \leq f_{N_\epsilon}$  then
    |  $P_i \leftarrow P_i + 1$ 
  end
  else
    if  $\exists i : |\mathbf{f}_{N_i}| \geq \bar{f}_N$  then
      if  $\exists i : |\mathbf{f}_{T_i}|/|\mathbf{f}_{N_i}| \geq \mu_i$  then
        |  $\theta \leftarrow \theta + \Delta\theta$  ( $\Delta\theta > 0, \theta \leq \pi/2$ ) else
        |  $P_i \leftarrow P_i - 1$ 
      end
    end
    else
      if  $\exists i : |\mathbf{f}_{T_i}|/|\mathbf{f}_{N_i}| \geq \mu_i$  then
        |  $P_i \leftarrow P_i + 1$  else
        | if  $|\sum_i \mathbf{f}_{z_i}| > (1 + \epsilon_W)|\mathbf{W}|$  then
        | |  $i_m = \arg \max\{|\mathbf{f}_{N_i}|\}$ 
        | |  $P_{i_m} \leftarrow P_{i_m} - 1$ 
        | else
        | |  $|\mathbf{W}| \leftarrow |\sum_i \mathbf{f}_{z_i}|$ 
        | end
        end
      end
    end
  end
end
end

```

8.3. System description

8.3.1. Robotic systems

A Robotiq three-finger adaptive gripper was installed at the end of a 6-DoF UR10 (Universal Robots) robotic arm. The gripper is under-actuated (see Fig. 8.1a), and its Finger A pushes against Finger B and Finger C. The gripper can manipulate objects less than 10kg by either enclosing them with its fingers and palm or pinching them by using only fingertips. When the gripper grasps an object using the built-in adaptive grasping mechanism, each finger stops moving as soon as the current sent to its motor exceeds a threshold, indicating a large exerted

force. Thus, the gripper can adapt its finger-positions to the shape of the grasped object, enabling an adaptive grasping.

The position range of each finger is divided into 255 counts, with 0 indicating fully open, and 255 the fully closed. In this chapter, I represent the position of each finger using counts.

8.3.2. Tactile sensors

I used OptoForce OMD-20-SE-40N 3D force sensor set. Three out of four sensors were fixed on each fingertip of the gripper using 3D-printed sensor adaptors. The OptoForce sensor can measure forces exerted on the contact surface in three directions, using infrared light to detect small deformation in the shape of the outer sensor surface. It has a wide range of measurement, with a nominal capacity of 40N in Z_{SCF} direction, and ± 20 N in both X_{SCF} and Y_{SCF} directions. The OptoForce sensor can measure forces exerted on the contact surface in three directions with a wide range of measurement. In this chapter, I discuss forces in two coordinate frames: world coordinate frame (WCF) (see Fig. 8.1a) and sensor coordinate frame (SCF) (see Fig. 8.1a). In SCF, I discuss the tangential force vector \mathbf{f}_{T_i} and the normal force vector \mathbf{f}_{N_i} exerted on the grasped object, with norms $|\mathbf{f}_{T_i}|$ and $|\mathbf{f}_{N_i}|$. The force vectors in WCF are represented as \mathbf{f}_{x_i} , \mathbf{f}_{y_i} , and \mathbf{f}_{z_i} , with corresponding norms $|\mathbf{f}_{x_i}|$, $|\mathbf{f}_{y_i}|$, and $|\mathbf{f}_{z_i}|$. The subscript i denotes the number of finger ($i = 1, 2, 3$), and P_i is the corresponding finger position. The weight of an object of mass m is calculated as $\mathbf{W} = m\mathbf{g}$, with \mathbf{g} being the gravitational acceleration.

8.3.3. Experimental Objects

I selected 10 everyday objects with deformable surfaces and various materials, including a disposable cup, a deformable bottle filled with 300mL water, a plastic bottle with three different surface textures (texture 1: uniform meshy texture; texture 2: non-uniform rough texture; texture 3: smooth texture), each of which is filled with 200g rice, a large flexible plastic jar, a golden aluminum can and a green aluminum can with different stiffnesses, a juice container and a tea box, both of which are made of cardboard with different stiffnesses (see Fig. 8.1b).

234

²www.optoforce.com

³www.universal-robots.com

⁴www.robotiq.com

8.4. Experimental results

The robotic system performed four groups of experiments. In the first three groups of experiments, the task was to grasp and then lift the deformable objects by applying three different grasping strategies, i.e. gripper's built-in adaptive grasping mechanism, manipulation with minimal grasping force, and my proposed framework. Furthermore, to evaluate and compare the performances of all grasping strategies, the weight of the grasped object was increased by either pouring rice or water inside, and then the object was manipulated and rotated by $\pm 2\pi/3$. The last group of experiments was carried out to evaluate the performance of the proposed strategy for manipulating deformable heavy objects. In this work, the UR10 robotic arm, the Robotiq gripper, and the OptoForce sensors were controlled in the framework of ROS (Robot Operating System). Tactile signals were sampled at a frequency of 333Hz and then processed by a 15Hz low-pass filter, while the gripper was controlled at 50Hz. In order to show the consistency of my proposed framework in a robotic system and experimentally validate the efficiency of the suggested approaches during manipulation of real world deformable objects via robotic gripper, my robotic system performed four groups of experiments. In the first three sets of experiments, the task of the robotic system was to grasp and then lift the deformable objects by applying three different grasping strategies, i.e. gripper's built-in adaptive grasping mechanism, manipulation with minimal grasping force, and the proposed grasping framework. Furthermore, to evaluate and compare the performance of all grasping strategies with each other, the weight of the grasped objects was increased by adding either rice or water inside and then manipulating as well as rotating (by $\pm 2\pi/3$) the grasped object with the robotic system. The last set of experiments was carried out to evaluate the performance of the proposed strategy for manipulating deformable heavy objects. In these experiments, the UR10 robotic arm, the Robotiq gripper, and the OptoForce sensors were controlled in the framework of ROS (Robot Operating System). Tactile signals were sampled at a frequency of 333Hz and then processed by a 15Hz low-pass filter, while the gripper was controlled at 50Hz.

8.4.1. *Gripper's built-in adaptive grasping mechanism*

In this scenario, the task of the gripper was to grasp the experimental objects using the built-in adaptive grasping mechanism without tactile feedback. When the gripper grasps an object, each finger stops moving as soon as the exerted force exceeds 15N, which is the minimum force can be detected by the gripper. Exploiting the built-in adaptive grasping approach, the gripper managed to grasp all the experimental objects without any slip; however, the objects were gravely deformed due to the large grasping force (see Fig. 8.6).

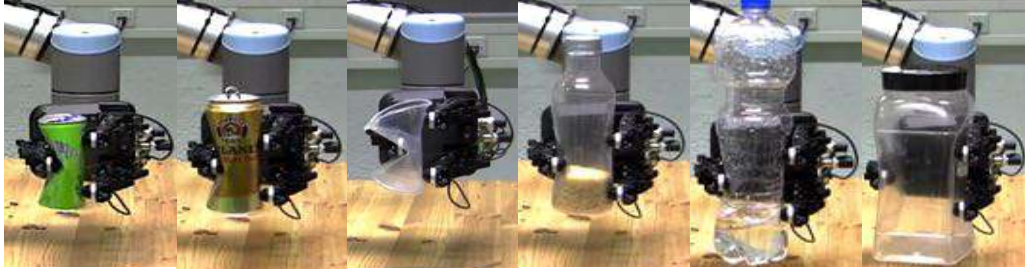


FIGURE 8.6. Grasping deformable objects using gripper’s built-in adaptive grasping mechanism.

8.4.2. *Minimum grasping force*

In this experiment, the minimum grasping force strategy was used (see Algorithm 8.1). The gripper first kept closing its fingers till the target object was grasped by a small contact force $f_{N\epsilon}$, with $0.2\text{N} \leq f_{N\epsilon} \leq 0.5\text{N}$, according to target object’s stiffness. As soon as the first slip was stopped, the minimum grasping force for each finger was determined (Algorithm 8.1-8.1, where $\delta = 5\%$ and $\Delta t = 300\text{ms}$). After the target object was grasped (see Fig. 8.7), I either increased the weight of grasped object manually, or rotated it using robotic system by $\pm 2\pi/3$. Experimental results in Fig. 8.7 show that the robotic system using minimum grasping force strategy is able to grasp the experimental objects with different stiffnesses and textures without large deformation. Nevertheless, objects slid out of the gripper. During manipulation, slips were caused by either weight increment or changes of the centers of mass, which the gripper could neither detect nor prevent. Therefore, the minimum grasping force can prevent the deformation of grasped objects to a great extent; however, it is not capable of preventing grasped objects from slipping in dynamic manipulation tasks.

8.4.3. *Evaluation of the proposed grasping strategy*

The task was to manipulate the experimental objects safely as described in the previous part. However, different from section 8.4.2, the robotic system was controlled by my proposed slip correction and grip force regulation framework (Algorithm 8.1). The upper bound of normal force was set to $2\text{N} \leq f_N \leq 5\text{N}$ in order to reduce local deformation, according to each target object’s stiffness. In order to tune the relative positions of the three fingers, the margin of resultant force was set in Z_{WCF} direction w.r.t. the estimated weight to $\varepsilon_W = 40\%$, according to the research result that the human central nervous system constantly adjusts the grip force with a margin of 10% – 40% [117]. In this experiment, the gripper closed its fingers for one position count once slip was detected, while the weight of the grasped object kept increasing.

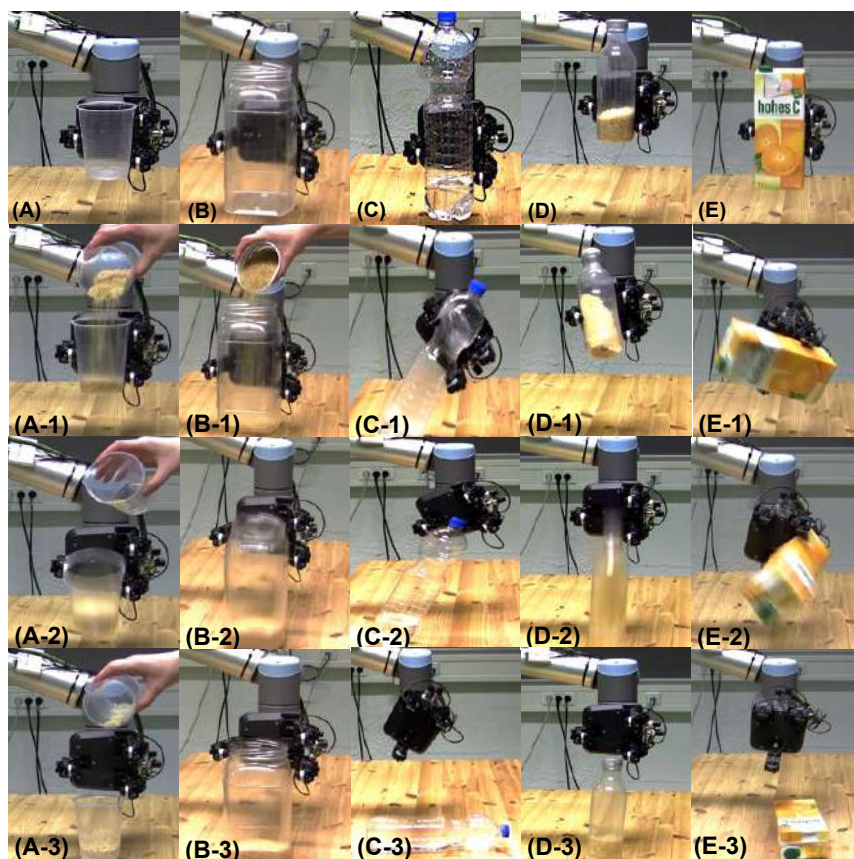


FIGURE 8.7. Manipulation of deformable objects with different characteristics, such as stiffness, surface texture, and center of mass, using minimum grasping force.

Hence, the target object was grasped stably without any slip during the entire process (see Fig. 8.8-A). In case of manipulation/rotation, the grasped object with dynamic center of mass (CoM) was manipulated stably by the robotic system, and the deformation of the object's surface was minimized as much as possible (see Fig. 8.8).

Normal and tangential force signals recorded in one of the dynamic manipulation experiments are plotted in Fig. 8.9. In this scenario, a deformable bottle filled with 300mL water was rotated (see Fig. 8.8-B). After initialization procedure (see Fig. 8.9-A), the robotic system grasped the bottle and lifted it up, till the first slip happened and was stopped (see Fig. 8.9-B). Then the robotic system started rotating the half-bottle of water by $\pm 2\pi/3$ for two times (see Fig. 8.9-C and 8.9-D). In the meantime, the gripper was controlled to correct slips and to regulate grasping force, in order to prevent the grasped bottle from sliding (especially as the abrupt changes of CoM happened) and large deformation. Compared to the minimum grasping force based manipulation, gripper reacted promptly either to correct slip or to regulate large normal force.



FIGURE 8.8. Manipulation of deformable objects with different characteristics, such as stiffness, surface texture, and center of mass, using Algorithm 8.1.

8.4.4. Comparison of Three Different Grasping Approaches

In order to measure the deformation extent of grasped objects, the difference between the average positions of fingers from the opposite sides (P_1 and $(P_2 + P_3)/2$) was calculated as an indication. Hence, a large finger position difference indicates a small deformation extent and vice versa. Maximum deformation values were recorded for experimental objects during manipulations by using both the adaptive grasping mechanism and the proposed gripper controller, respectively (see Fig. 8.11-A); while Fig. 8.11-B shows the deformation extent compared to the original size in percentage. Although the grasped objects were severely deformed in experiments using the adaptive grasping mechanism, deformation was largely reduced by taking advantage of the proposed gripper controller.

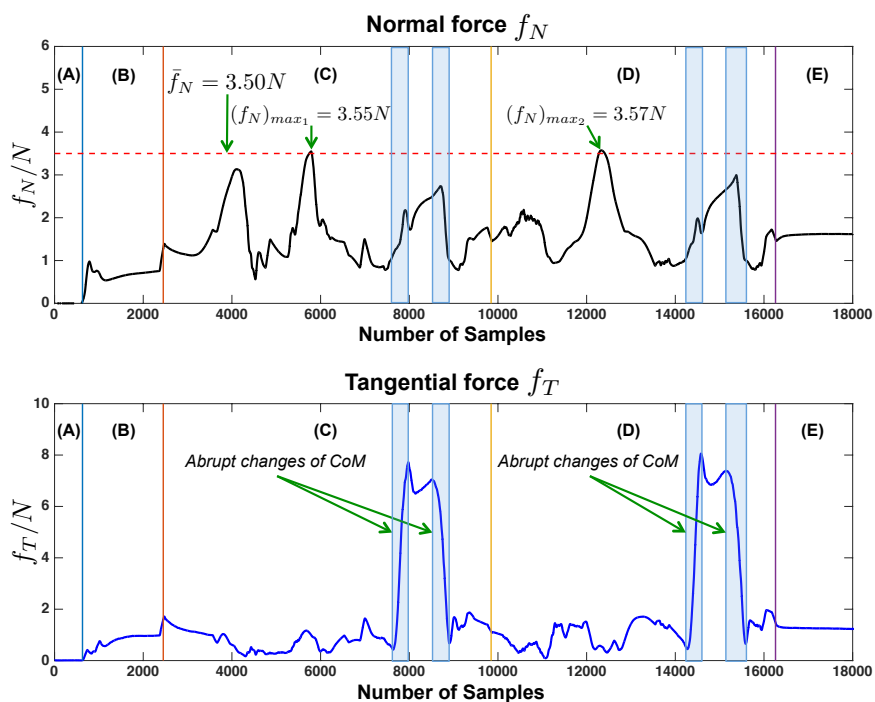


FIGURE 8.9. Normal force and tangential force exerted by one of the fingers (here finger A) recorded while manipulating a deformable bottle of 300mL water.

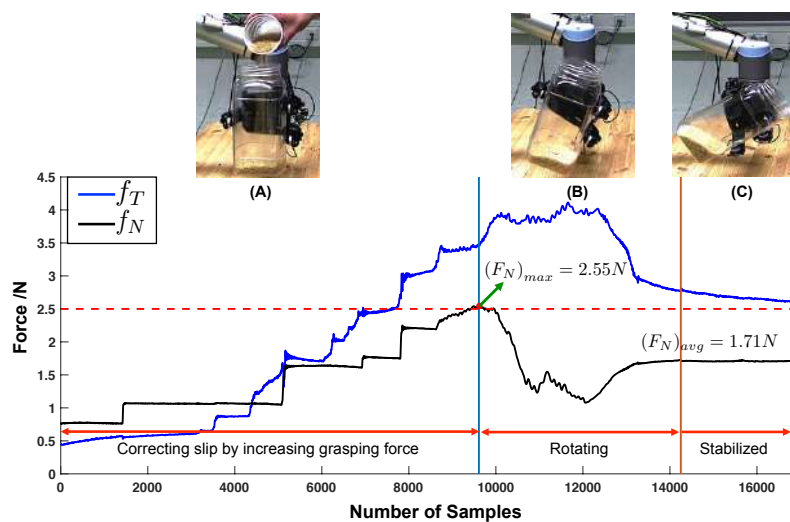


FIGURE 8.10. Manipulating a deformable heavy jar by applying Algorithm 8.2. Plots show the recorded normal and tangential forces exerted by (here finger B) during the manipulation process.

8.4.5. Evaluation of the proposed strategy for manipulation of deformable heavy objects

The objective of this experiment was to evaluate the performance of the proposed strategy for manipulating deformable heavy objects. The positive rotation direction ($\theta > 0$) of the gripper was specified as from finger A to finger B, through finger C. As θ increases from 0 to $\pi/2$, the resultant force $|\sum_i \mathbf{f}_{T_i}|$ required to balance the weight component $|\mathbf{W}| \cos \theta$ reduces. The difference between normal forces (\mathbf{f}_{N_i}) exerted by fingers from opposite sides should compensate $|\mathbf{W}| \sin \theta$, which increases during rotation. For the three-finger gripper, the condition for normal forces in stable state can be described as:

$$\left| |\mathbf{f}_{N_2}| + |\mathbf{f}_{N_3}| - |\mathbf{f}_{N_1}| \right| = |\mathbf{W}| \sin \theta \quad (8.3)$$

As θ gets close to $\pi/2$, both \mathbf{f}_{N_2} and \mathbf{f}_{N_3} approach $(|\mathbf{W}| - |\mathbf{f}_{N_1}|)/2$. In this experiment, the task of the robotic system was to grasp the deformable plastic jar safely, while exploiting the proposed strategy in Algorithm 8.1. After initialization and slip detection procedures, the empty jar was grasped with the determined minimum force. Then the weight of the grasped object was continuously increased by pouring rice into it. During this process, the gripper closed its fingers as soon as slip was detected (see Fig. 8.10-A). As the jar became heavier, the exerted normal force exceeded its upper bound (see Fig. 8.10, around 9500th sample of sensor signal), which means slip could not be stopped by increasing normal force any more. Thus, the gripper started rotating target object while tuning the relative positions of each finger simultaneously to find an equilibrium pose (see Fig. 8.10-B). Afterwards, tangential force reduced, indicating the stop of slip; and normal force converged, showing a stable grasping state (see Fig. 8.10-C). Fig. 8.10 shows that the robotic system managed to grasp and manipulate the deformable heavy jar successfully. It is worthwhile to mention that the position of each finger is kept being adjusted during the rotation process, in order to avoid the occurrence of re-orientation phenomenon, which means the grasped object has reached a new position in hand because of slippage.

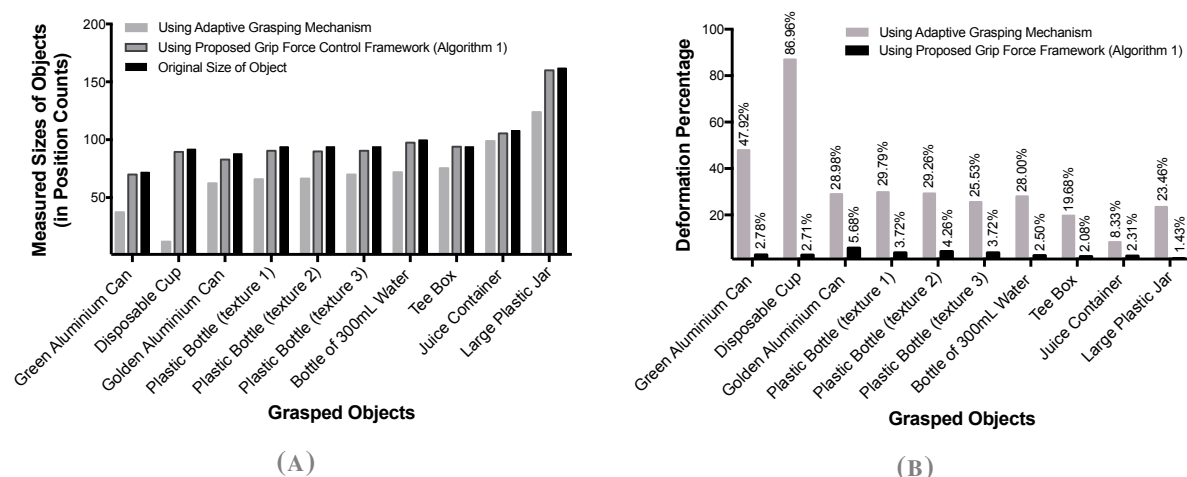


FIGURE 8.11. Comparison of deformation extents of grasped objects, using gripper’s built-in adaptive grasping mechanism and the proposed slip correction and force regulation framework, respectively.

8.5. Summary

Experimental results showed that although the built-in adaptive grasping mechanism of the gripper enables stable grasping during manipulation tasks, it mainly deformed grasped objects. Manipulating with minimum grasping force causes the least deformation; however, the stability of grasping cannot be guaranteed. With force signals measured on the contact surface, the grasped object can be manipulated stably with deformation being reduced as much as possible. It illustrates the significance of tactile information during manipulation tasks since tactile feedback can be used to complement the inadequate performance of the robotic system, such as the under-actuated gripper used in this work.

Approaches proposed in this work have several advantages over prior works. The approach utilized in this study can be executed online and does not require any prior knowledge of the contact surface (e.g., friction coefficient). Since my proposed approach does not rely on frequency analysis, it is insusceptible to the vibration signals generated by the robotic system during manipulation and also robust to external disturbances. Besides, my proposed framework can control multiple-fingers of the gripper individually in real time and is independent of the properties of the grasped object, such as stiffness, surface texture, and center of mass.

In the future, a low-level control (e.g., force control or torque control) of the gripper is expected for a more compliant behavior, which is not available currently for a finger position controller. Moreover, the performance could be improved by embedding the computation of break-away ratio into my framework.

CHAPTER 9

Touch Modality Identification on Humanoids with Sensitive Body

Touch is far more essential than our other senses. . . . It's ten times stronger than verbal or emotional contact.

(Saul Schanberg: A Natural History of the Senses)

9.1. Introduction

Recent advances in tactile sensing for robotics have opened up new pathways for humanoids to more accurately communicate with humans [133]. Through tactile interaction, various touch modalities may be carried out; a robot may be patted, slapped, punched, or tickled, with each action representative of a separate communicative intent. For any robotic system that is to work closely with humans, evaluation and classification of these touch modalities are vital. Humanoids should understand, just as humans do, that a slap is a form of negative feedback, that a pat is one of encouragement and so on [134]. To achieve this, a combination of several layers of technology is required. A large focus of the field has been on developing and extending tactile sensors utilized to collect and record tactile data. Less focus has been applied on the topic of processing and interpreting this data so as to provide meaningful and helpful information to the humanoid [26]. Taking advantage of my proposed tactile descriptors (chapter 3) I present a novel approach for touch modality identification (such as poking, tickling, push-

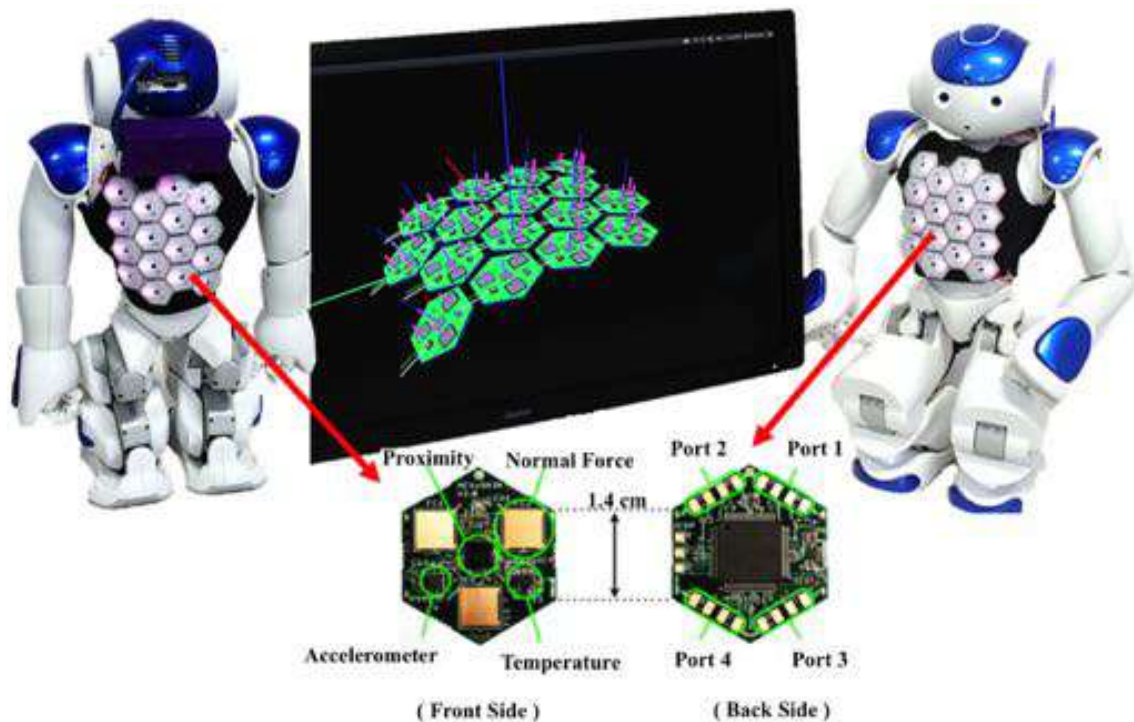


FIGURE 9.1. The upper body of the NAO was covered with 32 skin cells, 16 cells on the front and 16 cells on the back. The skin cells are called Cellular skin.

ing patting, rubbing, stroking, scratching, punching, and slapping) during tactile human-robot interaction. Using the proposed approach humanoids can distinguish between different touch modalities that are enacted on their body skin. In this respect, I equipped a NAO humanoid with whole upper body coverage of multi-modal artificial robotic skin.¹

9.2. Touch perception methodology

9.2.1. Touch perception via multi-modal robotic skin

Tactile information corresponding to applied touch was measured via the multi-modal artificial skin on the front and back of the NAO. The generated vibration during touch presentation was measured by the existing three-axis accelerometer on each skin cell. The intensity of the applied touch was sensed by the normal force sensors. Pre-contact sensing was carried out via proximity sensors in each cell. The thermal sensors were used to sense the temperature of objects in contact with NAO's skin. The robust tactile features were extracted from measured signals following procedure described in chapter 3.4.2.

¹The content of this chapter has been published in [170].

9.2.2. Data collection

Touch data collection was completed via 12 volunteers, (6 females and 6 males). Each participant was given a description of the actions as described in Table 9.1. In order to allow for human-robot interactions to be as natural as possible no instructions were given to the subjects regarding the duration, orientation or location of contact. Each subject was free to complete the actions as he or she would do normally. Tactile data from two touch scenarios was collected for each participant namely *single touch* and *multiple touch*.

9.2.3. *Single touch action*

Single touch refers to a singular enactment of one of the touch modalities from Table 9.1 upon the surface of the NAO's skin (see Fig. 9.3). Humans can identify touch modalities invariant to the body motion. Therefore, single touch data were collected while the NAO was stationary, as well as when the NAO was in motion.

9.2.3.1. NAO in stationary position

For the stationary case, the NAO was in sitting position such that subjects had free access to front and back of the NAO.

- **Training data collection**

The training dataset was obtained from six of the twelve subjects, comprised of three males and three females. Each subject carried out each single-instance touch modality on the back of the NAO three times. Consequently, for each touch modality, 18 samples were collected ($6 \text{ subjects} \times 3 \text{ trials} = 18 \text{ trials}$ or a single touch modality), with 162 training samples in total ($18 \text{ trials} \times 9 \text{ touch modalities} = 162$).

- **Test data collection**

Humans can discriminate touch modalities regardless of the location of the received touch on the body. Moreover, touch identification does not depend on the gender and age of the touch transmitter. Therefore, in this study, in order to assess the robustness of my proposed methods the unseen test data was collected from the remaining six subjects with different ages and nationalities. In addition, the test data was obtained

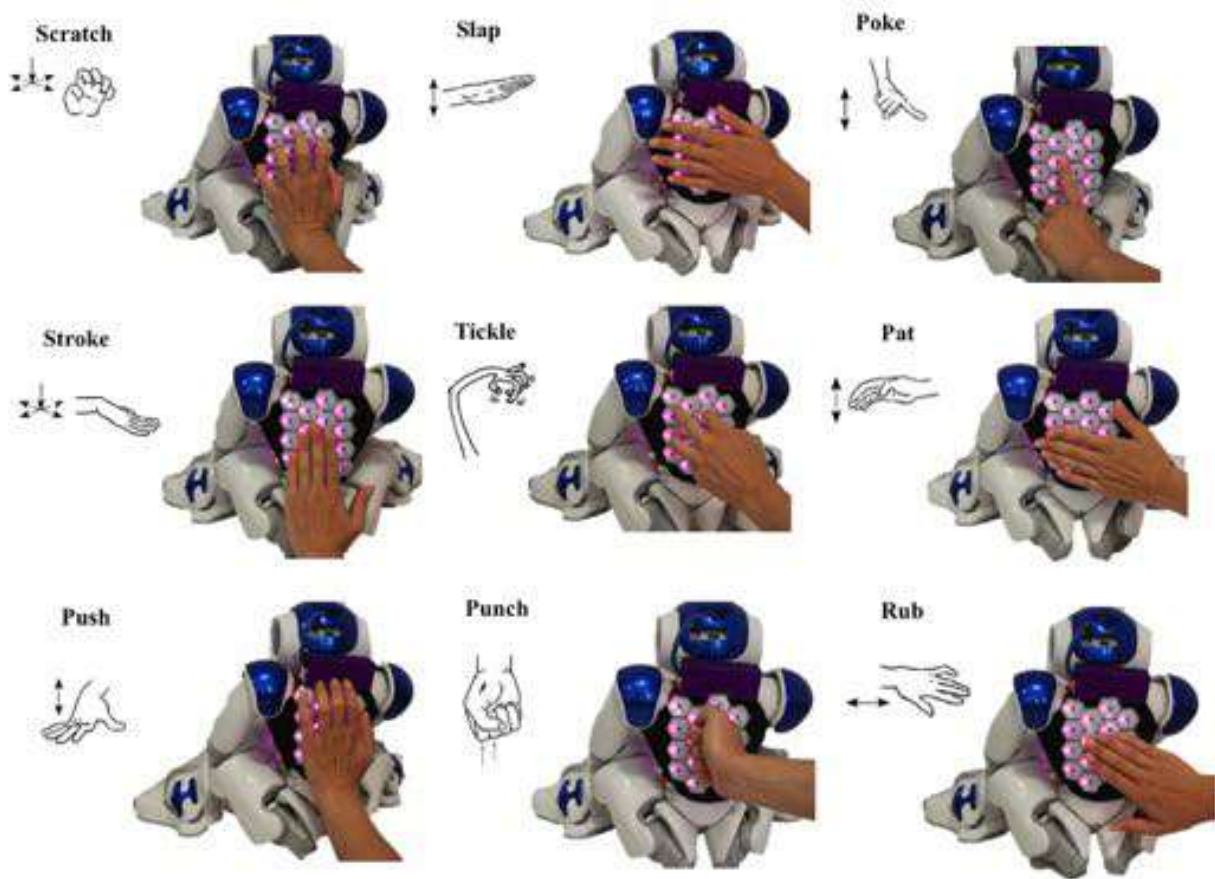


FIGURE 9.2. Illustrations of the nine touch modalities enacting on the NAO's body.

from actions applied to the front of the NAO instead of the back. In this scenario, each touch modality was carried out four times. Subsequently, for each touch modality, 24 samples were collected ($6 \text{ subjects} \times 4 \text{ trials} = 24 \text{ trials}$ for a single touch modality), with 216 unseen test samples in total ($24 \text{ trials} \times 9 \text{ touch modalities} = 216$).

9.2.3.2. NAO in motion

NAO was in motion state. NAO was either walking forward and backward or sitting down and standing up continuously.

Action	Description
Scratch	Contact with the fingertips or fingernails with movement tangential to the surface.
Tickle	Contact with the fingertips or fingernails with each finger moving independently and repeatedly along the skin.
Rub	Prolonged contact with the palm of the hand with movement tangential to the surface
Poke	Brief contact with the tips of one or more straightened fingers.
Stroke	Contact with the fingertips or upper sections of the finger moving simultaneously across the skin.
Punch	Brief contact applied by the base of a closed fist.
Pat	Two instances contact with the palm of the hand, relatively close together.
Push	Prolonged contact with the fingers or palm of the hand.
Slap	Brief contact with an open fist.

TABLE 9.1. Selected touch modalities.

- **Training data collection**

Training touch samples were collected from six of the twelve subjects while NAO was continuously sitting down and standing up. Each subject was free to decide when to carry out the actions during the position transition. The rest of the procedure was the same as described for the training data collection in Sec. 9.2.3.1.

- **Test data collection**

In this scenario, whilst NAO was walking toward or backward the remaining six subjects performed the touch actions on the front of the NAO. Each subject could decide when to present the touch actions on front of the NAO during the motion or walking. The rest of the process was the same as explained in Sec. 9.2.3.1.

9.2.4. Multiple simultaneous touch actions

Multiple touch actions consist of two or more single actions performed simultaneously on different areas of the NAO. It is desirable for humanoid to possess the human ability to distinguish and identify simultaneously applied touch modalities. To evaluate this property, a subset of combinatory actions was selected from the possible combinations of the 9 individual actions. This subset was selected so as to provide a representative set containing at least

TABLE 9.2. Multiple touch actions.

Body Part		Combined Action							
Front	Poke	Tickle	Push	Slap	Rub	Stroke	Punch	Scratch	Pat
Back	Poke	Tickle	Rub	Push	Stroke	Scratch	Pat	Punch	Slap

one instance of each single-action, as well as focus on those actions likely to be performed together in natural communication. These actions are listed in Table 9.2. For the multiple touch case, data was collected while the NAO was moving. As was done in the single-touch case, the movement was a continual loop of sitting to standing up movements and vice versa. Each pair of single-actions was enacted simultaneously on the NAO in order to create their respective multiple touch action.

- **Training data collection**

No training data was collected for the multiple touch case, as it is intended to be an evaluation dataset. The classifier used for evaluation was trained on the data previously collected in the single-touch case.

- **Test data collection**

A new group of six subjects not present in the previous single touch data collection, carried out the multiple touch actions on the NAO. Each action completed four times per subject (6 subjects \times 4 trials = 24 trials for each multiple touch modality). In total, this generated a dataset of 2 (front and back) \times 24 = 48 for each touch action.

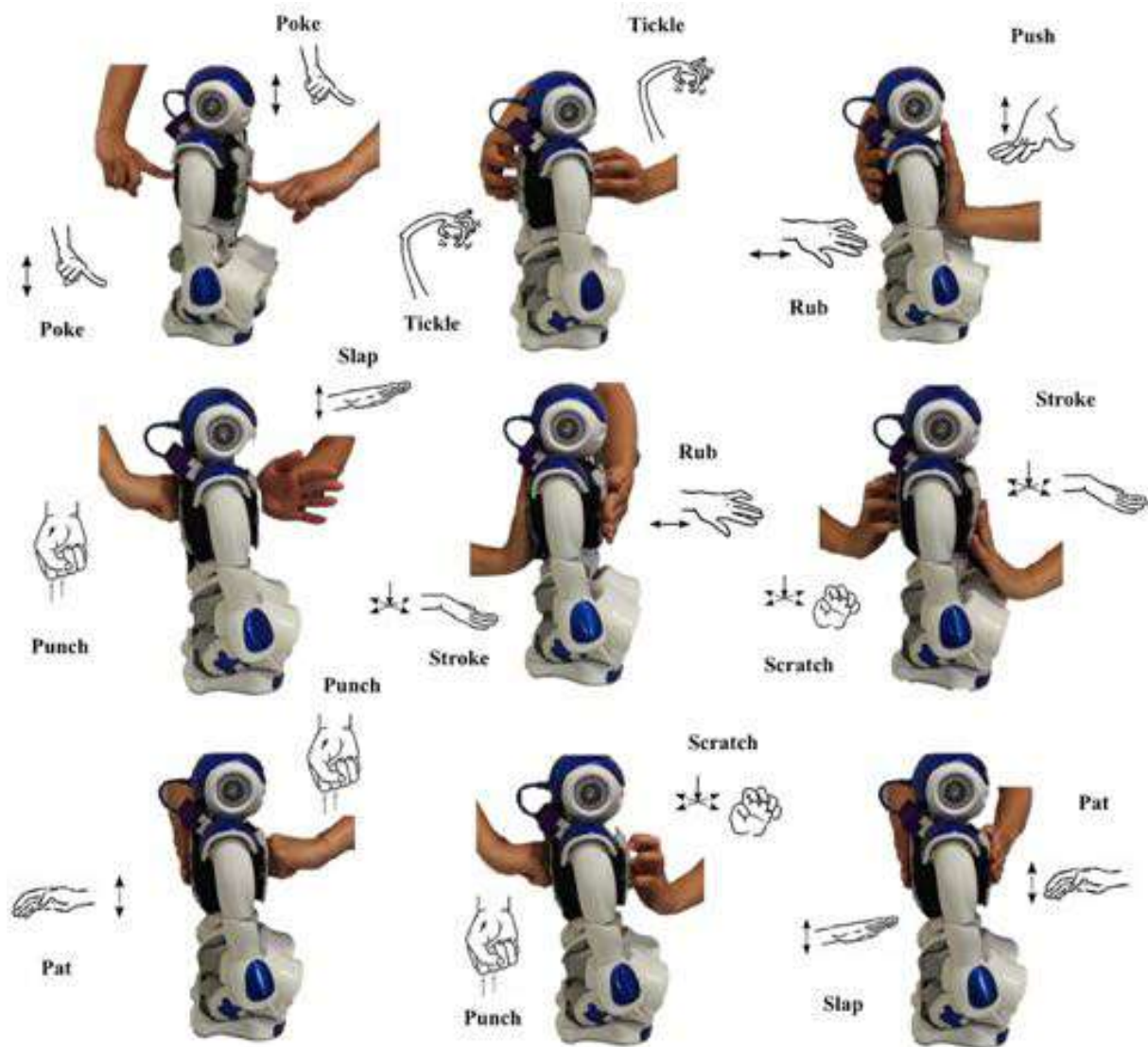


FIGURE 9.3. Illustrations of the multiple touch actions enacting simultaneously on the NAO's body.

9.3. Representative of touch signals

9.3.1. Dynamic Cell Selection

The contact may occur at any arbitrary location along the NAO skin during touch interaction. Therefore, NAO used the output of the proximity sensors existing on each skin cell to realize the location of a touch. In this experiment, all obtained proximity data were normalized to 0 and 1 (λ_{n_c} in 9.1), i.e., the proximity output was equal to value 1 if a skin cell was in contact

or in close contact ($d < 50\text{ mm}$) with the subjects's hand, otherwise equal to 0 ($d > 50\text{ mm}$).

$$\lambda_{n_c} = \begin{cases} 1 & \text{if } d < 50\text{ mm} & \text{Contact} \\ 0 & \text{if } d > 50\text{ mm} & \text{No-Contact} \end{cases} \quad (9.1)$$

where d is the distanced between hands of the subjects and NAO's skin and n_c is the assigned identification (ID) number of each cell. The output of the acceleration, normal force, and temperature sensors of the cells having proximity value equal to $\lambda_{n_c} = 1$ were considered for further data processing. This decreases the computational cost of signal and information processing during the feature extraction and touch modeling by the NAO.

9.3.2. Pre-Processing

Before computing the feature descriptors, pre-processing of each tactile signal was required. In this respect the mean value of each obtained signal during a touch action was subtracted with the original raw signal (zero mean) to maximize useful information and minimize the effect of artefacts.

9.4. Adapted existing touch classification approaches

In order to compare my proposed feature descriptors with the existing methods, I adapted the state-of-the art feature descriptors so they could function on my data. This was because the data-set and experimental setup varies from paper to paper, and the exact methods cannot be directly reapplied. In some cases, features were discarded as they were not relevant for my data - such as detecting a repeating action when all touch modalities are single-instance. Those features that were re-implemented are listed below. To the best of my knowledge there is only a few research that have addressed the problem of touch modality classification. There are three papers, in that they provide replicable, high-accuracy methodologies. In order to evaluate the effectiveness of the method presented in this paper, these methods which are summarised in table are adapted to my data, and evaluated in the paper [1–3]. The table 2.3 shows the summary of the existing touch classification approaches.

9.4.1. Adapted Naya [1]

1. *Max total intensity*: Max total force applied, calculated by finding the maximum of the total load datastream.

$$w_{peak} = \max \sum_{n_c=1}^{N_c} \sum_{n_f=1}^{N_f} F_{n_f}^{n_c}(t) \quad (9.2)$$

2. *Max contact area*: The contact area value obtained from the time of peak total load.

$$a_{peak} = \max \sum_{n_c=1}^{N_c} \sum_{n_f=1}^{N_f} b_{n_f}^{n_c}(t) \quad (9.3)$$

where

$$b_{n_f}^{n_c}(t) = \begin{cases} 1 & \text{for } F_{n_f}^{n_c}(t) \geq f_{thresh} \\ 0 & \text{otherwise} \end{cases} \quad (9.4)$$

3. *Temporal difference of total load*: Indicator of how sharp the peak for applied force is.

$$\delta_{w_{peak}} = \frac{\sum_{n_c n_f} |F_{n_f}^{n_c}(t_{max}) - F_{n_f}^{n_c}(t_{max} - 1)|}{\sum_{n_c n_f} F_{n_f}^{n_c}(t_{max})} \quad (9.5)$$

Where t_{max} is the time at which contact force was greatest.

4. *Temporal difference of contact area at total load*: Indicator of how sharply the contact area is changing at max force

$$\delta_{a_{peak}} = \frac{\sum_{n_c n_f} |b_{n_f}^{n_c}(t_{max}) - b_{n_f}^{n_c}(t_{max} - 1)|}{\sum_{n_c n_f} b_{n_f}^{n_c}(t_{max})} \quad (9.6)$$

9.4.2. Adapted Silvera-Tawil [2]

1. *Max Intensity*: Max value across all force sensors at any point in time during the action.
2. *Spatial resolution*: Ratio of elements containing at least 50% of the max intensity at the time of max intensity.

$$SR = \frac{1}{N_c N_f} \sum_{n_c=1}^{N_c} \sum_{n_f=1}^{N_f} c_{n_f}^{n_c}(t_{max}) \quad (9.7)$$

where

$$c_{n_f}^{n_c}(t) = \begin{cases} 1 & \text{for } F_{n_f}^{n_c}(t) \geq \frac{1}{2}w_{peak} \\ 0 & \text{otherwise} \end{cases} \quad (9.8)$$

3. *Mean of intensity*: Mean of the mean intensity across all sensors, across all time samples where action is observed.

$$MOI = \frac{1}{TN_cN_f} \sum_{t=0}^T \sum_{n_c=1}^{N_c} \sum_{n_f=1}^{N_f} F_{n_f}^{n_c}(t) \quad (9.9)$$

where T is the total number of time samples for the given action

4. *Contact Time*: Total time at least one force sensor is above threshold value, effectively measuring the duration of the action.
5. *Rate of intensity change*: Sum of the 2nd derivative of the absolute intensity change.

$$ROI = \sum_{n_c=1}^{N_c} \sum_{n_f=1}^{N_f} \frac{d^2 (|F_{n_f}^{n_c}(t) - F_{n_f}^{n_c}(t-1)|)}{dt^2} \quad (9.10)$$

9.4.3. Adapted Koo [3]

1. *Total Force*: Calculated using the variance of the accelerometer.

$$F_{total} = \text{var}(A_{rep}), \text{ where } A_{rep} \text{ is a representative accelerometer datastream} \quad (9.11)$$

2. *Contact Time*: Total time at least one force sensor is above threshold value, effectively measuring the duration of the action.
3. *Contact Area Change*: Sum of the changes in contact area

$$CAC = \sum_{n_c=1}^{N_c} \sum_{n_f=1}^{N_f} (b_{n_f}^{n_c}(t) - b_{n_f}^{n_c}(t-1)) \quad (9.12)$$

9.5. Experimental evaluation and results

9.5.1. Touch modality identification results

The Support Vector Machine (SVM) [171] algorithms as a common supervised marginal learning approach and the linear kernel method were used to discriminate different touch. In order to find the optimal learning parameters for SVM, 5-fold cross validation (CV) was used. In this respect, the training data set was randomly split into 5 folds and during each evaluation, 4 of those were used for training and one was used for testing. This process was repeated 10 times to obtain an average performance on the evaluation sets. This entire process was repeated 20 times using different values for the learning parameters to find the one with the lowest CV error. The SVM with optimal parameters was then re-trained with the entire training data set to obtain classification models. These classification models were used by NAO to predict the touch modalities for the unseen test data. The prediction results are reported in terms of recognition accuracy.

9.5.1.1. Single touch classification results

A. Enacted Touch Location Invariance

As is possible for humans, humanoid robot also should be capable of identifying various touch modalities irrespective of the location in which they occur. To provide this capability with the NAO, the SVM along with the best learning parameters found via cross validation process was trained with the data obtained from *single-touch actions* enacted solely on the back of the NAO having the stationary position. Then the constructed touch classification models was used by the NAO to predict with the unseen test data set collected on the front of the NAO. In this scenario, NAO could classify 9 touch modalities with 96.79% recognition accuracy substantially higher than chance classifier. Table 9.3 shows the confusion matrix obtained from the classification procedure. The confusion matrix indicates how often a given touch action was misclassified as another one. Perfect classification would result in a diagonally-filled table. However, Table 9.3 shows that most errors involve touch modalities having similar action properties. For instance, Rub was confused with Stroke as they both have almost similar action properties. Moreover, Slap was identified as Pat and Punch since these touch modalities share almost identical action properties. However, the confusion matrix and the obtained results

show that NAO was successfully able to discriminate different touch modalities regardless of the location of the enacted touch. Moreover, the achieved recognition results were independent on the subjects as the both training and unseen test data were collected with various subjects.

B. Enacted touch motion invariance

NAO employed SVM with the linear kernel method to discriminate 9 different received touch actions. The optimal learning parameters were obtained from 5-fold cross validation, the detailed procedure of which has been explained above. The classifier was trained with the training data which was collected from the back of the NAO while it was moving. Then the constructed learning models were used to predict the unseen touch modalities in test data enacted on the front of the NAO while it was sitting down and standing up continuously. In this case, NAO achieved 94.4% classification accuracy. Regarding to the confusion matrix Table 9.4, Poke and Push were confused with each other as they have similar action properties. The confusion matrix also shows that Rub was misclassified as Push and Poke. These touch modalities are sharing similar actions properties compare to the others. Furthermore, in order to evaluate the robustness of my proposed approach the collected training data from the back of the NAO having stationary position was used to train the classifier. The constructed touch classification models then was evaluated by predicting with the unseen test data while NAO was moving. In this case, NAO could successfully discriminate 9 touch modalities through the actions properties with 92.52% recognition accuracy. The confusion matrix in Table 9.5 shows that push and Poke, Pat and Slap, and Slap and Punch were confused two time with each other.

9.5.1.2. Multiple touch classification results

Multiple touch classification was carried out by training SVM classifier on stationary, single-touch actions enacted on back side of the NAO. The multiple touch dataset of the 9 combinatory actions collected as an unseen test set. Each multiple touch was evaluated as the combination of two single actions. The relative position of each skin cell from its assigned ID, combined with the output of the proximity sensors, records and splits the combinatory actions into its constituent parts. Table 9.6 shows the obtained confusion matrix in which NAO achieved 93.03% multiple touch classification accuracy. Table 9.6 illustrates that poke, stroke, and Rub were confused with push. Moreover, Pat and Punch miss-classified two time with slap.

9.5.2. *Touch clustering results*

An important task for NAO was to qualitatively differentiate between varying categories of touch modalities. This means that touch actions having the same properties tend to be in the same cluster (unsupervised learning). In this respect, Expectation Maximization (EM) [172] algorithm was employed to categorize the selected touch actions. NAO employed the EM algorithm as an unsupervised learning approach to categorize enacted touch modalities through actions properties. The EM was trained with the entire unsupervised data set. A class to clustering approach was used to evaluate how well NAO can recognize the correct category of an unseen touch. In this approach, classes were assigned to the categories, based on the majority value of the class attribute within each categories. Later on, these assignments were used to compute the classification performance. shows the results of this experiment for the single touch and NAO with stationary position, single touch while NAO was moving, and multiple touch individually, in which my proposed feature descriptor used by NAO to extract informative data from the collected touch tactile data. From table 9.7 it is clear that NAO managed to recognize the categories of touch modalities with an accuracy significantly higher than chance. NAO could categorize single touch (stationary case) and single touch (while NAO was moving) with the accuracy of 81.83% and 78.91% respectively. Using the EM and similar learning procedure as above NAO also categorized the received single touch while EM was trained with the touch collected from NAO's back having stationary position and evaluated with the touch received on the front side while moving. The obtained unsupervised classification accuracy by the NAO was 77.55%. Moreover, using EM NAO could categorized the multiple touch successful with recognition rate of 80.10%.

9.5.3. *Comparison with existing approaches*

The touch feature descriptors proposed to discriminate 9 touch modalities by NAO were compared against the adapted state of the art touch identification methods. Each method was evaluated using the classifier utilized in the original paper, as well as with a standard SVM classifier. This was done as in some cases, in particular Koo, had features that functioned well with a specific type of learning method. Comparison with both a specified and standardized learning method provides greater insight into the role of the feature extraction. For comparison, the proposed features were evaluated on all listed classifiers, as well as the standard SVM. Each classifier was trained with the collected single touch action data set from the back of the NAO in which NAO had the stationary position. The constructed touch models then were evaluated by predicting with the unseen touch samples applied on front side of

	Pat	Poke	Punch	Push	Rub	Scratch	Slap	Stroke	Tickle
Pat	24	0	0	0	0	0	0	0	0
Poke	0	23	0	1	0	0	0	0	0
Punch	0	0	24	0	0	0	0	0	0
Push	0	0	0	24	0	0	0	0	0
Rub	0	0	0	0	22	0	0	2	0
Scratch	0	0	0	0	0	23	0	0	1
Slap	1	0	1	0	0	0	22	0	0
Stroke	0	0	0	0	0	0	0	24	0
Tickle	0	0	0	0	0	1	0	0	23

TABLE 9.3. Confusion matrix for single touch classification (NAO in stationary position).

	Pat	Poke	Punch	Push	Rub	Scratch	Slap	Stroke	Tickle
Pat	24	0	0	0	0	0	0	0	0
Poke	0	22	0	2	0	0	0	0	0
Punch	0	0	23	0	0	0	1	0	0
Push	0	2	0	22	0	0	0	0	0
Rub	0	1	0	1	22	0	0	0	0
Scratch	0	0	0	0	0	23	0	0	1
Slap	1	0	1	0	0	0	22	0	0
Stroke	0	1	0	1	0	0	0	22	0
Tickle	0	0	0	0	0	0	0	0	24

TABLE 9.4. Confusion matrix for single touch classification (NAO in motion).

	Pat	Poke	Punch	Push	Rub	Scratch	Slap	Stroke	Tickle
Pat	22	0	0	0	0	0	2	0	10
Poke	0	23	0	1	0	0	0	0	0
Punch	0	0	22	0	0	0	2	0	0
Push	0	0	0	22	0	0	0	2	0
Rub	0	0	0	0	22	0	0	2	0
Scratch	0	0	0	0	0	22	0	0	2
Slap	0	0	2	0	0	0	22	0	0
Stroke	0	0	0	2	0	0	0	22	0
Tickle	0	0	0	0	0	1	0	0	23

TABLE 9.5. Confusion matrix for single touch classification (Training: NAO in stationary position. Evaluation: NAO in motion).

	Pat	Poke	Punch	Push	Rub	Scratch	Slap	Stroke	Tickle
Pat	48	0	0	0	0	0	0	0	0
Poke	0	44	0	4	0	0	0	0	0
Punch	0	0	46	0	0	0	2	0	0
Push	0	2	0	44	0	0	0	2	0
Rub	0	0	0	2	44	0	0	2	0
Scratch	0	0	0	0	0	46	0	0	2
Slap	2	0	2	0	0	0	44	0	0
Stroke	0	0	0	4	0	0	0	44	0
Tickle	0	0	0	0	0	2	0	0	46

TABLE 9.6. Confusion matrix for multiple touch action classification (Training: NAO in stationary. Evaluation: NAO in motion).

the NAO. The standardized SVM results placed the Hjorth-parameter based features with the highest accuracy, at 96.75% with the adapted Naya, Silvera-Tawil, and Koo features following with 67.3%, 56.2% and 53.6% respectively. The proposed features also demonstrated strong regularity across different learning methods. This strong regularity resulted in the proposed features outperforming other methods across the specified classifiers. Table 9.8 illustrates the results of the comparison between my proposed touch discriminating methods and the state-of-the-art methods.

Touch Modality	Clustering Accuracy
Single Touch stationary-stationary	81.83%
Single Touch moving-moving	78.91%
Single Touch stationary-moving	77.55%
Multiple Touch stationary-moving	80.10%

TABLE 9.7. Single and multiple touch modality categorization results using EM and the proposed tactile descriptors. Single touch stationary-stationary: EM was trained with unlabelled touch data from the back of the NAO (NAO was in stationary position) and evaluated with the test set obtained from the front of the NAO (NAO was in stationary position). Single touch-moving-moving: EM was trained and tested with touch data collected from back and front of the NAO respectively (in both case NAO was in motion). Single touch-stationary-moving: EM was trained and tested with touch data collected from back (NAO was in stationary position) and front of the NAO respectively (NAO was in motion). Multiple touch-stationary-moving: EM was trained with single touch data collected from the back of the NAO (NAO was in stationary position) and evaluated with multiple touch actions from front of the NAO (NAO was in motion)

9.6. Summary and discussion

This chapter addresses the problem of humanoid touch modality classification through the use of multi-modal tactile sensing and new feature descriptors. The results obtained from several experimental setups demonstrate the robustness of the feature descriptors. In the single action stationary case, the NAO was trained with actions applied to its backside and tested on actions performed on the front. The resultant high recognition rate shows the invariance of the features to the location of contact. It was extended in the multiple-touch case where actions were performed simultaneously to one another on alternate sides of the NAO. These actions comprised a test set which was evaluated on a classifier trained exclusively on the data from single touch case. The high level of discrimination demonstrates the ability for the humanoid to recognize both single and multi-touch actions. Evaluating on a test set comprised of subjects the NAO had not previously interacted with resulted in high classification accuracy illustrates invariance to the particular person performing the action. Finally, testing on data collected which the NAO was in motion, showed that performance was not affected.

To compare my method with the existing approaches, those that addressed the problem of touch modality classification were adapted to be compatible with my system. The comparison results show that my system, across multiple learning methods, for single touch classification, substantially outperforms the adapted approaches. Existing methods, such as Koo and Silvera-Tawil, commonly use a high spatial resolution sensor. The artificial skin used in my method, however, has a comparatively low spatial resolution. This reduction in tactile information should result in a decreased classification accuracy. However, this was compensated by the proposed feature descriptors. It is due to the features extracting key information from the raw signals without requiring further dimensionally reduction or feature selection.

Study	Features	Classifier (% correctly classified)			
		K-NN	Decision Tree	Logitboost	SVM
Adapted Naya	<ol style="list-style-type: none"> 1. Max total intensity 2. Max contact area 3. Temporal difference of total intensity at peak 4. Temporal difference of contact area at peak 	60.4 %	—	—	67.3%
Adapted Silvera	<ol style="list-style-type: none"> 1. Max intensity 2. Spatial resolution 3. Mean intensity 4. Contact time 5. Rate of change 	—	—	59.4%	56.2%
Adapted Koo	<ol style="list-style-type: none"> 1. Total Force 2. Contact time 3. Contact area change 	—	58.1%	—	53.6%
My Proposed Features	<ol style="list-style-type: none"> 1. Activity 2. Mobilty 3. Complexity 4. Linear Correlation 5. Non-linear Correlation 	95.1 %	96.8 %	94.4%	96.75%

TABLE 9.8. Comparison with the adapted existing touch classification approaches

An important advantage of the features is the built-in dynamic cell selection. By thresholding the proximity data to detect contact, only those cells being directly interacted with contributing towards the feature vector. The key result of this inclusion is the decrease in computational cost, as only those datastreams directly associated with the action are processed. It is especially significant when a lot of cells are used, such as if a full-size humanoid was to be covered. Furthermore, because only the in-contact cells are included in the features, actions of differing duration can be directly compared. Finally, the proximity thresholding also makes it trivial to differentiate between periods of contact and no-contact, simply by examining if any cells are being interacted with or not.

CHAPTER 10

Conclusion and future study

10.1. Conclusion

Our sense of touch is not only a passive receiver of tactile information but actively selects and refines sensations according to the current goals and perceptions. Our fingers, hands, and bodies are not external from the world, but direct actions within it to access the information that we humans need. Hence, tactile sensation, exploration, and perception, action, and learning cannot be considered simply as a forward process, but instead form a closed “active exploration and perception, action, and learning” loop. For cognitive robots that interact with dynamic environments, it is crucial to actively and efficiently perceive their surroundings and learn about objects via their physical properties (such as surface texture, stiffness, a center of mass, and thermal conductivity).

In this thesis, I tackled several challenges in active tactile object perception and learning in robotics; following exploration and perception, action, and learning loop. In this regard, I enabled the robotic systems to explore the unknown workspace actively. I proposed two novel probabilistic active workspace exploration methods; (I) an active pre-touch and (II) an active touch strategies. Using my proposed active pre-touch strategy, the robotic system autonomously and efficiently explored the unknown workspace and successfully determined the number of objects and estimated their location and their orientation. The experimental results show that the robot with the active pre-touch strategy obtained a maximum entropy reduction of 30% and 70% compared to uniform and random respectively, and also achieved a better estimation of the objects’ poses.

Taking advantage of my proposed active touch-based workspace exploration, the robot autonomously explored the unknown workspace from different directions and efficiently captured tactile point clouds, by strategically selecting the position to explore. By clustering the

constructed tactile point clouds, the robot successfully estimated the location, orientation, and geometric center of each object. Following the proposed active touch method, the robot reduced the uncertainty of the workspace up to 65% and 70% compared to uniform and random strategies respectively.

For the robotic system equipped with the sense of touch, the perception of the textural property of objects and determination of their center of mass in comparison with the perception of other objects' properties (such as thermal conductivity and stiffness) is more complicated and challenging. In this thesis, I tackled these problems in tactile perception. I proposed novel methods to enable the robotic systems to robustly perceive the textural properties of objects and explore and determine their center of mass.

I proposed a set of robust tactile descriptors to the robotic systems to enable them to sense the textural properties of objects by extracting robust tactile information while sliding their sensitive fingers or hands on the surface of the objects. The performance of the tactile descriptors was assessed with a broad range of materials, in-hand and large objects with periodic and non-periodic structural surfaces. The proposed robust tactile descriptors are shown to be robust across varying conditions. They are robust regardless of the position and orientation of objects in an unknown workspace, textural properties of objects and materials (periodic and non-periodic surface texture), and duration of sliding exploratory actions. I further evaluated the robustness of my tactile descriptors with multiple robotic systems equipped with large numbers of tactile sensors having various technologies, such as dynamic pressure sensors, accelerometers, capacitive sensors, and impedance electrode arrays. Using the proposed descriptors while executing human-like exploratory movements, the Shadow Hand classified 120 materials (100% accuracy) and 30 in-hand objects (98% accuracy) via their textural properties. Using the same methods, NAO identified 120 large objects with 90% accuracy, regardless of their weight.

For the first time, in this thesis, I proposed the strategy to explore the center of mass (CoM) of rigid objects. I formulated the CoM property as a constant feature of the object, which is not susceptible to the external properties of the object. Using my proposed approach the robot autonomously lifted objects from their different positions and then accurately determined their center of mass.

In order to close the exploration, perception, action and learning loop, in my study, I have designed a novel active tactile learning method as well as a new active object discrimination algorithm. I enabled the robotic systems to autonomously and efficiently learn about objects via their physical properties such as surface texture, a center of mass, stiffness, and thermal conductivity and then to discriminate among objects through their properties or search for the

targets objects.

Using my proposed active touch learning method, the robotic systems efficiently learned about objects based on their physical properties by selecting the next object to explore and the next physical property to learn. Then, the robot efficiently constructed reliable prior observation models of objects with a few number of training samples.

The performance of the active touch learning method was evaluated experimentally. The active touch learning provided high recognition accuracy with low number of training samples, reaching 50% fewer samples than the uniform and random learning strategy as baselines methods.

By taking advantage of the prior knowledge acquired previously and my proposed active discrimination algorithm, the robot successfully discriminated among objects via their physical properties. The robot took up to 15% fewer decision steps compared to the random method to achieve the same discrimination accuracy while using either my proposed method (CMUM) or the entropy reduction rate (EER) action selection strategy. However, taking advantage of my proposed CMUM action selection method, the robot achieved up to 10% higher decision accuracy in comparison with the EER.

Besides, to search for a target object, the robot reduced the decision steps up to 24% to find the target objects by following either the proposed CMUM method or the EER method, compared to the random method, whereas using the CMUM method, the robot reached 14% higher decision accuracy than EER to find the target object.

Furthermore, for the first time in this thesis, I introduced an online tactile transfer learning method to enable robotic systems to re-uses their past tactile experience while learning about new objects via their textural properties. I extended my online tactile transfer learning to enable robots with multi-modal artificial skin to actively leverage the prior tactile knowledge to learn new objects in the unknown workspace via multiple tactile properties named as active tactile transfer learning (ATTL).

Employing my proposed ATTL algorithm, the robot automatically leveraged the most relevant and informative prior tactile knowledge to learn about new unknown objects via their surface texture, stiffness, and thermal conductivity properties, with one or a few training samples with very high discrimination accuracy. The robot with the ATTL method achieved 72% discrimination accuracy with only one training sample plus 10 prior tactile knowledge (one-shot tactile learning). Moreover, it efficiently discriminated among new objects with 20% higher discrimination accuracy compared to uniform learning method.

So far, I have proposed several methods for active workspace exploration, tactile object perception and learning. In this thesis, I additionally proposed a novel tactile-based framework

to enable the robotic systems to manipulate target objects safely. My framework consists of a tangential-force based slip detection method to correct slip and a deformation prevention approach to regulating grasping force, which adjusts the relative positions of fingers in real time, and is realized by estimating the weight of the grasped object.

Approaches proposed in this work have several advantages over prior work. The method used in this study can be executed online and does not require any prior knowledge of the contact surface (e.g., friction coefficient). Since my proposed approach does not rely on frequency analysis, it is not susceptible to the vibration signals generated by the robotic system during manipulation, and also robust to external disturbances. Also, my proposed framework can control multiple-fingers of the gripper individually in real time and is independent of the properties of the grasped object, such as stiffness, surface texture, and center of mass.

For robotic system interacting with the environment and working closely with humans, evaluation and classification touch modalities are vital. Humanoids should understand, just as humans do, that a slap is a form of negative feedback, which a pat is one of encouragement. Through tactile interaction between humans and robots, various touch modalities might carry out, and each action is a representative of a separate communicative intent.

In this regard, I presented a novel approach for touch modality identification during the tactile human-robot interaction. By taking advantage of my proposed approach humanoids can distinguish between different touch modalities that are enacted on their sensitive body. My proposed features are demonstrated to be invariant to the location of contact and capable of processing single and multi-touch actions. To provide a comparison of my method, existing approaches were evaluated. The experimental results show that the humanoid can distinguish different single touch modalities with a recognition rate of 96.79% while using the proposed feature descriptors and SVM classifier. Furthermore, it can recognize multiple touch actions with 93.03% recognition rate.

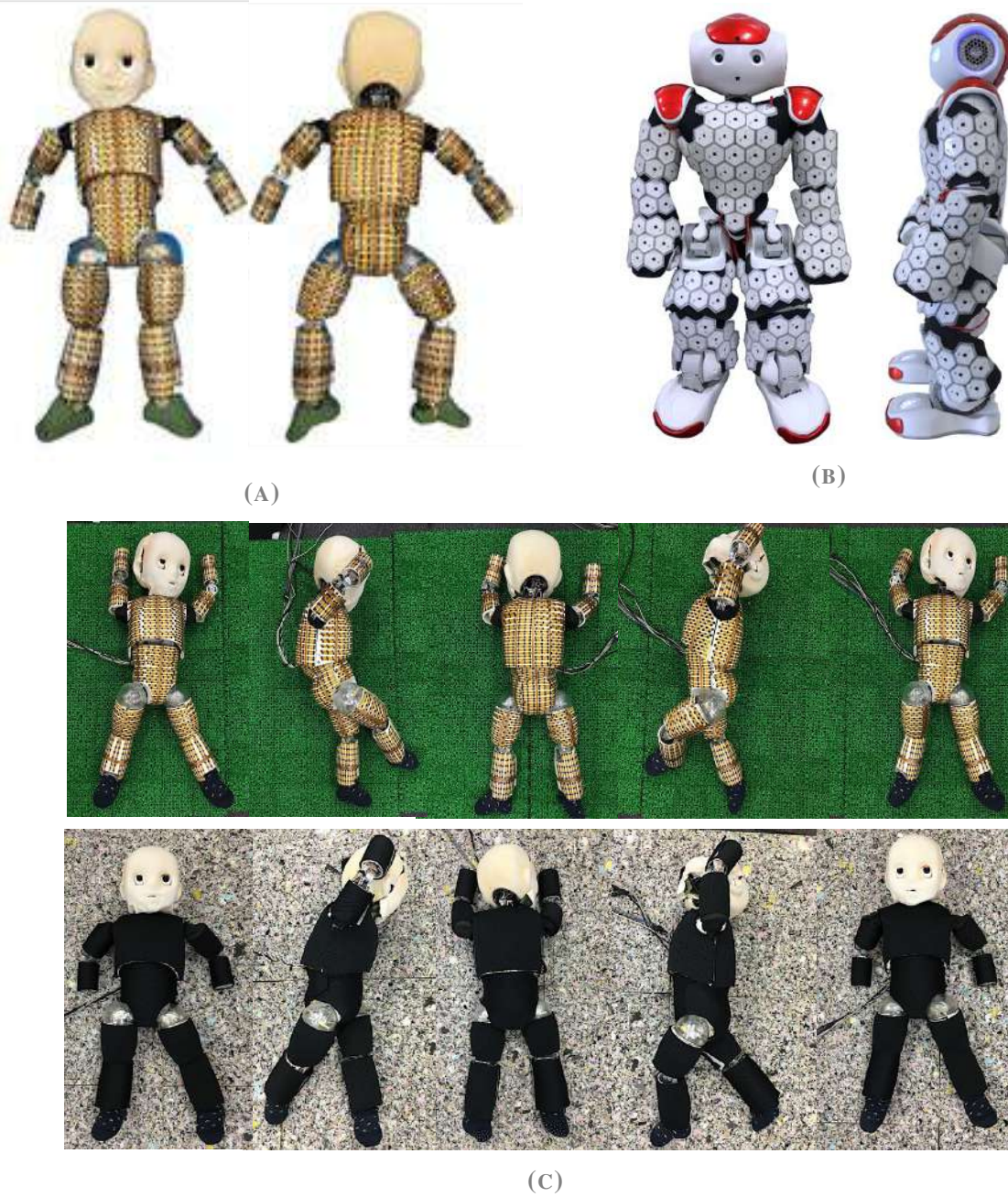


FIGURE 10.1. (A) shows the Noby robot (nine-month-old baby robot) which has built at the Intelligent System and Informatics lab (IS), the University of Tokyo directed by Prof. Yasuo Kuniyoshi. I have covered the whole body of Noby with 4000 foldable tactile sensors. (B) shows the NAO with the whole body multimodal skin cells. I have covered the NAO with robotic skin at the Institute for Cognitive System(ICS), Technical university of Munich directed by Prof. Gordon Cheng. (C) Illustrates that the Noby explores the floor with whole body to perceive the textural properties.

10.2. Future study

In the future, I would like to assess my proposed active tactile object perception and learning methods with humanoids having whole body tactile skin. In this regard, I have covered the whole body of a baby robot called Noby with 4000 tactile sensors (see Fig. 10.1-A). Moreover, I have covered the entire body of NAO with 250 multimodal skin cells (see Fig. 10.1-B). By taking advantage of my proposed active pre-touch exploration strategy the NAO with whole body proximity sensing (pre-touch) can autonomously explore workspace to find the objects and to estimate their poses (especially in case of a poor lighting condition). Using my proposed active touch learning method NAO can efficiently learn about objects via their physical properties. By taking benefit of my touch-based workspace exploration and active object discrimination methods the Noby will be able to explore the environment and discriminate among objects therein, solely based on touch information (see Fig. 10.1-C).

By employing my proposed active tactile transfer learning method, both humanoids can re-use their obtained tactile experiment while exploring the environment to learn about new objects with fewer trials or samples.

Moreover, in my future study, I will try to extend my proposed tactile transfer learning method to transfer tactile knowledge from one robotic platform (e.g., Noby) to another one (e.g., NAO) having with different sensing modalities.

Finally, I will extend my proposed strategies for in-hand object manipulation to whole body large object manipulation. Taking advantage of my proposed method NAO with whole body skin can grasp, carry, and manipulate deformable large objects with dynamic center of mass safely.

APPENDIX A

Uniform Pre-touch Strategy for Workspace Exploration

A.1. Workspace Definition

The workspace W_{XYZ} is defined as a discretized 3D grid bounded by the reaching capabilities of the robot (see Fig. A.1), where $X \in \{X_1, \dots, X_K\}$, $Y \in \{Y_1, \dots, Y_N\}$, $Z \in \{Z_1, \dots, Z_M\}$ and $K \times N \times M$ are length, width, and height respectively. The artificial skin of the robot has an array of N_c proximity sensors with known locations $l_{1:N_c}^n$ with respect to the end-effector position l^n at each observation n . The sensor array outputs a set of measurements $z_{1:N_c}^n$. I define $p(W_{XYZ}^n)$ as the probability of the presence of an object in every cell of the workspace at the n^{th} observation. The initial $p(W_{XYZ}^0)$ is a uniform distribution that will be updated using the new measurements. I assume that the robot's end-effector is horizontal to the X-Y plane of the workspace.

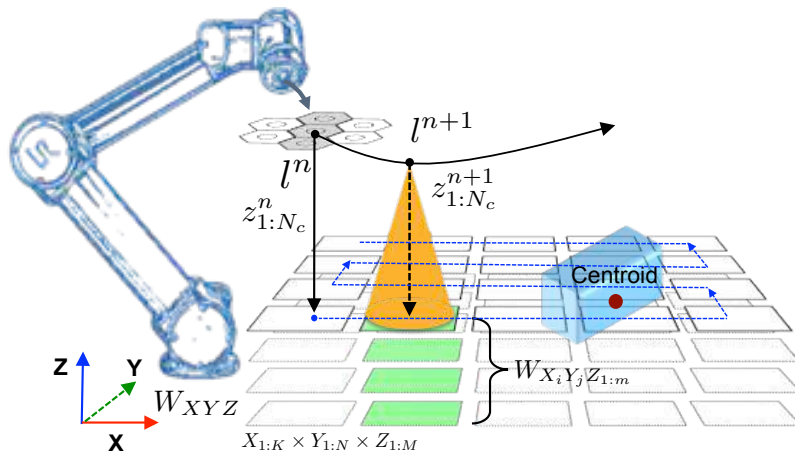


FIGURE A.1. An illustration of an unknown workspace exploration.

Algorithm A.1 Uniform strategy for workspace exploration

Input : $W_{XYZ}, l_{\text{init}}, \eta = 1$ ▷ Workspace definition, end-effector initial location.
Output: $\mathcal{L} = \{l_m\}_{m=1}^M$ ▷ Number of objects in the workspace (N) and their locations \mathcal{L} .
initialization: $p(W_{XYZ})$ ▷ Prior distribution of objects.
initialization: $moveTo(l_{\text{init}})$ ▷ move to initial position

Tactile-based unknown workspace exploration

for $n = 1 : N$ **do**

for $k = 1 : K$ **do**

$z_{1:N_c} \leftarrow moveTo(l^n)$ ▷ Robot moves to the position corresponds to the grid $W_{X_k Y_n}$
and collect observations
 $p(d^n | z^n, l^n) \leftarrow distanceEstimation(z_{1:N_c}, l^n)$
 $p(W_{XYZ}^n) \leftarrow p(W_{XYZ}^{n-1} | z_{1:N_c}, l^n)$ ▷ Update object distribution

end

end

$c_{1:M}, l_{1:M} \leftarrow localization(p(W_{XYZ}))$ ▷ Clustering and object localization

A.2. Methodology

First, the robot starts the exploration from a fixed location corresponding to a grid edge $W_{X_1 Y_1}$. Then, it moves to an adjacent location of the grid following the land-mower pattern (see Fig. A.1). In other words, the end-effector moves along X axis from $W_{X_1 Y_1}$ to $W_{X_2 Y_1}$ and continues until it reaches $W_{X_K Y_1}$. Then it moves one step along Y axis from $W_{X_K Y_1}$ to $W_{X_K Y_2}$ and continues until it arrives to $W_{X_1 Y_2}$. This process will be iteratively executed until the robot covers the entire workspace. At every location of the end-effector l^n the robot acquires sensor measurements $z_{1:N_c}^n$. With that information $p(W_{XYZ}^n)$ will be updated using Bayesian filtering. In order to fuse the measurements taken from all sensors of the array I assume that their readings are independent of each other. Therefore, the joint probability distribution is given by:

$$p(W_{XYZ}^n | z_{1:N_c}^{1:n}, l^{1:n}) \propto \prod_{i=1}^{N_c} p(z_i^n | l^n, W_{XYZ}^n) p(W_{XYZ}^{n-1} | z^{1:n-1}, l^{1:n-1}) \quad (\text{A.1})$$

By constraining the end-effector movement on the X-Y plane, I compute $p(z_i^n | l^n, W_{XYZ}^n)$ using the estimated distance d^n from the skin cells to the object. Then, I can compute $p(z_i^n | l^n, W_{XYZ_{1:m}}^n)$ as $p(z_i^n | l^n, d^n)$, where $Z_{1:m}$ are the cells below l^n (m is the number of cells in Z direction, the orange colored cells in Fig. A.1). $p(z_i^n | l^n, d^n)$ is the likelihood of having measurement z_i^n given that the object is at distance d^n and the end-effector is at l^n .

APPENDIX B

Gaussian Process

Here, I briefly introduce the Gaussian Process (GP) method [156] that has been used in this work. GP is a supervised learning method which describes the functional mapping $\mathbf{g} : \mathcal{X} \mapsto \mathcal{Y}$ between the input data set \mathcal{X} and the output data set \mathcal{Y} . The GP model is non-parametric and can be completely determined by its mean function $\mu(\mathbf{x})$ and covariance function $k(\mathbf{x}, \mathbf{x}')$:

$$\mu(\mathbf{x}) = \mathbb{E}[\mathbf{g}(\mathbf{x})], \quad (\text{B.1})$$

$$k(\mathbf{x}, \mathbf{x}') = \mathbb{E}[(\mathbf{g}(\mathbf{x}) - \mu(\mathbf{x}))(\mathbf{g}(\mathbf{x}') - \mu(\mathbf{x}'))]. \quad (\text{B.2})$$

The distribution of \mathbf{g} can be denoted as:

$$\mathbf{g}(\mathbf{x}) \sim \mathcal{GP}(\mu(\mathbf{x}), k(\mathbf{x}, \mathbf{x}')). \quad (\text{B.3})$$

In a regression task, GP is exploited to approximate the functional relation \mathbf{g} , in order to predict the output $\mathbf{y} = \mathbf{g}(\mathbf{x})$ given a test input \mathbf{x} . I explain the application of GP in exploration task through the example introduced in Sec. 5.3.1.

For the exploration of \mathbb{W}_{d_4} , all points that trajectory \mathbf{t}_n passes through have the same x_n and z_n coordinate, and \mathbf{p}_n^{obs} returns the y_n coordinate, i.e. the depth of the object surface from the start point \mathbf{p}_n^{start} in this direction.

I considered the single training input of the GPR model \mathbf{g}_{d_4} , $\mathbf{p}_n^{in} = (x_n, z_n)$, $\mathbf{p}_n^{in} \in \mathcal{X}_{d_4}$, $\mathcal{X}_{d_4} \subseteq \mathbb{R}^2$, $n \in \mathbb{N}$, and the corresponding training label (output) $\mathbf{p}_n^{out} = (y_n)$, $\mathbf{p}_n^{out} \in \mathcal{Y}_{d_4}$, $\mathcal{Y}_{d_4} \subseteq \mathbb{R}$, $n \in \mathbb{N}$, with (x_n, y_n, z_n) being the coordinates of the observed point \mathbf{p}_n^{obs} of the trajectory \mathbf{t}_n .

The entire training dataset of \mathbf{g}_{d_i} is denoted as $\Omega_{d_i} = \{\mathcal{X}_{d_i}, \mathcal{Y}_{d_i}\}$. Represent the universal set of the 2D coordinate \mathbf{p}_n all over the corresponding start plane as \mathbb{X}_{d_i} ; and $\mathbf{p}_n = (y_n, z_n)$ for $i = 1, 3$, whereas $\mathbf{p}_n = (x_n, z_n)$ for $i = 2, 4$.

Given N pairs of training data $\{\mathcal{X}_{d_4}, \mathcal{Y}_{d_4}\} = \{\mathbf{p}_n^{in}, \mathbf{p}_n^{out}\}_{n=1:N}$, the predicted distribution of target function $\mathbf{g}_{d_4}(\mathbf{p})$, $\mathbf{p} \in \mathbb{X}_{d_4}$ is denoted as $\hat{\mathbf{g}}_{d_4}(\mathbf{p}) \sim \mathcal{GP}(\hat{\mu}(\mathbf{p}), \hat{v}(\mathbf{p}))$, and the corresponding mean function and variance function are calculated as:

$$\hat{\mu}(\mathbf{p}) = \tilde{\mathbf{k}}^T (\mathbf{K} + \sigma_n^2 \mathbf{I})^{-1} \mathbf{y}, \quad (\text{B.4})$$

$$\hat{v}(\mathbf{p}) = k(\mathbf{p}, \mathbf{p}) - \tilde{\mathbf{k}}^T (\mathbf{K} + \sigma_n^2 \mathbf{I})^{-1} \tilde{\mathbf{k}}. \quad (\text{B.5})$$

where $k : \mathcal{X} \times \mathcal{X} \mapsto \mathbb{R}$ is the covariance function, $\tilde{\mathbf{k}}$ is the covariance vector with its n^{th} element indicating the covariance between the test input \mathbf{p} and the n^{th} training data point \mathbf{p}_n^{out} , and $\mathbf{y} \in \mathbb{R}^N$ is a vector of training outputs \mathbf{p}_n^{out} . The $(i, j)^{th}$ entry of the matrix \mathbf{K} represents the covariance between i^{th} and j^{th} training inputs, i.e. $K_{i,j} = k(\mathbf{p}_i^{in}, \mathbf{p}_j^{in})$.

The predicted target $\hat{\mathbf{p}}^{out}$ for the test input $\hat{\mathbf{p}}^{in}$ subjects to the Gaussian distribution: $\hat{\mathbf{p}}^{out} \sim \mathcal{N}(\hat{\mu}(\hat{\mathbf{p}}^{in}), \mathbf{K} + \sigma_n^2 \mathbf{I})$, and the probability of predicted $\hat{\mathbf{p}}^{out}$ is denoted as $p(\hat{\mathbf{p}}^{out})$.

In this work, I used the radial basis function (RBF) as the covariance function:

$$k(\mathbf{a}, \mathbf{b}) = \sigma_f^2 \exp\left(-\frac{(\mathbf{a} - \mathbf{b})^2}{2l^2}\right) + \sigma_n^2 \delta_{ab}, \quad (\text{B.6})$$

the hyper-parameters σ_f , σ_n , and l are selected through cross-validation.

APPENDIX C

Normalized Mutual Information method (NMI)

The Normalized Mutual Information method (NMI) that was proposed in [153] was used to measure the quality of the clustering results. To do this, consider $A = \{a_1, \dots, a_K\}$ and $B = \{b_1, \dots, a_S\}$ be two different partitions of the N data samples, i.e., two different clusterings. For instance, A might be the estimated clustering (predicted labels) and B is reference clustering derived from the class labels (true labels). Now, let assume $p_{AB}(i, j) = |a_i \cap b_j|/N$ is the probability that a randomly selected object or material belongs to cluster a_i in A and b_j in B . Moreover, consider $p_A(i) = |a_i|/N$ to be the probability that a randomly selected object/material belongs to category a_i in A ; Similarly let define $p_B(j) = |b_j|/N$ for object b_j in B . The mutual information between cluster A and B can be written as:

$$\mathbb{I}(A, B) = \sum_{i=1}^K \sum_{j=1}^S p_{AB}(i, j) \log(p_{AB}(i, j)/p_A(i)p_B(j)) . \quad (\text{C.1})$$

$\mathbb{I}(A, B)$ lies between 0 and $\min\{H(A), H(B)\}$ in which $H(A)$ and $H(B)$ are entropy of A and B respectively. The normalized mutual information (NMI) is defined as:

$$NMI(A, B) = \frac{\mathbb{I}(A, B)}{(H(A) + H(B))/2} . \quad (\text{C.2})$$

$NMI(A, B) \in [0, 1]$, $NMI(A, B) = 0$ means no mutual information and $NMI(A, B) = 1$ means perfect correlation.

Bibliography

- [1] A. Naya, J. Yamato, and K. Shinozawa. Recognizing human touching behaviors using a haptic interface for a pet-robot touching behaviors and experiment. *IEEE International Conference on Systems and Cybernetics*, pages 3–7, 1999. (Cited on pages xx, 28, 29, 188, and 189.)
- [2] A. S. Tawil, V. Rye, and M. Velonaki. Interpretation of the modality of touch on an artificial arm covered with an eit-based sensitive skin. *The International Journal of Robotics Research*, 31:1627–1641, 2012. (Cited on pages xx, 28, 29, 188, and 189.)
- [3] S. Y. Koo, J. G. Lim, and D. S. Kwondo. Online touch behavior recognition of hard-cover robot using temporal decision tree classifier. *IEEE International Symposium on Robot and Human Interactive Communication*,, pages 425—429, 2008. (Cited on pages xx, 28, 29, 188, and 190.)
- [4] C. G. Nunez, W. T. Navaraj, E. O. Polat, and R. Dahiya. Energy-autonomous, flexible, and transparent tactile skin. *Advanced Functional Materials*, 27(18), 2017. (Cited on pages xxi, 11, and 12.)
- [5] B. Heyneman and M. R. Cutkosky. Slip classification for dynamic tactile array sensors. *International Journal of Robotics Researhc*, 35:404–421, 2016. (Cited on pages xxi, 11, and 12.)
- [6] H. Kawasaki, T. Komatsu, K. Uchiyama, and T. Kurimoto. Dexterous anthropomorphic robot hand with distributed tactile sensor: Gifu hand ii. *Systems, Man, and Cybernetics, 1999. IEEE SMC '99 Conference Proceedings. 1999 IEEE International Conference on*, 2:782–787, 1999. (Cited on pages xxi, 11, and 12.)
- [7] Y. Ohmura, Y. Kuniyosh, and A. Nagakubo. Conformable and scalable tactile sensor skin for curved surfaces,. *IEEE International Conference on Robotics and Automation*, pages 1348–1353, 2006. (Cited on pages xxi, 11, and 13.)

- [8] T. Mukai, S. Hirano, and Y. Kato. *Fast and accurate tactile sensor system for a human-interactive robot*. INTECH Open Access Publisher, 2008. (Cited on pages xxi, 11, 13, and 28.)
- [9] Karla Stépánová, Matej Hoffmann, Zdenek Straka, Frederico B. Klein, Angelo Cangelosi, and Michal Vavrecka. Where is my forearm? clustering of body parts from simultaneous tactile and linguistic input using sequential mapping. *CoRR*, abs/1706.02490, 2017. (Cited on pages xxi and 13.)
- [10] N. Jamali and C. Sammut. Majority voting: Material classification by tactile sensing using surface texture. *IEEE Transactions on Robotics*, pages 508–521, 2011. (Cited on pages xxi, 14, 17, and 33.)
- [11] D. Xu, G. E. Loeb, and A. J. Fishel. Tactile identification of objects using bayesian exploration. *IEEE International Conference on Robotics and Automation*, pages 3056–3061, 2013. (Cited on pages xxi, 14, 15, 17, and 33.)
- [12] A. J. Fishel and G. E. Loeb. Bayesian exploration for intelligent identification of textures. *Frontiers in Neurorobotics*, Vol.6, 2012. (Cited on pages xxi, 14, 15, 33, and 107.)
- [13] Jivko Sinapov, Vladimir Sukhoy, Ritika Sahai, and Alexander Stoytchev. Vibrotactile recognition and categorization of surfaces by a humanoid robot. *IEEE Transactions on Robotics*, Vol.27(No.3):488–497, 2011. (Cited on pages xxi, 15, 16, 17, and 19.)
- [14] V. Chu, I. McMahon, L. Riano, C. G. McDonald, Q. He, et al. Robotic learning of haptic adjectives through physical interaction. *Robotics and Autonomous Systems*, 63:279–292, 2015. (Cited on pages xxi and 16.)
- [15] H. Soh, Y. Su, and Y. Demiris. Online spatio-temporal gaussian process experts with application to tactile classification. *IEEE International Conference on Intelligent Robots and Systems*, pages 4489–4496, 2012. (Cited on pages xxi, 15, and 16.)
- [16] Daisuke Tanaka, Takamitsu Matsubara, Kentaro Ichien, and Kenji Sugimoto. Object manifold learning with action features for active tactile object recognition. *IEEE International Conference on Intelligent Robots and Systems (ICRA)*, pages 608–614, 2014. (Cited on pages xxi, 19, 20, and 21.)
- [17] H. P. Saal, J. A. Ting, and S. Vijayakumar. Active sequential learning with tactile feedback. *AISTATS*, pages 677–684, 2010. (Cited on pages xxi and 19.)

- [18] N. Jamali, C. Ciliberto, L. Rosasco, and L. Natale. Active perception: Building objects models using tactile exploration. *IEEE International Conference on Humanoid Robots*, 2016. (Cited on pages xxi, 12, 19, and 92.)
- [19] Z. Su and et al. Force estimation and slip detection/classification for grip control using a biomimetic tactile sensor. *IEEE International Conference on Humanoid Robots*, pages 297–303, 2015. (Cited on pages xxii, 25, and 26.)
- [20] M. Stachowsky, T. Hummel, M. Moussa, and H. Abdullah. A slip detection and correction strategy for precision robot grasping. *IEEE ASME Transactions on Mechatronics*, PP(99):1–1, 2016. (Cited on pages xxii, 25, and 26.)
- [21] F. Veiga, H. van Hoof, J. Peters, and T. Hermans. Stabilizing novel objects by learning to predict tactile slip. *International Conference on Intelligent Robots and Systems (IROS)*, pages 5065–5072, 2015. (Cited on pages xxii, 25, and 26.)
- [22] Z. Su, J. Fishel, T. Yamamoto, and G. Loeb. Use of tactile feedback to control exploratory movements to characterize object compliance. *Frontiers in Neurorobotics*, 6(7):51, 2012. (Cited on pages xxii, 38, and 45.)
- [23] G. Westling and R. S. Johansson. Factors influencing the force control during precision grip. *Experimental Brain Research*, 53:277–284, 1984. (Cited on page 1.)
- [24] Susan.J Lederman and Roberta.L Klatzky. Hand movements: A window into haptic object recognition. *Cognitive psychology*, 19(3):342–368, 1987. (Cited on page 1.)
- [25] G. Robles-De-La-Torre. The importance of the sense of touch in virtual and real environments. *IEEE MultiMedia*, pages 24–30, 2006. (Cited on page 2.)
- [26] R. S. Dahiya, G. Metta, M. Valle, and G. Sandini. Tactile sensing—from humans to humanoids. *IEEE Transaction on Robotic*, 26(1):1–20, 2010. (Cited on pages 2, 11, 25, 27, and 181.)
- [27] M. Kaltenbrunner, T. Sekitani, J. Reeder, T. Yokota, K. Kuribara, et al. An ultra-lightweight design for imperceptible plastic electronics. *Nature*, Vol. 499:455–463, 2013. (Cited on page 11.)
- [28] M. W. Strohmayer, H. Worn, and G. Hirzinger. The dlr artificial skin parti: Uniting sensitivity and robustness. *IEEE International Conference on Robotics and Automation*, pages 1012–1018, 2013. (Cited on page 11.)

- [29] Sophon Somlor, Richard Sahala Hartanto, Alexander Schmitz, and Shigeki Sugano. A novel tri-axial capacitive-type skin sensor. *Advanced Robotics*, 29(21):1375–1391, 2015. (Cited on page 11.)
- [30] A. Schmitz, P. Maiolino, and et.al. Methods and technologies for the implementation of large-scale robot tactile sensors. *IEEE Trans. on Robotica*, 27(3):389–400, Jun 2011. (Cited on page 11.)
- [31] J. Ulmen and M. Cutkosky. A robust, low-cost and low-noise artificial skin for human-friendly robots. *IEEE International Conference on Robotics and Automation*, pages 4836–4841, 2010. (Cited on page 11.)
- [32] H. Xie, H. Liu, S. Luo, L. D. Seneviratne, and K. Althoefer. Fiber optics tactile array probe for tissue palpation during minimally invasive surgery. *IEEE International Conference on Intelligent Robots and Systems*, pages 2539–2544, 2013. (Cited on page 11.)
- [33] R. S. Dahiya, G. Metta, M. Valle, A. Adami, and L. Lorenzelli. Piezoelectric oxide semiconductor field effect transistor touch sensing devices. *Applied Physics Letter*, 95:034105, 2009. (Cited on page 11.)
- [34] T. V. Papakostas, J. Lima, and M. Lowe. A large area force sensor for smart skin applications. *IEEE Sensors*, 5(1620–1624), 2002. (Cited on page 11.)
- [35] D. Hughes and N. Correll. Texture ecognition and localization in amorphous robotic skin. *Bioinspiration and Biomimetics*, 10:055002, 2015. (Cited on page 11.)
- [36] S. Denei, P. Maiolino, E. Baglini, and G. Cannata. On the development of a tactile sensor for fabric manipulation and classification for industrial applications. *IEEE International Conference on Intelligent Robots and Systems*, pages 5081–5086, 2015. (Cited on page 11.)
- [37] S. Khan, S. Tinku, L. Lorenzelli, and R. S. Dahiya. Flexible tactile sensors using screen-printed p(vdf-trfe) and mwcnt/pdms composites. *IEEE Sensors Journal*, 15(6):3146–3155, 2015. (Cited on page 11.)
- [38] S. Stassi, V. Cauda, G. Canavese, and C. F. Pirri. Flexible tactile sensing based on piezoresistive composites: A review. *Sensors*, 14(3):5296–5332, 2014. (Cited on page 11.)

- [39] N. Yogeswaran, W. Dang, W.T. Navaraj, and et al. New materials and advances in making electronic skin for interactive robots. *Advanced Robotics*, 29(21):1359–1373, 2015. (Cited on page 11.)
- [40] A. R. Nawrocki, N. Matsuhisa, T. Yokota, and T. Someya. 300-nm imperceptible, ultraflexible, and biocompatible e-skin fit with tactile sensors and organic transistors. *Advanced Electronic Materials*, 2:n/a–n/a, 2016. (Cited on page 11.)
- [41] S. Lee, A. Reuveny, J. Reeder, S. Lee, H. Jin, et al. A transparent bending-insensitive pressure sensor. *Nature Nanotechnology*, 11:472–478, 2016. (Cited on page 11.)
- [42] Y. Jia and J. Tian. Surface patch reconstruction from ‘one-dimensional’ tactile data. *IEEE Transactions on Automation Science and Engineering*, 7:400–407, 2010. (Cited on page 12.)
- [43] H. Liu, X. Song, T. Nanayakkara, L. D. Seneviratne, and K. Althoefer. A computationally fast algorithm for local contact shape and pose classification using a tactile array sensor. *IEEE International Conference on Robotics and Automation (ICRA)*, pages 1410–1415, 2012. (Cited on page 12.)
- [44] H. Liu, J. Greco, X. Song, J. Bimbo, and K. Althoefer. Tactile image based contact shape recognition using neural network. *IEEE International Conference on Multisensor Fusion and Integration for Intelligent Systems (MFI)*, pages 138–143, 2013. (Cited on page 12.)
- [45] M. V. Liarokapis, B. Calli, A. J. Spiers, and A. M. Dollar. Unplanned, model-free, single grasp object classification with underactuated hands and force sensors. *IEEE International Conference on Intelligent Robots and Systems*, pages 5073–5080, 2015. (Cited on page 12.)
- [46] K. C. Nguyen and V. Perdereau. Fingertip force control based on max torque adjustment for dexterous manipulation of an anthropomorphic hand. *2013 IEEE/RSJ International Conference on Intelligent Robots and Systems*, pages 3557–3563, Nov 2013. (Cited on page 12.)
- [47] H. Liu, K. C. Nguyen, V. Perdereau, J. Bimbo, J. Back, M. Godden, L. D. Seneviratne, and K. Althoefer. Finger contact sensing and the application in dexterous hand manipulation. *Autonomous Robots*, pages 25–41, 2015. (Cited on page 12.)

- [48] Z. Yi, R. Calandra, F. Veiga, H. van Hoof, T. Hermans, Y. Zhang, and J. Peters. Active tactile object exploration with gaussian processes. *IEEE International Conference on Intelligent Robots and Systems*, pages 4925–4930, Oct 2016. (Cited on page 12.)
- [49] Z. Yi, R. Calandra, F. Veiga, H. van Hoof, T. Hermans, Y. Zhang, and J. Peters. Active tactile object exploration with gaussian processes. *2016 IEEE International Conference on Intelligent Robots and Systems (IROS)*, pages 4925–4930, 2016. (Cited on page 12.)
- [50] Stanimir Dragiev, Marc Toussaint, and Michael Gienger. Gaussian process implicit surfaces for shape estimation and grasping. *IEEE International Conference on Robotics and Automation*, pages 2845–2850, 2011. (Cited on page 12.)
- [51] S. J. Lederman. The perception of surface roughness by active and passive touch. *Bulletin of the Psychonomic Society*, 18:253–255, 1981. (Cited on pages 12 and 13.)
- [52] T. Bhattacharjee, J. Wade, and C. C. Kemp. Active tactile exploration with uncertainty and travel cost for fast shape estimation of unknown objects. *Proceedings of Robotics: Science and Systems*, pages 297–304, 2015. (Cited on page 12.)
- [53] G. Chirstopher C. Atkeson, C. H. An., and J. M Hollerbach. Rigid body load identification for manipulators. *IEEE Conference on Decision and Control*, pages 996–1002, 1985. (Cited on page 13.)
- [54] Yong Yu, K. Fukuda, and volume=4-pages=2893–2898 year=1999 S. Tsujio, journal=IEEE International Conference on Robotics and Automation. Estimation of mass and center of mass of graspless and shape-unknown object. (Cited on page 13.)
- [55] Y. Yu, T. Kiyokawa, and S. Tsujio. Estimation of mass and center of mass of unknown and graspless cylinder-like object. *International Journal of Information Acquisition*, 1(01):47–55, 2004. (Cited on page 13.)
- [56] Yong Yu, T. Arima, and S. Tsujio. Estimation of object inertia parameters on robot pushing operation. *IEEE International Conference on Robotics and Automation*, pages 1657–1662, 2005. (Cited on page 13.)
- [57] P. Dallaire, P. Giguere, D. Edmond, and B. Chaibdraa. Autonomous tactile perception: A combined improved sensing and bayesian nonparametric approach. *Robotics and Autonomous Systems*, pages 422–435, 2014. (Cited on pages 14 and 17.)

- [58] P.Giguere and G.Dudek. A simple tactile probe for surface identification by mobile robots. *IEEE Transactions on Robotics*, Vo.27(3):534–544, June 2011. (Cited on page 14.)
- [59] D. S. Chaturanga, Z. Wang, V. A. Ho, A. Mitani, and S. Hirai. A biomimetic soft fingertip applicable to haptic feedback systems for texture identification. *IEEE International Symposium on Haptic Audio Visual Environments and Games*, pages 29–33, 2013. (Cited on pages 14 and 17.)
- [60] V. Chu, I. McMahon, L. Riano, C. G. McDonald, Q. He, et al. Using robotic exploratory procedures to learn the meaning of haptic adjectives. *IEEE International Conference on Robotics and Automation*, pages 3048–3055, 2013. (Cited on pages 16 and 17.)
- [61] J. M. Romano and K. J. Kuchenbecker. Methods for robotic tool-mediated haptic surface recognition. *IEEE Haptics Haptics Symposium (HAPTICS)*, pages 49–56, 2014. (Cited on page 16.)
- [62] K. Watanabe, M. Sohgawa, T. Kanashima, M. Okuyama, and H. Norna. Identification of various kinds of papers using multi-axial tactile sensor with micro-cantilevers. *World Hap. Con.*, pages 139–144, April 2013. (Cited on page 16.)
- [63] C. M. Oddo, M. Controzzi, L. Beccai, C. Cipriani, and M.C. Carrozza. Roughness encoding for discrimination of surfaces in artificial active-touch. *IEEE Tran. on Robo.*, Vol.27(No.3):522–533, June 2011. (Cited on page 17.)
- [64] D. Tanaka, T. Matsubara, K. Ichien, and K. Sugimoto. Object manifold learning with action features for active tactile object recognition. *IEEE Int. Conf. on Intelligent Robots and Systems*, pages 516–523, 2014. (Cited on page 17.)
- [65] K. E. Friedl, A. R. Voelker, A. Peer, and C. Eliasmith. Human-inspired neurorobotic system for classifying surface textures by touch. *IEEE Robotics and Automation Letters*, 1:516–523, 2016. (Cited on pages 17 and 19.)
- [66] H. Hu, Y. Han, A. Song, S. Chen, C. Wang, and Z. Wang. A finger-shaped tactile sensor for fabric surfaces evaluation by 2-dimensional active sliding touch. *Sensors*, Vol. 14:4899–4913, 2014. (Cited on pages 18 and 19.)
- [67] A.Song, Y.Han, H.Hu, and J.Li. A novel texture sensor for fabric texture measurement and classification. *IEEE Transactions on Instrumentation and Measurement*, 63(7):1739–1747, 2014. (Cited on pages 18 and 19.)

- [68] W. W. Mayol-Cuevas, J. Juarez-Guerrero, and S. Munoz-Gutierrez. A first approach to tactile texture recognition. *IEEE Int. Conf. on Systems, Man, and Cybernetics*, 5:4246–4250, 1998. (Cited on pages 18 and 19.)
- [69] N. H. H. Mohamad Hanif, P. H. Chappell, A. Cranny, and N. M. White. Surface texture detection with artificial fingers. *37th Annual International Conference of the IEEE Engineering in Medicine and Biology Society*, pages 8018–8021, 2015. (Cited on pages 18 and 19.)
- [70] N. F. Lepora, M. Evans, C. W. Fox, M. E. Diamond, K. Gurney, and T. J. Prescott. Naive Bayes texture classification applied to whisker data from a moving robot. *The International Joint Conference on Neural Networks*, pages 1–8, 2010. (Cited on page 19.)
- [71] Danfei Xu, Gerald E. Loeb, and Jeremy A. Fishel. Tactile identification of objects using Bayesian exploration. *IEEE International Conference on Robotics and Automation*, pages 3056–3061, 2013. (Cited on page 19.)
- [72] Nathan F. Lepora, Uriel Martinez-Hernandez, and Tony J. Prescott. Active touch for robust perception under position uncertainty. *IEEE International Conference on Robotics and Automation*, pages 3020–3025, 2013. (Cited on page 20.)
- [73] Alexander Schneider, Jürgen Sturm, Cyrill Stachniss, Marco Reisert, Hans Burkhardt, and Wolfram Burgard. Object identification with tactile sensors using bag-of-features. *IEEE International Conference on Intelligent Robots and Systems*, pages 243–248, 2009. (Cited on pages 20 and 109.)
- [74] R. Martins, J. F. Ferreira, and J. Dias. Touch attention bayesian models for robotic active haptic exploration of heterogeneous surfaces. *International Conference on Intelligent Robots and Systems*, pages 1208–1215, 2014. (Cited on page 20.)
- [75] H. Saal, J. A. Ting, and S. Vijayakumar. Active sequential learning with tactile feedback. *AISTATS*, pages 677–684, 2010. (Cited on page 20.)
- [76] V. Vapnik. The nature of statistical learning theory. *Springer science and business media*, 2013. (Cited on page 22.)
- [77] C.C. Aggarwal. Data classification algorithms and applications. *CRC Press*, 2014. (Cited on page 22.)

- [78] S. J. Pan and A. Q. Yang. Survey on transfer learning. *IEEE Transactions on Knowledge and Data Engineering*, pages 1345–1359, 2010. (Cited on pages 22, 23, and 24.)
- [79] Y. Aytar and A. Zisserman. Enhancing exemplar svms using part level transfer regularization. *British Machine Vision Conference (BMVC)*, 2012. (Cited on pages 22 and 23.)
- [80] T. Tommasi, F. Orabona, M. Kaboli, and B. Caputo. Leveraging over prior knowledge for online learning of visual categories. *British Machine Vision Conference (BMVC)*, 2012. (Cited on pages 23, 130, 131, and 133.)
- [81] Y. Zhang and D. Y. Dit-Yan. Transfer metric learning by learning task relationships. *Proceedings of the 16th ACM SIGKDD international conference on Knowledge discovery and data mining*, pages 1199–1208, 2010. (Cited on page 23.)
- [82] J. Davis and P. Domingos. Deep transfer via second-order markov logic. *Proceedings of the 26th Annual International Conference on Machine Learning*, pages 217–224, 2009. (Cited on page 23.)
- [83] C. Wang, Y. Wu, and Z. Liu. Hierarchical boosting for transfer learning with multi-source. *Proceedings of the International Conference on Artificial Intelligence and Robotics and the International Conference on Automation, Control and Robotics Engineering*, pages 151–155, 2016. (Cited on page 23.)
- [84] W. Dai, Q. Yang, G. Xue, and Y. Yu. Boosting for transfer learning. *Proceedings of the 24th international conference on Machine learning*, pages 193–200, 2007. (Cited on page 23.)
- [85] B. Li, Q. Yang, and X. Xue. Transfer learning for collaborative filtering via a rating-matrix generative model. *Proceedings of the 26th Annual International Conference on Machine Learning*, pages 617–624, 2009. (Cited on page 23.)
- [86] M. Kaboli, T. De La Rosa, R. Walker, and G. Cheng. Re-using prior tactile experience by robotic hands to discriminate in-hand objects via texture properties. *IEEE International Conference on Robotics and Automation (ICRA)*, pages 2242–2247, 2016. (Cited on pages 23 and 130.)
- [87] X. Shi, W. Fan, and J. Ren. Actively transfer domain knowledge. *Machine Learning and Knowledge Discovery in Databases*, pages 342–357, 2008. (Cited on page 23.)

- [88] A. Saha, P. Rai, V. Suresh, D. Vall, and L. Scott. Active supervised domain adaptation. *Joint European Conference on Machine Learning and Knowledge Discovery in Databases*, pages 97–112, 2011. (Cited on page 23.)
- [89] D. Wu, B.J. Lance, and Thomas T.D. Parsons. Collaborative filtering for brain-computer interaction using transfer learning and active class selection. *PloS one*, 8(2):566–24, 2013. (Cited on page 24.)
- [90] G. Skolidis and G. Sanguinetti. Semisupervised multitask learning with Gaussian processes. *IEEE Transactions on Neural Networks and Learning Systems*, pages 12101–2112, 2013. (Cited on page 24.)
- [91] L. Fei-Fei, R. Fergus, and P. Perona. One-shot learning of object categories. *IEEE Transactions on Pattern Analysis and Machine Intelligence*, pages 594–611, 2006. (Cited on page 24.)
- [92] S. I. Lee, V. Chatalbashev, D. Vickrey, and D. Koller. Learning a meta-level prior for feature relevance from multiple related tasks. In *Proceedings of the 2007 international conference on Machine learning (ICML)*, pages 489–496, 2007. (Cited on page 24.)
- [93] A. Vedaldi, G. Guidi, and S. Soatto. Joint alignment up to (lossy) transformations. In *Proceedings of the 2008 IEEE Conference on Computer Vision and Pattern Recognition (CVPR)*, 2008. (Cited on page 24.)
- [94] V. Jain and E. Learned-Miller. Online domain adaptation of a pre-trained cascade of classifiers. In *Proceedings of the 2008 IEEE Conference on Computer Vision and Pattern Recognition (CVPR)*, 2011. (Cited on page 24.)
- [95] R. Salakhutdinov, A. Torralba, and J. Tenenbaum. Learning to share visual appearance for multiclass object detection. In *Proceedings of the 2008 IEEE Conference on Computer Vision and Pattern Recognition (CVPR)*, 2011. (Cited on page 24.)
- [96] C. Goring, E. Rodner, A. Freytag, and J. Denzler. Nonparametric part transfer for fine-grained recognition. *The IEEE Conference on Computer Vision and Pattern Recognition (CVPR)*, 2014. (Cited on page 24.)
- [97] R. Urtasun, A. Quattoni, N. D. Lawrence, and T. Darrell. Transfer learning for reinforcement learning domains: A survey. *The Journal of Machine Learning Research*, pages 1633–1685, 2011. (Cited on page 24.)

-
- [98] C. Do and A. Ng. Transfer learning for text classification. *In Advances in Neural Information Processing Systems*, pages 299–306, 2006. (Cited on page 24.)
- [99] Q. Wu, X. Zhou, Y. Yan, H. Wu, and H. Min. Online transfer learning by leveraging multiple source domains. *Knowledge and Information Systems*, pages 1–21, 2017. (Cited on page 24.)
- [100] J. T. Zhou. J. p. Sinno, W. T. Ivor, and H. Shen-Shyang, *Transfer Learning for Cross-Language Text Categorization through Active Correspondences Construction*, pages 2400–2406, 2016. (Cited on page 24.)
- [101] V. Jayaram, M. Alamgir, Y. Altun, B. Scholkopf, and M. Grosse-Wentrup. Transfer learning in brain-computer interfaces. *Pattern Recognition*, pages 20–31, 2016. (Cited on page 24.)
- [102] J. W. Tao, D. Song, S. Wen, and Wenjun Hu. Transfer learning for deep learning on graph-structured data. *Pattern Recognition*, pages 47–65, 2017. (Cited on page 24.)
- [103] E. D. Engeberg and S. G. Meek. Adaptive sliding mode control for prosthetic hands to simultaneously prevent slip and minimize deformation of grasped objects. *IEEE ASME Transactions on Mechatronics*, 18(1):376–385, 2013. (Cited on pages 24 and 26.)
- [104] S. Teshigawara, K. Tadakuma, A. Ming, M. Ishikawa, and M. Shimojo. High sensitivity initial slip sensor for dexterous grasp. *IEEE International Conference on Advanced Robotics*, 2010. (Cited on pages 24 and 26.)
- [105] M. Schöpfer, C. Schürmann, M. Pardowitz, and H. Ritter. Using a piezo-resistive tactile sensor for detection of incipient slippage. *International Symposium on Robotics and 6th German Conference on Robotics (ROBOTIK)*, pages 1–7, 2010. (Cited on page 24.)
- [106] D. P. Cotton, P.H. Chappell, A. Cranny, et al. A novel thick-film piezoelectric slip sensor for a prosthetic hand. *IEE Sensors Journal*, 7(5):752–761, 2007. (Cited on pages 24 and 26.)
- [107] F. Kobayashi, H. Kanno, H. Nakamoto, and F. Kojima. Slip based pick-and-place by universal robot hand with force/torque sensors. *IEEE Symposium on Robotic Intelligence In Informationally Structured Space*, pages 1–4, 2014. (Cited on pages 24 and 26.)

- [108] Y. Tada, K. Hosoda, and M. Asada. Learn to grasp utilizing anthropomorphic fingertips together with a vision sensor. *IEEE International Conference on Intelligent Robots and Systems*, pages 3323–3328, 2005. (Cited on pages 25 and 26.)
- [109] C. Melchiorri. Slip detection and control using tactile and force sensors. *IEEE ASME transactions on mechatronics*, 5(3):235–243, 2000. (Cited on page 25.)
- [110] B. Heyneman and M. R. Cutkosky. Slip interface classification through tactile signal coherence. *IEEE International Conference on Intelligent Robots and Systems*, pages 801–808, 2013. (Cited on page 25.)
- [111] Jens Reinecke, Andre Dietrich, Florian Schmidt, and Maxime Chalon. Experimental comparison of slip detection strategies by tactile sensing with the biotac® on the dlr hand arm system. *IEEE International Conference on Robotics and Automation*, pages 2742–2748, 2014. (Cited on pages 25 and 26.)
- [112] S. Shirafuji and K. Hosoda. Detection and prevention of slip using sensors with different properties embedded in elastic artificial skin on the basis of previous experience. *Robotics and Autonomous Systems*, 62(1):46–52, 2014. (Cited on pages 25 and 26.)
- [113] H. Kanno, H. Nakamoto, F. Kobayashi, F. Kojima, and W. Fukui. Slip detection using robot fingertip with 6-axis force/torque sensor. *Workshop on IEEE Symposium on Robotic Intelligence In Informationally Structured Space*, 2013. (Cited on page 26.)
- [114] X. Zhang and R. Liu. Slip detection by array-type pressure sensor for a grasp task. *International Conference on Mechatronics and Automation*, pages 2198–2202, 2012. (Cited on page 26.)
- [115] Nawid Jamali and Claude Sammut. Slip prediction using hidden markov models: Multidimensional sensor data to symbolic temporal pattern learning. In *Robotics and Automation (ICRA), 2012 IEEE International Conference on*, pages 215–222. IEEE, 2012. (Cited on page 26.)
- [116] S. Shirafuji and K. Hosoda. Detection and prevention of slip using sensors with different properties embedded in elastic artificial skin on the basis of previous experience. *IEEE International Conference on Advanced Robotics*, 2011. (Cited on page 26.)
- [117] L. Roberts, G. Singhal, and R. Kaliki. Slip detection and grip adjustment using optical tracking in prosthetic hands. *IEEE Annual International Conference of Engineering in Medicine and Biology Society*, pages 2929–2932, 2011. (Cited on pages 26 and 174.)

-
- [118] Nicholas Wettels and et al. Grip control using biomimetic tactile sensing systems. *IEEE ASME Transactions On Mechatronics*, 14(6):718–723, 2009. (Cited on pages 25, 26, and 170.)
- [119] D. Gunji, Y. Mizoguchi, S. Teshigawara, A. Ming, A. Namiki, M. Ishikawaand, and M. Shimojo. Grasping force control of multi-fingered robot hand based on slip detection using tactile sensor. *IEEE International Conference on Robotics and Automation*, pages 2605–2610, 2008. (Cited on page 26.)
- [120] Erik D Engeberg, Sanford G Meek, Mark Minor, et al. Hybrid force–velocity sliding mode control of a prosthetic hand. *Biomedical Engineering, IEEE Transactions on*, 55(5):1572–1581, 2008. (Cited on page 26.)
- [121] E. Engeberg and S. G. Meek. Adaptive object slip prevention for prosthetic hands through proportional-derivative shear force feedback. *IEEE International Conference on Intelligent Robots and Systems*, pages 1940–1945, 2008. (Cited on page 26.)
- [122] Y. Tada and K. Hosoda. Acquisition of multi-modal expression of slip through pick-up experiences. *Advanced Robotics*, 21(5-6):601–617, 2007. (Cited on page 26.)
- [123] Lionel Birglen, Clément M Gosselin, and CM Gosselin. Fuzzy enhanced control of an underactuated finger using tactile and position sensors. *IEEE International Conference on Robotics and Automation*, pages 2320–2325, 2005. (Cited on page 26.)
- [124] Nobutaka Tsujiuchi, Takayuki Koizumi, Akihito Ito, Hiroko Oshima, Yoshiro Nojiri, Yotaro Tsuchiya, and Shiro Kurogi. Slip detection with distributed-type tactile sensor. *IEEE International Conference on Intelligent Robots and Systems*, pages 331–336, 2004. (Cited on page 26.)
- [125] Takashi Maeno, Tomoyuki Kawamura, and Sen-Chieh Cheng. Friction estimation by pressing an elastic finger-shaped sensor against a surface. *Robotics and Automation, IEEE Transactions on*, 20(2):222–228, 2004. (Cited on page 26.)
- [126] Yoji Yamada, Takashi Maeno, Isao Fujimoto, Tetsuya Morizono, and Yoji Umetani. Identification of incipient slip phenomena based on the circuit output signals of pvdf film strips embedded in artificial finger ridges. In *Proceedings of the SICE Annual Conference*, pages 3272–3277, 2002. (Cited on page 26.)

- [127] Daisuke Yamada, Takashi Maeno, and Yoji Yamada. Artificial finger skin having ridges and distributed tactile sensors used for grasp force control. In *Intelligent Robots and Systems, 2001. Proceedings. 2001 IEEE/RSJ International Conference on*, volume 2, pages 686–691. IEEE, 2001. (Cited on page 26.)
- [128] Takashi Maeno, Shinichi Hiromitsu, and Takashi Kawai. Control of grasping force by detecting stick/slip distribution at the curved surface of an elastic finger. In *Robotics and Automation, 2000. Proceedings. ICRA'00. IEEE International Conference on*, volume 4, pages 3895–3900. IEEE, 2000. (Cited on page 26.)
- [129] M. R. Trembla and M. R. Cutkosky. Estimating friction using incipient slip sensing during a manipulation task. *IEEE International Conference on Robotics and Automation*, pages 429–434, 1993. (Cited on page 26.)
- [130] Giuseppe De Maria, Pietro Falco, Ciro Natale, and Salvatore Pirozzi. Integrated force/tactile sensing: The enabling technology for slipping detection and avoidance. *IEEE International Conference on Robotics and Automation*, pages 3883–3889, 2015. (Cited on page 25.)
- [131] G. D. Maria, C. Natale, and S. Pirozzi. Tactile sensor for human-like manipulation. *IEEE International Conference on Biomedical Robotics and Biomechatronics*, pages 1686–1691, 2012. (Cited on page 25.)
- [132] Joseph M Romano, Kaijen Hsiao, Günter Niemeyer, Sachin Chitta, and Katherine J Kuchenbecker. Human-inspired robotic grasp control with tactile sensing. *IEEE Transactions on Robotics*, 27(6):1067–1079, 2011. (Cited on page 25.)
- [133] B. D. Argall and A. G Billard. A survey of tactile human–robot interactions. *Robotics and Autonomous Systems*, 58:1159–1176, 2010. (Cited on pages 27 and 181.)
- [134] A. L. Thomaz, G. Hoffman, and C. Breazeal. Reinforcement learning with human teachers: Understanding how people want to teach robots. *IEEE International Symposium on Robot and Human Interactive Communication*, pages 352–357, 2006. (Cited on pages 27 and 181.)
- [135] A. Silvera-Tawil, D. Rye, and M. Velonaki. Artificial skin and tactile sensing for socially interactive robots: A review. *Robotics and Autonomous Systems*, 63:230–243, 2015. (Cited on page 27.)

-
- [136] H. Kozima, C. Nakagawa, and Y. Yasuda. Interactive robots for communication-care: A case-study in autism therapy. *IEEE International Workshop on Robots and Human Interactive Communication*, pages 341–346, 2005. (Cited on page 27.)
- [137] A. Lucarotti, C. M. Oddo, N. Vitiello, and M. C. Carrozza. Synthetic and bio-artificial tactile sensing: A review. *IEEE Sensors*, 13:1435–1466, 2013. (Cited on page 28.)
- [138] K. Kim, K. R. Lee, D. S. Lee, and et al. A silicon-based flexible tactile sensor for ubiquitous robot companion applications. *Journal of Physics: Conference Series*, 34:399–403, 2006. (Cited on page 28.)
- [139] T. Minato, Y. Yoshikawa, T. Noda, S. Ikemoto, H. Ishiguro, and M. Asada. A child robot with biomimetic body for cognitive developmental robotics. *IEEE-RAS International Conference of Humanoid Robot*, pages 557–562, 2008. (Cited on page 28.)
- [140] T. Tajika, T. Miyashita, H. Ishiguro, and N. Hagita. Automatic categorization of haptic interactions -what are the typical haptic interactions between a human and a robot? *IEEE International Conference on Humanoid Robots*, pages 490–496, 2006. (Cited on page 29.)
- [141] A. Iwata and S. Sugano. Human-robot-contact-state identification based on tactile recognition. *IEEE Transaction on Industrial Electronics*, 52:1468–1477, 2005. (Cited on page 29.)
- [142] A. Flagg, D. Tam, K. MacLean, and R. Flagg. Conductive fur sensing for a gesture-aware furry robot. *IEEE Haptics Symposium (HAPTICS)*, 99, 2012. (Cited on page 29.)
- [143] P. Gastaldo, L. Pinna, L. Seminara, and M. Valle. and r. zunino. *A tensor-based approach to touch modality classification by using machine learning*, 63:268–278, 2015. (Cited on page 29.)
- [144] Mohsen Kaboli, Philipp Mittendorfer, Vincent Hugel, and Gordon Cheng. Humanoids learn object properties from robust tactile feature descriptors via multi-modal artificial skin. *IEEE International Conference on Humanoid Robots (Humanoids)*, pages 187–192, 2014. (Cited on page 32.)
- [145] Mohsen Kaboli, Rich Walker, Gordon Cheng, et al. In-hand object recognition via texture properties with robotic hands, artificial skin, and novel tactile descriptors. *IEEE International Conference on Humanoid Robots (Humanoids)*, pages 1155–1160, 2015. (Cited on page 32.)

- [146] Mohsen Kaboli and Gordon Cheng. Robust tactile descriptors for discriminating objects from textural properties via artificial robotic skin. *IEEE Transactions on Robotics Journal, Accepted*, 2017. (Cited on page 32.)
- [147] B. Hjorth. Eeg analysis based on time domain properties. *Electroencephalography and Clinical Neurophys.*, 29:306–310, 1970. (Cited on page 32.)
- [148] P. Mittendorf and G. Cheng. Humanoid multimodal tactile-sensing modules. *IEEE Transactions on Robotics*, 27:401–410, 2011. (Cited on page 37.)
- [149] S. J. Lederman and R. L. Klatzky. Haptic perception: A tutorial. *Attention, Perception, & Psychophysics*, 71:1439–1459, 2009. (Cited on page 43.)
- [150] M. Kaboli, K. Yao, and G. Cheng. Tactile-based manipulation of deformable objects with dynamic center of mass. *IEEE International Conference on Humanoid Robots (Humanoids)*, pages 752–757, 2016. (Cited on pages 51 and 164.)
- [151] Rong-En Fan, Kai-Wei Chang, Cho-Jui Hsieh, Xiang-Rui Wang, and Chih-Jen Lin. Liblinear: A library for large linear classification. *Journal of Machine Learning*, 9:1871–1874, 2008. (Cited on pages 57 and 58.)
- [152] A. P. Dempster, N. M. Laird, and D. B. Rubin. Maximum likelihood from incomplete data via the em algorithm. *Journal of the Royal Statistical Society.*, 39(1):1–38, 1977. (Cited on page 57.)
- [153] A.L.N. Anil and A.K. Jain. Robust data clustering. *IEEE Computer Society Conference on Computer Vision and Pattern Recognition, CVPR*, 3:128–136, 2003. (Cited on pages 58 and 207.)
- [154] M. Kaboli, D. Feng, K. Yao, P. Lanillos, and G. Cheng. A tactile-based framework for active object learning and discrimination using multimodal robotic skin. *IEEE Robotics and Automation Letters*, 2(4):2143–2150, 2017. (Cited on page 70.)
- [155] P. Lanillos, E. Besada-Portas, J. Lopez-Orozco, A. de la Cruz, and M. Jesus. Minimum time search in uncertain dynamic domains with complex sensorial platforms active sequential learning with tactile feedback. *Sensors*, pages 14131–14179, 2014. (Cited on page 73.)
- [156] C. E. Rasmussen and C. K. I. Williams. Gaussian processes for machine learning. 2006. (Cited on pages 76, 91, 146, 147, and 205.)

-
- [157] M. Kaboli, D. Feng, K. Yao, and G. Cheng. Tactile-based active object discrimination and target object search in an unknown workspace. *Autonomous Robots, under review*, 2017. (Cited on page 85.)
- [158] Kunpeng Yao, Mohesn Kaboli*, and Gordon Cheng. Tactile-based object center of mass exploration and discrimination. *IEEE International Conference on Humanoids Robot (Humanoids), *corresponding author*, 2017. (Cited on page 85.)
- [159] Ruben Martinez-Cantin, Nando de Freitas, Arnaud Doucet, and José A Castellanos. Active policy learning for robot planning and exploration under uncertainty. *Robotics: Science and Systems*, pages 321–328, 2007. (Cited on page 92.)
- [160] Yizong Cheng. Mean shift, mode seeking, and clustering. *IEEE Transactions on Pattern Analysis and Machine Intelligence*, 17(8):790–799, 1995. (Cited on page 93.)
- [161] Antons Rebguns, Daniel Ford, and Ian R Fasel. Infomax control for acoustic exploration of objects by a mobile robot. *Lifelong Learning*, 2011. (Cited on page 109.)
- [162] L. Csato and M. Opper. Sparse on-line gaussian processes. *Neural Computation*, 14(3):641–668, 2002. (Cited on page 126.)
- [163] M. Kaboli and G. Cheng. Novel tactile descriptors and a tactile transfer learning technique for active in-hand object recognition via texture properties. *IEEE International Conference on Humanoid Robots (Humanoids)-workshop on tactile sensing for manipulation: new progress and challenges*, 2016. (Cited on page 130.)
- [164] M. Kaboli. Leveraging over prior knowledge for online learning of visual categories across robots. *Thesis, KTH, The Royal Institute of Technology, Stockholm Sweden*, 2012. (Cited on pages 130, 131, and 133.)
- [165] J. A. K. Suykens and J. Vandewalle. Least squares support vector machine classifiers. *Neural Process. Lett.*, 9:293–300, 1999. (Cited on page 131.)
- [166] T. Tommasi, F. Orabona, and Barbara B. Caputo. Safety in numbers: Learning categories from few examples with multi model knowledge transfer. *IEEE Conference on Computer Vision and Pattern Recognition (CVPR)*, pages 3081–3088, 2010. (Cited on page 132.)
- [167] K. Crammer, O. Dekel, J. Keshet, S. Shalev-Shwartz, and Y. Singer. Online passive-aggressive algorithms. *The Journal of Machine Learning Research*, Vol.7:551–585, December 2006. (Cited on pages 132 and 133.)

- [168] M. Kaboli, Di Feng, and G. Cheng. Active tactile transfer learning for object discrimination in an unstructured environment using multimodal robotic skin. *International Journal of Humanoid Robotics (IJHR)*, 15(1), 2017. (Cited on page 143.)
- [169] Chai Kian.M. Generalization errors and learning curves for regression with multi-task gaussian processes. *Advances in neural information processing systems*, pages 279–287, 2009. (Cited on page 148.)
- [170] Mohsen Kaboli, Alex Long, and Gordon Cheng. Humanoids learn touch modalities identification via multi-modal robotic skin and robust tactile descriptors. *Advanced Robotics*, 29(21):1411–1425, 2015. (Cited on page 182.)
- [171] C. Cortes and V. Vapnik. Support-vector networks. *Journal in Machine learning*, 20:273–297, 1995. (Cited on page 191.)
- [172] A. P. Dempster, N. M. Laird, and D. B. Rubin. Maximum likelihood from incomplete data via the em algorithm. *Journal of the Royal Statistical Society*, 39:1–38, 1977. (Cited on page 193.)